AD_____

Award Number: DAMD17-00-1-0105

TITLE: Growth Inhibitory and Stimulatory Signals in Prostate Cancer

PRINCIPAL INVESTIGATOR: Robert J. Matusik, Ph.D.

CONTRACTING ORGANIZATION: Vanderbilt University Medical Center
Nashville, Tennessee 37232-2103

REPORT DATE: April 2003

TYPE OF REPORT: Final

PREPARED FOR: U.S. Army Medical Research and Materiel Command
Fort Detrick, Maryland 21702-5012

DISTRIBUTION STATEMENT: Approved for Public Release;
Distribution Unlimited

REPORT DOCUMENTATION PAGE

Form Approved
OMB No. 074-0188

Public reporting burden for this collection of information is estimated to average 1 hour per response, including the time for reviewing instructions, searching existing data sources, gathering and maintaining the data needed, and completing and reviewing this collection of information. Send comments regarding this burden estimate or any other aspect of this collection of information, including suggestions for reducing this burden to Washington Headquarters Services, Directorate for Information Operations and Reports, 1215 Jefferson Davis Highway, Suite 1204, Arlington, VA 22202-4302, and to the Office of Management and Budget, Paperwork Reduction Project (0704-0188), Washington, DC 20503

1. AGENCY USE ONLY (Leave blank)	2. REPORT DATE April 2003	3. REPORT TYPE AND DATES COVERED Final (1 Apr 00 – 31 Mar 03)

4. TITLE AND SUBTITLE
Growth Inhibitory and Stimulatory Signals in Prostate Cancer

5. FUNDING NUMBERS
DAMD17-00-1-0105

6. AUTHOR(S)
Robert J. Matusik, Ph.D.

7. PERFORMING ORGANIZATION NAME(S) AND ADDRESS(ES)
Vanderbilt University Medical Center
Nashville, Tennessee 37232-2103

E-Mail: Robert.matusik@vanderbilt.edu

20031222 018

9. SPONSORING / MONITORING AGENCY NAME(S) AND ADDRESS(ES)
U.S. Army Medical Research and Materiel Command
Fort Detrick, Maryland 21702-5012

10. SPONSORING / MONITORING AGENCY REPORT NUMBER

11. SUPPLEMENTARY NOTES
Original contains color plates: All DTIC reproductions will be in black and white.

12a. DISTRIBUTION / AVAILABILITY STATEMENT
Approved for Public Release; Distribution Unlimited

12b. DISTRIBUTION CODE

13. Abstract (Maximum 200 Words) (abstract should contain no proprietary or confidential information)
Substantial progress has been made by the DOD funded Vanderbilt Prostate Cancer Center (VPCC) to evaluate the growth stimulator and growth inhibitory pathways in the development of prostate cancer. The VPCC research group has expanded both in personnel and disciplinary approaches to study prostate cancer. A number of investigators are now working on existing and developing new mouse models for prostate cancer. In addition the researchers have developed new funding to start translational programs on the treatment of prostate cancer. The established of the VPCC by the DOD funding has made this possible. The VPCC will continue to exist and is pursuing new sources of funding to maintain and expand the existing program. The research program funded has established that a loss of the growth inhibitory signal (TGFβ) in the prostate will increase prostatic metastatic tumor burden. We have been surprised to discover that the loss of this inhibitory signal process by the stromal cells rather then the epithelial cells are key to this process. Further, we have shown that overexpression of the growth stimulatory signal (TGFα) plus loss the inhibitory signal gives a selective advantage to the prostate tumor to survive in the face of androgen ablation therapy. Although funding of this Center is ending, the research started has now expanded into other programs with support from both the DOD and NIH which will allow the programs to continue.

14. SUBJECT TERMS
TGFα, TGFβ, prostate cancer, transgenic mice probasin, Large T antigen

15. NUMBER OF PAGES
165

16. PRICE CODE

17. SECURITY CLASSIFICATION OF REPORT Unclassified	18. SECURITY CLASSIFICATION OF THIS PAGE Unclassified	19. SECURITY CLASSIFICATION OF ABSTRACT Unclassified	20. LIMITATION OF ABSTRACT Unlimited

NSN 7540-01-280-5500

Standard Form 298 (Rev. 2-89)
Prescribed by ANSI Std. Z39-18
298-102

Table of Contents

PROGRESS REPORT

Project 1: *The role of the TGFβ pathway in prostate cancer progression to an androgen-independent disease.*

In breast and colon cancer, transforming growth factor-β (TGF-β) signaling initially has an anti-neoplastic effect, inhibiting tumor growth, but eventually exerts a pro-neoplastic effect, increasing motility and cancer spread. Prostate cancer is the most commonly occurring cancer and the second leading cause of cancer death in American men. In human prostate cancers, loss of functional Transforming Growth Factor-β (TGF-β) receptor type II (TβRII) has been correlated with higher tumor grade and poor prognosis. However, no proof exists that demonstrates that the loss of TβRII actually promotes tumor progression.

To determine the effect of an inhibited TGF-β pathway on prostate cancer, we disrupted this pathway in transgenic mice that used the large probasin promoter (LPB) to target expression the tumorigenic SV40 large T antigen (Tag) in the prostate[1; 2]. This was accomplished by cross-breeding the LPB-Tag mice with transgenic mice which used the metallothionein (MT) promoter to drive a dominant negative TGF-β type II receptor (DNIIR) mutant in the prostate (termed bigenic mice). LPB-Tag develops high-grade prostatic intraepithelial neoplasia (HGPIN) that progresses to locally invasive carcinoma by 20 weeks of age. MT-DNIIR mice develop prostatic lesions comparable to HGPIN. Transgene(s) and TGF-β1 expression was identified in the prostate and decreased protein levels of plasminogen activator inhibitor type 1, as a marker for TGF-β signaling, correlated with expression of the dominant negative TGF-β type II receptor mutant. Although the sizes of the neoplastic prostates were not enlarged, increased amounts of metastasis were observed in mice expressing both transgenes compared to age-matched control mice expressing only the large T antigen transgene. Bigenic offspring aged 12-23 weeks were studied to determine the effect of loss of TGF-β signaling on prostate cancer progression. While age-matched MT-DNIIR and LPB-Tag develop only HGPIN at comparable time points, Bigenic mice develop invasive prostate cancer with both glandular and neuroendocrine differentiation at 16 weeks. Some Bigenic mice develop metastatic lesions – especially to the lung – that are not observed in age-matched LPB-Tag mice. *This study demonstrated for the first time that a disruption of TGF-β signaling in prostate cancer plays a causal role in promoting tumor metastasis.*[3]

To identify the gene changes that accompany increase metastatic burden, microarray analyses was performed. Microarray analyses of Bigenic versus LPB-Tag dorsolateral prostate samples at 12, 16, 18.5, 20, and 23 weeks showed a total of 996 out of 5000 genes examined with differential fold expression of either ≥ 1.5 or ≤ 0.7. Using the top 50 differentially expressed genes, the mice within each transgenic age group clustered together upon pair-wise comparison, showing there are age-dependent differential gene expression patterns. The top 50 genes were selected based on four statistical methods: Significance Analysis of Microarrays, weighted gene analysis, mutual-information scoring, and permutation t-test. Comparing the early and late ages (by the agglomerative hierarchical clustering algorithm) revealed that the early ages (12,16 weeks) and late ages (20,23 weeks) clustered together as distinct groups. The microarray data correlated

4

with the histological results showing a significant difference between Bigenic and LPB-Tag mice starting at 16 weeks. The temporal patterns of expression will allow us to identify the TGF-β mediated pathways contributing to prostate cancer progression and potential therapeutic targets. Our analysis of the selected genes and the role of the TGF-β in prostate cancer will continue through the funded NCI grant entitled "Transgenic mouse models for prostate cancer".

Project 2: *Tumorigenic effects of partial versus complete ablation of the TGFβ type II receptor in prostatic epithelial cells.*

Several approaches have been taken to characterize TGF-ß receptor expression in the prostate during postnatal development (1, 3, 5 and 6 weeks) in the mouse. The first try was the immunostaining using a published antibody and technique for detecting TßRII[4]. While this technique works well in human tissue, we were not able to overcome specificity problems in mouse tissues. Real time PCR using RNA isolated from above time points and primers to TßRII was done in collaboration with the Pathology Core and *in situ* hybridization attempts were unsuccessful, likely because of very low RNA abundance. More recent attempts utilizing a technique previously published by us[5] for detection of TßRII have been successful. These results suggest that TßRII expression is not present in the prostate epithelium in one week old animals but is present at 3, 5 and 6 weeks. Validation of specificity was carried out by showing lack of TßRII staining in tissues with conditional knock-out of the TßRII gene.

Three lines of ARR₂PB-DNIIR mice have been generated by the VICC Transgenic Mouse/ES Cell Shared Resource by microinjecting a previously assembled ARR₂PB-DNIIR construct. Offspring of founder mice from the three ARR₂PB-DNIIR lines (lines A, B, and C) have been shown to have the appropriate genotype. Prostates have been harvested from the three lines of ARR₂PB-DNIIR animals, and expression of the DNIIR was determined. Transgene expression was not obtained in any of the lines, and there was no discernable phenotype. Testing of these lines for expression of the endogenous probasin gene revealed that probasin levels decreased almost 100-fold compared to wild type mice. The normal rodent prostate dorsolateral lobes contain two types of epithelium, one that expresses high levels of probasin and one that expresses low levels of probasin. Apparently, when we target expression of the DNIIR to the epithelium with the probasin promoter, the DNIIR must inhibit the growth of the epithelium such that high expression of the DNIIR is selected against. The only epithelium that remain develop normal prostate histology but express very low levels of probasin. Thus, this mouse cannot be successfully made to express the DNIIR under the control of the probasin promoter. However, Task 3, conditional KO of the Tgfbr2 in prostatic epithelium, accomplished the goal of Task 2.

A line of ARR₂PB-Cre+/+ mice generated in the laboratory of Dr. Pradip Roy-Burman[6] was crossed with mice carrying the *Tgfbr2^{floxE2}* allele developed in our laboratory[7]. As a preliminary experiment, 7wk prostates from animals carrying the *Tgfbr2^{pko}* allele were harvested and examined for a phenotype. Initial results indicate that 7wk prostates from these bigenic animals may exhibit some epithelial disorganization in the anterior prostate. Further examination of the prostate phenotype in *Tgfbr2^{pko}* animals has shown disappointingly minimal changes. However, we have verified Cre-mediated recombination of Tgfbr2 in the anterior, dorsolateral

and ventral prostate lobes by PCR. This result was surprising since the MT-DNIIR mice develop PIN lesions and we expected that complete loss of the type II receptor in the epithelium would have at least the same phenotype. Our conclusion was that the MT-DNIIR expression in the stromal cell layer must be more important then in the epithelium.

In order to determine the role of the type II receptor in the stromal cell, new experiments were conducted that were not originally proposed in this grant. To test this hypothesis, we expanded this specific aim to specifically remove the type II receptor from the stromal cell layer. We have developed an interesting and likely very significant model that indicates TGF-ß signaling in prostate stromal cells are important in the development of prostate cancer. We targeted fibroblastic recombination by crossbreeding transgenic mice with homozygous floxed exon 2 *TβRII* gene with transgenic mice expressing *Cre* under the FSP-1 (fibroblast specific protein, S100A4) promoter (FSP-*Cre*[8]. The use of a FSP promoter-driven GFP transgenic mouse illustrated fibroblast specificity of expression in various tissues. Further, Cre-specific immuno-staining of the prostate indicate only stromal expression. The homozygous conditional-knock out of the type II TGF-ß receptor (*Tgfbr2^{fspKO}*) resulted in little to no histologic abnormality in the colon, lung, liver, kidney, or skin. However, pancreas, bladder, mammary gland, and prostate gland of *Tgfbr2^{fspKO}* displayed stromal hypercellularity. The prostate of 6-7 week old *Tgfbr2^{fspKO}* mice specifically had focal hyperchomatic epithelial nuclei with atypia, phenotypically similar to low-grade prostate intraepithelial neoplastic (PIN) lesion in humans. Although grossly normal, the heterozygous conditional-knockout had epithelial hyperproliferation of the anterior prostate ducts and limited phenotypic effect on the dorsolateral ducts compared to age matched FSPCre⁻ littermates. Since the *Tgfbr2^{fspKO}* mice die at approximately 8 weeks of age, extended analysis of the prostate was performed by xenografting prostates into sub-renal capsules. After two months the *Tgfbr2^{fspKO}* prostate xenografts showed significant hyperproliferative progression to a phenotype similar to human high grade PIN. Together, the data reveal the requirement of TGF-ß signaling in stromal fibroblasts of the prostate for the regulation of epithelial development and neoplastic differentiation. And further establish the *Tgfbr2* gene as being haploinsufficient in its ability to protect against hyperplasia. The data indicate that TGF-ß signaling in stroma may be more important than TGF-ß signaling in epithelia in influencing the development of prostate cancer and in metastases. The results of Tu et al. (2003)[3] with a metallothionein driven DNIIR may be due more to expression of the dominant-negative type II receptor in stroma than in prostate epithelium as the metallothionein promoter drives expression in both stromal and epithelial cells.

Project 3: *Tumorigenic effect of TGFα in mouse prostatic epithelial cells and the therapeutic efficacy of combined blockade of the EGF receptor and TGFα cleavage in mouse prostate cancer.*

TGFα, one of the ligands of the Epidermal Growth Factor Receptor (EGFR) is overproduced in human prostate cancer. Using a mouse model that over-expresses TGFα, we have shown that this expression promotes prostatic intraepithelial neoplasia (PIN) in these animals. These lesions are concurrent with hyperphosphorylation of the EGFR as well as both

MAP kinase and AKT, effector molecules thought to act down stream of TGFα signaling and involved in mediating the increased proliferation and decreased apoptosis which we also observe in the prostate of the transgenic animals. In addition, by combining over-expression of TGFα to stimulate the EGFR axis while simultaneously inhibiting the TGFβ axis via a MT-DNIIR results in a HGPIN earlier than either transgene alone. The EGFR axis lends itself to pharmacological manipulation but targeting to inhibit EGFR kinase activity show a modest effect on prostate growth in a mouse model of prostate cancer (LPBTag). Inhibiting the EGFR kinase activity leads to a modest reduction in overall prostate size and reduction in epithelial proliferation as well as downstream markers. Our findings thus far indicate that TGFα plays a role in growth and development of prostate cancer but that it is insufficient to drive the development of the disease on its own. Pharmacological targeting the EGFR axis may prove useful in combination with other drugs for treating prostate cancer but is unlikely to be effective therapy on its own.

Four independent ARR$_2$PB-TGFα transgenic lines were generated which carried the DNA construct. Unfortunately, a sensitive radioimmuno assay did not detect any expression of human TGFα in the prostates of these lines and blinded histological analysis of the prostate tissue found no difference compared to non-transgenic littermates. Given the lack of detectable protein expression in ARR$_2$PB-TGFα transgenic mice, a comparison to the MT-TGFα mice cannot be made.

However, to study the effect of the combination of both the increased stimulating effect of TGFα and the loss of TGFβ inhibitory effect, twenty male bigenic MT-TGFα MT-DNIIR mice were generated and sacrificed at 15, 22, 32 and 38 weeks of age, along with the appropriate age match controls. The bigenic mice were found to develop high-grade PIN lesions earlier (at 15 weeks) than animals with only one of the transgenes (22 weeks). These lesions did not progress beyond PIN by 38 weeks of age. These animals did, however, develop primary liver tumors by 38 weeks of age, much earlier than tumors have been seen to develop in MT-TGFα mice, indicating a synergistic relationship between the two transgenes. Histological analysis indicates that the transgenic mice have hyperphosphorylated MAP kinase and AKT and both an increase in epithelial proliferation and a decrease in apoptosis. Further analysis is in progress to determine why prostatic lesions do not progress beyond the PIN stage. Preliminary results suggesting down regulation of the AKT pathway may be involved.

Additional experiments have been conducted to determine the interaction of EGFR axis the androgen stimulus axis. MT-TGFα and non-transgenic controls were castrated and their prostate tissue analyzed. Preliminary results indicate that the MT-TGFα transgene retards the rate of prostate regression by promoting continued proliferation after androgen withdrawal and by reducing the level of apoptosis in the tissue.

As already described, none of the established ARR$_2$PB-DNIIR and the ARR$_2$PB-TGFα transgenic lines expressed the transgenes. Also, as describe earlier, we believe this is due to expression of these genes under the probasin promoter selects against epithelial cells that expression probasin. Therefore, the probasin promoter will not work to make these transgenic lines. The LPB-CRE/TGFβR2$^{floxE2/floxE2}$ mice do not develop PIN as does the MT-DNIIR mice[9]

7

suggesting that disruption of the stromal cell TGFβ is more important (See the report for project 2).

As the MT-TGFα line did not develop cancer, the LPB-Tag 12T-7f line[1] was utilized and animal's prostate tumors were treated with EGFR tyrosine kinase inhibitor, the EKI-785 compound from Wyeth-Ayerst. A modest decrease in gross weight of the dorsolateral lobe of the treated animals was detected when compared to the untreated controls. Molecular and histological analysis of tissues from these animals indicated a modest reduction in the amount of cell proliferation and a reduction in the activity of the downstream marker phosphoMAPK.

KEY RESEARCH ACCOMPLISHMENTS

Project 1: *The role of the TGFβ pathway in prostate cancer progression to an androgen-independent disease.*

Task I: Characterization of MT-DNIIR-27 and MT-DNIIR-4 mice. Task completed
- With aging, the MT-DNIIR-27 and MT-DNIIR-4 transgenic mice show the most significant changes in the dorsolateral prostate which include the development of high grade prostatic intraepithelial neoplasia (HGPIN).
- In one MT-DNIIR-4 transgenic mouse, invasive prostate cancer developed at 33 weeks of age. However, due to skeletonal defects that these mice also develop after 30 weeks of age, we are not able to maintain the animals past this time. Therefore, all long term studies are now being carried out with the MT-DNIIR-27 transgenic line.
- With androgen removal (castration) the prostate of the MT-DNIIR mice regress at a slower rate. Slowing down prostate regression by the loss of the TGFβ signaling pathway suggest that a loss of this pathway in prostate cancer can play a role in tumor progression

Task II: MT-DNIIR x LPB-Tag transgenic lines. Studies Completed on the DNIIR cross with two different lines of LPB-Tag: 12T-7f (PIN and invasive cancer model, rare metastasis) and 12T-10 (Neuroendocrine, NE, cancer that with NE metastasis) LPB-Tag tumors. Task completed, publication in press (attached)

MT-DNIIR x 12T-7f Cross
- The incidence of primary prostate cancer was analyzed in a blinded study by Scott Shappell by comparing MT-DNIIR x 12T-7f to 12T-7f alone.
- The incidence of metastatic NE cancer increases when the MT-DNIIR gene is expressed in the 12T-7f but not statistically significant.

MT-DNIIR x 12T-10 Cross
- The primary NE prostate cancer still occurs in the cross as seen in the 12T-10 alone [6].
- The incidence of primary NE prostate cancer is the same between the cross and 12T-10 alone.

- The incidence of metastatic NE cancer burden increases in the cross and is statistically significant ($p < 0.05$).

Conclusion: The loss of the TGFβ pathway contributes to the spread of prostate cancer. Since animals in Task IV died rapidly, not allowing us to complete that task, we have expanded Task II to conduct new MicroArray experiments to identify downstream targets to the type II receptor that are potentially responsible for the rapid increase in tumor burden.

Additional New Research:
- MicroArray chips containing 5,000 mouse genes were used to identify changes in gene expression patterns between the 12T-7f and the MT-DNIIR cross 12T-7f. A time course during tumor growth was analyzed.
- Clustering Analysis identified three genes as showing statistically significant changes: MT, VL30, and embigin. These changes were confirmed by real time PCR.
- MT is the zinc inducible metallotheinen gene, thus we have decided not to pursue this gene. The sameVL30 is a mouse virus sequence that has been reported to increase tumor metastasis. However, no human counterpart has been identified and again we are not pursuing this gene. We have identified the human counterpart to the mouse embigin.
- An antibody to embigin was obtained from Martin Tenniswood. Immunohistochemistry reveals that it is upregulated in mouse models in response to the loss of TGFβ signaling
- Immunohistochemistry on human prostate cancer microarrays reveals that embigin is upregulated as the prostate tumor grade increases

Future Direction: We are now constructing expression vectors for embigin and will overexpress the gene in prostatic cell lines to determine its effect on cell growth and invasion in cell culture and tumor formation *in vivo*. *The research will be continued under a newly funded renewal of my grant entitled "Transgenic animal models for prostate cancer" (NCI R01-CA76142; 4/1/03-3/31/08).*

Task III: Progression after androgen ablation in the LPB-Tag mice. Animal study and MRI analysis of tumor regression completed. Immunohistological studies completed.
- Animals have been castrated, tumors regressed and 74% regrowth following 2-6 months.
- Pathological analysis shows that the regrowing tumors are PIN, sarcomas, and NE cancers.
- Metastatic tumors appear frequently in the castrated mice, mostly as NE cancers.

Task IV: Progression after androgen ablation in the MT-DNIIR x LPB-Tag Mice.
These studies have not been possible to complete since after castration of the MT-DNIIR x 12T-7f, mice die at an extremely high rate. Task I has taught us that the prostate of MT-DNIIR mice regresses slowly and the data of Project 2 now suggests that the change in regression is due blocking the Type II R in the stromal cells rather then the epithelium. Task II has taught us that the cross between the MT-DNIIR and LPB-Tag develops a more aggressive cancer and routinely

develop NE cancer in intact mice. Also, the NE cancer that develops in the 12T-10 starts as a PIN lesion that is AR positive and chromogranin A (a NE cell marker) positive but progresses to invasive and then metastatic NE cancer that is AR negative. The normal route of dedifferentiation of NE cells is that they lose AR. Taken together, this data suggest that castration of the MT-DNIIR x 12T-7f could actually accelerate the dedifferentiation of the NE cancer resulting in death. Removing androgens by castration is equal to removing the AR since both cases result in a loss of AR activity. Our crosses of MT-DNIIR with the 12T-10 line that develops NE cancer show that NE tumor burden is significantly and rapidly increased.

The results of Project 1 & 2 demonstrated that the stroma plays an important role in prostate cancer progression. Expansion of these studies has now been submitted the DOD by Dr. Neil Bhowmick as a new grant application. This work will have to be done in tissue recombination and grafting models since the crosses we proposed in this Center rapidly progress and die if castrated.

Project 2: *Tumorigenic effects of partial versus complete ablation of the TGFβ type II receptor in prostatic epithelial cells.*

Task I: Characterize TβRI and TβRII expression during prostate development in the mouse. Three different methods were used in effort to detect TGFβ Type II Receptor in mouse prostates of 1,3,5,6 weeks old animals.

- The first try was the immunostaining using new to us Rabbit Polyclonal Antibody (Gift from Antonia Teresita) to TGFβ RII.
- Problems with specificity could not be overcome.
- Real Time PCR using RNA isolated from above time points and primers to TGFβ RII, done in collaboration with Scott Shappell laboratory.
- Technical difficulties using this method did not led to any results.
- In Situ Hybridization on paraffin sections of prostates. The 35 S labeled Exon 2 and 3 of TGFβ RII was hybridized to 1, 3, 5, 6 weeks old prostate sections in an approach to exclude previous problems such as CG rich regions and 3' overhang ends of template during digestion.
- The slides are exposed to research emulsion (for 2 month) and experiments were completed.

Conclusion: TβRII expression is not present in the prostate epithelium in one week old animals but is present at 3, 5 and 6 weeks. Validation of specificity was carried out by showing lack of TβRII staining in tissues with conditional knock-out of the TβRII gene.

Task II: Disrupt the TGF-β pathway specifically in epithelium with the ARR₂PB-DNIIR transgene.

- We have made eleven transgenic lines with the Large PB promoter construct and three lines with the new ARR₂PB promoter to target prostate specific expression of the DNIIR to the prostate of transgenic mice. None the lines express the DNIIR gene.

- Two types of luminal epithelial cells exist in the rodent prostate, one type expresses high levels of probasin and the second type very low levels of probasin. By RT-PCR, we have confirmed that in the ARR$_2$PB-DNIIR transgenic mice, 100-fold lower levels of probasin exist compared to non-transgenic mice.

Conclusion: Expression of the DNIIR selects during prostatic development and growth for a population of luminal epithelial cells that have a differentiation pattern that does not express probasin. Since these cells express very low levels of probasin, the probasin promoter construct we used are also downregulated such that DNIIR is no longer expressed. Thus, the MT-DNIIR is the only construct that will work.

Task III: Create and cross breed ARR$_2$PB-Cre mice with Tgrbr2^{floxE2} mice for complete abrogation of TGF-ß signaling.
- A line of ARR$_2$PB-Cre+/+ mice was generated in the laboratory of Dr. Pradim Roy-Burman.
- This line of ARR$_2$PB-Cre+/+ mice is presently being crossbred with mice carrying the Tbrbr2^{floxE2} allele. As a preliminary experiment, 7wk prostates from animals carrying the Tbrbr2^{pk} allele were harvested and examined for a phenotype. Initial results indicate that 7wk prostates from these bigenic animals may exhibit some epithelial disorganization in the anterior prostate. Furthermore, Cre expression was detected in the epithelial cells of the anterior prostate only.
- ARR$_2$PB-Cre+/-: Tbrbr2$^{floxE2/wt}$ were crossbred with Tbrbr2$^{floxE2/ffloxE2}$ animals to generate more animals carrying the Tbrbr2^{pko} allele. Animals carrying the Tbrbr2^{pk} will be evaluated for the absence of TßRII in prostatic epithelial cells at E18.5, post-natal stages of 1,3,5, and 6 weeks.
- Prostates were examined for the presence of PIN lesions and invasive/metastatic prostatic adenocarcinoma at 3, 6, 9 and 12 months of age. No lesions were found.

Conclusion: Removal of the epithelial type II receptor has no effect on the formation of PIN in the prostate. This result is surprising since the MT-DNIIR develop PIN. These data suggested that the stromal type II receptor was more important. To test the role of the type II receptor in the stroma cells, a new set of experiments were undertaken that were not previously proposed.

Additional new Research:
We expanded this specific aim to specifically remove the type II receptor from the stromal cell layer.
- We targeted fibroblastic recombination by crossbreeding transgenic mice with homozygous floxed exon 2 TßRII gene with transgenic mice expressing Cre under the FSP-1 (fibroblast specific protein, S100A4) promoter (FSP-Cre)
- Cre-specific immuno-staining of the prostate indicate only stromal expression
- The homozygous conditional-knock out of the type II TGF-ß receptor (Tgfbr2^{fspKO}) resulted in little to no histologic abnormality in the colon, lung, liver, kidney, or skin. However,

11

pancreas, bladder, mammary gland, and prostate gland of $Tgfbr2^{fspKO}$ displayed stromal hypercellularity.

- The prostate of 6-7 week old $Tgfbr2^{fspKO}$ mice specifically had focal hyperchomatic epithelial nuclei with atypia, phenotypically similar to low-grade prostate intraepithelial neoplastic lesion in humans.

- Since the $Tgfbr2^{fspKO}$ mice die at approximately 8 weeks of age, extended analysis of the prostate was performed by xenografting prostates into sub-renal capsules. After two months the $Tgfbr2^{fspKO}$ prostate xenografts showed significant hyperproliferative progression to a phenotype similar to human high grade PIN. Together, the data reveal the requirement of TGF-ß signaling in stromal fibroblasts of the prostate for the regulation of epithelial development and neoplastic differentiation.

Conclusion: The data indicate that TGF-ß signaling in stroma may be more important than TGF-ß signaling in epithelia in influencing the development of prostate cancer and in metastases. The results of Tu et al. (2003) with a metallothionein driven DNIIR may be due more to expression of the dominant-negative type II receptor in stroma than in prostate epithelium as the metallothionein promoter drives expression in both stromal and epithelial cells.

Project 3: *Tumorigenic effect of TGFα in mouse prostatic epithelial cells and therapeutic efficacy of combined blockade of EGF receptor and TGFα cleavage in mouse prostate cancer.*

Task I: To develop and characterize ARR$_2$PB-TGFα transgenic mice and compare them to MT-TGFα mice.

- Our latest advance in constructs has replaced the LPB promoter with the ARR$_2$PB promoter[10]. Using this construct, four independent transgenic mouse lines have been generated carrying a ARR$_2$PB driven TGFα gene.

- Unfortunately, a sensitive radioimmuno assay did not detect any expression of human TGFα in the prostates of these lines.

- A blinded histological analysis of the prostate tissue found no difference between ARR$_2$PB-TGFα compared to non-transgenic littermates.

- Twenty male MT-TGFα mice have been generated for comparison with the ARR$_2$PB-TGFα mice but were used instead as a control for the mice in task II.

Conclusion: Similar to our results with the ARR$_2$PB-DNIIR, the ARR$_2$PB-TGFα transgenic lines to not make the transgene. Again, we believe that a selection for an epithelial population that cannot express the probasin protein and thus the probasin driven transgene has occurred. Given the lack of detectable protein expression with the ARR$_2$PB–TGFα construct, we do not believe comparison to MT-TGFα mice will prove informative.

Task II: To cross MT-TGFα mice to MT-DNIIR mice as well as to cross ARR$_2$PB-TGFα mice to ARR$_2$PB-DNIIR and/or ARR$_2$PB-CRE/$Tgfbr2^{floxE2/floxE2}$ mice.

- Twenty male bigenic MT-TGFα crossed with MT-DNIIR mice have been generated, along with equal numbers of non-transgenic mice and animals with either the MT-TGFα or MT-DNIIR transgenes alone. Five of each group of mice were sacrificed at 15, 22, 32, and 38 weeks of age.
- The bigenic mice were found to develop high-grade PIN lesions earlier (15 weeks) than animals with only one of the transgenes (22 weeks). These lesions did not progress beyond PIN by 38 weeks of age. These animals did, however, develop primary liver tumors by 38 weeks of age, much earlier than tumors have been seen to develop in MT-TGFα mice, indicating a synergistic relationship between the two transgenes.
- The non-transgenic animals were found to be free of prostatic lesions while transgenic animals showed PIN like lesions.
- The bigenic animals consistently showed lesions of a higher grade than those of animals with only one of the transgenes. The most significant lesions were found in the anterior and dorsal lobes.
- Histological analysis indicates that the transgenic mice have hyperphosphorylated MAP kinase and AKT and both an increase in epithelial proliferation and a decrease in apoptosis. Further analysis is in progress to determine why prostate lesions do not progress beyond the PIN stage, with preliminary results suggesting down regulation of the AKT pathway may be involved.
- Additional experiments have been conducted to determine the interaction of EGFR axis the androgen stimulus axis. MT-TGFα and non-transgenic controls were castrated and their prostate tissue analyzed. Results indicate that the MT-TGFα transgene retards the rate of prostate regression by promoting continued proliferation after androgen withdrawal and reducing the level of apoptosis in the tissue.
- As the ARR$_2$PB-TGFα and ARR$_2$PB-DNIIR lines did not produce protein, they were not crossed.

Conclusion: TGFα overexpression is sufficient to result in PIN but not prostate cancer. By combining this growth stimulatory pathway TGFα with the loss of the growth inhibitory TGFß prostatic intraepithelial neoplasia develops at an earlier age. When overexpressing TGFα, the 12T-7f tumors are more resistant to androgen ablation. Although these data does not show a direct causal role for TGFα, the data does show that tumor cells which overexpress this gene can have a selective advantage to grow and become resistant to androgen ablation therapy.

Task III: To treat mouse prostate tumors with EGFR tyrosine kinase inhibitor and/or selective TACE inhibitor.

- Given that the MT-TGFα line did not develop cancer, the LPB-Tag line was utilized and animals were treated with the EKI-785 compound from Wyeth-Ayerst.
- A small decrease in gross weight of the dorsolateral lobe of the treated animals was detected when compared to the untreated controls.

13

- Molecular and histological analysis of tissues from these animals are nearing completion to determine the effects of inhibiting the EGFR kinase activity.

Conclusion: Alone, EKI-785 would have a small effect on a decrease in prostate tumor growth but it maybe useful in combination with conventional androgen ablation therapy since the overexpression of TGFα (Task 2) is protective against androgen ablation and tumor regression.

CORE: Pathology Core Laboratory and Provision of Basic Histopathology Support:

- As describe in previous years, equipment has been purchased for the Pathology Core. It now services all the individual projects. The following techniques are provided.

Adjuctive diagnostic techniques:

- Establishment of immunohistochemical protocols and application to various models, supplementing immunostaining assays performed by individual labs, including:

  - General/model characterization: Pan cyto-keratin, High molecular weight cytokeratin, CK5, PCNA, Apo-tag, AR, Chromogranin, CD31 (including on frozen sections)

  - Antibody assays for Shappell Mouse-based research: 8-lipoxygenase, platelet 12-lipoxygenase, leukocyte 12-lipoxygenase, cyclooxygenase-2

  - Antibodies currently being investigated/validated: Laminin, N-cadherin, E-cadherin, Beta-catenin.

  - Performance of ultra-structural studies on DLP/VP on LPB-Tag 12T-7f x MT-DNIIR mouse.

  - Establishment of quantitative Real Time RT-PCR assays on Roche LightCycler system, utilizing cDNA standard curves with cloned templates and cDNA binding fluorescent probe SYBR green or oligo specific hybridization probes.

REPORTABLE OUTCOMES: The reportable outcomes of the Vanderbilt Prostate Cancer Center are divided into three sections: 1) Institutional Commitments and VPCC; 2) Research Projects, and 3) Pathology Core.

1) Institutional Commitments and VPCC: Due to the DOD funding of the Center, Vanderbilt University Medical Center, the Vanderbilt-Ingram Cancer Center, the Section of Surgical Sciences, and the Department of Urologic Surgery have made major institutional commitments that have allowed the scope of the Center to expand beyond the initial research projects.

Importantly, this commitment has now resulted in the promotion of Susan Kasper from Research Assistant Professor to Assistant Professor (2001), the recruitment of Simon Hayward as an Assistant Professor (2001), a secondary appointment of Scott Shappell to Urologic Surgery (2001). In addition, over 3,700 sq ft of space is now in Urologic Surgery for prostate cancer research.

Administration: Dr. Robert Matusik serves as the Director of the VPCC. The Center holds research meetings on the first Wednesday of the month at 1:00 pm. In addition, a second meeting is also being held the first Wednesday of the month at 5:00 pm to discuss new programs and potential grant application. Since the DOD Center will not be renewed, we have submitted a NCI proposal for the Mouse Models for Human Cancer Consortium (MMHCC) for a grant entitled "Mouse Models of Prostate Cancer". In addition, for October 2004, we will be submitted a SPORE on Prostate; The Specialized Programs of Research Excellences on Prostate are NCI funding programs that must have a large translational component to each grant plus COREs that would support these clinical undertakings. Lastly, we are looking to develop a Program Project Grant (PPG) on Prostate; The Program Project Grants that will cover basic research on prostate cancer. These can be strong on basic research without a clinical program.

Our Steering Committee for the last year of the grant was as follows:
Vanderbilt Prostate Cancer Center Members:

>Dr. Robert J. Matusik, Prostate Cancer Center Director and Director of Urologic Research
>Dr. Harold Moses, Director of Vanderbilt-Ingram Cancer Center
>Dr. Robert Coffey, Director of the GI Cancer Program/ or Dr. Shane Cutler
>Dr. Scott Shappell, Assistant Professor, Department of Pathology
>Dr. Susan Kasper, Research Assistant Professor, Department of Urologic Surgery
>**Internal Advisors:**
>Dr. Joseph A. Smith, Chairman, Department of Urologic Surgery / or Dr. Sam Chang
>Dr. Michael Cookson, Department of Urologic Surgery
>Dr. Simon Hayward, Department of Urologic Surgery
>**External Advisor:**
>Dr. Chung Lee, Department of Urology, Northwestern University
>**Consumers:**
>Mr. Jerry Savells
>Mr. Norman Wayne Simpson

Budget: The budget commitments have remained the same as last year and include the following:

- The Vanderbilt University Medical Center has provided the salary for Ms. Debbie Thompson to serve as an administrative assistant to the VPCC.

15

- The Vanderbilt-Ingram Cancer Center has provided $200,000/ year as support for operating expenses of the Center, for equipment, administrative assistant (Ms. Beth Deits) and pilot projects to expand the research endeavor.

- The Department of Urologic Surgery has provided the start-up funds to recruit Dr. Simon Hayward as a new faculty member.

- The Department of Urologic Surgery provided the funds to renovate the four offices for the Prostate Cancer Center.

- For the Urologic Oncology Fellowship Training program, Dr. Jen (MD/Ph.D) has replaced Dr. Naoya Masumori (MD/PhD) as the Urologist.

Space for VPCC: Although the planned move in date was for July 2001, the actually move in date for the Laboratories was August 2001 and the offices was November of 2001.The commitment made last year has been realized. The Floor plan was attached last year and it remains as it was attached. To review, we now have increased by 2168 sq ft. from the previous1533 sq. ft. to new total of 3701 sq. ft. laboratory space. This includes the laboratories of Drs. Matusik, Kasper, and Hayward. These individuals and Ms. Lisa Howell, secretary, have moved into the new office space (596 sq. ft.). Two offices (136 sq. ft.) have been provided for the post-doctoral fellows. These offices will have to be shared but they will provide space for the post-doctoral fellows to work on data and write manuscripts. A conference room has been made available for routine meeting with personnel. (See previous report for detailed floor plan).

New Faculty: Last year it was reported that Drs. Susan Kasper and Simon Hayward were recruited as Assistant Professors in Urologic Surgery. They both have joint appointment in Cancer Biology. Dr. Kasper started in January 2001 and Dr. Hayward in August.

- Dr. Susan Kasper has received two NIH grants. One grant entitled "Developmental Biology of the Normal Mouse Prostate" and a second grant entitled "Regulation of Prostate Cancer Progression."

- Dr. Simon Hayward is funded by grants entitled "Paracrine Regulation of Prostatic Carcinogenesis" (DOD), "Hormonal Carcinogenesis in Rb-Knockout Mouse" (NIH), and "Therapy Selection by Gene Profiling" (DOD), Biological Activity of IGF and FGF in the human prostate." (NIDDK), and "Spectral Imaging (SIm) for Phenotype Analysis of Cancer" (NCI).

- Dr. Robert Matusik has had both NIH grants successfully renewed: "Transgenic Mouse Models for Prostate Cancer" and Control of Prostate-Specific Gene Expression"

16

Post-doctoral Fellows

- Dr. Shane Cutler currently is working in Dr. Coffey's laboratory on Project 3 to study the role of TGFα in prostate tumor development.

- Dr. Ren Jie Jin on May 1, 2001. He is a trained Urologist from China that has also completed a Ph.D. from Seoul National University, Korea. Dr. Jin is working with Dr. Matusik's laboratory on Project 1 and on the LPB-Tag transgenic animal models. He is a new recruit to the Urology Fellowship Training Program

- Mr. Janni Mirosevich arrived September 1, 2001. Mr. Mirosevich will study gene expression on Project 1.

- Ms. Tiina Pitkänen-Arsiola arrived in July, 2001. Ds. Pitkänen-Arsiola works with Dr. Kasper's laboratory to study progression in prostate cancer from an androgen-dependent to an androgen-independent disease.

Students

- Mr. William Tu is a MD/Ph.D. student at Vanderbilt working for Dr. Matusik. (see Curriculum Vitae, Appendices). He is studying how combining the disruption of the TGFβ pathway and the p53/RB pathway results in developing adenocarcinoma in Project 1. He has completed his Ph.D. on this project and will return to medical school in July 2003.

- Miss Aparna Gupta is a Ph.D student at Vanderbilt. She has just starting working in Dr. Matusik's laboratory using MicroArray analysis of gene expression in the mouse prostate tumors.

2) Research Projects: A number of manuscripts are now in preparation on the role that TGFα and TGFβ pathway plays in developing prostate cancer. A number of abstracts have been presented. Also, as a result of this work, symposium lecture at meetings have resulted.

Published Abstracts, Papers, Presentations (2002-2003)

ABSTRACTS:

1. Tu WH, Shyr Y, Larsen P, Levy S, Kasper S, Moses HL, Roberts RL, Shappell SB, Matusik RJ. Differential gene expression from disrupted TGF-beta signaling in two transgenic mouse models with prostate cancer metastasis. The American Association for Cancer Research 94rd Annual Meeting, April 5-9, 2003. Toronto, Ontario, Canada.

2. Tu WH, Shyr Y, Larsen P, Levy S, Kasper S, Moses HL, Roberts RL, Shappell SB, Matusik RJ. Inhibition of TGF-beta signaling increases prostate cancer metastasis in transgenic mice and modifies gene expression. The 10th Annual Society for Basic Urologic Research Fall Symposium in Urologic Research, December 5-8, 2002. Tucson, Arizona.

3. Cutler, NS, Coffey, RJ. Targeting the Epidermal Growth Factor Receptor In a Mouse Model of Prostate Cancer. Modeling Human Cancer in Mice: Pre-clinical Trials, Bar Harbor, ME October 24-26, 2002

Manuscripts

1. Tu, W, Thomas, TZ, Masumori N, Kasper, S, Shry Y, Larsen P, Levy S, Roberts RL, Shappell SB, and Moses H, and Matusik RJ. Loss of the TGFβ pathway promotes prostatic metastasis. Neoplasia, In press 2003.

2. Shappell, SB, Roberts RL, George TV, Herbert R, Rubin MA, Humphrey PA, Ittmann MM, Sundberg JP, Rozengurt N, Barrios R, Ward JM, Cardiff RD. Prostate pathology of genetically engineered mice: The consensus report from the Bar Harbor Meeting. Cancer Res. Submitted.

3. Thomas TZ, Tu WH, Shappell S, Kasper S, Moses HL, Matusik RJ, and Serra RA. Disruption of the TGFβ pathway in transgenic mice prevents castration-induced prostatic regression. In preparation.

4. Cutler, NS, Roberts, R, Shappell, S, Coffey, RJ. Overexpression of TGFα induces prostatic intraepithelial neoplasia in mice. In preparation.

5. Cutler, NS, Washington, K, Deane, NG, Coffey, RJ. Interaction of the EGFR axis and TGFβ axis in liver cancer. In preparation.

INVITED PRESENTATIONS:

1. Tu WH, Shyr Y, Larsen P, Levy S, Kasper S, Moses HL, Roberts RL, Shappell SB, Matusik RJ. Loss of TGF-β signaling alters gene expression patterns and accelerates prostate tumorigenesis in transgenic mice. The American Association for Cancer Research 93rd Annual Meeting, April 6-10, 2002. San Francisco, California.

2. Dr. Matusik presented his work at the NIH sponsored MMHCC Workshop on *Transgenic Models for Prostate Cancer* in October 2001, and in October 2002 at a special joint meeting of the MMHCC and prostate SPORE investigators, Washington DC.

Personnel:

The personnel of the VPCC include those supported by the DOD award, institutional commitments, and individuals that may be on trainee awards [For example, Dr. Ren Jie Jin (Matusik) and Dr. Shane Culter (Coffey) are on training grants]. Listed below are only individuals supported directly by the DOD award over the fiscal year covered by this report.

PROJECT 1:

Robert J. Matusik, PhD	PI and Director
Susan Kasper, PhD	Co-Investigator
Richard L. Roberts, PhD	Research Instructor
Yong Qing Wang, PhD	Research Fellow

| Janni Mirosevich, Ph.D. | Research Fellow |
| William Tu | Graduate Student |

PROJECT 2:

Harold L. Moses, MD	PI
Agnieszka E. Gorska	Research Tech Senior
Mary E. Aakre	Research Tech Senior
Anna Chytil	Research Tech Senior

PROJECT 3

| Robert J. Coffey, Jr, MD | PI |
| Ping Lin Jih | Research Fellow |

PATHOLOGY CORE

Scott B. Shappell, MD,	PI
Richard L. Roberts, PhD	Research Instructor
Sabrina "Erin" Hannah	Research Assistant II
Cathy Hibbs-Brown	HistoTech

3) Pathology Core: Dr. Scott Shappell is director of the Pathology Core. He Chaired the NCI sponsored Mouse Models of Human Cancer Consortium (MMHCC) workshop on transgenic mouse prostate cancer models[11]. This Workshop report, written by Dr. Shappell, establishes the standards for the characterization of mouse models for prostate cancer.

CONCLUSIONS:

Substantial progress has been made on the three individual grants and in the establishment of the Pathology Core. In addition, Vanderbilt University Medical Center, Section of Surgical Sciences, Department of Urologic Surgery, and the Vanderbilt-Ingram Cancer Center have meet their commitments to the DOD Center grant which are beyond the initial research projects allowing use to expand the program as a new Vanderbilt Prostate Cancer Center. As a result of these commitments, a MMHCC for "Mouse Models for Prostate Cancer" grant has been submitted. Without question, the support by the DOD to establish this Center has had a major impact on developing a prostate cancer program at Vanderbilt. The VPCC has been able to leverage the DOD support to addition money from foundations, new DOD awards, and NIH grants. New personnel, including students, post-doctoral fellows, and faculty members have been

recruited and have made major career choices to focus their research on prostate cancer. Although the DOD will not continue the Centers, the award became the seed money that has established an ever expanding group of prostate cancer researchers at Vanderbilt.

References:

1. Kasper S, Sheppard PC, Yan Y, et al. Development, Progression and Androgen-Dependence of Prostate Tumors in Transgenic: A Model For Prostate Cancer. Laboratory Investigation. 1998;78:319-334.

2. Masumori N, Thomas TZ, Case T, et al. A probasin-large T antigen transgenic mouse line develops prostate adeno and neuroendocrine carcinoma with metastatic potential. Cancer Res 61, 2239-2249. 2001.

3. Tu WH, Thomas TZ, Masumori N, et al. Loss of TGF-beta signaling alters gene expression patterns and accelerates prostate tumorigenesis in transgenic mice. Neoplasia. 2003; In press.

4. Muro-Cacho CA, Rosario-Ortiz K, Livingston S, Munoz-Antonia T. Defective transforming growth factor beta signaling pathway in head and neck squamous cell carcinoma as evidenced by the lack of expression of activated Smad2. Clin Cancer Res. 2001;7:1618-1626.

5. Joseph H, Gorska AE, Sohn P, Moses HL, Serra R. Overexpression of a kinase deficient TGF-beta type II receptor in mouse mammary stroma results in increased epithelial branching. Mol Biol Cell. 1999; 10:1221-1234.

6. Wu X, Wu J, Huang J, et al. Generation of a prostate epithelial cell-specific Cre transgenic mouse model for tissue-specific gene ablation. Mech Dev. 2001;101:61-69.

7. Chytil A, Magnuson MA, Wright CV, Moses HL. Conditional inactivation of the TGF-beta type II receptor using Cre:Lox. Genesis. 2002;32:73-75.

8. Iwano M, Plieth D, Danoff TM, Xue C, Okada H, Neilson EG. Evidence that fibroblasts derive from epithelium during tissue fibrosis. J Clin Invest. 2002;110:341-350.

9. Serra R, Johnson M, Filvaroff EH, et al. Expression of a truncated, kinase-defective TGF-beta type II receptor in mouse skeletal tissue promotes terminal chondrocyte differentiation and osteoarthritis. J Cell Biol. 1997;139:541-552.

10. Zhang ZF, Thomas TZ, Kasper S, Matusik RJ. A small composite probasin promoter confers high levels of prostate-specific gene expression through regulation by androgens and glucocorticoid *in vitro* and *in vivo*. Endocrinology. 2000;141:4698-4710.

11. Shappell SB, Roberts RL, Thomas GV, et al. Prostate Pathology of Genetically

Enigineered Mice: The Consensus Report from the Bar Harbor Meeting. Cancer Res. 2003, In press.

The Loss of TGF-β Signaling Promotes Prostate Cancer Metastasis[1]

William H. Tu[*,†,‡,§], Tania Z. Thomas[*], Naoya Masumori[¶], Neil A. Bhowmick[§], Agnieszka E. Gorska[§], Yu Shyr[§], Susan Kasper[*,†,‡,§], Tom Case[*], Richard L. Roberts[†,#], Scott B. Shappell[†,‡,#], Harold L. Moses[†,‡,§] and Robert J. Matusik[*,†,‡,§]

*Department of Urologic Surgery, †Vanderbilt Prostate Cancer Center, ‡Department of Cancer Biology, §Vanderbilt–Ingram Cancer Center, #Department of Pathology, Vanderbilt University Medical Center, Nashville, TN, USA; ¶Department of Pathology, Sapporo Medical University School of Medicine, Sapporo, Japan

Abstract

In breast and colon cancers, transforming growth factor (TGF)-β signaling initially has an antineoplastic effect, inhibiting tumor growth, but eventually exerts a proneoplastic effect, increasing motility and cancer spread. In prostate cancer, studies using human samples have correlated the loss of the TGF-β type II receptor (TβRII) with higher tumor grade. To determine the effect of an inhibited TGF-β pathway on prostate cancer, we bred transgenic mice expressing the tumorigenic SV40 large T antigen in the prostate with transgenic mice expressing a dominant negative TβRII mutant (DNIIR) in the prostate. Transgene(s) and TGF-β1 expression were identified in the prostate and decreased protein levels of plasminogen activator inhibitor type I, as a marker for TGF-β signaling, correlated with expression of the DNIIR. Although the sizes of the neoplastic prostates were not enlarged, increased amounts of metastasis were observed in mice expressing both transgenes compared to age-matched control mice expressing only the large T antigen transgene. Our study demonstrates for the first time that a disruption of TGF-β signaling in prostate cancer plays a causal role in promoting tumor metastasis.

Neoplasia (2003) **5**

Keywords: transforming growth factor-β; prostate cancer; metastasis; probasin; transgenic mice

Introduction

Prostate cancer is a heterogeneous disease that typically progresses from prostatic intraepithelial neoplasia (PIN) to locally invasive to potentially metastatic carcinoma. Surgical treatment of locally invasive cancer yields a 10-year progression-free survival probability of greater than 90%. In contrast, the development of metastatic cancer drops the survival probability to about 30% [1]. Metastasis occurs in late-stage prostate cancer wherein some cancers with the loss of *p53*, *RB*, and the TGF-β type II receptor (TβRII) have been identified [2–5].

The TβRII transduces signal for the ubiquitous, pleiotropic cytokine transforming growth factor (TGF)-β that is involved in many pathways including growth inhibition, apoptosis, and differentiation [6–8]. TGF-β signaling involves the binding of ligand to the extracellular domain of TβRII, the transphosphorylation of the TGF-β type I receptor by the cytoplasmic domain of TβRII, and the subsequent phosphorylation of Smad signaling molecules that can activate the transcription of downstream targets such as plasminogen activator inhibitor type I (PAI-I) [9,10]. Although the loss of the TβRII has been associated with prostate cancer, its effect on tumor progression has not been determined. We have studied transgenic mouse models of prostate cancer to examine the effect of blocking the TGF-β signaling pathway on tumor development and progression.

The large probasin (LPB) promoter directed the prostatic epithelial cell expression of the SV40 large T antigen (*Tag*) [11], with a deletion in the early region to remove the small t antigen. The oncogenic *Tag* has been reported to induce neoplasia by sequestering and inactivating two tumor suppressor genes, *p53* and *RB*, that have been associated with prostate cancer [2,3]. Two LPB-*Tag* lines, 12T-7f and 12T-10, were used to study different aspects of prostate tumor progression. The 12T-7f line developed prostate tumors of lethal size by 23 weeks of age that contained high-grade prostatic intraepithelial neoplasia (HGPIN) and occasional foci of invasive carcinoma (IC) [12]. We chose this line to test whether blocking TGF-β

signaling would promote progression from cancer precursors to more locally invasive and/or metastatic cancer. However, the 12T-10 line developed small prostate lesions containing HGPIN and invasive neuroendocrine carcinoma that became metastatic after 6 months of age [13]. This line was selected to determine whether inhibiting the TGF-β pathway would modify the metastatic phenotype.

Although multiple lines were made with the probasin promoter to target the dominant negative TβRII mutant (*DNIIR*) in the prostate of transgenic mice, none of the lines expressed the *DNIIR* transgene (unpublished observation). The zinc-inducible metallothionein (MT) promoter was well suited to express the transgene in the prostate because the prostate contains naturally high levels of zinc and expresses several MTs in the epithelium [14]. The *DNIIR* construct had a Flag epitope and contained the extracellular, transmembrane, and juxtamembrane domains (aa 1–191) of the human TβRII, but lacked the cytoplasmic kinase domain for downstream signaling [15]. Overexpressing the *DNIIR* transgene has been shown to create a dominant negative mutation in transgenic mice by competing with the naturally low levels of endogenous TβRII for TGF-β ligand and by binding to endogenous TGF-β receptor type I [16]. By breeding the MT-DNIIR mice with 12T-7f and 12T-10 mice, we hypothesized that expression of the *DNIIR* transgene in the *Tag* tumors would inhibit TGF-β signaling and alter the neoplastic phenotype.

Materials and Methods

Generating and Genotyping Transgenic Mice

LPB-*Tag* transgenic mice lines were generated with the 5'-flanking region of the rat LPB gene (−10,834 to +28 bp) linked to the *Tag* gene deletion mutant (*d1 2005*), which removed expression of the small t antigen [12]. Both 12T-7f and 12T-10 lines were maintained in the CD1 mouse strain. MT-DNIIR transgenic mice (MT-DNIIR-27) were generated using a truncated human TβRII with a Flag epitope as the *DNIIR* transgene under the control of the MT promoter [15]. The MT-DNIIR line used in this study was maintained in the B6D2 mouse strain. 12T-7f$^{Tag+/−}$ females were mated with MT-DNIIR$^{DNIIR+/+}$ males to generate 12T-7f/MT-DNIIR and MT-DNIIR mice in the similar mouse background. The 12T-7f/MT-DNIIR and MT-DNIIR mice were supplemented with 25 mM zinc sulfate in the drinking water to enhance transgene expression. 12T-7f$^{Tag+/−}$ females were mated with B6D2F1 males to generate control 12T-7f and nontransgenic (NT) mice in the same mouse background. Some of the control 12T-7f and NT mice were supplemented with 25 mM zinc sulfate in the drinking water. 12T-10$^{Tag+/+}$ females were mated with MT-DNIIR$^{DNIIR+/+}$ males to generate 12T-10/MT-DNIIR mice. To control for genetic background, 12T-10$^{Tag+/+}$ females were mated with B6D2F1 males to generate 12T-10 mice. None of the 12T-10/MT-DNIIR or 12T-10 mice were supplemented with 25 mM zinc sulfate in the drinking water. Mice were genotyped for the *DNIIR* transgene by polymerase chain reaction (PCR) analysis of

genomic DNA isolated from mouse tails using proteinase K digestion and ethanol extraction. The forward TβRII primer (5'-TCCCACCGCACGTTCAGAAG-3') and reverse Flag primer (5'-ATCGTCATCGTCTTTGTAGTC-3') produced an amplimer of 506 bp [15]. Mice were genotyped for the *Tag* transgene by PCR analysis using the forward LPB primer (5'-TAGCATCTTGTTCTTAGTCTT-3') and reverse *Tag* primer (5'-CTCCTTTCAAGACCTA-GAAGGTCCA-3') to produce an amplimer of 430 bp [12]. Exon 7 of the endogenous mouse casein gene served as an internal control for the *Tag* PCR reaction using the forward casein primer (5'-GATGTGCTCCAGGCTAAAGTT-3') and the reverse casein primer (5'-AGAAACGGAATGTTGTG-GAGT-3') to generate a 540-bp amplimer [12].

Tissue Preparation and Histopathologic Analysis

Mice were sacrificed by cervical dislocation after the inhalation of an anesthetic agent according to the policy of the Vanderbilt University Animal Care Committee. The prostates were generally dissected into four different lobes (ventral, lateral, dorsal, and anterior lobes) under a dissecting microscope. When it was not possible to separate the lateral and dorsal lobes, the tissues were taken together as the dorsolateral lobe. Seminal vesicle, vas deferens, testis, periurethral gland, bladder, bulbourethral gland, para-aortic lymph nodes (LNs), neck LNs, lumbar spine, liver, lung, kidney, spleen, brain, adrenal, parotid gland, and submandibular gland were also harvested for histologic examination. Tissues were either frozen on dry ice and stored at −80°C, or fixed in 10% formalin and processed and embedded in paraffin using standard techniques. Paraffin-embedded tissues were cut at 5 μm and sections were used for H&E staining, immunohistochemistry, and *in situ* hybridization. Histology was classified in a blinded manner by two pathologists (S.B.S. and R.L.R.) based on histopathologic definitions from the Prostate Pathology Committee of the National Cancer Institute Mouse Models of Human Cancer Consortium [17].

Immunohistochemistry

Immunostaining was performed on 5-μm-thick paraffin sections, which were deparaffinized and rehydrated using standard techniques [13]. The following primary antibodies were used (with the indicated dilutions in PBS): (a) *SV40 Tag*, Ab-2 (1:100; Oncogene Research Products, Boston, ME); (b) CG, bovine SP-1 (1:1000; DiaSorin, Stillwater, MN); and (c) TGF-β1, sc-146 (1:200; Santa Cruz Biotechnology, Santa Cruz, CA). For *Tag*-immunostained sections, the same concentration of control mouse ascites fluid (Sigma, St. Louis, MO) was used as a negative control. For CG-immunostained sections, the same concentration of normal rabbit immunoglobulin, X903 (Dako, Carpinteria, CA), was used as a negative control. For TGF-β1–immunostained sections, control peptide (sc-146P) was added at 10 times the primary antibody concentration along with the primary antibody as a negative control, or the same concentration of normal rabbit immunoglobulin was used as negative control. Color development was performed with 3,3'-diaminobenzidine
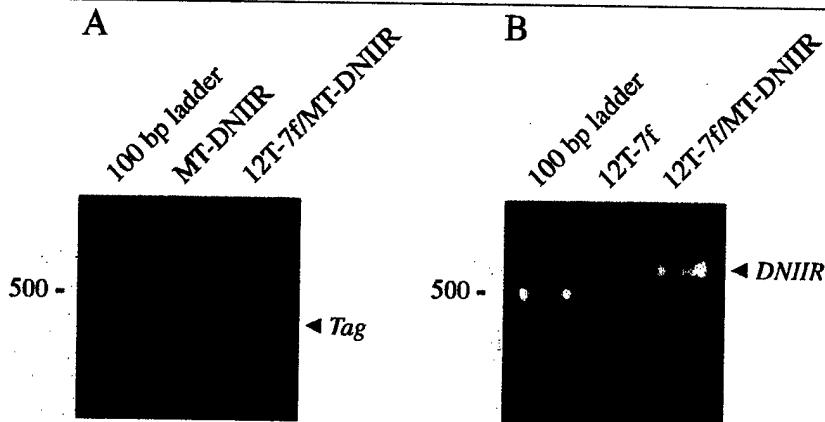
Figure 1. *Detection of transgene in transgenic mice. (A) An example of PCR genotyping using primer sets for the Tag transgene. The expected size of the Tag-amplified product is 430 bp. Transgene was detected in the 12T-7f/MT-DNIIR sample but not in the MT-DNIIR sample. (B) An example of PCR genotyping using primer sets for the DNIIR transgene. The expected size of the DNIIR-amplified product is 506 bp. Transgene was detected in the 12T-7f/MT-DNIIR sample but not in the 12T-7f sample.*

tetrahydrochloride (Dako). Slides were counterstained with hematoxylin, dehydrated, and coverslipped. Some of the immunostaining was quantitated using the MetaMorph image analysis program.

In Situ Hybridization for DNIIR

In situ hybridization was performed on 5-μm-thick paraffin sections, which were deparaffinized and rehydrated using standard techniques [15]. Sections were hybridized to ^{35}S-labeled sense and antisense riboprobes. The MT-DNIIR plasmid was linearized with EcoRI, and the antisense probe was made with T7 polymerase. The sense probe was made from XbaI-linearized plasmid and T3 polymerase.

Slides were exposed to photographic emulsion at 4°C for 1 month and then developed with D19 developer, fixed in 1% acetic acid, and cleared in 30% sodium thiosulfate. Sections were counterstained with 0.2% toluidine blue. Kodak Ektachrome film (Eastman Kodak, Rochester, NY) was used to take photographs under phase contrast, bright field, and dark field illumination using a microscope (Zeiss, Thornwood, NY).

Quantitative Real-Time Reverse Transcriptase Polymerase Chain Reaction (RT-PCR)

RNA was extracted from frozen samples using the RNeasy Midi Kit 75144 including treatment with DNase
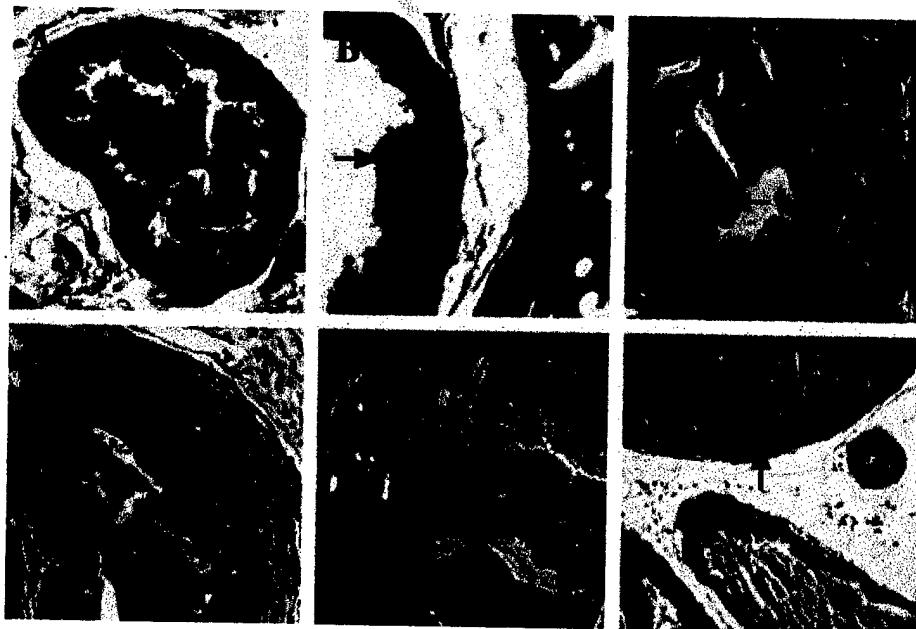
Figure 2. *Illustrations of histopathology of transgenic animals (H&E). (A) NHA in a DLP of a 12-week-old NT mouse. (B) LGPIN (arrow) in a DLP of a 23-week-old MT-DNIIR mouse. (C) HGPIN (arrow) in a DLP of an 18-week-old 12T-7 mouse. (D) MI (arrow) in a DLP of a 9-month-old 12T-10 mouse. (E) IC (arrow) in a DLP of a 20-week-old 12T-7f/MT-DNIIR mouse. (F) UC (arrow) in a VP of a 10-month-old 12T-10/MT-DNIIR mouse.*

Table 1. Histopathology of Mice Expressing the *Tag* Transgene.

Line	Mouse number	Age	AP	DLP	VP	Metastatic site
12T-7f/MT-DNIIR	9237	12 weeks	HGPIN	HGPIN	NHA	None
12T-7f/MT-DNIIR	9240	12 weeks	HGPIN	HGPIN	NHA	None
12T-7f/MT-DNIIR	9241	12 weeks	HGPIN	HGPIN	NHA	None
12T-7f/MT-DNIIR	A3474	12 weeks	HGPIN	HGPIN	HGPIN	None
12T-7f/MT-DNIIR	A3476	12 weeks	HGPIN	HGPIN	NHA	None
12T-7f/MT-DNIIR	A3477	12 weeks	HGPIN	HGPIN	LGPIN	None
12T-7f/MT-DNIIR	A3478	12 weeks	HGPIN	HGPIN	LGPIN	None
12T-7f	A3231	12 weeks	HGPIN	HGPIN	LGPIN	None
12T-7f	A3242	12 weeks	HGPIN	HGPIN	LGPIN	None
12T-7f	A3246	12 weeks	HGPIN	HGPIN	LGPIN	None
12T-7f	A3479	12 weeks	HGPIN	HGPIN	HGPIN	None
12T-7f	A3483	12 weeks	HGPIN	HGPIN	HGPIN	None
12T-7f	A3484	12 weeks	HGPIN	HGPIN	NHA	None
12T-7f/MT-DNIIR	9201	16 weeks	HGPIN	HGPIN	HGPIN	None
12T-7f/MT-DNIIR	9207	16 weeks	HGPIN	HGPIN	HGPIN	None
12T-7f/MT-DNIIR	9208	16 weeks	HGPIN	HGPIN, IC	HGPIN	Lung
12T-7f/MT-DNIIR	A3187	16 weeks	HGPIN	HGPIN	HGPIN	None
12T-7f/MT-DNIIR	A3190	16 weeks	HGPIN	HGPIN	HGPIN	None
12T-7f/MT-DNIIR	A3199	16 weeks	HGPIN	HGPIN	HGPIN	None
12T-7f/MT-DNIIR	A3203	16 weeks	HGPIN	HGPIN	HGPIN	None
12T-7f/MT-DNIIR	A3204	16 weeks	HGPIN	HGPIN	HGPIN	None
12T-7f/MT-DNIIR	A3207	16 weeks	HGPIN	HGPIN	HGPIN	None
12T-7f/MT-DNIIR	A3208	16 weeks	HGPIN	HGPIN	HGPIN	None
12T-7f/MT-DNIIR	A3209	16 weeks	HGPIN	HGPIN	HGPIN	None
12T-7f/MT-DNIIR	A3499	16 weeks	HGPIN	HGPIN	HGPIN	None
12T-7f/MT-DNIIR	A3505	16 weeks	HGPIN	HGPIN	HGPIN	None
12T-7f	A3117	16 weeks	HGPIN	HGPIN	NHA	None
12T-7f	A3120	16 weeks	HGPIN	HGPIN	HGPIN	Lung
12T-7f	A3218	16 weeks	HGPIN	HGPIN	HGPIN	None
12T-7f	A3221	16 weeks	HGPIN	HGPIN	HGPIN	None
12T-7f	A3228	16 weeks	HGPIN	HGPIN	LGPIN	None
12T-7f	A3232	16 weeks	HGPIN	HGPIN	HGPIN	None
12T-7f	A3233	16 weeks	HGPIN	HGPIN	LGPIN	None
12T-7f	A3234	16 weeks	HGPIN	HGPIN	HGPIN	None
12T-7f	A3235	16 weeks	HGPIN	HGPIN	HGPIN	None
12T-7f	A3239	16 weeks	HGPIN	HGPIN	HGPIN	None
12T-7f	A3243	16 weeks	HGPIN	HGPIN	LGPIN	None
12T-7f	A3244	16 weeks	HGPIN	HGPIN	HGPIN	None
12T-7f	A3247	16 weeks	HGPIN	HGPIN	LGPIN	Lung
12T-7f	A3249	16 weeks	HGPIN	HGPIN	LGPIN	None
12T-7f	A3251	16 weeks	HGPIN	HGPIN	NHA	None
12T-7f	A3252	16 weeks	HGPIN	HGPIN	HGPIN	None
12T-7f	A3276	16 weeks	HGPIN	HGPIN, IC, UC	HGPIN, IC, UC	LN
12T-7f/MT-DNIIR	9215	18 weeks	HGPIN	HGPIN	HGPIN	None
12T-7f/MT-DNIIR	9218	18 weeks	HGPIN	HGPIN, IC	HGPIN	Lung, liver, LN, spine
12T-7f/MT-DNIIR	9239	18 weeks	HGPIN	HGPIN	HGPIN	None
12T-7f/MT-DNIIR	A3028	18 weeks	HGPIN	HGPIN	HGPIN	Lung
12T-7f/MT-DNIIR	A3078	18 weeks	HGPIN	HGPIN	HGPIN	None
12T-7f/MT-DNIIR	A3194	18 weeks	HGPIN	HGPIN	HGPIN	None
12T-7f/MT-DNIIR	A3195	18 weeks	HGPIN	HGPIN	HGPIN	None
12T-7f/MT-DNIIR	A3490	18 weeks	HGPIN	HGPIN	HGPIN	Lung
12T-7f/MT-DNIIR	A3491	18 weeks	HGPIN	HGPIN	HGPIN	Lung, liver
12T-7f	A3104	18 weeks	HGPIN	HGPIN	HGPIN	None
12T-7f	A3108	18 weeks	HGPIN	HGPIN	HGPIN	None
12T-7f	A3283	18 weeks	HGPIN	HGPIN	HGPIN	None
12T-7f	A3285	18 weeks	HGPIN, IC	HGPIN	LGPIN	None
12T-7f	A3286	18 weeks	HGPIN	HGPIN	HGPIN	None
12T-7f/MT-DNIIR	9212	20 weeks	HGPIN, IC	HGPIN	HGPIN	None
12T-7f/MT-DNIIR	9219	20 weeks	HGPIN	HGPIN	HGPIN	None
12T-7f/MT-DNIIR	9223	20 weeks	HGPIN, IC	HGPIN, IC	HGPIN	None
12T-7f/MT-DNIIR	A3087	20 weeks	HGPIN	HGPIN	LGPIN	None
12T-7f/MT-DNIIR	A3210	20 weeks	HGPIN	HGPIN, IC	LGPIN	Lung
12T-7f	9194	20 weeks	HGPIN	HGPIN	HGPIN	None
12T-7f	9195	20 weeks	HGPIN	HGPIN	HGPIN	None
12T-7f	9197	20 weeks	HGPIN	HGPIN	HGPIN	None
12T-7f	A3271	20 weeks	HGPIN	HGPIN	HGPIN	Lung, liver, spine
12T-7f	A3274	20 weeks	HGPIN	HGPIN	HGPIN	None
12T-7f	A3384	20 weeks	HGPIN	HGPIN	HGPIN	None
12T-7f	A3387	20 weeks	HGPIN	HGPIN	HGPIN	None
12T-7f	A3391	20 weeks	HGPIN	HGPIN	HGPIN	None
12T-7f/MT-DNIIR	9220	23 weeks	HGPIN	HGPIN	HGPIN	None
12T-7f/MT-DNIIR	9227	23 weeks	HGPIN	HGPIN, IC	NHA	Lung

Table 1. (continued)

Line	Mouse number	Age	AP	DLP	VP	Metastatic site
12T-7f/MT-DNIIR	A3018	23 weeks	HGPIN	HGPIN	LGPIN	None
12T-7f/MT-DNIIR	A3030	23 weeks	HGPIN	HGPIN	HGPIN	None
12T-7f/MT-DNIIR	A3081	23 weeks	HGPIN	HGPIN	HGPIN	None
12T-7f	9245	23 weeks	HGPIN	HGPIN	HGPIN	None
12T-7f	9246	23 weeks	HGPIN	HGPIN	HGPIN	None
12T-7f	A3258	23 weeks	HGPIN	HGPIN, IC	HGPIN	None
12T-7f	A3265	23 weeks	HGPIN	HGPIN	LGPIN	None
12T-7f	A3278	23 weeks	HGPIN	HGPIN	HGPIN	None
12T-10/MT-DNIIR	A3130	6 months	HGPIN	HGPIN	HGPIN, MI	None
12T-10/MT-DNIIR	A3131	6 months	HGPIN	HGPIN, MI	HGPIN	None
12T-10/MT-DNIIR	A3132	6 months	HGPIN	HGPIN, MI	HGPIN	None
12T-10/MT-DNIIR	A3133	6 months	HGPIN	HGPIN	HGPIN	Lung
12T-10/MT-DNIIR	A3134	6 months	HGPIN	HGPIN, MI	HGPIN	None
12T-10	A3158	6 months	HGPIN	HGPIN	HGPIN	None
12T-10	A3159	6 months	HGPIN	HGPIN	HGPIN	None
12T-10	A3160	6 months	HGPIN	HGPIN	HGPIN	None
12T-10	A3161	6 months	HGPIN	HGPIN	HGPIN	None
12T-10	A3164	6 months	HGPIN	HGPIN	HGPIN	None
12T-10/MT-DNIIR	A3142	7 months	HGPIN	HGPIN	HGPIN	None
12T-10/MT-DNIIR	A3143	7 months	HGPIN	HGPIN	HGPIN	None
12T-10/MT-DNIIR	A3144	7 months	HGPIN	HGPIN	HGPIN	None
12T-10/MT-DNIIR	A3145	7 months	HGPIN	HGPIN	HGPIN	None
12T-10/MT-DNIIR	A3146	7 months	HGPIN	HGPIN	HGPIN	None
12T-10	A3162	7 months	HGPIN	HGPIN, MI	HGPIN	Lung
12T-10	A3163	7 months	HGPIN	HGPIN	HGPIN	None
12T-10	A3169	7 months	HGPIN	HGPIN, MI	HGPIN	None
12T-10	A3170	7 months	HGPIN	HGPIN, MI	HGPIN	None
12T-10	A3171	7 months	HGPIN	HGPIN, MI	HGPIN	Lung
12T-10/MT-DNIIR	A3150	8 months	HGPIN	HGPIN	HGPIN	None
12T-10/MT-DNIIR	A3151	8 months	HGPIN	HGPIN, IC	HGPIN	None
12T-10/MT-DNIIR	A3152	8 months	HGPIN	HGPIN, MI, IC	HGPIN	None
12T-10/MT-DNIIR	A3407	8 months	HGPIN	HGPIN, MI	HGPIN, MI	Lung, liver
12T-10	A3175	8 months	HGPIN	HGPIN, MI	HGPIN	None
12T-10	A3176	8 months	HGPIN	HGPIN, MI	HGPIN	None
12T-10	A3177	8 months	HGPIN	HGPIN	HGPIN	None
12T-10	A3178	8 months	HGPIN	HGPIN, MI	HGPIN	None
12T-10	A3179	8 months	HGPIN	HGPIN	HGPIN	None
12T-10/MT-DNIIR	A3403	9 months	HGPIN	HGPIN, MI	HGPIN	None
12T-10/MT-DNIIR	A3404	9 months	HGPIN	HGPIN, MI	HGPIN, MI	Lung, liver, LN
12T-10/MT-DNIIR	A3405	9 months	HGPIN	HGPIN, MI	HGPIN	None
12T-10/MT-DNIIR	A3406	9 months	HGPIN	HGPIN, MI	HGPIN, MI	Lung, liver
12T-10/MT-DNIIR	A3408	9 months	HGPIN	HGPIN, MI	HGPIN	Lung, liver
12T-10	A3394	9 months	HGPIN	HGPIN, MI	HGPIN	None
12T-10	A3395	9 months	HGPIN	HGPIN, MI	HGPIN	Lung
12T-10	A3396	9 months	HGPIN, MI	HGPIN, MI, IC	HGPIN	Lung, liver
12T-10	A3397	9 months	HGPIN	HGPIN, MI	HGPIN	Lung
12T-10/MT-DNIIR	A3135	10 months	HGPIN, MI	HGPIN, MI	HGPIN, IC, UC	Lung, liver, LN
12T-10/MT-DNIIR	A3137	10 months	HGPIN	HGPIN, IC	HGPIN, IC, UC	Lung, LN
12T-10/MT-DNIIR	A3138	10 months	HGPIN, IC	HGPIN, MI	HGPIN	Lung
12T-10	A3168	10 months	HGPIN	HGPIN, IC	HGPIN, MI	None
12T-10	A3180	10 months	HGPIN	HGPIN, MI	HGPIN	Lung
12T-10	A3184	10 months	HGPIN	HGPIN, MI	HGPIN	None
12T-10	A3185	10 months	HGPIN	HGPIN	HGPIN, MI	Lung, liver

AP = anterior prostate; VP = ventral prostate.

79254 (Qiagen, Valencia, CA). RNA concentration was determined based on absorbance on a spectrophotometer, and RNA quality was assessed by agarose gel electrophoresis. *DNIIR* copy numbers were determined using a Lightcycler fluorescence temperature rapid air cycler (Roche Molecular Biochemicals, Indianapolis, IN) with cDNA standard curves and the double-stranded DNA-binding fluorescent probe SYBR Green. The cDNA template was generated from the MT-DNIIR plasmid. The forward *DNIIR* primer (5′-AGAAGAATATAACACCAG-CAATCC-3′) and reverse *DNIIR* primer (5′-ATC-CAACGCGGTAGCAGTAGAAGA-3′) generated a 128-bp

amplimer. The specificity of the amplimer in each reaction was confirmed by the melting curve analysis. Copy numbers of mRNA were calculated, using the Lightcycler software (version 3.5), from serially diluted (1:10) standard curves (10^9–10^3 copies). The serially diluted standards were simultaneously amplified with the unknown samples to generate a linear standard curve using the fit points method of analysis with seven points. Additionally, real-time RT-PCR was developed for β-actin as a loading control using a cDNA template, the forward β-actin primer (5′-ACGGC-CAGGTCATCACTATTG-3′) and the reverse β-actin primer (5′-ATGCTACTCAGGCCGGGGA-3′).

Western Blot and Band Quantification

Protein was extracted by sonication and centrifugation of frozen tissues in RIPA buffer (PBS, pH 7.4, 1% NP-40, 0.5% sodium deoxycholate, 0.1% SDS) supplemented with 1 mM PMSF and Complete Mini protease inhibitor cocktail, 1836153 (Roche, Mannheim, Germany). Protein concentration was determined by the Lowry method using the Bio-Rad Protein Assay 500-0006 (Bio-Rad Laboratories, Hercules, CA). Protein lysates were treated with β-mercaptoethanol and heated at 70°C for 10 minutes then electrophoresed in NuPage 7% Tris−acetate gels EA035A (Invitrogen, Carlsbad, CA). Proteins were transferred overnight at 30 V to Invitrolon PVDF membranes LC2005 (Invitrogen). Membranes were blocked with blocking buffer containing 5% skim milk in TBS with 0.1% Tween. For PAI-I detection, anti−PAI-I polyclonal antibody TP223 (Torrey Pines Biolaboratories, Houston TX) at 1:1000 dilution in blocking buffer was used, followed by horseradish peroxidase−linked antirabbit Ig NA9340 (Amersham Biosciences, Buckinghamshire, England, UK) at 1:2000 dilution in blocking buffer. Bands were visualized using ECL plus RPN2132 (Amersham Biosciences) and Kodak BioMax MR Film 870-1302 (Eastman Kodak).

For β-actin detection, the PAI-I western membranes were stripped by incubation in stripping buffer (2% SDS, 62.5 mM Tris−HCl, pH 7.4, 100 mM β-mercaptoethanol) for 30 minutes at 70°C. Then the membranes were blocked and probed with monoclonal anti−β-actin antibody A5441 (Sigma) at 1:5000 in blocking buffer, followed by horseradish peroxidase−linked antimouse Ig NA931V (Amersham Biosciences) at 1:2000 dilution in blocking buffer. Bands were visualized using ECL plus RPN2132 and Kodak BioMax MR Film 870-1302.

For band quantitation, the exposed film was scanned to obtain TIFF images in Adobe Photoshop. With each membrane image, the band intensities in a constant area were measured using the Scion Image analysis program (Scion, Frederick, MD). The band intensity values were transferred to the Microsoft Excel program for statistical analysis.

Statistical Analysis

Heteroskedastic *t*-test was performed to compare the Western blot data between two groups. Fisher's exact test as well as the Generalized Linear Mode (Logistic Regression Model) were used to compare the metastasis data between two groups. *P* value <.05 was considered statistically significant. The analyses were performed in collaboration with the Vanderbilt Cancer Center Biostatistics Shared Resource.

Results

### Generation and Characterization of Transgenic Mice

The 12T-7f line was heterozygous for the *Tag* transgene, whereas the 12T-10 line was homozygous for the *Tag* transgene. The MT-DNIIR line was homozygous for the *DNIIR* transgene. Therefore, 12T-7f mice were bred with MT-DNIIR mice to generate 12T-7f/MT-DNIIR offspring and MT-DNIIR control offspring. 12T-7f mice were bred with B6D2F1 mice to generate 12T-7f control offspring and NT offspring. 12T-10 mice were bred with MT-DNIIR mice to generate 12T-10/MT-DNIIR mice. 12T-10 mice were bred with B6D2F1 mice to generate 12T-10 control offspring. Offspring were genotyped by PCR using genomic DNA isolated from mouse tail (*arrow*, Figure 1, A and B).

Histologic examination of the prostates showed progressive tumor development in the mice expressing the T antigen, but minimal or no lesions in the other mice. The prostates were classified in a blinded manner by two pathologists (S.B.S. and R.L.R.) as containing no histologic abnormality (NHA), low-grade prostatic intraepithelial neoplasia (LGPIN), HGPIN, microinvasive carcinoma (MI), IC, or undifferentiated carcinoma (UC) [13,17]. Compared to normal areas, LGPIN and HGPIN were characterized by stratification and crowding of the epithelial cells within basement membrane-bound preexisting glands along with cytologic abnormalities such as nuclear enlargement (*arrow*, Figure 2, A−C). HGPIN was distinguished from LGPIN based on the accentuation of these features including marked nuclear atypia, more hyperchromatic nuclei, and higher mitotic and apoptotic rates (*arrow*, Figure 2, B and C). MI was recognized as foci of single cells or groups of cells breaking through the basement membrane of HGPIN-containing glands into the surrounding stroma (*arrow*, Figure 2D). Lesions were designated as IC when they were more extensive than those described above as MI, with foci of glands demonstrating invasion (*arrow*, Figure 2E). UC was characterized by invasive lesions that frequently showed destructive overgrowth of normal prostate architecture and lacked glandular differentiation but had cytologic and histologic features typical of neuroendocrine differentiation (*arrow*, Figure 2F). The MT-DNIIR and NT mice showed predominately NHA or LGPIN and rarely HGPIN but not cancer in the prostate. Given that carcinoma was identified only in the mice expressing the T antigen and predominantly in the dorsolateral lobes, we focused on the dorsolateral prostate (DLP) in these mice for further experiments (Table 1).

Both Transgenes and TGF-β1 Were Expressed in Prostate Lesions

Because human prostate carcinomas arise from the glandular epithelium, it was important to demonstrate the presence of both transgenes in the epithelium. Both *Tag* and *DNIIR* transgenes were expressed in luminal epithelial cells of 12T-7f/MT-DNIIR and 12T-10/MT-DNIIR mice according to immunohistochemical analyses for *Tag* (*arrow*, Figure 3A) and *in situ* hybridization analyses for *DNIIR* (*arrow*, Figure 3B). We found stable levels of *DNIIR* expression throughout tumor progression as measured by real-time RT-PCR (Table 2). Additionally, TGF-β1 was identified in the prostate and localized to the epithelium according to immunohistochemical analyses (*arrow*, Figure 3C). The staining intensities of TGF-β1 were similar based on MetaMorph analysis. The presence of TGF-β justified the use of a dominant negative TβRII to block TGF-β signaling. Thus, expression of both transgenes and TGF-β1 was seen in the
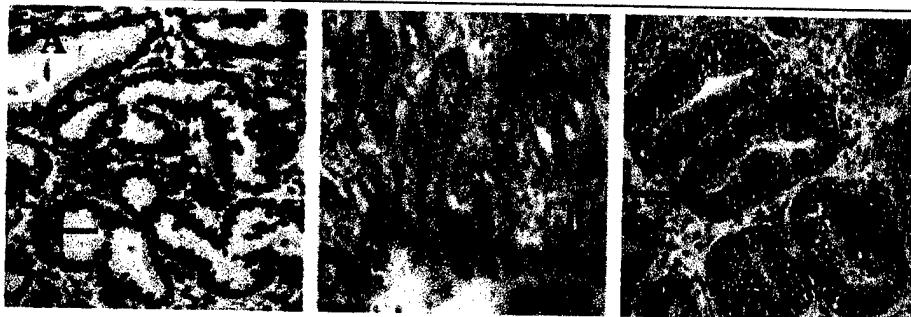
Figure 3. Detection of transgene expression in transgenic mice. (A) An example of immunohistochemical analysis shows expression of Tag in an HGPIN lesion (arrow) in a DLP of a 12T-7f/MT-DNIIR mouse. (B) A light field view of in situ hybridization shows expression of DNIIR in an HGPIN lesion (arrow) in a DLP of a 12T-7f/MT-DNIIR mouse. (C) An example of immunohistochemical analysis shows localization of TGF-β1 in an HGPIN lesion (arrow) in a DLP of a 12T-7f mouse. (D) An example of immunohistochemical analysis shows localization of TGF-β1 in an HGPIN lesion (arrow) in a DLP of a 12T-7f/MT-DNIIR mouse. (E) An example of immunohistochemical analysis shows localization of TGF-β1 in an HGPIN lesion (arrow) in a DLP of a 12T-10 mouse. (F) An example of immunohistochemical analysis shows localization of TGF-β1 in an HGPIN lesion (arrow) in a DLP of a 12T-10/MT-DNIIR mouse.

prostatic epithelial lesions that developed in the 12T-7f/MT-DNIIR and 12T-10/MT-DNIIR.

Expression of the DNIIR Transgene Decreased Levels of a TGF-β Downstream Target, PAI-I

PAI-I expression is positively regulated by TGF-β [9,10]. Using PAI-I as a marker for TGF-β signaling, the presence of the DNIIR transgene was shown to disrupt TGF-β signaling. Western blot analyses were performed to determine the PAI-I and β-actin levels in tissues from age-matched mice. The PAI-I levels were quantitated using the Scion Image analysis program and normalized for protein loading by the β-actin levels. The average normalized level of PAI-I in 12T-7f/MT-DNIIR mice was significantly lower than the average normalized level of PAI-I in 12T-7f mice ($P<.05$) (Figure 4, A and B). Similarly, the average normalized level of PAI-I in 12T-10/MT-DNIIR mice was significantly lower than the average normalized level of PAI-I in 12T-10 mice ($P<.05$) (Figure 4, C and D). Therefore, the DNIIR transgene actively inhibited TGF-β signaling in the prostate.

12T-7f/MT-DNIIR Mice Tended to Develop More IC But Not Larger Prostates Compared to 12T-7f Mice

The histologic progression of prostatic neoplasia in 12T-7f/MT-DNIIR ($n=39$) mice was similar to that of

12T-7f mice ($n=41$) from 12 to 23 weeks old. Both lines predominantly developed HGPIN with glandular proliferation and hypercellular stroma in the prostate. To determine whether the loss of TGF-β inhibition in the tumors stimulated growth, we measured the wet prostatic weights and normalized for differences in animal size by calculating the percentage of body weight. Comparing the prostate weights, as percentage of body weight, of 12T-7f/MT-DNIIR and 12T-7f mice revealed no increase in tumor size (data not shown). Invasive periurethral and bulbourethral tumors were rarely observed in 12T-7f/MT-DNIIR mice ($n=2$) and 12T-7f mice ($n=1$). Focal lesions of locally invasive carcinoma were observed more frequently in routine sections of the prostates of 12T-7f/MT-DNIIR mice ($n=6$) than in 12T-7f mice ($n=3$) (Table 1). None of the control MT-DNIIR mice ($n=50$) and NT mice (NT, $n=56$) from 12 weeks to 10 months old developed IC.

12T-7f/MT-DNIIR Mice Tended to Develop Metastasis More Frequently and Extensively Than 12T-7f Mice

Both 12T-7f/MT-DNIIR and 12T-7f mice developed microscopic neuroendocrine metastases to the para-aortic LNs (arrow, Figure 5A), lungs (arrow, Figure 5B), liver (Figure 5C), and rarely bones (12T-7f/MT-DNIIR, $n=1$; 12T-7f, $n=1$) (arrow, Figure 5D). Metastases were identified histologically

Table 2. Quantitation of DNIIR Transgene Expression by Real-Time RT-PCR.

Line	Mouse number	Age	Tissue	DNIIR level	β-Actin level	Ration of DNIIR/β-Actin
12T-7f/MT-DNIIR	9237	12 weeks	DLP	3.65E+04	1.00E+10	3.7E−06
12T-7f/MT-DNIIR	9241	12 weeks	DLP	1.85E+05	4.24E+10	4.4E−06
12T-7f/MT-DNIIR	9201	16 weeks	DLP	7.65E+04	1.19E+10	6.4E−06
12T-7f/MT-DNIIR	9208	16 weeks	DLP	1.06E+05	1.03E+10	1.0E−05
12T-7f/MT-DNIIR	9218	18 weeks	DLP	1.80E+04	5.53E+09	3.3E−06
12T-7f/MT-DNIIR	A3028	18 weeks	DLP	6.02E+04	2.60E+10	2.3E−06
12T-7f/MT-DNIIR	9212	20 weeks	DLP	4.98E+04	4.35E+10	1.1E−06
12T-7f/MT-DNIIR	9223	20 weeks	DLP	3.10E+04	4.07E+10	7.6E−07
12T-7f/MT-DNIIR	9227	23 weeks	DLP	2.40E+04	1.07E+10	2.2E−06
12T-7f/MT-DNIIR	A3030	23 weeks	DLP	5.76E+04	1.08E+10	5.3E−06
12T-7f/MT-DNIIR	A3407	8 months	Liver metastasis	1.69E+07	5.89E+10	2.9E−04
12T-7f/MT-DNIIR	A3404	9 months	Liver metastasis	1.79E+03	5.67E+10	3.2E−08
12T-7f/MT-DNIIR	A3135	10 months	Liver metastasis	1.30E+03	6.02E+10	2.2E−08

Levels are listed as copy numbers per 200 ng of total RNA.

A

12T-7f   *12T-7f/MT-DNIIR*

9194 9195 9245 9246 9219 9223 9227 9212

PAI-1

β-actin

C

12T-10   *12T-10/MT-DNIIR*

A3169 A3163 A3159 A3158 A3143 A3142 A3130 A3133

PAI-1

β-actin

B

Mouse	Age	PAI-1	Actin	Ratio
9194	20 wk	133.11	22.33	6.0
9195	20 wk	37.74	13.22	2.9
9245	23 wk	68.89	23.58	2.9
9246	23 wk	51.25	11.95	4.3
9219	20 wk	115.13	162.02	0.7
9223	20 wk	44.32	110.40	0.4
9227	23 wk	68.36	37.00	1.8
9212	20 wk	155.59	46.07	3.4

D

| Mouse	Age	PAI-1	Actin	Ratio
A3169	7 mo	86.73	57.59	1.5
A3163	7 mo	68.23	91.73	0.7
A3159	6 mo	99.45	114.99	0.9
A3158	6 mo	79.91	85.90	0.9
A3143	7 mo	61.20	107.61	0.6
A3142	7 mo	78.30	215.67	0.4
A3130	6 mo	68.68	153.50	0.4
A3133	6 mo	80.15	174.23	0.5

Figure 4. *Quantitation and normalization of PAI-I levels in transgenic mice. (A) Western blots for PAI-I and for β-actin as a loading control in 12T-7f and 12T-7f/MT-DNIIR mice. (B) Summary of band intensities from Western blots in (A) along with ratios of PAI-I to β-actin. The average ratio is significantly lower in 12T-7f/MT-DNIIR mice than in 12T-7f mice (P<.05). (C) Western blots for PAI-I and for β-actin as a loading control in 12T-10 and 12T-10/MT-DNIIR mice. (B) Summary of band intensities from Western blots in (C) along with ratios of PAI-I to β-actin. The average ratio is significantly lower in 12T-10/MT-DNIIR mice than in 12T-10 mice (P<.05).*

and showed typical features of neuroendocrine differentiation. The metastatic lesions were immunopositive for *Tag* (*arrow*, Figure 5A), TGF-β1 (*arrow*, Figure 5B), and chromogranin A (CG), a neuroendocrine marker confirming their transgene expression and neuroendocrine differentiation (*arrow*, Figure 5D). More 12T-7f/MT-DNIIR mice (n=7) developed metastasis than age-matched 12T-7f mice

(n=4) (Table 1). Lung metastasis occurred most commonly whereas liver metastasis occurred in a subset of those animals, seemingly indicating more widespread metastasis. Comparing liver metastasis in the 12T-7f line (n=1) (*arrow*, Figure 5E) and the 12T-7f/MT-DNIIR line (n=2) (*arrow*, Figure 5F) showed more extensive metastasis in the 12T-7f/MT-DNIIR mice. These results in the 12T-7f
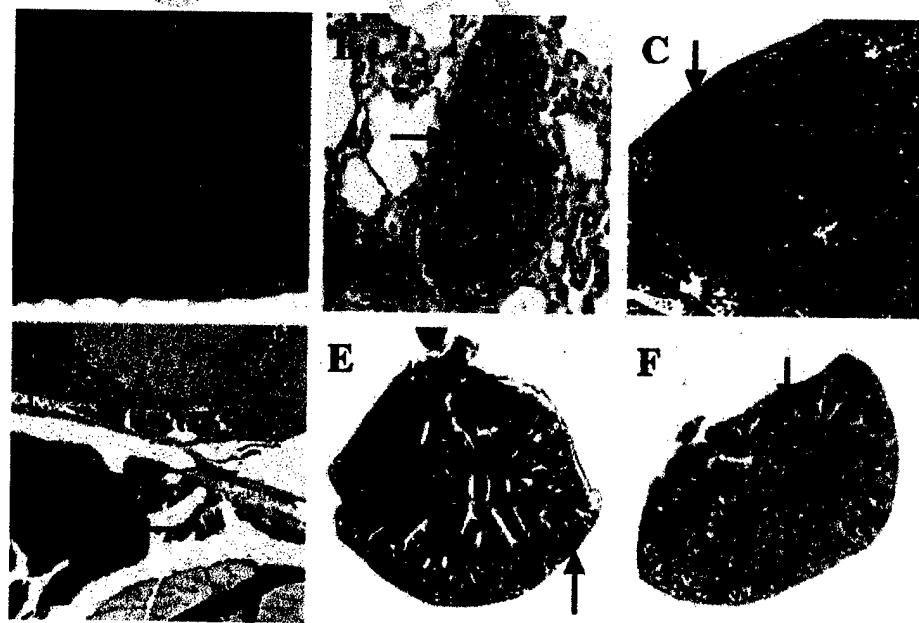
Figure 5. *Metastatic lesions along with immunohistochemical analyses in 12T-7f/MT-DNIIR mice and 12T-7f mice. (A) Tag-expressing metastatic lesion (arrow) in the para-aortic lymph node of a 12T-7f/MT-DNIIR mouse. (B) TGF-β1-expressing metastatic lesion (arrow) in the lung of a 12T-7 mouse. (C) Metastatic lesion (arrow) on H&E stain in the liver of a 12T-7 mouse. (D) CG-expressing metastatic lesion (arrow) in the lumbar spine of a 12T-7f mouse. (E) Micrometastases (arrow) in the liver of a 20-week-old 12T-7f mouse. (F) Extensive micrometastases (arrow) in the liver of an 18-week-old 12T-7f/MT-DNIIR mouse.*

mouse model suggested that loss of the TGF-β pathway in prostate tumors promotes metastatic disease.

12T-10/MT-DNIIR Mice Tended to Develop More IC But Not Larger Prostates Compared to 12T-10 Mice

Characterizing the effects of DNIIR overexpression on the tumors in the 12T-10 line showed an even more pronounced effect on tumor progression. The histologic progression of the primary prostatic neoplasia in 12T-10/MT-DNIIR mice was similar to that of 12T-10 mice. The 12T-10/MT-DNIIR mice (n=22) and 12T-10 mice (n=23) from 6 to 10 months old progressively developed HGPIN, locally invasive neuroendocrine carcinoma in the prostate, and neuroendocrine metastasis. Comparing the prostate weights, as percent of body weight, of 12T-10/MT-DNIIR and 12-T10 mice showed no increase in tumor size (data not shown). Invasive peri-

urethral and bulbourethral tumors were rarely observed in 12T-10/MT-DNIIR (n=3) and 12T-10 (n=1) mice. The incidence of IC was higher in the 12T-10/MT-DNIIR mice (n=5) than 12T-10 mice (n=2) (Table 1).

12T-10/MT-DNIIR Mice Developed Significantly More Extensive Metastasis Than 12T-10 Mice

The 12T-10/MT-DNIIR and 12T-10 mice developed LN, lung, and liver metastases similar to, but more frequently than, 12T-7f/MT-DNIIR and 12T-7f mice. According to immunohistochemical and real-time RT-PCR analyses, the metastatic lesions expressed Tag, TGF-β1, CG, and DNIIR (Table 2). Based on histologic examination, the cumulative incidence of metastasis was not different between the 12T-10/MT-DNIIR (n=8) and 12T-10 (n=7) mice (Table 1). However, the extent of metastatic disease was prominently
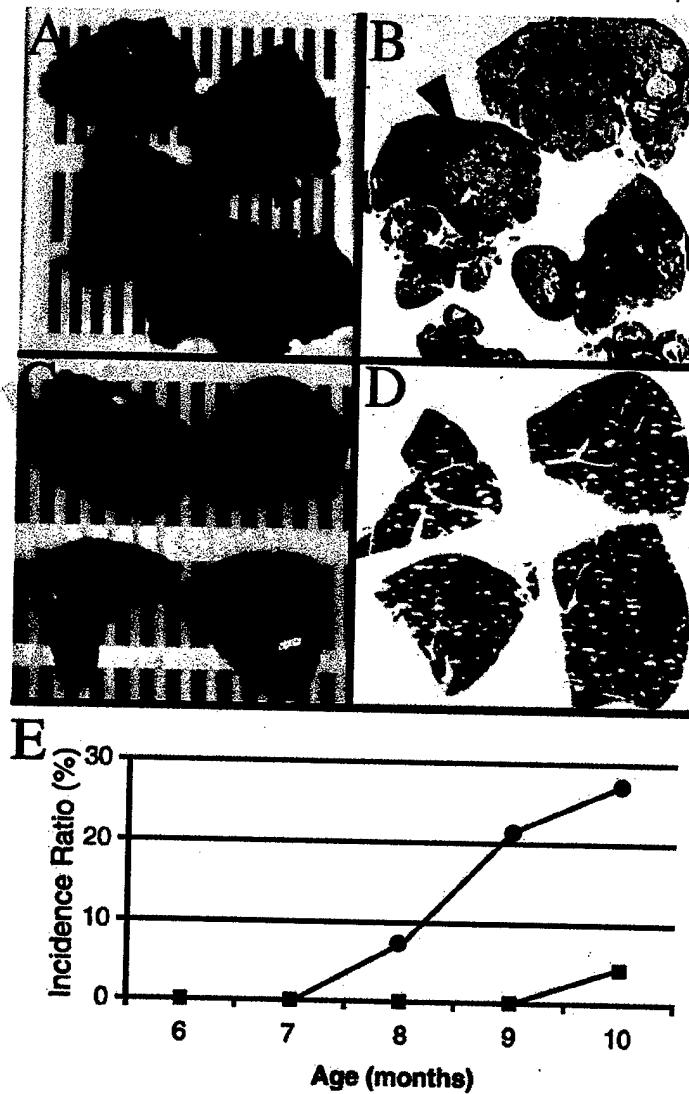
Figure 6. Comparison of metastasis in 12T-10/MT-DNIIR mice and 12T-10 mice. (A and B) Gross metastatic lesions (arrow) in the liver of a 12T-10/MT-DNIIR mouse and accompanying histology. (C and D) No gross lesions in the liver of an age-matched 12T-10 mouse and accompanying histology. (E) Comparison of incidence (%) of gross metastasis over time in 12T-10/MT-DNIIR (●, n=22) mice versus 12T-10 (■, n=23) mice. The incidence ratio of metastasis is significantly greater in 12T-10/MT-DNIIR mice than in 12T-10 mice (P<.05).

increased in the 12T-10/MT-DNIIR mice compared to 12T-10 mice. Grossly evident metastatic nodules in the liver and lungs from 12T-10/MT-DNIIR mice (*arrow*, Figure 6, *A* and *B*) were noted but no grossly evident metastases were observed in those organs from age-matched 12T-10 mice (Figure 6, *C* and *D*). Comparing the cumulative incidence of gross metastasis over time between 12T-10/MT-DNIIR mice (●, $n = 6/22$) and 12T-10 (■, $n = 1/23$) mice showed a statistically significant ($P < .05$) increase in the 12T-10/MT-DNIIR mice (Figure 6*E*). Furthermore, comparing only mice with metastasis showed a statistically significant ($P < .05$) increase in gross metastasis in 12T-10/MT-DNIIR mice ($n = 6/8$) compared with 12T-10 mice ($n = 1/7$). These results in the 12T-10 mouse model demonstrated that a loss of TGF-β signaling in metastatic prostate cancer increases the amount of metastatic lesions.

Discussion

In summary, this study has demonstrated that disruption of TGF-β signaling modulates progression in late-stage prostate cancer, specifically metastasis. Although more IC foci were noted in routine sections in the mice expressing the *DNIIR* and *Tag* transgenes, the increases were not statistically significant (Table 3). Therefore, the effect on metastasis was not simply due to the development of more IC. Instead, the effect must have been either on the development of metastasis and/or growth at the metastatic site. Because the MT promoter is not prostate-specific, more direct effects on the immune system or angiogenesis cannot be ruled out. Nevertheless, the *DNIIR* transgene had a direct effect of disrupting the TGF-β pathway in the prostate tumors as demonstrated by the significant reduction in levels of PAI-I. Decreased levels of PAI-I, an inhibitor of urokinase-type plasminogen activator (uPA) that mediates extracellular matrix proteolysis, may be a possible mechanism for the increased metastasis in our model because it has been demonstrated that PAI-I is present at low levels in several human prostate cancer cell lines including PC-3 cells and increasing PAI levels by stable transfection decreases metastasis of PC-3 cells in mice [18,19]. Other intracellular effectors of TGF-β might also be causally involved in induction of prostate cancer metastasis. It has been reported in breast and colon cancers that TGF-β signaling initially has a negative effect but eventually exerts a positive effect on tumor progression. For example, blocking TGF-β is important for tumor growth, but subsequent restoration of the TGF-β pathway contributes to tumor cell motility, epithelial-to-mesenchymal transition, and ultimately metastasis [20,21]. Those reports focused on nonprostatic cancer and used different systems such as injection of cell lines into mice for tumor and metastasis formation.

In human prostate cancer, the loss of the TβRII occurs most commonly in advanced stage disease [4,5], suggesting that this pathway does not function as a positive influence on the spread of this disease. These studies correlated a dysfunctional TGF-β receptor pathway with tumor grade at the primary site but did not prove that the loss of the receptor

Table 3. Summary of Histopathology.

Line	Age	IC	Metastasis
12T-7f/MT-DNIIR	12–23 weeks	6 of 39	7 of 39 (2 to liver)
12T-7f	12–23 weeks	3 of 41	4 of 41 (1 to liver)
12T-10/MT-DNIIR	6–10 months	5 of 22	8 of 22 (6 gross*)
12T-10	6–10 months	2 of 23	7 of 23 (1 gross*)
MT-DNIIR	12 weeks–10 months	0 of 50	0 of 50
NT	12 weeks–10 months	0 of 56	0 of 56

*Significant difference with $P < .05$.

was responsible for cancer progression. Our study in two transgenic animal models provides proof, rather than a pathologic correlation, that disruption of TGF-β regulation is important for increasing metastatic burden. This is especially critical in human prostate cancer that metastasizes in end-stage disease mainly to the bone, where high TGF-β levels are naturally found [22]. Metastatic initiation and growth will be important targets for future study and possibly therapy because limiting metastasis would allow for more successful treatment of prostate cancer [1]. The majority of human prostate cancer metastases are moderate to poorly differentiated adenocarcinomas, but these mouse models, similar to other SV40 T antigen models, develop invasive and metastatic poorly differentiated carcinomas with neuroendocrine differentiation [17]. Murine trangenic models to study human prostate cancer have some limitations because mice do not naturally develop prostate cancer and results in mice do not always translate directly to humans. Nevertheless, a recent report has identified the neuroendocrine phenotype and TGF-β pathway as important prognostic factors in human prostate cancer [23]. Although TGF-β loss has been associated with human prostate cancer progression, it has not been determined whether that loss was a cause or consequence of tumor progression. Our data, in an animal model of prostate cancer that demonstrates genetic and histopathologic changes analogous to those in human prostate cancer, suggest for the first time that there is a clinically relevant selective advantage for loss of TGF-β regulation as a cause of increased metastatic burden. We hope to use this model to identify novel TGF-β targets that would be tested in human samples.

References

[1] Ohori M, Goad JR, Wheeler TM, Eastham JA, Thompson TC, and Scardino PT (1994). Can radical prostatectomy alter the progression of poorly differentiated prostate cancer? *J Urol* **152**, 1843–49.

[2] Quinn DI, Henshall SM, Head DR, Golovsky D, Wilson JD, Brenner PC, Turner JJ, Delprado W, Finlayson JF, Stricker PD, Grygiel JJ, and Sutherland RL (2000). Prognostic significance of p53 nuclear accumulation in localized prostate cancer treated with radical prostatectomy. *Cancer Res* **60**, 1585–94.

[3] Bookstein R, Rio P, Madreperla SA, Hong F, Allred C, Grizzle WE, and

Lee WH (1990). Promoter deletion and loss of retinoblastoma gene expression in human prostate carcinoma. *Proc Natl Acad Sci USA* **87**, 7762–66.

[4] Kim IY, Ahn HJ, Lang S, Oefelein MG, Oyasu R, Kozlowski JM, and Lee C (1998). Loss of expression of transforming growth factor-beta receptors is associated with poor prognosis in prostate cancer patients. *Clin Cancer Res* **4**, 1625–30.

[5] Guo Y, Jacobs SC, and Kyprianou N (1997). Down-regulation of protein and mRNA expression for transforming growth factor-beta (TGF-beta1) type I and type II receptors in human prostate cancer. *Int J Cancer* **71**, 573–79.

[6] Morton DM and Barrack ER (1997). Modulation of transforming growth factor β1 effects on prostate cancer cell proliferation by growth factors and extracellular matrix. *Cancer Res* **55**, 2596–602.

[7] Brodin G, ten Dijke P, Funa K, Heldin CH, and Landstrom M (1999). Increased smad expression and activation are associated with apoptosis in normal and malignant prostate after castration. *Cancer Res* **59**, 2731–38.

[8] Danielpour D (1999). Transdifferentiation of NRP-152 rat prostatic basal epithelial cells toward a luminal phenotype: regulation by glucocorticoid, insulin-like growth factor-I and transforming growth factor-beta. *J Cell Sci* **112** (Part 2), 169–79.

[9] Datta PK, Blake MC, and Moses HL (2000). Regulation of plasminogen activator inhibitor-1 expression by transforming growth factor-β–induced physical and functional interactions between Smads and Sp1. *J Biol Chem* **275**, 40014–19.

[10] Hua X, Miller ZA, Wu G, Yigong S, and Lodish HF (1999). Specificity in transforming growth factor β–induced transcription of the plasminogen activator inhibitor-1 gene: interactions of promoter DNA, transcription factor, μE3, and Smad proteins. *Proc Natl Acad Sci USA* **96**, 13130–35.

[11] Yan Y, Sheppard PC, Kasper S, Lin L, Hoare S, Kapoor A, Dodd JG, Duckworth ML, and Matusik RJ (1997). A large fragment of the probasin promoter targets high levels of transgene expression to the prostate of transgenic mice. *Prostate* **32**, 129–39.

[12] Kasper S, Sheppard PC, Yan Y, Pettigrew N, Borowsky AD, Prins GS, Dodd JG, Duckworth ML, and Matusik RJ (1998). Development, progression and androgen-dependence of prostate tumors in transgenic: a model for prostate cancer. *Lab Invest* **78**, 319–34.

[13] Masumori N, Thomas TZ, Case T, Paul M, Kasper S, Chaurand P, Caprioli RM, Tsukamoto T, Shappell SB, and Matusik RJ (2001). A probasin-large T antigen transgenic mouse line develops prostate ad-

eno and neuroendocrine carcinoma with metastatic potential. *Cancer Res* **61**, 2239–49.

[14] Ghatak S, Oliveria P, Kaplan P, and Ho SM (1996). Expression and regulation of metallothionein mRNA levels in the prostates of noble rats: lack of expression in the ventral prostate and regulation by sex hormones in the dorsolateral prostate. *Prostate* **29**, 91–100.

[15] Serra R, Johnson M, Filvaroff EH, LaBorde J, Sheehan DM, Derynck R, and Moses HL (1997). Expression of a truncated, kinase-defective TGF-beta type II receptor in mouse skeletal tissue promotes terminal chondrocyte differentiation and osteoarthritis. *J Cell Biol* **139**, 541–52.

[16] Wang XJ, Greenhalgh DA, Bickenbach JR, Jiang A, Bundman DS, Krieg T, Derynck R, and Roop DR (1997). Expression of a dominant-negative type II transforming growth factor beta (TGF-beta) receptor in the epidermis of transgenic mice blocks TGF-beta–mediated growth inhibition. *Proc Natl Acad Sci USA* **94**, 2386–91.

[17] Matusik R, Masumori N, Thomas T, Case T, Paul M, Kasper S, and Shappell S (2001). Transgenic mouse models of prostate cancer. In *Contemporary Endocrinology: Transgenics in Endocrinology*. M Matzuk, C Brown, T Kumar (Eds.) Totowa, Canada Humana Press Inc, 401–25.

[18] Lyon PB, See WA, Xu Y, and Cohen MB (1995). Diversity and modulation of plasminogen activator activity in human prostate carcinoma cell lines. *Prostate* **27**, 179–86.

[19] Soff GA, Sanderowitz J, Gately S, Verrusio E, Weiss I, Brem S, and Kwaan HC (1995). Expression of plasminogen activator inhibitor type 1 by human prostate carcinoma cells inhibits primary tumor growth, tumor-associated angiogenesis, and metastasis to lung and liver in an athymic mouse model. *J Clin Invest* **96**, 2593–600.

[20] Yin JJ, Selander K, Chirgwin JM, Dallas M, Grubbs BG, Wieser R, Massague J, Mundy GR, and Guise TA (1995). TGF-beta signaling blockade inhibits PTHrP secretion by breast cancer cells and bone metastases. *J Clin Invest* **103**, 197–206.

[21] Derynck R, Akhurst RJ, and Balmain A (2001). TGF-beta signaling in tumor suppression and cancer progression. *Nat Genet* **29**, 117–29.

[22] Pfeilschifter J and Mundy GR (1987). Modulation of type beta transforming growth factor activity in bone cultures by osteotropic hormones. *Proc Natl Acad Sci USA* **84**, 2024–28.

[23] Singh D, Febbo PG, Ross K, Jackson DG, Manola J, Ladd CP, Tamayo, P, Renshaw AA, D'Amico AV, Richie JP, Lander ES, Loda M, Kantoff TR, Golub TR, and Sellers WR (2002). Gene expression correlates of clinical prostate cancer behavior. *Cancer Cells* **1**, 203–209.

Prostate Pathology of Genetically Engineered Mice: The Consensus Report from the Bar Harbor Meeting[1]

Scott B. Shappell[2], Richard L. Roberts, George V. Thomas, Ron Herbert, Mark A. Rubin, Peter A. Humphrey, Michael M. Ittmann, John P. Sundberg, Nora Rozengurt, Roberto Barrios, Jerrold M. Ward, Robert D. Cardiff

Department of Pathology and Vanderbilt Prostate Cancer Center (S.B.S. R.L.R.), Department of Urologic Surgery and Vanderbilt-Ingram Cancer Center (S.B.S.), Vanderbilt University Medical Center, Nashville, TN; Department of Pathology, University of California at Los Angeles, Los Angeles, CA (G.V.T., N.R.), National Institute of Environmental Health Sciences, Research Triangle Park, N.C., (R.H.), Departments of Pathology and Urology, University of Michigan, Ann Harbor, MI (M.A.R.), Departments of Pathology and Urology, Washington University of St. Louis, St. Louis, MO (P.A.H.), Department of Pathology, Baylor College of Medicine, Houston, TX (M.I., R.B.), Jackson Laboratories, Bar Harbor, ME (J.P.S.); Veterinary and Tumor Pathology Section, Office of Laboratory Animal Resources, National Cancer Institute, Frederick, MD (J.M.W.), Center for Comparative Medicine, University of California, Davis, Davis, CA (R.D.C.)

Running Title: Bar Harbor Classification of Mouse Prostate Pathology

Footnotes

[2]Correspondence: Scott B. Shappell, M.D., Ph.D.
Department of Pathology, C-3321 Medical Center North
Vanderbilt University Medical Center
Nashville, TN 37232-2561
Phone: 615-343-2338
Fax: 615-343-7023
e-mail: scott.shappell@vanderbilt.edu

[3]Abbreviations: MMHCC, Mouse Models of Human Cancer Consortium; GEM, genetically engineered mouse (mice); PZ, peripheral zone; TZ, transition zone; CZ, central zone; PIN, prostatic intraepithelial neoplasia; HGPIN, high grade PIN; LGPIN, low grade PIN; Pca, prostate carcinoma; BPH, benign prostatic hyperplasia; RP, radical prostatectomy; ECE, extracapsular extension; HMWCK, high molecular weight cytokeratin; PAH, post-atrophic hyperplasia; CK, cytokeratin; NE, neuroendocrine; CG, chromogranin; Tag, large T-antigen; LOH, loss of heterozygosity

Abstract

The Pathologic Classification of Prostate Lesions in Genetically Engineered Mice is the result of a directive from the National Cancer Institute Mouse Models of Human Cancer Consortium (MMHCC) Prostate Steering Committee to provide a hierarchical taxomony of disorders of the mouse prostate to facilitate classification of existing and newly created mouse models and the translation to human prostate pathology. The proposed Bar Harbor Classification system is the culmination of three meetings and workshops attended by various members of the Prostate Pathology Committee of the MMHCC. Most recently, a formal two day Pathology Workshop was held at Jackson Laboratories in Bar Harbor Maine in October 2001. Study sets of 93 slides from 22 genetically engineered mouse (GEM) models were provided to individual panel members. Developmental, inflammatory, benign proliferative, and neoplastic disorders of the prostate have been classified. Much attention was given to prostatic intraepithelial neoplasia (PIN). High grade PIN (HGPIN) in the human is routinely recognized by histologic features, which have been noted in several GEM models. However, human HGPIN has additional molecular, genetic, and clinical features that support its role as a precursor lesion for peripheral zone prostate carcinomas (Pcas). Such properties have not been established for the majority of histologic alterations suggested to represent PIN in the mouse. Hence, criteria for mouse PIN (mPIN) were established as histologic, with separate classification for those models that progress to invasive carcinoma and those in which regular progression to invasion has not been documented. It was the consensus opinion that mPIN should not currently be graded, as histologic features that might predict invasion in any given model (as implied by high grade) are not presently recognized. Several SV40 based models have in situ lesions (mPIN) that progress to invasion. The nuclear atypia in these models is marked and greater than that characteristic of human HGPIN. The cytologic features of several models based on manipulations of growth factors, their receptors, or tumor suppressor genes were felt to be more similar to those of human HGPIN. However, very few examples of models with even rare progression have been reported or were represented at the meeting. PIN is distinguished from epithelial hyperplasia with atypia by criteria of focality and progression. The lack of provision for grading PIN in the Bar Harbor classification does not preclude descriptions of progression in the characterization of individual models. Of models reviewed, unequivocal invasive carcinoma was noted consistently only in SV40 early region or large T antigen based models, utilizing either supposed androgen regulated prostate specific or non-androgen regulated promoters. Invasive carcinoma in these models typically has the appearance of neuroendocrine (NE) differentiation, including finely granular "salt and pepper" chromatin with rosetting and/or features typical of small cell carcinoma, with high nuclear to cytoplasmic ratios, hyperchromatic nuclei, and nuclear molding. Such NE differentiation has been confirmed immunohistochemically and ultrastructurally in some models. Tumors with this morphology should be designated as NE carcinoma. Similar tumors possibly arising in or involving other male accessory glands such as the peri-urethral and bulbourethral glands were noted in sections from all mice utilizing AR-dependent promoters and SV40 early region or large T antigen. As these tissues are androgen regulated and transgenic mice created with androgen dependent promoters may develop tumors in these sites as well as the prostate, a pathologic classification of tumors arising in these other male accessory glands is included in the Bar Harbor Classification. Few examples of unequivocal invasive adenocarcinoma of the prostate were provided, but some microinvasive and more extensively invasive adenocarcinomas were clearly demonstrated. Increased gland spaces (relative to wild type mice) with cytologic atypia is not in itself diagnositic of adenocarcinoma. Although stromal desmoplasia is not a routinely recognized histologic feature in invasive acinar forming human Pca, focality and

desmoplasia were recognized as important supportive features for true invasive adenocarcinoma. Adenocarcinoma is classified as well, moderately, and poorly differentiated based on extent of glandular formation. It is intended that the Bar Harbor Classification of Prostate Pathology in GEM will prove helpful in allowing for more uniform characterization of newly generated models as well as in ongoing investigational use of current mouse models of Pca.

Introduction and Objectives:

The increased generation of potential models of prostate neoplasia in genetically engineered mice (GEM) and their use in investigations of possible cancer therapies in prostate carcinoma (Pca) mandates the development of a standardized pathology classification scheme. As mice and other rodents do not spontaneously develop Pca, histologic criteria have been attempted based on the disorders observed in newly created GEM models and by efforts to translate these lesions to the familiar histopathology of human Pca and its precursor lesions. As the goal of the MMHCC is to model human neoplasia, use of criteria and terminology applied to human prostate pathology is logical. However, as detailed herein, there are anatomic and natural history issues that impact on the ability to make straightforward analogies between GEM models of Pca and the human disease being modeled. Further, in addition to pathologic criteria, other criteria that can be incorporated into characterization and validation of GEM models include genetic and other molecular alterations and the natural history of the prostate lesions and the similarity of these aspects to human Pca.

GEM models will be useful for delineating novel causative molecular alterations in the development and/or progression of Pca and useful in testing interventions that will translate to treatments in human Pca patients if such models are similar, at least in some regards, to this heterogenous human neoplasia at initiating or secondary molecular alterations. As histopathologic features are a phenotypic consequence of these underlying molecular alterations, pathology assessment will be useful for characterizing new models and for detecting potentially meaningful changes as a consequence of genetic crosses or therapeutic interventions.

Protocols for tissue submission are necessary for characterizing the prostate and other organs in new GEM models, including the assessment of the natural history of any prostatic neoplasia and possible development of metastases. In addition to histologic assessment in standard microscopy sections, tissue based analysis of cellular differentiation can be useful in thorough characterization of GEM models. Biologic parameters including proliferation, apoptosis, and microvessel density can provide mechanistic insight into effects of genetic manipulations and therapeutic interventions.

Hence, the specific objectives of the MMHCC Prostate Pathology Committee to facilitate characterization and application of GEM models of prostatic disease were as follows:

1) Development of a classification scheme for disorders of the prostate and related organs in GEM.
2) Provision of histopathologic definitions for these disorders.
3) Collection and annotation of images illustrating these disorders, utilizing as many of the provided models as possible.
4) Collection, organization, and distribution of pathology protocols useful in characterization of prostate disorders in GEM.

The researchers involved in the development and use of GEM models of Pca range from basic molecular scientists to clinicians actively engaged in patient care. Research endeavors in the use of GEM models in Pca will be most productive if investigators are familiar with the full spectrum of basic prostate developmental biology, the cell biology of normal and abnormal prostate cell growth, and the spectrum of histopathologic features and clinical history of human Pca. Many GEM investigators have very little experience with human Pca, including familiarity with the zones of the human prostate in which neoplasia occurs or in which specific precursor lesions are found, anatomic considerations involved in clinically relevant staging of human Pca, and the morphologic appearances of human Pca. As the research community supported by the MMHCC is attempting to generate and use models that may have limited or wide application to specific or broad subsets of

5

human Pca patients, respectively, it is fundamental to understand GEM prostate pathology in the context of human prostate pathology. For this perspective, knowledge of the basic anatomic and histologic similarities and differences between the mouse and human prostate is necessary. As such, this review includes detailed considerations of prostate anatomy and clinical and pathologic features of the full spectrum of both benign and neoplastic human prostate disorders, similarities to which have been or can potentially be encountered in GEM models. Each section for the classification scheme is in general divided into: definitions of that disorder, clinical considerations and morphologic features in human prostate pathology, and the pathologic features of that entity in GEM models. For human prostate pathology, references are typically made to standard textbook chapters commonly utilized by human Genitourinary pathologists and that should be available to investigators from their human pathology colleagues. Specific references on described entities can be found in those standard texts and are occasionally cited herein for certain lesions.

The images illustrating the various lesions in the mouse pathology classification were taken from the slides of the models provided to the MMHCC Prostate Pathology Committee or additional materials made available to the author. Where possible, multiple models are illustrated for a specific lesion, to emphasize the common features of the disorder and to allow visualization of the process against different histologic backgrounds, etc. The inclusion of a model or the reference to a model regarding a specific lesion is not intended as a potential endorsement or criticism of that specific model. Similarly, the illustration of a specific lesion in a single slide is not intended to be taken as a generalization regarding the natural history of that model. However, as descriptions of specific GEM models in the literature have used non-uniform pathology criteria and terminology, making comparisons between models difficult, the pathology classification is followed by a description of the natural history of several models. The intention was to be able to describe the natural history of these models using the newly proposed Bar Harbor Classification scheme. In addition to the histopathology features of these models, reported molecular alterations that provide supplemental information to the pathology and natural history of these GEM models is included. It is hoped that this will provide useful information to investigators interested in learning about GEM models of Pca or utilizing them in future investigations. Characterization of GEM models is an integrated endeavor incorporating pathology, natural history, and molecular characterizations. This section illustrates how pathology characterization can be applied to existing models, and hence provides examples for characterization of future models as well. This section includes some models that were included in the Bar Harbor Pathology Workshop and/or accompanying meeting and some that were not. Particularly in the latter instance, descriptions of the pathology are inferred largely from the literature. It is impossible for a review to include all relevant studies in this expanding area of investigation. We have attempted to be thorough, with the major goal of illustrating, supporting, and applying the Pathology Classification Scheme. Inclusion or omission of any individual model is not intended as a specific endorsement or criticism of a specific model.

A protocols section is included, primarily in Appendices. Guidelines regarding tissue submission are provided. Information on specific immunohistochemical studies that have been successfully employed in mouse prostate are included. In addition to consulting individual references for information on the use of the specific antibodies, general protocols for immunohistochemistry an in situ hybridization are included in the Appendices. A glossary defining terms utilized herein and which may be useful as modifiers in describing specific lesions is also included in the appendices. Finally, web sites that provide information complementing that included herein on the characterization and use of GEM models for Pca are included in an appendix.

General Considerations: In addition to examination of the histopathologic features demonstrated in reviewed models and consideration of the criteria for specific pathologic diagnoses, several general principles regarding characterization of GEM models for Pca were elaborated at the Bar Harbor Pathology Workshop.

Low frequency of spontaneous genitourinary pathologic lesions in mice: The low incidence of spontaneous pathologic lesions in the mouse prostate was emphasized. This is true not only for neoplastic proliferations, but also for non-neoplastic disorders, and includes aged mice. The experience for large numbers of mice of different genetic backgrounds, including at the Jackson Laboratories and National Institute of Environmental Health Sciences (NIEHS) emphasizes this general impression. In a recent survey of 612 control B6C3F1 mice for two year toxicology and carcinogenicity studies conducted in the National Toxicology Program, not a single example of a spontaneous carcinoma was observed in the prostate of these wild type mice, with fairly uniform sampling of APs, DLPs, and VPs (1). Epithelial hyperplasia was rare, noted in 0.7 % of VPs and 0.9 % of APs and DLPs (1). Adenocarcinoma of the seminal vesicles was noted in two mice (0.3 %). Other pathologic diagnoses that are included in the current proposed Bar Harbor GEM classification scheme were also uncommon in two year old control B6C3F1 mice. Whereas lymphocytic infiltration in the prostate was fairly common (approximately 30 % of DLPs and VPs, 20 % of APs), more pronounced degrees of inflammation, including neutrophilic infiltrates within prostate acini as described for the classification of active prostatitis herein, were uncommon (approximately 1, 3, and 5 % for AP, VP, and DLP respectively) (1). Atrophy was noted in only the AP of two of 612 mice and possible mucinous metaplasia in only one DLP (1).

The low incidence of pathology in the prostate of wild type mice suggests that any of the lesions described herein, including inflammatory and other non-neoplastic disorders, could be a consequence of the genetic manipulation involved. Mechanisms for these lesions could involve systemic effects (e.g., immunologic or endocrinologic effects) as well as direct consequences in the prostate and careful consideration must be given to the possible biology of the genetic manipulations as well as to the pathology in other organ systems. Some differences in the frequency of spontaneous lesions could exist between different genetic strains of mice. This should be borne in mind, particularly for mild phenotypes occurring in a small percentage of examined animals.

Importance of adequate controls, especially for aged mice, and of blinded histopathologic assessment: Obviously it is important when characterizing new GEM models to have appropriate controls, typically composed of aged matched mice of identical genetic background. As some of the lesions developing spontaneously in wild type mice may be more frequent with aging, adequate controls and blinded histopathologic assessment is particularly important for more subtle phenotypes that may be detected only in older mice. Blinded histopathologic analysis is highly desirable in all studies characterizing lesion development and progression in new models, as well as in genetic crosses where the phenotype may be altered or in interventional trials where histopathology is an endpoint. Blinded histopathologic analysis for data collection can be performed in a blinded fashion after initial review of possible pathology in engineered mice. Characterization of GEM models for Pca should, when at all possible, include the participation of an experienced pathologist, and preferably one with experience in human prostate pathology and mouse pathology. Members of the MMHCC Prostate Pathology Committee are available for review of pathology material generated by investigators engaged in GEM research, both within and outside the MMHCC. Centralized review of particularly promising models, including in future Pathology Workshops is desirable.

Importance of genetic background: It is certainly anticipated that the genetic background could have modifying influences on lesion development and/or progression in GEM models of prostate disorders. Some examples of the possible influence of different genetic backgrounds on neoplastic progression have been observed in some of the models described herein (2, 3). A corollary to this is that great care should be taken in describing the genetic background and breeding strategies involved in the creation of new GEM models or in the production of mice for other studies from breeders of existing models, including those obtained from other laboratories. Subtle or even pronounced differences in phenotype or natural history of existing models could be observed when alternate genetic backgrounds are obtained from different breeding strategies. Rigid data has not been thoroughly collected or reported on the precise reproducibility of lesion progression between one set of animals and sequential sets in some models employing strategies involving genetic instability. Hence environmental or other more random factors influencing the ultimate phenotype cannot always be excluded, but these are in general more difficult to control.

The role of natural history in model characterization: The importance of the natural history of neoplasia progression was stressed as fundamental to the characterization of any given model. The time course of lesion development and progression and any defined accompanying molecular alterations are important characteristics of a model that may allow for determination of its suitability for specific research applications that may be relevant to a particular aspect of the biology of human Pca. Individual GEM models may show different histopathologic features at different ages, and a careful description of the frequency of specific lesions at specific time points is vital.

Certain general features of the natural history of human Pca are well known and considered as clinically relevant and desirable in mouse models of Pca, such as development of invasive gland forming cancer from in situ precursor lesions, progression to locally advanced disease, metastases to lymph nodes and bone, and progression to hormone refractory disease. It is unlikely that any given model will faithfully mimic even these general aspects, aside from other issues of heterogeneity in the morphologic and molecular aspects and clinical behavior of human Pca. In addition to accurate descriptions of the temporal progression of histopathologic alterations, any detected molecular alterations with progression are important parameters of model characterization. Many of the genetic and molecular alterations observed so far in individual models are described herein. In addition to the possible prediction of novel genetic changes in human Pca progression, identification of molecular alterations in GEM models that are already known in some human Pcas will identify models that may be useful for elucidating the role of those changes in tumor progression as well as for testing targeted therapeutic strategies. In addition to pathologic features based on the classification scheme described herein, it is intended that the natural history and accompanying molecular and genetic alterations will be part of the information available on WEB sites described in the Appendix for GEM models of Pca.

Anatomic Considerations:

Anatomy of the human prostate and zonal origin of prostate carcinoma (Pca): There are some similarities between the mouse and human prostate, which help support the application of mouse models for elucidation of molecular alterations that accompany Pca development and progression. However, there are also some crucially important differences between the prostate in the two species, including in the gross and micro anatomy, that have implications for certain basic aspects of pathology analysis in mouse models and for the application of the models to certain clinicopathologic issues in human Pca. Despite the recognition of distinct lobes in the developing human prostate, these are not identifiable in the adult prostate, which does not have a defined

discreet lobe structure. Past use of terms such as lateral and posterior lobes have been supplanted by the concept of specific zones within the prostate that are anatomically recognizable, have characteristic histologic features, and importantly, have specific predispositions to benign or malignant neoplastic growth.

As described by McNeal (4-6), the human prostate is composed of the anterior fibromuscular stroma, occuping up to one-third of the prostate volume in the normal prostate and with no or minimal glandular tissue, the periurethral transition zone (TZ), the peripheral zone (PZ), and the central zone (CZ) (Figure 1). The CZ surrounds the ejaculatory ducts (Figure 1c) and comprises an increasing portion of the prostate from where the ejaculatory ducts enter the urethra, near the prostatic utricle at the verumontanum, superiorly towards the base. The CZ glands have characteristic morphology, with large complex glands showing a more irregular luminal border, with epithelial tufting, papillary formations, and frequent Roman arches or even cribriforming (Figure 1c-e). Such glands can be distinquished from high grade prostatic intraepithelial neoplasia (HGPIN) on biopsy by their lack of significant cytologic atypia. Although the CZ is typically encased by the prostatic capsule, it can rarely be seen to extend beyond the capsule medially at the prostate base (7). The human prostate is derived from the urogenital sinus, whereas the seminal vesicles and ejaculatory duct are Wolffian-duct derived (6). The histologic characteristics of the CZ and its spatial relationship to the ejaculatory ducts have raised speculation of a Wolffian duct-origin, which was supported in part by morphologic analysis of the prostate in patients with unilateral agenesis of seminal vesicles and vas deferens (8). However, there remains insufficient data at present to counter the presumed urogenital sinus origin for the CZ. The CZ is a rare site of origin for Pca (Pca), although it is not uncommonly seen in prostatectomy specimens to be secondarily involved by extension from a PZ tumor.

The TZ is exclusively the site of benign prostatic hyperplasia (BPH) in the human prostate (Figure 1a,h; Figure 4). BPH is not synonymous with benign prostate, and this term should not be used to refer to benign PZ prostate tissue intended as a control for usual PZ Pca tissues. BPH is a specific common TZ-confined abnormality, composed typically of nodules of glandular and stromal hyperplasia with or without more interior stromal nodules, that can be associated with urinary obstructive symptoms (6). This condition, which requires androgens, occurs microscopically in approximately 50% of men between the age of 51-60 years, increasing even further with age. Including lesser degrees of these changes, BPH-type histologic alterations in the TZ are present in as many as 90 % of radical prostatectomy (RP) specimens (removed for Pca). Although conceptually located in different regions of the normal human prostate, the morphologic distinction between TZ and PZ is made primarily by the "after the fact" involvement of the former by BPH changes (Figure 1a,b,h,j). Although composed of lobules of glands with shorter ducts compared to those reaching out to the PZ, in the young post-pubertal adult, architectural and histologic differences in the glands of the TZ and the PZ are not well defined. These more interior regions of the human prostate are somehow predisposed to the nodular glandular and stromal hyperplasia that once developed allows us to recognize and define the TZ in the aged prostate.

The mouse prostate does not undergo such spontaneous nodular glandular and stromal hyperplasia in regions potentially analogous to the human TZ. Hence, no anatomically defined lobes or regions of multiple lobes in the mouse prostate are analgous to the human TZ. This has bearing on some of the specific entities in the mouse prostate pathology classification scheme described herein and their translation between human and mouse. For example, epithelial hyperplasia in the human prostate is most typically used as a pathologic description in the context of TZ BPH (described below), and the term well differentiated adenocarcinoma for the human prostate

9

is typically reserved for tumors containing Gleason patterns 1 and 2, located primarily in the TZ (i.e., as in Gleason score 2-4 tumors). However, in the Bar Harbor classification scheme for mouse prostate pathology, the designation well differentiated is applied to invasive adenocarcinomas composed predominantly or exclusively of well formed glands, without any implied translational meaning to region of origin.

Only approximately 20 % of clinically significant Pcas, but perhaps a higher percentage of latent or autopsy cancers originate in the TZ (5, 7, 9). Such TZ tumors often have at least characteristic, if not specific, histology (10, 11) (Figure h,i), and evidence supports that such tumors may arise from different genetic alterations and precursor lesions than Pca that occurs in the PZ (12). TZ tumors, especially when small, are often seen in association with BPH nodules (9). However, BPH as a clinical condition is NOT considered to be a risk factor or precursor for Pca. Prostatic intraepithelial neoplasia (PIN), including HGPIN, is rarely seen in the TZ (in contrast to its common occurrence in the PZ, where it is the presumed precursor for most PZ tumors). In contrast, a lesion defined by pathologic criteria referred to as atypical adenomatous hyperplasia (AAH) (or adenosis) is a putative precursor lesion for usual TZ tumors (12). TZ tumors are often Gleason pattern 2 and occasionally even Gleason pattern 1, being comprised of fairly circumscribed proliferations of closely spaced malignant glands, which often have ample clearer cytoplasm and larger gland profiles than the more usual Gleason pattern 3 PZ tumors (Figure 1h,i). Such lesions can infiltrate amongst benign glands, constituting Gleason pattern 3, and hence many TZ tumors detected clinically are Gleason score 4 or 5. TZ localized or tumors apparently originating in the TZ not uncommonly contain areas of less differentiated Gleason pattern 4. However, even in the latter case, whether due primarily to a more interior location and hence less propensity to extend beyond the prostate, or due to as yet undefined biologic differences, TZ tumors appear to have a better prognosis than more usual PZ tumors (13, 14).

The PZ contains the majority of the glandular tissue in the normal human prostate, approximately 75 % in prostates without BPH, and represents the most frequent site of Pca origin (7, 9, 10). It is located predominantly in the posterior and lateral aspects of the gland (Figure 1 a,b,h,j) extends to the apex and variably anteriorly, and laterally surrounds the CZ at the base. This predominantly posterior and lateral location explains why digital rectal examination is important in clinical detection of Pca, why most palpable tumors (i.e., clinical stage T2 vs. T1c) are located in the PZ (14, 15), and why transrectal biopsies are typically targeted to the PZ rather than the TZ. The PZ origin of most Pcas also dictates important anatomic relationships for prostate capsule penetration and extracapsular extension (ECE). Normal benign prostate glands, in their lobular configuration, are surrounded by a prominent stroma of contracting spindle cells and collagen (6, 16). This fibromuscular stroma, which is so much more abundant in the human compared to the rodent, extends beyond the outer perimeter of the glands and forms a more or less distinct capsule, separating the prostate from periprostatic fat. The capsule is best defined in the posterior and lateral portions of the human prostate (Figure 1 h,j) (6, 16). Standard pathologic staging of radical prostatectomy (RP) specimens addresses the absence or presence of ECE (i.e., pT2 or pT3 tumors), a major prognostically significant cutoff for increased risk of progression following surgical treatment (7, 9, 17). Progressive levels of capsule invasion short of extension into periprostatic fat (ECE) may also have prognostic significance (18). Nerve bundles which facilitate ECE are located particularly in the posterolateral aspect of the gland, with the largest nerve plexus at the base, and a smaller one at the apex (5). The typical site of ECE is thus at the posterolateral aspect of the human prostate gland, particularly at the base, which is also a common route for invasion of seminal vesicles, which are at the superior posterior aspect of the prostate (5, 7, 9).

The PZ is the predominant, essentially exclusive site of PIN in the human prostate. Epithelial hyperplasia analogous to that seen in TZ BPH does not occur. Instead epithelial proliferation occurs within the confines of pre-existing normal gland profiles, and is designated as low or high grade PIN based predominantly on nuclear features as described below. Invasive acinar forming carcinomas associated with HGPIN in the PZ are generally considered moderately differentiated; that is, Gleason pattern 3 (7, 9) (e.g., see Figure 6a). Especially with progressive tumor growth, potential dedifferentiation with deveopment of morphologies assigned higher Gleason patterns (Figure 1k) is thought to occur as a common manner of tumor progression in usual PZ tumors (7, 9, 10). However, HGPIN may also be observed in association with smaller volume high grade (Gleason score 8-10) tumors in the PZ (19).

Histology and phenotype of human prostate glands: In the human prostate, benign glands are composed of a basal cell layer and luminal differentiated secretory cells (i.e, two cell types), with some immunophenotypically defined transitional or intermediate forms and a small subpopulation of cells showing neuroendocrine (NE) differentiation (6, 20, 21). Benign glands are larger than typical cancer glands, and have an undulating or slight tufting luminal contour due in part to stratification or pseudostratification of secretory cells and the mechanisms of secretion (6, 22) (Figure 1f). Basal cells in benign human prostate glands are the dividing or progenitor cell (a subset of which may be the true prostatic "stem cells"), giving rise to the differentiated secretory cells lining the gland lumens and most likely to NE cells as well (21, 23). Basal cells tend to be oriented parallel to the basement membrane, are not always conspicuous by light microscopy, and can be difficult to distinguish from underlying spindle stromal cells (6). They are routinely recognized by immunostaining with antibodies to high molecular weight cytokeratin (HMWCK) (Figure 1g). Malignant prostate glands do not possess such a basal cell layer, with the atypical cells presumably representing aberrantly differentiated or neoplastic counterparts of secretory cells. Pragmatically, the absence of an immunophenotypically defined basal cell layer is a useful adjunct for recognizing malignant glands and distinguishing them (particularly in biopsies) from small gland profiles of benign glands or certain well described mimics of Pca, such as atrophy, partial atrophy, and atypical adenomatous hyperplasia (adenosis) (7, 9, 24-26).

Anatomy and histology of the mouse prostate: In contrast to the human, the rodent prostate is divided into añatomically distinct lobes, which are not encased by abundant fibromuscular stroma and a "capsule" into a single discreet gland demarcated from periprostatic adipose tissue as in the human prostate. The mouse prostate can be separated into the anterior prostate (AP) or coagulating gland, the ventral prostate (VP), and dorsal and lateral lobes, often grouped together as the dorsolateral prostate (DLP) (Figure 2 a,b) (27). The individual glands making up each lobe of the mouse prostate are surrounded by an extremely thin fibromuscular stroma, composed of only a few layers of bland spindle cells interspersed amongst eosinophilic collagen (Figure 2c-h). The stroma of each duct or gland is immediately surrounded by loose connective tissue (Figure 2c-h), imparting a lobular architecture to the prostate. The abundant intervening dense stroma surrounding the glands and immediate stroma of adjacent "lobules" is not present as in the human prostate (compare to Figure 1 a,b,h,j) (16). In addition, nerve bundles which are seen within the prostate fibromuscular stroma (interior to the capsule) in the posterolateral aspects of the human gland, are not observed within the thin rim of contractile mouse stroma. Rather, nerves and ganglia are typically appreciated microscopically in the peristromal loose connective tissue, often in sections of the DLP. Hence, there are clearly differences between the species regarding anatomic relationships fundamental to carcinoma extension outside of the prostate in the human (e.g., amount of stroma, location of nerves, presence of a "capsule" between prostate and periprostatic fat, seminal vesicle proximity to

sites commonly involved by ECE in the human). *It was therefore the opinion of the Bar Harbor Pathology Panel that mouse models may not be adequate or suited to address these particular clinicopathologic or staging issues related to ECE in human Pca.* Although in the human, lymph node metastases are rarely seen in organ confined Pca vs. tumors with ECE (7, 9), mechanisms relevant to regional or distant metastases may still be related between the two species.

It has been stated that the mouse DLP is the most homologous to the human PZ (16, 28-30), which may be particularly emphasized by investigators whose models develop lesions exclusively or primarily in the DLP as a further validation of the model. The embryologic development of the mouse prostate has been examined in detail and reviewed previously (27-29). The specific developing lobes identifiable in the embryo remain recognizable in the postnatal and adult mouse prostate, as the lobes described above. These developing lobes are recognizable as such in the human ONLY in the embryo (28). *It was the consensus opinion of the Bar Harbor Pathology Panel that there is no direct or currently defined relationship between the specific mouse prostate lobes and the specific zones in the human prostate.* As such, there is currently no data to *a priori* consider it better or worse or more relevant to human Pca to have neoplasia involving one lobe or another in the mouse prostate. It is possible in the human prostate that the zones described above contributed to by more than one embryologically recognizable "lobe". A corollary to this principle of not prejudging GEM models based on lobes involved includes the mouse VP. In the human, the periurethral buds representing the potential VP anlage in the embryo regress or fail to develop. Concluding that lesions in the mouse VP are not as relevant to human Pca compared to lesions developing in other mouse lobes would at present appear to be a tremendous oversimplification. Such anatomic restrictions would imply that the other lobes are in themselves greatly analogous to the histology, function, and gene expression profiles of the human prostate. Such comparisons are far from established. Dissimilarity is evident between the human and mouse prostate not only structurally, but from the very fact that the mouse prostate does not develop Pca spontaneously. Perhaps another way of looking at this issue is the fact that the mouse prostate lobes are sufficiently dissimilar from the human prostate, that each of the lobes (including the VP) is essentially equally dissimilar. Although there are some established differences in the secretory products of the individual lobes of the mouse prostate (29), how this translates to the zones of the human prostate is also not known. Therefore, the VP lobe that persists in the mouse may be essentially just as homologous as the other mouse lobes to the portions of the human prostate that do develop. It is likely that the closer the genetic manipulations and the secondary molecular alterations that ensue in any mouse model are to the complex sequence and combinations of genetic alterations in human Pca the more likely any model is to have particular relevance to at least a subset of human Pcas. Support for this position on anatomic considerations in mouse models includes the fact that similar alterations in gene expression have been demonstrated between human Pca and mouse tumors arising in the VP in multiple GEM models. When attempting to characterize a new GEM model of Pca, all lobes (including the AP) should be processed, analyzed and described.

The mouse AP is closely apposed to the seminal vesicles, along its entire curving length (Figure 2a). Histologically, it normally demonstrates a more papillary and cribriform growth pattern than the other lobes, with cuboidal to columnar epithelial cells containing typically central nuclei with inconspicuous to small nucleoli, and eosinophilic granular cytoplasm. The gland lumens contain abundant slightly eosinophilic secretions (Figure 2c). The growth patten of the epithelium in the AP and its close spatial relationship to the Wolffian duct derived seminal vesicles are somewhat analogous to the growth pattern of the glands in the human CZ and its relationship to the also Wolffian duct-derived ejaculatory ducts. This leads to some speculation that the mouse AP is

12

homologous to the human CZ, the origins of which are discussed above. The mouse AP is clearly derived from the urogenital sinus (27). The mouse DP is composed of branching ducts and glands lined by simple columnar and occasionally slightly stratified and tufting epithelium (Figure 2d,e). The moderate degree of infolding is intermediate between the AP and the flatter luminal borders of the lateral and ventral prostate. The secretory cells of the DP are typically columnar with lightly eosinophilic granular cytoplasm, and the central to basally located small uniform nuclei contain inconspicuous or small nucleoli. Gland lumens contain homogenous eosinophilic secretions (Figure 2e). The LP has flatter luminal edges, with only sparse infoldings, with the abundant luminal space containing more particulate eosinophilic secretions (Figure 2d). The epithelium is cuboidal to short columnar, with more clear to lightly granular cytoplasm and small uniform basally located nuclei. The VP also has flatter luminal edges and only focal epithelial tufting or in-folding (Figure 2f,g). The abundant luminal spaces typically contain homogenous pale serous secretions. The nuclei are small, uniform, typically basally located, and have inconspicuous to small nucleoli (Figure 2g).

The glands of each of the mouse prostate lobes appear to have normal cell populations homologous to the human prostate, including luminal secretory cells, a basal cell layer, and a minor population of NE cells. In the mouse, as in normal human prostate glands, a basal cell layer is not conspicuous by routine light microscopy, and ultrastructural studies had previously reported the lack of a continuous basal cell layer in normal mouse prostate glands (31). A previous study had reported that antibodies to HMWCK (66kDa and 57KDa), which identify the basal cell layer in benign human glands, did not identify a similar phenotypic basal cell layer in normal mouse glands (32). However, a more recent study utilizing a rabbit polyclonal antibody to mouse cytokeratin (CK) 5 showed staining of an apparent basal cell layer in histologically normal prostate glands with possible reduced expression in PIN-containing glands in a transgenic mouse model with overexpression of human insulin like growth factor-I (IGF-I) on a bovine keratin 5 promoter (33). This antibody has been successfully utilized by other laboratories, confirming the presence of this immunophenotypically defined basal cell layer in normal mouse prostate glands (Figure 2h), as well as its variable expression in PIN glands in other transgenic mouse models (S.B.S., R.L.R., unpublished observations). Similar results have been achieved with antibodies to CK14 (34) (R.D.C., unpublished observations) and even with a murine antibody against human HMWCK that is commonly employed in human prostate pathology (35). Possible application and limitations of these antibodies to HMWCK in facilitating recognition of invasive carcinoma in mouse models are described below. Limited markers exist for secretory cell differentiation in the mouse prostate, such as antibodies to the dorsolateral prostate protein (36). Immunostaining for chromogranin (CG) demonstrates a very minor population of immunophenotypically defined NE cells in the normal mouse prostate (32, 37). Such cells appear to represent < 0.3 % of the normal mouse prostate cell population (P.A.H., unpublished observations).

Ampullary glands: The ampullary glands in the mouse have no known human counterpart. The ampullary glands in rodents add secretions to the semen that contribute to fertility (38). Familiarity with their gross and microscopic anatomy is important for the proper interpretation of lesions that may be noted in the male accessory glands of GEM (39). The ampullary glands are of Wolffian duct origin, in contrast to the urogenital sinus origin of the prostate. These structures are androgen-dependent glandular outpouchings of the proximal ductus deferens, with one gland on each side. Duct budding and branching occurs in the postnatal period. The single proximal ducts of the ampulary glands enter into the ductus deferens proximal to the seminal vesicles. Although they may be separately dissected to facilitate their identification, they can also be identified by their characteristic location and their characteristic secretions when seen in sections of male reproductive

13

organs submitted en bloc as described in the protocols section below. The epithelium is simple columnar and in comparison to the prostate ducts, the surrounding fibromuscular stroma is thicker in the ampullary glands. The secretions have a characteristic "swiss cheese" appearance, with holes noted in the dense eosinophilic secretions. Enlargment with epithelial hyperplasia was noted in the ampullary glands (and other Wolffian duct derived tissues, such as seminal vesicle), but not the prostate lobes, in mice overexpressing int2/Fgf-3 under the control of the mouse mammary tumor virus long terminal repeat (MMTV-LTR) (39).

Bulbourethral glands: The bulbourethral glands (BUGs) and periurethral glands are also androgen regulated derivatives of the urogenital sinus. As some strategies for targeting transgenes to the mouse prostate have also resulted in transgene expression and pathology in these other male accessory glands, familiarity with their location and histologic features is important for adequate pathologic characterization of GEM models of Pca. In contrast to the prostate, which does not show histologically distinct acini and excretory ducts, the periurethral and bulbourethral glands have a "biphasic" appearance, with lobules of secretory acini and central excretory ducts that empty into the urethra.

The bulbourethral glands in the male mouse are analgous to Cowper's glands in human males, which are located subjacent to the urethra in the suburothelial connective tissue at the membranous portion of the urethra, immediately distal to the prostatic apex. Such glands can occasionally be seen in apical portions of radical prostatectomy specimens and are rarely sampled "accidentally" in transrectal biopsies, where they may cause diagnostic confusion. In the human, the bulbourethral or Cowper's glands are rarely the site of origin of carcinoma, with these tumors being the subject of only a few case reports.

In the mouse, the bulbourethal glands are located more distally along the urethra, separated more distinctly from the prostate, and lying under the bulbocavernous muscle (28). They are composed of acini arranged in lobules, the cells of which have basally located nuclei and abundant pale mucinous cytoplasm. These acini empty into centrally located short excretory ducts that are lined by cuboidal epithelium (40).

Periurethral glands: In the human, the periurethral glands (glands of Littre) are located along the penile or spongy urethra. Again, these glands are rarely the site of cancer origin. Of note, in keeping with their developmental relationship to the prostate, these tissues can express PSA. In the mouse, the periurethral glands are located in the suburothelial tissue distal to the portion of the urethra that the prostate ducts empty into. They are not routinely dissectable from the prostate and other male accessory tissues grossly, but are commonly seen in "en bloc" sections (e.g., see Figure 12 in the Protocols section) or in sections of remaining tissue (including urethra and proximal SV and prostate ducts) submitted after dissection and separate submission of individual prostate lobes. The periurethral glands are composed of lobules of acini and short excretory ducts that open into the urethra (e.g., see Figure 11). In wild type mice, the acinar epithelium is cuboidal with oval nuclei and a denser more eosinophilic granular cytoplasm compared to secretory cells of the BUGs, and in which secretory granules may occasionally be seen (40).

The Bar Harbor Pathology Workshop - Materials and Methods:

The Pathologic Classification of Prostate Lesions in GEM is the result of a directive from the MMHCC Prostate Steering Committee to provide a specific hierarchical taxomony of disorders of the mouse prostate to facilitate classification of existing and newly created mouse models and their translation to human prostate pathology. The classification system described herein is the

14

culmination of three meetings and workshops attended by various members of the Prostate Pathology Committee of the MMHCC. In April 2001, an initial two day meeting was held at Vanderbilt University Medical Center (organized by S.B.S. and attended by S.B.S., R.L.R., R.H., N.R., R.B., J.M.W., R.D.C.), in which models were presented, slides were reviewed, approaches to classification of mouse prostate disorders were discussed, and plans were made for the eventual Pathology Workshop to be held in conjunction with the October 2001 MMHCC Prostate Organ Site meeting. These processes were continued and a hierarchical taxonomy of mouse prostate diseases was drafted with annotated images at the two day Pathology Committee meetings (attended by S.B.S., R.L.R., G.V.T., N.R., J.M.W., R.D.C.) accompanying the MMHCC Steering Committee meeting in San Francisco in July 2001. Finally, a formal two day Pathology Workshop was held at Jackson Laboratories in Bar Harbor Maine in October 2001, preceeding the NCI MMHCC sponsored Conference on Modeling Human Pca in Mice at Jackson Laboratories on Oct. 18-21, 2001. This session was organized by S.B.S. and attended by members of the MMHCC Prostate Pathology Committee (S.B.S., R.L.R., G.V.T., R.H., J.M.W., R.D.C.), a representative of Jackson Laboratories (J.P.S.), and three invited "outside" prostate pathology experts (M.A.R., P.A.H., M.M.I.), who were chosen by the Prostate Pathology Committee Chairman on the basis of their well recognized expertise in human prostate pathology, their research interests in Pca, and their experience with characterization and utilization of GEM models of Pca. The combined efforts leading to the Bar Harbor Classification represent a balanced effort of investigational human (M.D. and/or M.D./Ph.D.) pathologists (S.B.S., R.L.R., G.V.T., M..A.R., P.A.H., M.I., R.B., R.D.C.) and veterinary (D.V.M. and/or D.V.M./Ph.D.) pathologists (R.H., J.P.S., N.R., J.M.W.), typically with specific research interests in Pca and in studies employing GEM.

For the Bar Harbor meeting, paraffin blocks and/or glass slides from 24 models of GEM were made available to the organizer of the Prostate Pathology Workshop (S.B.S.) through generous donation by investigators from across the country (Table 1). A complete set of these slides was brought to the Bar Harbor meeting and slides and images derived from them were shared with all of the pathologists. Provided paraffin blocks were sectioned and H & E stained before hand and supplemented with sets of H & E stained slides from individual investigators to allow for the creation of personal study sets of individual slides from 22 of these models (Table 1). Some models included different ages of mice and/or different tissues, such that study sets of 93 slides from these 22 models were provided to the 10 panelists at the Bar Harbor meeting. For some models, paraffin blocks or slide sets were not provided, but a single slide set was provided to S.B.S.. These slides and images derived from them were also brought to the meeting. All of these slides were reviewed in detail at the meeting and the individual slide sets were retained by the individual pathologists for later review.

The specific objectives for the Pathology Panel were the following: 1) Development of a classification scheme for disorders of the prostate and related organs in GEM; 2) Provision of histopathologic definitions for these disorders; 3) Collection and annotation of images illustrating these disorders, utilizing as many of the provided models as possible; 4) Collection, organization, and distribution of pathology protocols useful in characterization of prostate disorders in GEM. S.B.S. organized the meetings with input from R.D.C. S.B.S. prepared the entire text of this manuscript, incorporating ideas and comments made at the time of the meeting and subsequently by the Panel members. S.B.S. composed the figures contained herein with the valuable participation of R.L.R. G.V.T. compiled the protocols contained in the Appendices, with input from R.H. G.V.T. and R.H. provided images to S.B.S. for figure 12. J.M.W. and R.D.C. provided input in editing of protocols. The photomicrographs in Figures 1 through 11 were prepared from images of the slide

sets of the Bar Harbor meeting obtained with a Nikon Professional Digital SLR D1 camera, resolution 2012 x 1324 pixels and 12 bits per color, attached to an Olympus BX50 5-headed microscope with U-PLAN objectives. Images were captured using Nikon Capture software and processed in Photoshop, with final figures generated as JPEGs at 200 d.p.i. In figure legends, images referred to as low, intermediate, and high magnification typically represent original magnifications of 40x, 100x, and 400x, respectively.

Pathologic Classification of Disorders of the Prostate in Genetically Engineered Mice (The Bar Harbor Classification-Table 2):

Disorders of Development. Agenesis/Aplasia and Hypoplasia: *Agenesis* describes the absence of an organ due to the lack of formation and development of its primordium in the embryo. Absence of the prostate should be distinguished from a small prostate due to developmental reasons, that is hypoplasia, or due to secondary regression, as in atrophy. *Hypoplasia* refers to inadequate development or underdevelopment of an organ. The prostate should be small for age and may or may not have associated histologic abnormalities (Figure 3a).

Developmental abnormalities of the prostate may be associated with more widespread abnormalities of the genitourinary tract and/or other organ systems. Very few specific prostate developmental disorders are described in the human. The prostate is not appropriately developed in patients with disorders of androgen synthesis or signaling. The prostate is small in patients who have autosomal recessive deficiency of type II 5α-reductase (41), due to absent or inadequate formation within the prostate of dihydrotestosterone (DHT) from circulating testosterone. DHT is necessary for normal prostate development as well as the development of BPH. 5α-reductase occurs in two different isozyme forms, type 1 and type 2. Although individual studies differ slightly regarding tissue specific expression, the prostate predominantly expresses type 2, whereas type 1 is expressed primarily in liver and skin (42). Patients with 5α-reductase deficiency have a 46 XY karyotype. In addition to a small prostate, these patients have features of male pseudohermaphrotidism, with a clitoriform penis and bifid scrotum at birth and with the development of the penis and scotum at puberty (41).

Given the utility of rodents and particularly GEM in deciphering key factors in normal prostate development and differentiation, it can be expected with increasing frequency that genetic manipulation of pathways implicated in prostate development will lead to mouse models with prostate abnormalities. Further, given the potential relationship between pathways regulating normal development and their altered expression or function in neoplasia, genetic manipulations intended to result in prostate neoplasia may also be characterized by abnormal development. Examples of abnormal prostate development have already been reported in GEM, including as part of a constellation of more widespread abnormalities. For example, although the vast majority p57^{Kip2} deficient mice die within 24 hr and exhibit multiple skeletal abnormalities, examination of the 10 % that survive beyond weaning shows "immaturity" of the prostate, seminal vesicles, and testes, along with growth retardation (43).

p63 knockout mice also have abnormal prostate development. *p63* is a recently identified homologue of the *p53* tumor suppressor gene. The *p63* gene encodes multiple isotypes, some of which are able to transcribe *p53* reporter genes and induce apoptosis. Other isotypes transcribed from an internal promoter localized within intron 3 appear to be capable of acting as dominant-negatives to suppress transactivation by *p53* and the other p63 isotypes (44). *p63* is selectively expressed in the basal cell layer of a variety of epithelial tissues, including prostate (44). By

immunostaining, *p63* is expressed in the basal cell layer of both the human and mouse prostate. In contrast, in human Pca, *p63* immunostaining is absent (45) , similar to the "loss" of a basal cell layer in malignant prostate glands as determined by immunostaining for HMWCK. However, p63 knockout (p63 -/-) mice die at birth (46), making it difficult to demonstate the role of this gene in normal prostate development. *p63*-deficient mice show severe defects in the development of multiple epithelial organs that express p63 protein (46). To assess the role of p63 in prostate development, Signoretti et al. histologically analyzed the periurethral region in day 1 p63 -/- male mice and demonstrated that the prostate does not develop in these animals (45). Histological examination showed no ducts or epithelial buds either in the ventral or in the dorsolateral region of the periurethral mesenchyme compared to the presence of these solid buds and small gland epithelial structures in similar sections of the periurethral region in control mice (45).

Homeobox genes are important in prostate development and cell determination within the developing male genitourinary tract (29, 47). Hoxd-13 is expressed in mesenchyme and epithelium of the lower genitourinary tract in the perinatal period, including focally in the budding nascent ducts of the developing mouse prostate (48). Temporal expression correlates with prostate duct morphogenesis in the post-natal period. Transgenic Hoxd-13 deficient mice have multiple abnormalities in development of the male accessory glands, including agenesis of the bulbourethral glands, diminished seminal vesicle luminal folding, and decreased size and ductal branching in the dorsal and ventral prostate (48). Hoxa-13 is also widely expressed in the developing lower genitourinary tract. In animals with a spontaneously occurring heterozygous mutation involving a 50 base pair deletion in exon one of one Hoxa-13 allele, there is decreased size and branching of the dorsolateral and ventral prostate as well as abnormal seminal vesicle morphology, a phenotype that overlaps that observed in Hoxd-13 deficient mice (49). Bhatia-Gaur et al. recently reported abnormalities in prostate ductal morphogenesis and reduced development of secretory differentiation in both the prostate and BUGs, compatible with hypoplasia, in mice homozygous for a null mutation in the androgen regulated murine Nkx3.1 homeobox domain (50). This abnormality and the associated PIN like lesions that develop in these mice are described further below.

Regarding androgen metabolism defects, 5α-reductase type 2 knockout mice have abnormal development of the prostate, similar to human patients with autosomal recessive 5α-reductase type 2 deficiency, whereas 5α-reductase type 1 knockout mice have an apparently normal prostate phenotype (42).

Metaplasia: Metaplasia refers to the replacement of one adult cell type (epithelial or mesenchymal) by another adult cell type. Metaplasia is presumably a reversible process, potentially occurring in response to some sort of stress for which the new cell type is better suited. In the human prostate, well recognized forms of metaplasia include transitional (urothelial) metaplasia, mucinous metaplasia, and squamous metaplasia. However, unlike implicated metaplasia-dysplasia-carcinoma sequences in some organ sites, these are exceedingly uncommon precursor lesions for carcinomas in the prostate. Invasive mucinous carcinoma, an uncommon form of high grade Pca (7, 9) has rarely been observed to be associated with HGPIN with similar signet ring mucinous cells (51).

In addition to the prostatic urethra, urothelial or transitional epithelium typically extends a variable length along primary periurethral ducts (Figure 3b). Urothelial metaplasia is not uncommonly seen admixed with more typical secretory cells for variable lengths along secondary periurethral ducts and is not uncommonly seen in prostatectomy specimens or biopsies to involve even more distal PZ glands (6). Transitional metaplasia is commonly observed following anti-androgen therapy, including with castration or synthetic estrogen administration in the past, and

perhaps less frequently and/or less extensively with currently employed Lupron/Flutamide therapy (6, 7, 9). Metaplasia likely arises from altered differentiation of basal cells rather than from differentiated secretory cells. Transitional or urothelial metaplasia is recognized by its resemblance to normal bladder urothelium (Figure 3c), and its cells commonly exhibit focal nuclear grooves characteristic of urothelial cells. Also, similar to normal urothelium, it stains strongly and uniformly with antibodies to HMWCK, such that this property cannot be used to distinguish basal cell hyperplasia and transitional metaplasia. Indeed the two may be seen together, for example, in response to anti-androgen therapy. The prostatic urethra, periurethral ducts, and even peripheral lobules of the prostate can be involved extensively by urothelial carcinoma in situ with or without stromal invasion (7, 9), which is almost uniformly associated with urothelial carcinoma in the bladder (52). Prostate involvement by urothelial carcinoma is either by direct extension of the urinary bladder disease or as part of a "field effect".

The prostatic urethra not uncommonly shows squamous metaplasia, possibly in response to chronic irritation, and squamous metaplasia can be seen focally in more distal or peripheral regions of the prostate and adjacent to infarcts involving BPH nodules in the TZ (6). Squamous metaplasia can occur more extensively in the prostate in response to anti-androgen treatment or with estrogen treatment for Pca (6), and is in fact a well documented response to estrogens in a variety of species, including in rodents.

Mucinous metaplasia, in which prostate secretory cells show cytoplasmic mucin, often with basilar displacement of the nucleus, similar to intestinal goblet cells is usually a very focal process (6). It is of no clinical significance, but it is important to not confuse it for carcinoma, for example, when it is associated with intraluminal blue-tinged mucin, as the latter is more common in Pca than benign glands (7, 9, 53). There is certainly no established precursor relationship to the unusual mucin-rich or mucinous carcinomas of the prostate (7, 9).

Metaplasia is rarely noted in wild type mouse prostates. For example, in the survey of 2 year old B6C3F1 mice referred to above, a form of possible mucinous metaplasia (with less pronounced goblet cells compared to GEM examples described herein) was noted in only one of 612 mice (1). Metaplasia in the prostate of GEM may arise in response to similar initiating stimuli as described above for human prostate or may more uniquely arise as a consequence of the specific genetic manipulation. Foci compatible with transitional metaplasia have been observed in the partially atrophic or regressing PIN-like lesions in faster growing lines of LPB-Tag mice following castration (29, 54) (S.B.S., unpublished observations) (Figure 3d). An interesting form of intestinal or adenomatous metaplasia has been observed in GEM created with H-ras expressed in the prostate with a probasin promoter (Pb-ras +/+), with or without crossing to mxil -/- mice (R.D.C., Schreiber-Agus, N. unpublished observations) (Figure 3e). The type of metaplasia observed in GEM should be specified and if nuclear atypia (potentially constituting dysplasia) is present, it too should be noted and described.

Atrophy: Atrophy is a common "spontaneous" histologic alteration in the human prostate, in which shrunken or dilated glands are lined by a flattened epithelial lining. In the TZ, it often takes the form of cystically dilated glands imparting a "swiss cheese" appearance. In the PZ, atrophy may have a similar appearance, but is often seen as angulated dark appearing glands in which the flat luminal lining gives a high nuclear to cytoplasmic ratio and hence a hyperchomatic appearance (Figure 3f). A somewhat infiltrative sclerotic appearance can be seen with atrophic glands, and such foci are well recognized histologic mimicks of Pca in human biopsy samples (6). A possibly related entitiy is post-atrophic hyperplasia (PAH), recognized histologically as a somewhat lobular configuration of small acini surrounding a larger, more angulated gland with flatter lining cells (55).

18

The cells in the small gland profiles have more cytoplasm than usual atrophy and can have prominent nucleoli, especially when associated with admixed inflammation, leading to diagnostic difficulties regarding distinction from Pca (56). A possible relationship to inflammation has been suggested for usual forms of atrohpy, and possible preneoplastic potential has been suggested for inflammation associated atrophy and PAH (57, 58). Spontaneous atrophy may represent, at least in part, a failure of cells to differentiate. The proliferation rates are actually higher in these "usual" forms of atrophy compared to normal benign glands (59), and epithelial cells in atrophic glands fail to express some antigens which are strongly expressed in differentiated secretory cells (60). Proliferation rates are even higher in PAH (59). In contrast, atrophy seen with hormone deprivation in humans may be more of an "active" involution, possibly involving apoptosis. Although foci similar to usual atrophy can be seen, especially in the PZ, other characteristic features such as basal cell hyperplasia and apical cell clearing (in addition to transitional and squamous metaplasia) can be seen with neoadjuvant hormone deprivation therapy (e.g., with combined Lupron/Flutamide) [Civantos, 1995 #801; Vaillancourt, 1996 #662].

In contrast to its common occurrence in prostates of middle aged and especially older humans (e.g., as seen in prostates obtained at autopsy or RP for Pca), spontaneous atrophy in the wild type mouse prostate is apparently extremely uncommon. In the survey of control 2 year old B6C3F1 mice, atrophy was noted only in the AP of two of 612 mice and approximately 1 % of seminal vesicles (1). Atrophy, with dilated gland profiles and flattened epithelium, typically associated with prominent inflammation, has been observed in castrated GEM (29, 54, 61) compared, for example, to the PIN lesions in intact similarly aged mice from these models (Figure 3i). Of note, HGPIN in the human also appears to be an androgen-responsive lesion (62).

Inflammatory Disorders

Prostatitis, active or chronic active: Clinicopathologic entities involving prostate inflammation or related disorders in the human include acute prostatitis, chronic bacterial prostatitis, chronic abacterial prostatitis, and prostadynia (63). These disorders are typically diagnosed by clinical features and laboratory procedures, although the histology when seen has characteristic features. Acute prostatitis is usually seen in younger patients and is caused by organisms associated with urinary tract infections and less commonly those associated with sexually transmitted diseases. Tissue is rarely procured, but demonstrates neutrophilic infiltrates within epithelium, gland lumens, and surrounding stroma, as well as stroma congestion and edema. Chronic prostatitis is common and is usually caused by organisms typically associated with urinary tract infections, especially E. coli and other coliforms and less commonly enterococcus. Patients are commonly symptomatic, and treatment is difficult. Reflux of infected urine is a likely contributing factor. Prostatic concretions (corpora amylacea and larger concretions) can serve as a nidus or reservoir for offending organisms and complicate eradication. Similar symptoms and laboratory evidence of inflammation in expressed seminal fluid but without culturable etiologic organisms is known as chronic abacterial prostatitis. Similar symptoms without laboratory evidence of inflammation is referred to as prostadynia, which may in part be due to increased contractal function of prostatic stroma, the bladder neck and urethral sphincter. Histologic features of chronic prostatitis are not uncommonly seen in transrectal biopsy (performed for abnormal digital rectal examination or elevated serum PSA) , and may be important to note as active inflammation may cause mild elevation in serum PSA.

Importantly, chronic prostatitis implies an active ongoing process ("chronic active prostatitis") and is NOT diagnosed by just the presence of possibly increased lymphocytes within the prostate stroma. Lymphocytes, including small lymphoid aggregate, are common in the prostate

19

stroma, may increase with age, and may be a particularly conspicuous component of glandular and stromal hyperplasia in BPH. Similarly, in mouse prostates, scattered lymphocytes in the stroma and small lymphoid aggregates in the stroma or peri-prostatic fat can be observed. In the pathology survey of 2 year old control B6C3F1 mice, such lymphocytic infiltration in the prostatic stroma was noted in approximately 30 % of DLPs and VPs and 20 % of APs (1). Although this feature can be described and assessed as it could be variable depending on genetic manipulation, it should not be classified as chronic prostatitis or active prostatitis in GEM. Chronic active prostatitis is characterized by neutrophils and monocytes (not readily distinguishable from lymphocytes in routine histology sections) within the prostatic epithelium and gland lumens (Figure 3g). This type of active inflammation, including with neutrophils and cellular debris within gland lumens, was noted in only approximately 3-5 % of DLPs and VPs and 1 % of APs in 2 year old control wild type B6C3F1 mice (1). It is important to keep in mind in diagnostic human prostate pathology that inflammation can lead to reactive atypia and proliferation (even cribriforming) in prostatic epithelial cells, including the presence of nucleoli (6). Similar reactive atypia can be seen in mouse prostate epithelium in association with active inflammation. In addition to its importance in producing symptoms and accounting for significant costs in patient care, recent attention has begun to focus on a possible connection between inflammation associated atrophy and epithelial proliferation as a predisposing condition or precursor for Pca (57, 58). Although little attention has focused thus far on inflammatory disorders, similar inflammatory infiltrates can occur in the GEM prostate (Figure 3i). Regarding possible etiologies of active inflammation in the GEM prostate, stasis complicating obstruction due to large size of the prostate as a consequence of the transgenic manipulation can likely contribute to and be complicated by infection. Consideration should also be given to modulation of the immune or inflammatory response as a consequence of non-prostate selective genetic manipulations. Inflammation in the mouse prostate can also be accompanied by reactive epithelial proliferation and nuclear atypia, although such alterations are expected to be relatively mild (1). Such lesions in the GEM prostate should be classified as inflammatory, with specification of reactive atypia, rather than proliferative, as in hyperplasia or PIN.   *Granulomatous prostatitis:* Non-specific granulomatous prostatitis in the human prostate is not uncommon, being present in up to 1 % of transrectal biopsies (6). It is the most common form of "non-infectious" granulomatous prostatitis in humans. Importantly, it can mimic Pca, both on rectal examination, as it can produce a firm, irregular prostate, and on histopathologic examination, as the sheet like growth of histiocytes can resemble high grade (e.g., Gleason pattern 5) carcinoma on cursory examination (6). It is likely due to inflammatory reaction to prostatic secretions, potentially complicating intra-prostatic duct obstruction and acinar rupture. Clinically, it is commonly associated with a history of recurrent or persistent urinary tract infections. Histologically, it is characterized by a mixed inflammatory infiltrate, without well formed granulomas or giant cells, but with sheet like growth of histiocytes (macrophages) (Figure 3h). Admixed eosinophils are an important diagnostic feature (6).

The most common form of infectious granulomatous prostatitis in humans is an iatrogenic condition, caused by the instillation of BCG (Mycobacterium bacillus Calmette-Guerin) for the treatment of urinary bladder carcinoma in situ or superficial bladder cancer. Necrotizing granulomatous lesions with multinucleated giant cells identical to those in tuberculosis can be seen in the prostate following BCG treatment (6). Characteristic necrotizing granulomatous lesions with irregularly outlined zones of necrosis surrounded by palisading histiocytes can be seen in the human prostate after transurethral resection of the prostate (TURP) for BPH. For obvious reasons, we don't expect to see these clinicopathologic lesions in GEM. However, similar necrotizing or non-

20

necrotizing granulomatous inflammation can be seen in the human prostate as a part of systemic infections with fungal organisms or tuberculosis and with involvement by vasculitis in Wegener's granulomatosis (6). Fungal or other infectious etiologies could in theory be observed in the prostate of mouse models, especially if the genetic manipulation resulted in immunocompromise. The pathology of such processes has not been well described in GEM. However, infection should always be kept in mind as a cause of unusually prominent inflammation in the mouse prostate, especially if only observed in a subset of examined mice.

Abscess: An abscess is characterized histologically by sheet-like infiltration of neutrophils, with a cavity formed in areas of frank tissue destruction. It may be surrounded by a wall of granulation tissue, with prominent small capillary formation and may resolve by leaving a cavity surrounded by fibrosis. It is essentially always caused by infection, particularly bacterial and fungal. It is rare in the human prostate, with the availability of antibiotic treatment (6). It can be seen as a complication of acute prostatitis, potentially associated with urinary obstruction and infection with coliforms, or due to hematogenous seeding from another source, usually associated with staphylococcal infecton. It is more likely to occur in the setting of immunocompromise. If identified in the prostate of GEM, local or systemic infection should be suspected. Frequent occurrence could also accompany immunosuppression due to the specific genetic manipulation involved.

Coagulative necrosis: Coagulative necrosis is a form of tissue necrosis in which the basic outline of the cells and tissues is maintained. Often these areas are eosinophilic in H & E stained sections, and lack normal nuclear staining. It is quite characteristic of hypoxic cell death. It is seen in the human prostate, for example, when BPH nodules undergo infarction, where central coagulative necrosis may be seen surrounded by atypical reactive epithelium and squamous metaplasia (6). It has been seen either focally or more extensively in the prostate and seminal vesicles in occasional older transgenic animals with markedly enlarged prostates and subsequently engorged seminal vesicles (S.B.S., unpublished observations), which is likely due to an ischemic process.

Fibrosis: Fibrosis refers to the deposition of extracellular collagen and such "scarring" is a potential consequence of inflammation. With time, these areas evolve from more cellular regions in which plump spindled fibroblasts may be seen in an edematous stroma to hypocellular regions with dense eosinophilic collagen. In addition to a sequalae of inflammatory injury, transgenic manipulations involving growth factors or their receptors can lead more directly to stromal cell or fibroblast activation, with increased deposition of extracellular matrix. Such stomal alterations have been observed in the prostates of GEM, and should be considered when the "fibrosis" or stromal hyalinization is not accompanied or preceeded by prominent inflammation.

Non-neoplastic proliferations of the Prostate/Hyperplasia

Epithelial Hyperplasia: A variety of characteristic epithelial hyperplasias occur in the human prostate, most notably adenomatous or glandular hyperplasia in the TZ as part of the glandular and stromal hyperplasia typical in BPH (Figure 4 a,b,c) (6). Basal cell hyperplasia can be seen in association with BPH (Figure 4d) as well as in a morpholically distinct form in the PZ, which when accompanied by prominent nucleoli can mimic PIN (6, 64). Another described morphologic entity is clear cell cribriform hyperplasia (Figure 4e), which is also most commonly observed in the TZ with BPH (6). Basal cell hyperplasia is also one of several characteristic alterations seen in benign human prostate following standard neoadjuvant anti-hormonal therapy with Lupron and Flutamide (65, 66), a change which may be more prominent in the TZ (S.B.S., unpublished observations).

21

Importantly, the creation of new glandular spaces IS NOT a diagnostic criterion specific for cancer per se in the human prostate; nor should this be regarded as an absolutely specific feature for adenocarcinoma in GEM. Glandular hyperplasia in BPH in the human can involve an increase in the amount of glandular tissue, with increased gland profiles as well as epithelial proliferation within gland spaces, as evidenced by stratification. Importantly, this glandular proliferation is NOT accompanied by appreciable cytologic atypia in human BPH. Again, BPH in the human prostate is NOT the same as "benign prostate", when the latter term is used to refer to normal prostate glands (e.g., control tissue for studies on Pca as typically arising in the PZ). BPH is a specific clinicopathologic entity essentially confined to the TZ and is characterized by glandular as well as stromal proliferation (6). Hypercellular BPH nodules can be observed and atypical adenomatous hyperplasia (AAH), or adenosis, is characterized by a proliferation of admixed larger and small gland profiles, with similar nuclear and cytoplasmic features in each, and retention of at least a fragmented basal cell layer (6). Although regarded as a possible precursor lesion for well differentiated TZ carcinomas (e.g., Gleason pattern 2 carcinomas) often seen at the edge of BPH nodules (12), it is not malignant per se and does not warrant definitive treatment. Other lesions with increased glandular or epithelial tissue include sclerosing adenosis, also typically seen in the TZ, and which can have nuclear atypia and mimic higher grade Pcas (6). Hence, many benign lesions in the prostate demonstrate increased glandular spaces in addition to or instead of increased epithelial cell stratification within pre-existing gland or duct spaces.

Epithelial proliferation classified as hyperplasia is not typically recognized per se in the human prostate PZ. Lesions referred to as PAH are described above with atrophy. Epithelial proliferation in normal PZ gland spaces is either difficult to distinguish from just a variation of normal gland morphology or is usally accompanied by at least mild nuclear enlargement and atypia and more appropriately classified as low grade PIN (LGPIN) (9, 64). The distinction between LGPIN and "normal" or benign PZ glands is not always easy or reliably made (9, 64). Further, although LGPIN is presumed to be able to progress to HGPIN, it does not have the same defined spatial and molecular relationship with Pca as HGPIN. It also does not share the clinically important association of an increased likelihood of detecting Pca on subsequent biopsies when it is found without invasion in transrectal biopsies, and hence is not usually reported as a pathologic finding on biopsies (7, 9). However, the anatomic restrictions of hyperplasia as a typical TZ histologic alteration and PIN as a generally PZ restricted entity in human prostate cannot be translated to specific lobes or regions within lobes of the mouse prostate. Hyperplasia is the appropriate designation for epithelial proliferations in the mouse prostate not satisfying the definition of mouse PIN, with appropriate modifiers regarding extent and the presence of atypia.

Hyperplasia defined as an increase in glandular tissue compared to age matched wild type control mice could certainly be a "developmental" consequence of transgene expression during prostate development. Attention should be given to the extent (diffuse vs. focal) or possible uniform symmetry of such epithelial proliferations (even if atypia is present) in effort to distinguish a generalized phenomenon vs. a possible manifestation of the development of an epithelial neoplasm in GEM. Hyperplasia may also be seen as an increase in epithelial cells within gland spaces. As seen in Table 2, hyperplasia is broken down further as focal or diffuse, and as epithelial, stromal, or both. Prostate epithelial hyperplasia has been observed in GEM (Figure 4f,g). The presence or absence of atypia should be noted. As epithelial proliferation with nuclear atypia is the histologic hallmark of PIN, atypia should be diagnosed with caution and preferably in a blinded fashion so that confidence can be had in the presence of this potentially subjective feature. As described below, other criteria are necessary for a classification of PIN in the mouse prostate, such

as focality and progression. Epithelial proliferation can involve basal cells or secretory cells. When possible, this should be specified. Adjunctive immunohistochemical stains can be helpful, as described in the protocol section. The modifier term focal refers to the involvement of one or a few gland spaces. Diffuse refers to a more extensive and uniform process. In practice, this can be distinquished as ≥ 50 % of gland profiles in adequately sampled prostate lobes. Although some gland lumens will be cut more longitudinally and others more transversely in any given section and many of these are different profiles of the same connecting ducts or glands, the semi-quantitative estimation of percent involvement or rigid counting of gland spaces involved may be a useful objective parameter. This is particularly true when sufficiently large numbers of animals and sections are included and assessed in a blinded fashion, as hyperplasia may be relatively subtle and subjective. Also, as normal proliferation and apoptosis in the rodent prostate may occur differentially along proximal and distal portions of ducts and glands, attention should be given if possible to differential involvement of proximal and distal portions of the duct/gland profiles within well oriented sections (see Protocol section regarding sectioning). This is desirable as genetic manipulations could accentuate, modulate, or negate these normal cell turnover mechanisms. As a supplement to blinded histopathologic assessment, more objective parameters of epithelial proliferation and turnover can be employed, such as immunostaining for proliferation markers and tissue stains for apoptosis (see Protocol section). Such parameters can be assessed in an objective quantitative fashion, as long as sampling is random and equal and/or attention is again given to the proximal vs. distal portion of examined prostate lobes.

Stroma and combined epithelial and stromal hyperplasia: Attention should be given to possible stromal abnormalities accompanying prostatic epithelial hyperplasia in GEM. Stromal hypercellularity in the human prostate is an extremely common, almost characteristic, accompaniment to the glandular hyperplasia that occurs in the TZ in BPH. Pure stromal nodules are not uncommonly seen as generally small circumscribed foci in the more immediate periurethral region (6). The cells are oval or spindled and similar to normal prostate stroma and the associated matrix is characteristically myxoid to hyalinized. Stromal hypercellularity is noted in other typically TZ lesions, such as basal cell hyperplasia and sclerosing adenosis (6), whereas it is not a usual accompanying feature to the malignant glanular elements in typical PZ Pcas in the human (7, 9).

Prominent stromal hypercellularity has been observed along with epithelial cell proliferation in multiple GEM models (Figure 5a,b,c). Whether a direct consequence of transgene expression or a possible paracrine effect from transformed epithelial cells is not defined. When uniform or diffuse, it is certainly unlikely to be a desmoplastic response to what is hopefully a focal invasive event (see below). Often the stromal hypercellularity has been observed to be progressive and has a general resemblance, especially in the early stages, to normal prostate stroma. In some models (Figure 5a,c), there is also noted a more condensed hypercellular stroma in closer proximity to the proliferating atypical epithelial compartment. Atypia and mitotic activity in this stroma can be conspicuous. In addition to possible classification as combined epithelial and stromal hyperplasia, in some models, the epithelial lesion is properly regarded as PIN. There is epithelial atypia and progression in both the extent of epithelial involvement and in the severity of the atypia, qualifying the epithelial abnormality as PIN, and there has been development of subsequent invasion. Such lesions can be descriptively designated as "PIN with hypercellular stroma". Atypia in the stromal component should be addressed as well. In contrast to these rather diffuse processes, focally prominent proliferations of epithelium and associated stroma raise consideration of discrete neoplasms, potentially classifiable as adenoma or papilloma.

23

Neoplastic Proliferations of the Prostate

Benign epithelial neoplasms. Adenoma, papillary adenoma or papilloma: These designations are intended for true neoplastic proliferations that lack the hallmarks of malignancy, such as destructive invasion and metastatic potential. There are essentially no counterparts in human prostate pathology, in terms of benign neoplasms of variably differentiated secretory epithelial cells (e.g., compared to the common occurrence of adenomas in such tissues as colon). There are rare basal cell lesions described as basal cell adenomas (7, 9), but in general, this category was created based on already observed or possible lesions more comparable to those in other tissue sites or in veterinary pathology. Although in theory such lesions are clonal neoplasms, certainly this is not routinely demonstrated for the vast majority of lesions classified as such. Instead these benign tumors are recognized by a combination of pathologic features, including discrete growth that can be expansile or nodular or protrude into a lumen, but without destructive invasion. Cytologic atypia can be present, and if so, it should be described. Further, if such atypia progresses this should be noted and described (e.g., potentially paralleling the development of high grade dysplasia in some human adenomas). Similarly, if focally architecturally distinct epithelial regions are identified, perhaps characterized by greater crowding or accentuated atypia or apparent invasion into the stromal compartment of the lesion itself, this should be noted and described (e.g., potentially paralleling the development of early invasive carcinoma in some adenoma-carcinoma sequences).

When occurring in the background of extensive or even diffuse epithelial and stromal hyperplasia, such focal intraluminal polypoid protrusions may represent foci of essentially intraluminal herniations or a pattern of growth into an area of "less resistance" than surrounding stroma or adjacent tissue (Figure 5d,e). Some such foci in a few SV40 or Tag based models develop a very characteristic edematous stroma as well, and lesions either representing combined epithelial and stromal hyperplasia or true neoplasms have been described by the term "phyllodes-like" on the basis of their histologic resemblance to phyllodes tumors in the human. These tumors are particularly characteristic (although not necessarily common) in the human breast. Histologically similar lesions have very rarely been described in the human prostate (7, 9). The term "phyllodes" for the human neoplasm derives from the "leaf-like" pattern of epithelial growth within the very prominent and typically edematous appearing stroma. The hyperplastic vs. neoplastic nature of the described lesions in the prostate of GEM, which are seen especially with advancing age in certain models, is not established and no consensus was reached on this matter. We do not recommend the term phyllodes tumor as a precise designation for these foci because of a lack of demonstrated homology to these uncommon neoplasms in the human (e.g., in terms of potential clinical behavior and the lack of more widespread background epithelial and stromal abnormalities in human). However, the descriptive adjective "phyllodes-like" is certainly useful in describing the characteristic histology of such combined epithelial-stromal lesions.

Papilloma refers to a benign neoplasm similar to adenoma, but with a well defined fibrovascular stroma, imparting a characteristic papillary growth pattern (Figure 5f-h). Papillary adenoma and papilloma are hence synonymous. Again, a homologous lesion is not recognized in the human prostate per se, but lesions satisfying typical histologic criteria for papilloma in human and veterinary pathology have been observed in the prostate and seminal vesicles of GEM. When seen in a background of more widespread hyperplasia or PIN, such lesions are recognized by their focally distinct growth pattern, again without destructive invasion. Although such tumors are seen in a variety of tissues (e.g., human breast), as described for adenoma and phyllodes-like lesions above, they are not usually encountered in the human in a background of widespread hyperplasia occurring throughout the entire organ. Molecular data to support that such foci in mouse prostates are truly

24

distinct clonal neoplasms and not part of a more widespread process would be welcomed. For now, such lesions can be classified as adenomas or papillomas or as combined epithelial stromal proliferations, but they should be described in detail, including the presence or absence of atypia, as should the histology of the rest of the prostate in which they are arising.

Prostatic Intraepithelial Neoplasia: Considerations, Controversy, Compromise, Consensus, and Challenge for the Future

Human prostatic intraepithelial neoplasia (PIN): Human PIN is the neoplastic proliferation of epithelial cells within preexisting gland spaces, which occurs predominantly in the PZ (Figure 6a)(7, 9, 67, 68). The proliferating, stratified cells are neoplastic and less differentiated counterparts of secretory or luminal cells and do not immunostain with antibodies to high molecular weight cytokeratin. In fact, with increasing grades of PIN the basal cell layer is progressively lost or fragmented (69). Human PIN is now classified as low or high grade, replacing a previous three tiered system whereby PIN I is low grade PIN (LGPIN) and PIN II and PIN III are high grade PIN (HGPIN) (7, 9, 67). The two tiered system has improved interobserver agreement, is relatively easy to apply in daily clinical practice settings, and has biologic and clinical implications (7, 9, 64, 70, 71).

Grading human PIN: Human PIN is characterized by progressive epithelial proliferation, as manifested by nuclear stratification. With progressive severity, there is greater nuclear enlargement and increasingly prominent nucleoli (7, 9, 67). Macronucleoli (> 2-3 um) are typical and diagnostic of high grade PIN (HGPIN) (Figure 6b). HGPIN is considered the likely precursor lesion for most or all human PZ invasive Pcas (Figure 6a) (12). HGPIN architecturally can show multiple growth patterns, including tufting and micropapillary (most common) (Figure 6b), flat or cribriform (72). Multiple lines of evidence support the relationship between HGPIN and PZ-located Pca (9, 12, 68, 69). These include the earlier age occurrence of HGPIN compared to invasive Pca in autopsy studies. There is an increased incidence of HGPIN (but not LGPIN) in autopsy or RP prostates with cancer compared to those without. There is frequently close spatial association of HGPIN and invasive acinar-forming Pca (Figure 6a). Numerous studies examining various molecular markers, including expression of oncogenes, growth factors and their receptors, have demonstrated alterations in HGPIN that are intermediate between benign prostate and Pca or that are similar in HGPIN and Pca (69). Similar to the frequent multifocality of invasive Pca in the human prostate, HGPIN is frequently multifocal, and genetic evidence supports that HGPIN and Pca are commonly multiclonal (69, 73). On a practical level, the finding of HGPIN alone (without invasive Pca) in transrectal prostate biopsies performed for clinical indications (abnormal digital rectal exam or elevated serum PSA) is associated with an increased incidence of detecting invasive Pca on repeat biopsy (9, 70, 71, 74).

Significance of cribriform lesions with intact basal cell layers in human Pca: Although HGPIN as a true potential precursor lesion for invasive carcinoma may demonstrate a cribriform growth pattern within pre-existing ducts and glands (72), several recent studies have shown that "cribriform HGPIN" has a worse prognosis than cribriform invasive carcinoma in RPs or imparts an independent increased risk for progression when identified in RPs (75, 76). Such data have raised speculation that these lesions, which are associated with higher grade and larger volume Pcas, actually represent the spread of invasive carcinoma within ducts, so-called "intraductal carcinoma", a post-invasive rather than pre-invasive lesion (75-77). Even solid foci with comedo necrosis, classified as a Gleason pattern 5 in the Gleason grading scheme (78), can now be recognized as

potentially having a basal cell layer on HMWCK immunostaining, indicating neoplastic growth within a pre-existing duct. Solid and cribriform patterns of "intraductal carcinoma" with necrosis are particularly associated with adverse outcome (increased progression) following RP (76). These cribriform intraductal lesions have been shown to have advanced molecular alerations more in keeping with relationship to or progression from Gleason pattern 4 carcinoma than a relationship to Gleason pattern 3 carcinomas or PIN (79). Thus, evidence is emerging supporting the relationship of at least some of these cribriform lesions in human Pca to more advanced disease, rather than HGPIN, which as a precursor lesion in the PZ, is typically associated with Gleason pattern 3 carcinoma.

The possible biologic implications of these lesions in humans should not prematurely be extended to mouse models based solely on the architectural and histologic similarities of "non-invasive" cribrifrom proliferations. Atpical cribriform lesions within ducts have been observed in numerous GEM models of Pca. In the mouse, however, these can be seen without associated invasion anywhere in the prostate (e.g., in contrast to the large volume of typically high grade invasive tumor in human RPs) or with only small foci of invasion. Hence, these lesions likely represent PIN in the mouse (i.e., as a true potential precursor lesion), as they have typically been interpreted.

Invasion in association with HGPIN: The earliest invasive forms of Pca associated with HGPIN (conceptually analogous to microinvasion being discussed in the mouse prostate tumor classification scheme) are not clearly defined and are difficult to recognize. Not recognized in the human is the penetration through the HGPIN gland basement membrane of individual tumor cells or small groups of cells with possible cytologic alterations or stromal response, features pathologists are used to assessing for early invasive carcinoma in association with in situ carcinoma lesions in such sights as the uterine cervix or urinary bladder. Possible early invasive lesions composed of microscopic foci of larger HGPIN-like glands with closely arranged "sprouting" small acini have been described in RPs as "transitive forms" by McNeal (80), but the application of such concepts to diagnosing early invasive carcinoma on biopsy is not established. The finding of small acini with cancer nuclei adjacent to HGPIN raises the differential diagnosis of HGPIN with invasion vs. HGPIN suspicious for invasion because of the possibility of tangential sectioning of outpouchings of HGPIN glands (64, 81). There is room for interobserver variability in this setting, and only sufficient spatial separation of the small acini in question from adjacent HGPIN glands to a degree where the morphology is incompatible with outpouchings of HGPIN can allow for a definitive diagnosis. This has important implications clinically (81) and highlights some potential differences in human and mouse prostate pathology. First of all, the extremely thin rim of fibromuscular stroma surrounding mouse prostate ducts and glands would not allow for similar sufficient spatial separation of small gland profiles from overlying PIN glands. However, the outer or basalar contours of mouse glands appear more regular or smoother than those in the human prostate, such that tangential sectioning of PIN glands may be less of an issue in the mouse. Further, early invasive forms in certain mouse models do appear to take the form of individual cells or small numbers of cells invading through the basement membrane into surrounding stroma. The ability to sample evolving mouse lesions with time in contrast to tissue sampling issues in human patients is one advantage for defining these lesions. Obviously, progression of lesions such as these to more extensive invasion will render greater confidence in the truly invasive nature of such "microinvasive" foci. Other issues relevant to microinvasion, such as loss of a basal cell layer and possible stromal response are described below in the section of microinvasive carcinoma.

Neoplastic proliferation of potential pre-malignant potential. Mouse Prostatic Intraepithelial Neoplasia (mPIN)/
> *With documented progression to invasive carcinoma*
> *Without documented progression to invasive carcinoma*

General considerations: Similar to human PIN, mouse PIN (mPIN) is defined histologically as proliferation of atypical epithelial cells within pre-existing or basement membrane lined glands and ducts. Hence, it may be recognized by stratification of epithelial cells with nuclear atypia. With progressive neoplastic epithelial growth, the focus can acquire a tufting, micropapillary, or cribriform growth pattern. In some previously published descriptions of mouse models, grading PIN as low grade or high grade has been accomplished based predominantly on progressive nuclear atypia. However, it should be borne in mind that human HGPIN represents a broader concept than just its morphologic features; that is, by virtue of its being seen in association with invasive carcinoma and by having documented molecular alterations similar to Pca, it is considered to have potential for progression to invasion (12, 69). Obviously, documentation of progression to invasion and characterization of progressive molecular alterations in PIN have not been accomplished in all mouse models. Because of the association of HGPIN with invasive Pca in the human, consideration was given to classifying as high grade only those mouse PIN lesions which occur in models that have documented progression to invasive carcinoma (and in which the invasion appears to be related to the PIN lesions). However, it was the opinion of the Pathology Panel that this definition may discourage devopment and characterization of models that could be useful for deciphering early changes leading to PIN in Pca development and for testing possible chemoprevention agents. Further, as insufficient data exists on morphologic features of PIN that correlate with progression (regardless of the specific mouse model), it was decided that mPIN should not at present be graded as low grade or high grade. Any attempts to do such in a formal general classification scheme would be premature. For example, PIN has progressed in multiple SV40 early region or large T antigen based models. If based on these observations, the profound nuclear atypia in the PIN lesions of these mice were to serve as the histologic hallmarks of HGPIN in GEM, few if any non-SV40 based models would ever develop a lesion classified as HGPIN. Some non-SV40 based models have reportedly progressed to invasion with a fairly high frequency. However, based on the published morphology of such models and that of other non-SV40 GEM models, there are certainly no readily identifiable features of the PIN lesions in such mice that would be expected to translate to likely progression if seen de novo in a different GEM model. As a consequence of these well considered limitations in the current knowledge regarding PIN morphology and outcome in a diversity of models and because of the implications of calling a lesion HGPIN, it was decided that mPIN should not at present be graded.

A grading scheme for PIN applied to a specific non-SV40 based model was recently described by a group of investigators including a member of the MMHCC Prostate Pathology Committee (82). PIN was divided into four categories based on progressive architectural and cytologic abnormalities. Although it was not clear if all histologic assessments were blinded, the application of this scheme allowed for the documentation of lesion progression in Nkx -/- x PTEN +/- mice (34, 82). Lesions similar to these PIN categories have been noted in several other non-SV40 based models listed in Table 1 (82). However, similar detailed time course analyses (with sufficient numbers of animals at a range of time points) have not been reported in other models utilizing this classification scheme, in order to determine whether similar progression can be documented. Further, the reproducibility and interobserver agreement of this or any other

classification scheme have not been thoroughly documented. As non-SV40 models that actually progress to invasive carcinoma become increasingly reported, the ability of this or other classification schemes to recognize lesions with true potential to progress to invasion can be investigated. The morphologic appearance of the PIN lesions in SV40 and non-SV40 models is quite distinct, such that a classification scheme developed in non-SV40 models may not apply to those based on the SV40 early region or large T antigen. Grading schemes capable of documenting progression within an individual model will also be useful for blinded histologic assessment of possible therapeutic benefit of chemoprevention strategies designed to inhibit or reduce progression. Therefore, just because there is not a single grading scheme that can be adequately applied to all SV40 based and non SV40 models in a meaningful way does not mean that progressive alterations in extent and nuclear atypia in PIN lesions should not be well described within any individual model being characterized (34, 82). Modifiers for such progression are described below.

 Classification of mPIN: Although mPIN should not be graded morphologically, this category is divided into those models that have documented progression to invasion or the capacity to invade and those that do not (Table 2). Diagnosing invasive carcinoma is described below. Hence, mPIN without documented invasion can be considered initially as a tentative category when a PIN lesion is observed in a new mouse model. If invasion is subsequently documented, the classification is appropriately modified to reflect this. The frequency with which such invasion should occur to warrant such designation was not established. However, it is intended that this should not be an exceedingly rare, isolated, or equivocal event. Progression should be reproducible. For example, development of unequivocal invasive carcinoma in ≥ 5- 10 % of animals in a particular age range in multiple breedings of a model would be far more convincing than a single microscopic focus of possible invasion in a single mouse.

 Although human HGPIN is regarded as a precursor lesion, the natural history of HGPIN is not established. The frequency with which progression would occur and over what time course is not known. The "potential" for invasion or the "capacity to progress to invasion" are important concepts in precursor lesions. As such, it was further decided that demonstration of progression to invasive carcinoma of a PIN lesion in a transplant model would warrant classication as "PIN, with documented progression". The criteria for recognizing subsequent invasion in a transplant model were not clearly delineated, but in general, invasive carcinoma should be recognized on the basis of the sound criteria for invasion in the intact prostate as described below. Further, standardized protocols for such acceptable transplantation models were not developed or approved, and may be a necessary focus for future workshops. For now, complete details should be provided by investigators using this experimental approach, including the age of the source animal and the size, lobe, and histologic nature of the transplanted material and the time course for subsequent histologic investation of the transplanted tissue. In contrast, crossing of one GEM line with another (Table 1) with resulting progression of PIN lesions to invasion, which has been specifically reported in some instances (30), does not warrant classification of the PIN lesions in the parent lines as PIN with invasion. Such bigenic lines are considered distinct "models" and should be characterized fully and classified separately. The future collection of well described morphologic data on models of PIN that do or do not progress may allow for subsequent development of specific diagnostic criteria for HGPIN in the mouse that can be applied to all models or specific subsets of models and which will have similar meaning as in the human. It is possible and quite likely that nuclear or other histologic features that will correlate with progression in non SV40 models will be different than those in SV40 or T antigen-based models. It is also possible that similar qualities and degrees of nuclear atypia in the in situ lesions in some models may NOT reflect similar invasive potential in different

28

models. Progression to invasion in different mice may be associated with molecular alterations not necessarily reflected in appreciably different nuclear or other morphologic features.

Definition: mPIN is diagnosed by the combined presence of epithelial proliferatin and nuclear atypia. In rare instances, the pattern may be flat, in which proliferation is not conspicuous, but the nuclear atypia and its progression are sufficient for the diagnosis of mPIN. Nuclear atypia can be in the form of nuclear enlargement, nuclear membrane irregularity, hyperchromasia, chromatin clumping, prominent nucleoli, or a combination of these features. As the category of epithelial hyperplasia can have atypia as described above, two other features which much be present for a designation of mPIN are **focality and progression**. The lesion should begin focally, as a manifestation of neoplasia, rather than being present uniformly throughout the prostate, as a perhaps more direct consequence of transgene expression or other genetic manipulation. Progression refers to either extent of involvement or nuclear atypia or both; with both being particularly supportive. Rigid criteria for the degree of these changes that constitute "progression" were not established. However, they should be well documented, described, and hopefully illustrated over an appropriate time frame (depending on the rapidity of neoplasia development) in any given new model. Examples are shown in Figures 6 and 7. A recent example of an attempt to document progression in PIN lesions in non-SV40 models that do not progress to unequivocal invasive carcinoma utilized a scoring scheme for PIN (82). Although initial evaluation of the spectrum of possible lesions in a new model can be unblinded, subsequent evaluation of lesions in mice of different ages using objective schemes to describe architectural and cytologic abnormalities that may allow for documentation of temporal progression should be blinded.

Descriptions and biology of mPIN: The morphology of PIN in the GEM models is distinct from that of the human prostate PZ in many aspects, including with regard to nuclear features. These differences are particularly pronounced for SV40 early region and large T antigen transgenic mouse lesions (Figure 6). Compared to human HGPIN, in SV-40 based mouse PIN lesions, the atypical nuclei appear to be more elongated, are more hyperchromatic, and have a greater mitotic and apoptotic rate (Figures3c-h) (16). In at least one SV-40 model, the high proliferative and apoptotic rates have been confirmed by PCNA immunostains and tissue assays for apoptotic bodies. These indices increased with time in PIN lesions, paralleling other nuclear abnormalities in PIN, and were indeed much higher than those reported in human prostate (31).

Nuclear atypia appears to be of a different quality in PIN lesions of growth factor and tumor suppressor gene manipulated models. Although nuclear enlargement occurs, there is less hyperchromasia and nuclear membrane abnormalities. Nucleoli, occasionally multiple, are prominent (Figure 7). The nuclear atypia in these models is thus more reminiscent of that seen in human HGPIN. However, as described below, progression to invasion has been much less documented and is certainly less common or typical in such models compared to SV-40 based models. In GEM models, observed growth patterns for PIN lesions include tufting, micropapillary, cribriform, and flat. Hence, the architectural patterns are similar to those well noted in human PIN.

The degree of nuclear enlargement, chromatin clumping, and nuclear membrane abnormalities in PIN of SV40 early region and Tag antigen based models is suggestive of aneuploidy. Few cytogenetic data exist on mouse prostate neoplasms. Karyotype analyses in tumors derived from the LPB-Tag 12T-10 mouse show a near tetraploid chromosome content (83). Whether this degree of nuclear atypia and possible aneuploidy is a consequence of genomic instability due to p53 inactivation is not known. Some PIN lesions in SV-40 based models have even demonstrated necrosis (e.g., CR2-SV-40; P.A.H., unpublished observations), which is not seen in human HGPIN, but such lesions were still compatible with in situ lesions and not intraductal

carcinoma as described and defined above in human Pca. All of the reported SV40 early region and Tag antigen based models have progressed from this PIN lesion to invasive carcinoma (31, 32, 36, 37, 84-86). In contrast, progression to invasion in non SV40 models (Table 1) is less common in general and potentially less frequent in individual models that do progress.

Modifiers of PIN lesions in individual models: The pattern of growth should be described; e.g., flat, tufting, micropapillary, cribriform, and combinations. The extent of involvement should be described, with documented temporal progression; either as rare, focal, multifocal, extensive, diffuse, or as the number of ducts/glands involved compared to the total assessed (or expressed as percentage). Nuclear atypia should be described (see glossary of terms) and its progression rigidly described. In all studies, but especially in models with perhaps more subltle alterations (e.g., Figure 7e,f), blinded pathologic analysis compared to aged matched controls should be performed. Supportive objective studies utilizing tissue markers can be employed, such as proliferation and apoptosis assessment, which are known to be altered in human PIN (69) and thus far in mPIN lesions that have been examined (30, 31, 50).

Microinvasive Carcinoma:
Microinvasive carcinoma in human Pca: Microinvasive carcinoma is conceptually the earliest form of invasive carcinoma, with extension of malignant cells through the basement membrane of PIN-involved glands into the surrounding stroma. A histologically recognizable form of such microinvasion is not well defined for human Pca. Clinically, it is crucially important to distinguish on transrectal biopsy a diagnosis of "HGPIN suspicious for invasion" (which may warrant a repeat biopsy) vs. "HGPIN with invasion" (which is sufficient for definitive therapy, such as radical prostatectomy). However, even in the latter situation, this refers to small acini of malignant cells nearby larger HGPIN glands rather than the penetration through HGPIN containing glands of individual tumor cells or small numbers of tumor cells. Hence, despite the biologically crucial stage of initial invasion in Pca progression, the concept of microinvasive carcinoma has little clinical meaning in the human. Although small tumor volumes (e.g., <0.2 or 0.5 cc) in RP specimens may have implications regarding the "clinical significance" of an invasive Pca, these tumors cannot yet be reliably identified by histologic or other parameters preoperatively (87-89). A category of microinvasive carcinoma in terms of limited extent of invasion from overlying or adjacent in situ lesions is not defined for prostate in a manner analogous to some other organs, such as the uterine cervix or in colon polyps.

Microinvasive carcinoma in GEM:
General Considerations: Despite the above issues in human Pca, there are several reasons why microinvasive carcinoma is considered to be a definable and potentially extremely useful category in the pathology of GEM. Biologically, the ability to identify early invasive carcinoma forms may allow for the characterization of the genetic alterations necessary for this crucial stage in the progression of Pca. Secondly, as many models are being generated which appear to be predominantly characterized by PIN, having histologic criteria (or criteria based on ancillary techniques such as immunohistochemistry) to make a definitive diagnosis of microinvasion will allow for the identification of which models truly progress. This can include assessment of possible progression to invasion by combinations of genetic alterations in bigenic or even more complicated breeding combinations. Thirdly, unlike the difficulty in recognizing such a stage in human Pca progression because of histologic reasons such as gland shape and the inability to sample lesions over time in the same individual, it appears that such a stage of early progession can be reliably recognized in the mouse. Recognition of microinvasion in the GEM prostate may be facilitated by

30

the more uniform or smoother gland contours, with a generally flat or smooth epithelial-stromal interface. This is in contrast to the more undulating contours of the epithelial- stromal interface in the human prostate, raising the issue of tangential sectioning of outpouchings of HGPIN containing glands yielding small acinar profiles, as described above. However, given the extremely thin rim of fibromuscular stroma in the mouse prostate, there cannot be a physically large amount of separation between PIN glands and invasive foci in a normal, non-desmoplastically thickened stroma. Hence, recognizing microinvasive foci arising from PIN is still a potentially challenging issue in mouse prostate pathology (16). The ability to define microinvasion in the mouse prostate is supported by several convincing reported examples of such early invasion, particularly in models based on the SV40 early region or large T antigen (31, 32, 37) (Figure 8), but also potentially in growth factor and cell cycle regulator manipulated models (30). Blinded histopathologic analyses in such models support that this stage relative to HGPIN increases with time (32, 37). Furthermore, histopathologic analyses in bigenic models to begin addressing key factors in tumor progession have shown that this is a definable endpoint with documentable inhibition of progression to microinvasion from HGPIN lesions (90).

Definition: Microinvasion is defined as the extension of individual tumor cells or small nests or acini of cytologically atypical cells into the thin rim of stroma underlying PIN containing ducts or glands. Borrowing from human pathology (not necessarily just human prostate pathology) possible other criteria for microinvasion (and invasion in general) in the GEM prostate include: for microinvasion, small nests or acini adjacent to larger PIN glands with adequate spatial separation of such small acini, unequivocal penetration through the basement membrane of PIN glands based on special stains, immunohistochemistry or electron microscopy, and a stroma response (e.g., desmoplasia); for more pronounced degrees of invasion, obvious destructive or extensive involvement of stroma, extension into periprostatic fat or loose connective tissue surrounding the contractile stroma, perineural invasion, lymphovascular invasion, and metastases (16).

Definitive classification and possible adjunctive techniques: Obviously, greater confidence in the classification of microinvasion is obtained in models that clearly progress to unequivocal more extensive invasion. This has been demonstrated in several SV40 early region and large T antigen based models (Figure 8c). In terms of biology, it may be more important to distinquish microinvasion from PIN than microinvasion from invasive (more extensively invasive) carcinoma. Possible useful parameters for the latter are described below. The transition to larger foci of invasive carcinoma may be a question of degree and related to more usual properties of cell proliferation and survival, as well as expression of genes such as matrix metalloproteinases and other proteases allowing for continued invasion through the stroma. For example, regarding possible effects of interventions to slow tumor growth or prevent tumor dedifferentiation (possible crucial targets in human Pca as secondary chemopreventive strategies), with larger invasive carcinoma foci amenable to tissue based molecular studies, histopathologic assessment can be supplemented with immunostains for proliferation markers, TUNEL assays for apoptosis, immunostains for differentiation factors as they are developed, or quantitative gene expression studies. For demonstrating unequivocal penetration into surrounding stroma in models with PIN and questionable invasion, adjunctive methodologies (special stains, immunostains, EM) may be warranted, especially in models not showing progression to more definitive and unequivocal invasive carcinoma (82). Some of these adjunctive techniques are described in the Protocols section. However, these have not been rigorously applied in a manner addressing this specific issue of invasion vs. in situ lesions. Application of candidate techniques to tissue sections in models

31

clearly progressing to microinvasive and more extensive invasive carcinoma may allow for the establishment of standards to apply to models with more questionable early invasion from PIN.

Stromal alterations with early invasion: It is important to note that routinely detectable stromal alterations are NOT a typical feature in invasive human Pca. Although phenotypic alterations may be demonstrable using special techniques, prostate stroma does not show hitologically defined inflammation, edema, or desmoplasia in response to usual invasive acinar carcinoma. Perhaps the only unique stromal alteration in human Pca is that referred to as stromal collagenosis, characterized by rounded foci of acellular eosinophilic material adjacent to invasive carcinoma foci, and possibly related in some cases to organiziation of mucinous material within gland lumens (mucinous fibroplasia), such that the hyalinosis sometimes involves gland lumens and surrounding stroma (7, 9). Although this is essentially diagnostic of Pca, it is rarely seen on biopsies and not particularly commonly in radical prostatectomies. Stromal hypercellularity is NOT seen in association with invasive Pca as a common or characteristic feature, and in fact, can sometimes argue against carcinoma in suspicious foci, being more typical in certain benign mimics of carcinoma in biopsy or TURP specimens (such as basal cell hyperplasia and sclerosing adenosis) (7, 9). This does not mean that stromal hypercellularity or desmoplasia cannot accompany invasive carcinoma in GEM models and that it will not be a useful feature in recognizing invasion in some models. However, it is fundamentally crucial that such stromal alterations be truly focal and found in association with the possible invasive focus in question. It should not be observed more uniformly in association with proliferating atypical epithelium as a possible paracrine effect or even more uniformly as a possible more direct consequence of transgene expression in stromal cells. Immunostaining has variably shown possible transgene expression in prostate and seminal vesicle stromal cells in multiple models with supposedly prostate epithelial specific promoters (multiple panel pathologists, unpublished observations). However, immunostaining methods can vary from assays not particularly sensitive (such that negative staining does not exclude transgene expression) to not particularly specific (such that positive staining does not reflect true positive expression). This issue awaits further resolution. For now, attention should be paid to the focality of desmoplasia. Different pathologists may have different sensitivities or skills for recognizing such alterations and it can be complicated by a more general background of stromal hypercellularity in some models (16, 29, 36, 85). No consensus opinion was reached regarding the validity of proposed examples of such desmoplasia in association with less than extensive in the study sets for the Bar Harbor Pathology Workshop. However, this feature has been reported in association with invasion in some models (85), may be dependent in part on the genetic background of the mouse, and has been personally observed by some of the involved pathologists (M.M.I., unpublished observations). Desmoplasia is certainly not a uniformly appreciable feature of early invasive carcinoma in general in GEM prostates, as it has not been observed or described in some published models having convincing early invasion (32, 37). Hence, other criteria for microinvasion may need to be considered as outlined above.

Invasive Carcinoma:
Criteria for invasive carcinoma: The distinction of invasive carcinoma from microinvasive carcinoma is essentially one of degree. Recommended criteria include extension into a widened (potentially desmoplastic) stroma (e.g., Figure 8c) compared to a more normal width stroma in microinvasion (e.g., Figure 8a,b), extension into periprostatic fat (e.g., Figure 8g-i; Figure 9) (37), and a focus size of > 1 mm (32). Other possible morphologic indicators of invasive carcinoma include perineural invasion, lymphovascular invasion, and metastases. However, experience from

32

human pathology and preliminary experience in GEM models thus far would indicate that these parameters are less likely to be observed in the absence of more obvious destructive stromal invasion.

Perineural invasion in Pca: In human prostate pathology, properly defined perineural invasion (i.e., circumferential perineural growth and cytologic atypia) is pathognomic of carcinoma on biopsy (7, 9). It is observed in approximately 20 % of transrectal biopsies with Pca, in which case it may correlate with ECE in univariate but not multivariate analysis (91, 92). It may also help in the pre-operative or intra-operative decision to sacrifice the neurovascular bundle ipsilateral to the side with perineural invasion on biopsy, potentially reducing the risk of positive surgical margins at foci of ECE and improving outcome (93). Perineural invasion is present in the vast majority (75-90 %) of totally submitted RP specimens, including those with Pca confined to the prostate, as Pca has an apparent predilection for invading the perineural space, and there are many nerve bundles within the prostatic stroma, especially in the posterolateral aspects of the gland toward the base. The prognostic significance in RP specimens of perineural invasion, perineural invasion qualified by parameters of extent of involvement, and in the context of specific patient subsets is the subject of ongoing investigation (94). In the mouse prostate, nerve bundles are not histologically conspicuous within the thin rim of fibromuscular stroma surrounding individual acini, but rather are seen in the surrounding loose connective tissue. Prostatic perineural invasion has been observed by carcinoma in multiple GEM models (29, 32). However, these models develop obvious destructive prostatic stromal and periprostatic invasion by carcinoma, so that it is not yet known if perineural invasion will be observed in mouse models as the only definitive parameter of invasion in occasional cases.

Lymphovascular invasion in Pca: Lymphovascular invasion can be identified in a significant minority of human RP specimens, including without identifiable pelvic lymph node metastases. Lymphovascular invasion can be seen in lymphatic channels within the prostate stroma, those associated with the ejaculatory duct complex, and those immediately outside the prostate (95, 96). Interestingly, although there are abundant lymphatic channels within the prostate itself, lymphovascular invasion is only uncommonly noted with invasive Pca that is confined to the prostate (that is, without ECE). The frequency of lymphovascular invasion is greater in stage T3 (vs.T2) tumors, suggesting perhaps that molecular alterations that allow for extension outside the prostate may also be related to the ability to invade lymphatics. In such patients, tumor lymphatic invasion may have independent prognostic significance for biochemical progression (elevated serum PSA) following RP (95, 96). Lymphovascular invasion has been reported with carcinoma in the prostate of GEM (32, 36), presumably in lymphatic spaces in the loose connective tissue between acini rather than within the thin rim of fibromuscular stroma surrounding acini. It is also presumed that lymphovasular invasion in mouse prostate tumor models will uncommonly be identified in the absence of obvious (stromal) invasive carcinoma, but there is little specific information regarding this so far. Furthermore, as in routine surgical pathology, caution must be exercised regarding possible artefactual lymphovascular invasion. The presence of large amounts of potentially fragile or friable in situ atypical proliferations can lead to artefactual implantation of tumor within vessel spaces either during grossing poorly fixed specimens or during histologic sectioning. Pathologists are typically experienced with interpretation of such possible artifacts in microscopic examination of sections. For now, attention should be paid to the usual morphologic features of true lymphovascular invasion as described in human Pca (e.g., shape of focus, adhesion to vessel wall, subtle cytologic changes) (95) as well as presence or absence of associated

unequivocal invasion, its extent, and its spatial relationship to the focus of possible lymphovascular invasion.

Metastases in Pca: The presence of metastatic Pca is essentially diagnostic of invasive carcinoma, as neoplasia confined to in situ basement membrane contained lesions should not have access to lymphatic or vascular spaces necessary for regional or systemic spread. However, as in human Pca, tumor metastasis would not be expected to be a very sensitive indicator of invasive disease. For example, all patients undergoing RP have invasive disease; that is, definitive treatment is not performed for HGPIN alone, and the 2-4 % of totally submitted specimens that are negative for residual Pca on histologic examination (14, 97, 98) are typically due to sampling issues for very small tumors, and invasion was present on the pre-operative biopsy. However, in most current practise settings, lymph node metastases are present in only 2-5 % of RP and bilateral pelvic lymph node dissection specimens (14, 17, 99). All GEM models of Pca reported thus far as developing metastatic tumor have had unequivocal invasion at similar or earlier time points. However, metastases are occasionally noted in individual animals without documentable invasive histologically similar primary tumors in the prostate. This could represent a sampling issue, as there is some indication that metastases from mouse prostate carcinomas can occur in association with very small foci of invasive tumor (37). However, if this situation is encountered several other explanations should be considered: 1) the metastasis could come from another completely unrelated site, which should always be excluded in transgenic mice made with non-selective promoters or in genomic knockout models; 2) the primary could be in other male accessory glands, such as the periurethal or bulbourethral glands, which develop invasive tumors histologically similar to prostate tumors in some models made with reportedly "prostate-selective" promoters; 3) a poorly differentiated spindle cell tumor in a distant site could actually represent a metastatic sarcoma, which should be a consideration in models that are developing stromal hyperplasia in association with neoplastic epithelial proliferation. Ancillary studies, such as cytokeratin immunostains and electron microscopy can be useful in this setting. It should be borne in mind that sarcomas typically metastasize by hematogenous routes, very characteristically to liver and lung. However, several NE carcinoma models have shown liver and lung metastases, and this pattern of visceral metastasis is actually quite characteristic of Pca with NE differentiation in the human (100). Lymph node metastases are quite characteristic of carcinoma. It was the consensus opinion of the Pathology Panel that immunostains for a particular transgene (e.g., large T antigen in the case of SV-40 or large T-antigen based models) cannot be used as *a priori* evidence of origin from the prostate for a potential metastatic focus. This is poor pathology practise, and numerous examples are well recognized of transgene expression in other sites besides the prostate with anticipated prostate selective promoters. However, in well characterized models in which extensive autopsy studies (covering age ranges in question) have shown absence of transgene expression in other organs (the list can never be too complete), transgene expression documented by in situ hybridization or immunostains can be an important adjunct to more traditional means of establishing the site of a primary for metastases in question. Currenlty, well documented markers for prostate origin independent of a specific transgene, analogous to human PSA, are not defined for mouse. More data needs to be acquired for newer techniques, such as mass spectrometric analysis of protein expression patterns (37), for identifying or confirming a prostate origin for a metastatic focus.

Classification of invasive carcinoma in GEM: When an invasive focus is identified, it should be histologically classifed as to a specific type of carcinoma if possible, such as adenocarcinoma or NE carcinoma, or otherwise classified as an undifferentiated carcinoma (Table 2). Adenocarcinoma refers to tumors that histologically demonstrate unequivocal glandular

34

formation. In the Bar Harbor Classification, adenocarcinomas of the prostate of GEM should be classified as well-, moderately-, or poorly-differentiated, according to the extent or percentage of glandular formation. Well differentiated tumors refer to those in which all or the majority of the invasive focus in composed of discreet, well formed glands (Figure 8e,f). Moderately differentiated adenocarcinomas refer to tumors in which extensive gland formation is still evident, but there are admixed foci showing gland fusion or solid areas (Figure 8 g,h,i). Poorly differentiated adenocarcinomas are those in which invasive foci are composed predominantly of nests or solid sheets, but in which glandular formation is focally present. It was the opinion of the Pathology Panel that specific percentages for the amount of an invasive tumor showing gland formation would not be specified for this classification purpose. If progressive dedifferentiation is observed in a given model, with less gland formation observed in invasive foci with age, the approximate percentage of gland formation in individual tumors can be stated as a function of time. It should be noted that these terms do NOT translate to similar terms in human prostate pathology. Although differentiation in human Pca is more often stated by Gleason score or pattern, there is a general translation, such that well differentiated tumors correspond to typically TZ located Gleason pattern 1 and 2 (Gleason score 2-4) tumors (Table 3). Moderately differentiated tumors are compsed of Gleason score 5 and 6 tumors, and hence include Gleason pattern 3 tumors, composed completely of well formed small glands, as commonly seen in PZ tumors associated with HGPIN. A morphologically similar tumor arising in association with mPIN in a mouse model would be classifed as well differentiated if composed entirely or predominantly of discreet and well formed glands. A summary of the classification of adenocarcinoma in GEM prostate is shown in Table 4. Note that some invasive carcinomas previously classified as moderately differentiated or poorly differentiated in some models have morphologies quite typical of NE carcinoma, and should be classified as such if possible according to criteria described below. Poorly differentiated carcinomas which do not show such NE differentiation may be classified as poorly differentiated adenocarcinomas if focal gland formation is evident of if ultrastructural examination or other ancillary techniques show focal glandular or secretory differentiation. Otherwise, tumors that do not show specific differentiation as outlined in Table 2 should be classified as undifferentiated.

Invasive NE carcinoma has been observed in several SV40 and large T-antigen based transgenic mouse models, based on recognition of typical morphology with subsequent confirmation by immunohistochemistry and electron microscopy (Figure 9 A-I) (32, 37, 86). Similar NE differentiation in other SV40 based models is suggested by similar morphologic features to these documented NE carcinomas in GEM and typical NE carcinomas in a variety of human sites (Figure 9 K-L). It should be stressed that NE differentiation can be seen focally in many and maybe even most otherwise typical human prostate adenocarcinomas using immunohistochemistry (7, 9). The prognostic significance of such NE differentiation, the increase in such differentiation with progression, and its relationship to the development of hormone refractoriness remain a subject of controversy in human prostate pathology (7, 9). In addition, there is a minority of human Pcas that show typical morphologic features of NE carcinomas, especially small cell carcinomas, as more typically associated with other organ sites such as the lung (7, 9). The designation of a mouse tumor as an NE carcinoma is based on the presence of characteristic histologic and cytologic properties, which can be confirmed by ancillary techniques, and not the demonstration of focal immunostaining for traditional NE markers in an otherwise histologically-recognized adenocarcinoma. Further, the designation of a mouse prostate tumor as an NE carcinoma is for precise pathologic characterization. Correct tumor classification will allow the possible accumulation of information regarding phenotype and tumor behavior, genetic alterations, and treatment response. Although

there are several preliminary observations relating this phenotype to androgen insensitivity (described in association with specific models below), there is currently insufficient data to allow any specific biologic inferences regarding this morphology in GEM models.

NE carcinomas can take the form of solid and cribriform growth with interspersed gland-like spaces or rosette formation. Hence, glandular spaces per se are not incompatible with a diagnosis of NE carcinoma. In this pattern of NE carcinoma, somewhat reminiscent of large cell NE carcinomas in the human lung and those seen in many other human sites, tumor cells may have moderate eosinophilic cytoplasm, often appreciated in areas of rosetting. The nuclei are often oval or round and have finely granular chromatin (Figure 9). Admixed more spindled cells with scant cytoplasm and hyperchromatic nuclei can be seen. Indeed such tumors may be admixed with or appear to transition to foci with the appearance highly reminiscent of human lung small cell carcinoma, either classic "oat cell" carcinoma or intermediate cell type. This appearance is also similar or essentially identical to that of small cell carcinoma of the human prostate (7, 9, 100). Small cell carcinomas are characterized by tumor cells with scant cytoplasm (high nuclear/cytoplasmic ratio), with oval or spindled markedly hyperchromatic nuclei, which may show nuclear "molding", in which one nucleus appears to indent into an adjacent nucleus, which conforms to the shape of the former. Crush artefact, in which smeared hyperchromatic material is seen in hypercellular areas, corresponding to DNA-rich material ("Azzopardi effect ") is also highly characteristic. Small cell carcinoma in the human prostate may be immunopositive for PSA and negative for NE markers such as neuron specific enolase (NSE) or negative for PSA and postive for NSE. Importantly, it is classified based on its cytologic features, regardless of its immunophenotype, as this high grade tumor does seem to have certain clinicopathologic associations. Although data is based on relatively small numbers of patients, patients with these tumors appear to be hormone insensitive, have an increased incidence of visceral (i.e., liver and lung) rather than lymph node metastases, and may respond to established small cell chemotherapy (100). As tumors in human and mice with this small cell carcinoma morphology can be seen in association with NE carcinomas with rosetting and more cytoplasm, small cell carcinoma is currently regarded as a less differentiated form of NE carcinoma (as documented immunohistochemically and ultrastructurally in lung NE carcinomas), rather than as a separate entity. The current Bar Harbor Classification System incorporates this concept (Table 2). Effort should be made to distinguish these tumors in invasive foci or the relative contribution of each morphology in an admixed tumor, so that any specific genetic alterations, correlation with androgen receptor expression, structural alterations, or function, and response to treatment can be potentially discerned.

Currently, tumors identified with the morphologies described above and illustrated in Figure 9 should be tentatively classified as NE carcinomas, and attempts should be made to confirm NE differentiation by immunohistochemistry and/or EM. Currently established NE markers for which immunostains have been successfully applied to mouse formalin-fixed paraffin embedded sections include chromogranin (32, 37) and synaptophysin (See protocols sections). A practical approach to the classification of possible tumors in this category is summarized in Table 5. As more invasive prostatic adenocarcinomas are recognized in GEM models, the specificity of these markers for unequivocally NE carcinomas vs. possible focal expression in otherwise typical adenocarcinomas will be addressed. However, thus far in a model in which CG immunostaining was noted in NE carcinoma foci, definitive adenocarcinoma foci were negative (37), and in a model in which synaptophysin immunostaining was noted in small cell carcinoma foci, well differentiated adenocarcinoma foci were negative (N.Greenberg, personal communication). However, NE marker immunostaining may not be particularly sensitive for detecting NE carcinomas, especially since

36

expression can be focal and invasive foci can be extremely small. Hence, as in standard human pathology practice, negative immunostaining for a single NE marker or even two NE markers cannot exclude true NE differentiation. Therefore, if a tumor with morphology identical or similar to that shown in Figure 9 is encountered, exhaustive effort to confirm or exclude NE differentiation should be applied. Immunostains for NE markers should be supplemented with other ancillary studies, such as the possible presence of very characteristic punctate or dot-like immunostaining with CK 8 antibodies or the presence of diagnostic dense core NE-type secretory granules on electron microscopic examination (32, 37). It should be remembered that the latter can be focal or rare, especially in less differentiated small cell carcinomas, so that adequate sampling should be applied and described before concluding that a tumor is undifferentiated. Such ultrastructural studies can also help in recognizing characteristic secretory differentiation in poorly differentiated adenocarcinomas.

Squamous cell carcinomas are extremely rare in the human prostate, and most typically arise from the prostatic urethra. They have not been reported in the prostate of GEM. The same is true for adenosquamous carcinoma. These lesions should be diagnosed based on their same recognized features in human and veterinary pathology in prostate and other sites (7, 9). Spindle cell or sarcomatoid carcinoma refers to a spindle cell lesion in which there is unequivocal epithelial differentiation immunophenotypcially or ultrastructurally (7, 9). It has not been specifically reported in the prostate of GEM, although it needs to be considered in the differential of poorly differentiated carcinomas, carcinosarcomas, and sarcomas, as described below.

Benign soft tissue neoplasms and sarcomas: Neoplastic growths satisfying usual human and veterinary pathology diagnostic criteria for benign and malignant mesenchymal neoplasms have rarely been observed or reported in GEM and less commonly reported. For now, if such lesions are encountered, they should be diagnosed and classified according to standard pathology practice. A few practical considerations are offered. In the human prostate, the most common sarcoma in the pediatric population is rhabdomyosarcoma, usually of the embryonal type (7, 9). In the adult human prostate, stromal nodules are extremely common, increasing with age (Figure 10 A,B). They are located typically in the glandular poor periurethral region, and are usually accompanied by glandular and stromal hyperplasia in the TZ as part of BPH and. Benign circumscribed lesions with histology and immunophenotype of smooth muscle, and hence classifiable as leiomyomas occur uncommonly (Figure 10 C,D) (7, 9). In addition to common usual stromal nodules, rare proliferations of the specialized prostate stroma occur that demonstate increased cellularity, atypia, and mitoses. Such lesions have been reported as "prostatic stromal proliferation of uncertain malignant potential" or "PSPUMP" (7). Some stromal proliferations appear to have an associated epithelial component, imparting a biphasic appearance. The epithelial or glandular spaces can exhibit a "leaf-like" growth pattern, quite similar to the phyllodes tumor more typical in the human breast (7, 9). Such lesions in the human prostate are best regarded as low grade and less commonly high grade malignant neoplasms (rather than hyperplasias) as they have occasionally demonstrated local recurrence and even metastases (7, 9). The most common sarcoma in the adult human prostate is leiomyosarcoma (7, 9). Although the relative rarity of these lesions (e.g., compared to the human female uterus) precludes the establishment of rigid criteria for distinguishing potentially malignant from benign smooth muscle neoplasms, the presence of infiltration, nuclear atypia, significant pleomorphism, necrosis, and appreciable mitotic activity are all suggestive of leiomyosarcoma over leiomyoma. Other mesenchymal neoplasms, with the same histologic and immunophenotypic features as their

37

more common soft tissue counterparts, have been reported in the human prostate, such as synovial sarcoma, hemangiopericytoma, and solitary fibrous tumor (7, 9).

Stromal hypercellularity is a prominent feature of the prostate in some GEM models (Figure 5a-c). It is a prominent feature of the anterior and dorsal/dorsolateral prostate of the faster growing LPB-Tag lines (36) (Figure 5a). The stromal hypercellularity is diffuse in these lobes (accompanying the marked epithelial proliferation), generally increases with age, and the cells and surrounding extracellular collagenous stroma have morphology in keeping with prostate stroma. Similar, but potentially lesser, stromal hypercellularity has been observed in the prostate of TRAMP mice in the experience of some investigators (85) (Figure 5b) (R.H., unpublished observations). Similar extensive or focal stromal hypercellularity has also been observed in the smooth muscle wall of the seminal vesicle in LPB-Tag and TRAMP mice (multiple members of the Prostate Pathology Panel, unpublished observations). In the prostate, these changes are too diffuse and too morphologically similar to normal mouse prostate stroma to represent desmoplasia. Whether they occur as a paracrine response to neoplastic epithelial cells or as a more direct consequence of at least minor (lesser magnitude than prostate epithelium) transgene expression in these cells remains to be further resolved. It is currently the responsibility of the MMHCC Prostate Pathology Panel to simply offer guidelines for classifying such lesions. When not associated with a distinct circumscribed or destructive growth pattern suggestive of neoplasia, they should be described as hyperplasia, either focal or diffuse, with or without atypia, as described above.

We have noted in the background of more diffuse stromal hypercellularity in some LPB-Tag mice, somewhat circumscribed foci that stand out as more cellular, and which show increased pleomorphism and mitoses (S.B.S., unpublished observations). The natural history of such lesions in this or other models has not been examined, as focus has been placed more on epithelial proliferations. Neoplasms properly classified as sarcomas have rarely been noted in the prostate of GEM, so that their true incidence in different models or under different experimental manipulations remains to be clarified. In addition to poorly differentiated carcinomas with histologic features suggestive of NE differentiation emerging in castrated animals from fast-growing Tag lines, foci of increased stromal hypercellularity with atypia similar to that described above and lesions compatible with frank sarcomas are occasionally noted (54). One lesion in a 12T7s mouse castrated at 25 wks and maintained for an additional 25 wks developed a sarcoma with histologic features compatible with leiomyosarcoma. The tumor is composed of highly atypical and mitotically active spindle cells organized in well formed intersecting fasicles typical of leiomyosarcoma (Figure 10 e,f). As the mouse had other foci involved by poorly differentiated carcinoma with NE differentiation, consideration could be given to a carcinosarcoma as described below. Some of the specific sarcoma subtypes are included in the Bar Harbor Classification for completeness and anticipation of the possible spectrum of neoplasms possible in the GEM prostate. However, to our knowledge, tumors such as rhabdomyosarcoma, chondrosarcoma, and osteosarcoma have not been observed. If encountered, they should be diagnosed based on standard practices in veterinary and human pathology.

When a poorly differentiated neoplasm with oval or spindle cells is encountered in the prostate and/or as a metastatic lesion, it should be definitively characterized as such by either convincing cytokeratin (CK) (typically a pan cytokeratin or CK8, not HMWCK such as CK5 or CK14) immunostaining or ultrastructrual examination. Spindle cell neoplasms may also be small cell carcinomas as described above, which can have weak CK immunostaining. Inclusion of appropriate NE markers (chromogranin, synaptophysin) can address this potential differentiation (along with electron microscopy). Vimentin immunostaining is also theoretically useful in this

setting, as strong vimentin and absent CK staining supports a sarcoma. However, few if any successful mouse vimentin immunostaining protocols have been described. If the differential diagnosis includes a specific sarcoma, antibodies for characteristic differentiation markers, such as smooth muscle actin for possible smooth muscle tumor, can be added. Sarcomatoid carcinoma, similar to its appropriate use in human pathology, refers to a lesion that has sarcomatoid histologic/cytologic features, such as spindle cell growth, but is demonstrated to have epithelial differentiaion, such as by CK immunostaining or electron microscopy. Vimentin immunostaining could be seen focally or weakly in such neoplasms

The designation of carcinosarcoma should be reserved for truly biphasic lesions, in which areas of unequivocal carcinoma and unequivocal sarcoma are both present. Carcinosarcomas are rare, highly aggressive tumors in the human prostate. Most have been observed with disease progression following hormonal or radiation treatment in patients with previously diagnosed more typical prostate adenocarcinoma (7, 9). Although radiation treatment in patients with that history could in theory contribute to the tumor "dedifferentiation", these tumors can develop without the history of such pretreatment, precluding definitive association. The epithelial component may be poorly differented adenocarcinoma, or show morphology of another carcinoma, such as squamous cell carcinoma. The sarcoma may be a sarcoma, not otherwise specified (NOS), show features of leiomyosarcoma, or show heterologous differentiation, such as a rhabdomyosarcoma or osteosarcoma (7, 9). Any detected similar lesions in GEM should be diagnosed according to similar principles.

Pathology of Disorders of the Periurethral and Bulbourethral Glands:

Developmental Disorders of the Periurethral and Bulbourethral Glands: Developmental disorders of these male accessory glands in GEM have not been frequently described in the literature. However, given the relationship between the embryonic development of the prostate and these other ductular/glandular derivatives of the urogenital sinus and their shared androgen dependence, genetic manipulations resulting in abnormal prostate development may be expected to also give rise to related abnormalities in these other male accessory glands. As such, agenesis and hypoplasia should be defined and applied as described above for the prostate. For example, abnormal development of secretory differentiation compatible with hypoplasia in the BUGs, with reduced mucin-producing epithelium compared to a corresponding increase in ductular epithelium, was noted in Nkx3.1 knockout (Nkx3.1 -/-) mice (50).

Neoplastic Proliferations of the Periurethral and Bulbourethral Glands: The relationship of these tissues to the prostate embyologically, their regulation by androgens, the documented and possible expression of transgenes in these tissues with prostate selective or prostate "specific" promoters, and the observed occurrence of neoplasms in these sites in GEM all contributed to the decision to include a classification of their neoplastic proliferations (Table 2). Neoplasms arising in the corresponding human sites are extremely rare. However, in situ and invasive tumors involving these tissues have been observed in essentially all mouse models generated with androgen dependent and even androgen independent potentially prostate specific promoters (Figure 11). Whether tumors can arise in these sites or secondarily involve them is not always clear. However, origin of tumors in the periurethral glands and BUGs has been described in some models, along with likely precursor lesions. Description of these lesions is not intended to detract from such models; after all, even with this potential complicating factor, models made with prostate selective promoters are still less likely to be complicated by neoplasms arising in multiple organs, as can be observed with "non-selective" promoters or genomic knockouts.

39

From the perspective of pathology analysis, there are several issues relevant to gross and microscopic examination: tumors arising in the prostate can extend to involve the periurethral region, either by growth along prostatic ducts to where they enter the urethra or by direct invasion into periurethral stroma; conversely, tumors arising in the periurethral glands can extend into prostate lobes, potentially mimicking a primary prostate tumor; neoplasms may originate in both the prostate and the periurethral and/or bulbourethral glands (either synchronously or metachronously) and give rise to metastases. As reported and unreported observed examples of periurethral and bulbourethral carcinomas have morphologic characteristics quite similar or identical to those arising in the prostate in given models, the latter also raises issues of determining the primary site for metastases.

Periurethral and bulbourethral gland neoplasms have been best characterized in the C3(1)-SV40 mouse model (40) (Figure 11a-dD). In these mice, atypical hyperplasia was present in the periurethral glands in 100 % and in the bulbourethral glands in > 75 % of mice ≥ 5 months old. Invasive carcinomas were identified in approximately 40 % of periurethral glands and approximately 20 % of bulbourethral glands in mice 10-12 months old (40). Lung metastases with similar morphology were noted in approximately 15-20 % of mice ≥ 9 months old and in which such invasive carcinomas were present in these other male accessory glands (40). In fact, most metastases in this model may come from periurethral and bulbourethral gland tumors (J.M.W., unpublished observations). Invasive tumors, essentially uniformly with NE differentiation, have also been noted in the periurethral and bulbourethral glands of intact LPB-Tag 12T-10 and castrated and even intact faster growing LPB-Tag lines (37, 54) (Figure 11e,f). Similar tumors were noted to involve the periurethral region of TRAMP mice from multiple institutions (Table 1) based on slides reviewed by the Pathology Panel (R.B., R.H., unpublished observations) (Figure 11g). However, the isolated occurrence of such tumors in this model or their simultaneous occurrence with similar morphology tumors in the prostate have not been described. The combined experience in different models with androgen dependent promoters would certainly support the possibility of neoplastic transformation due to transgene expression in these androgen-dependent other male accessory glands, and transgene expression in these sites has been documented with C3(1)-SV40 and LPB-Tag models (37, 40). Interestingly, atypical hyperplastic lesions have been noted in the ducts of periurethral glands in CR(2)-SV40 mice (P.A.H., unpublished observations) (Figure 11h). As this androgen-independent promoter appears to selectively target NE cells in the prostate (32), this suggests possible targeting of a normal likely very minor NE component in these other male accessory gland sites. However, these lesions do not appear to progress in this model, and involvement of the periurethral region by more extensive NE carcinomas appears to be by direct extension from unequivocal prostate tumors (P.A.H., unpublished observations).

Even though tumors originating in the homologous sites in the human are vanishingly rare, given the relationship of the development of these sites to that of the prostate and the potential similar androgen dependence or independence of tumors arising therein, if mouse models of Pca have relevance to human Pca, tumors in these other related sites may share at least some of that relevance (40, 101). Pathways regulating cell proliferation, apoptosis, invasion, and angiogenesis and the role of hormones and stromal interactions may be closely related in tumors of the prostate and other male accessory glands in the mouse. Future studies may shed some insight on this matter. Additionally, promoters that can selectively target transgenes to the prostate vs. these other male accessory glands may be developed. Knowledge of how to grossly procure these sites for pathologic analysis and how to classify neoplasms therein is essential for understanding the natural history of

40

current models, characterizing future models, and analyzing selectivity of new promoters. Techniques for tissue sampling are described below in the Protocols section.

Hyperplasia and atypical hyperplasia: Epithelial and/or stromal hyperplasias should be described as for prostate, with attention to their focal or diffuse nature and presence or absence of atypia. Description of extent can include involvement of multiple discreet periurethral gland lobues as well as that within any given focus. Presence or absence of bilaterality of involvement should be noted for the bulbourethral glands. Thus far, reported and observed epithelial proliferations in these sites have been uniformly accompanied by cytologic atypia, similar to the prostate lesions in their corresponding mouse models, and stromal proliferation has not been appreciated. Possible precursor lesions in which atypical epithelium is noted in periurethral or bulbourethral glands without obvious stromal invasion can be designated as atypical hyperplasia (Figure 11a,b,h). These lesions show nuclear enlargement and hyperchromasia with frequent mitotic figures and apoptotic bodies. These foci typically appear to conform to the normal glandular architecture, the smallest of which appear to be localized in the ducts of these accessory glands. More expansile forms, which may be associated with an apparent increase in slightly irregular new ductular or glandular profiles, but still without extension into surrounding stroma, may be seen with progression (40). More extreme forms with a nodular or micropapillary growth pattern, have been described, and reported as atypical nodular hyperplasia (40). These lesions (without frank invasion) should be classified as atypical hyperplasia, and terms such as nodular or micropapillary can be added as modifiers, along with other descriptions, such as increased nuclear atypia, to document apparent progression of the lesion in any given model.

Carcinoma: Invasive carcinomas in the periurethral and bulbourethral glands should in general be classified according to the same guidelines described above for the prostate. Carcinomas with focal and ill defined, but definitive glandular formation, have been observed, including associated with prominent stromal fibrosis and referred to as scirrhous carcinoma (J.M.W., personal communication). Such a lesion would be classified as poorly differentiated adenocarcinoma in the current classification scheme. In addition, invasive tumors with histologic and cytologic features typical of NE carcinoma have been observed in multiple models (Figure 11, c-g). As described above for prostate, such tumors should be tentatively classified as NE carcinoma, but efforts should be made to confirm the diagnosis by immunohistochemistry and/or electron microscopy. As for prostate, negative immunostaining for chromograninin does not exclude an NE carcinoma, as this marker can be negative or show only focal, rare, and weak immunostaining. Rather, a panel of immunostains should be employed, including other NE markers, such as synaptophysin, and cytokeratins, such as CK8, which may show characteristic punctate or "dot-like" perinuclear immunostaining. Electron microscopy should show typical dense core secretory granules. However, these may be rare and focal, depending on the degree of differentiation.

Pathology and Natural History of Selected Published Transgenic and Knockout Mouse Models of Pca:

Models with Pathology Reviewed by MMHCC Prostate Pathology Panel:

C3(1)-SV40 Early Region: Lines established from mice overexpressing the SV 40 early-region under the control of the rat prostatic steroid binding protein [C3(1)] gene consistently develop prostate epithelial proliferations with nuclear atypia (PIN), with documented progression to microinvasive and invasive carcinoma (84). Prostate changes in this model appear confined to the

41

VP and DLP, occuring earlier and perhaps more extensively in the VP, correlating with greater expression of the large T antigen (Tag) and the C3(1) gene in normal VP compared to the DLP. By three months of age, 100 % of mice developed epithelial hyperplasia in the DP and VP, with nuclear statification, elongation and hyperchromasia. These atypical proliferative epithelial lesions are confined to normal basement membrane lined structures, and show progression in extent and in the degree of nuclear atypia (previously referred to as LGPIN and HGPIN) (84).

Approximately one third of mice subsequently showed exuberant papillary forms of atypical proliferative epithelial lesions, reported previously as an adenoma (84). It is not known if this represents a true clonal benign lesion, as opposed to a focal accentuation of epithelial hyperplasia/dysplasia. Although adenoma as a benign neoplasm with risk of malignant transformation does not occur per se in the human prostate, this designation for the described mouse lesion is acceptable under the current Bar Harbor classification scheme in GEM. No early (micro) invasive lesions were described in this initial report, but were illustrated in a subsequent morphologic and molecular characterization of this line (31). It would be interesting to note any histologic evidence of malignant progression in foci described as adenomas vs. the relationship of progression to foci classified as PIN.

The majority of C3(1)-SV40 mice showed frankly invasive poorly differentiated carcinoma within the prostate after 8 months of age (84), although invasion and metastases are even more likely to be associated with neoplastic lesions in the periurethral and bulbourethral glands (40). The invasive tumors are composed of solid sheets and nests of cells with a high nuclear to cytoplasmic ratio. The illustrated unequivocally invasive lesions show little glandular differentiaton (84). Vague acinar structures are observed, consistent with poorly differentiated adenocarcinoma in the Bar Harbor Classification. Large well circumscribed cribriform and papillary lesions surrounded by more poorly differentiated tumor may represent in situ lesions rather than more definitive glandular differentiation in invasive foci (84). The stroma in this model was not described in detail, so it is assumed that it is largely unremarkable, an impression confirmed by the Bar Harbor Pathology Panel review of provided materials. One C3(1)-SV40 mouse reportedly developed pulmonary metastases in the original report (84). The overall frequency with which metastases are observed in these mice was subsequently confirmed to be low, and more likely to be associated with morphologically similar invasive lesion in the periurethral and bulbourethral glands (40), where the histologic and cytologic features are commonly suggestive of NE differentiation. NE differentiation was not pursued in the initial C3(1)-SV40 model report, and remains to be more definitively addressed (J.M.W., unpublished observations). Although the segment of the C3(1) 5' flanking region employed in this mouse has hormone response elements, the responsiveness of this model to androgens was not reported. In addition, there is widespread expression of the transgene in other organs, with invasive carcinomas arising in the submandibular salivary glands, as well as other male accessory organs as described (40, 84).

Shibata et al. subsequently more rigidly characterized the time course and nature of the progressive epithelial abnormalities in the C3(1)-SV40 mouse, including examination of ultrastructural correlates of the light microscopic lesions regarded as LGPIN and HGPIN, proliferation and apoptotic rates, and possible additional genetic alterations occurring with progression (31). In addition to nuclear atypia, the authors also used retention of cell polarity in the "basal layer" as a criterion for low grade PIN. Loss of polarity of epithelial cells was used as a surrogate for fragmentation or loss of the "basal" cell layer, as well characterized in progressive human PIN lesions (7, 9, 69). Whether these ultrastructural features correlate with progressive loss of a basal cell layer as defined by more recently available anti-HMWCK antibodies for mouse is not

42

clear. In addition, the authors also state that HGPIN was generally distinguished from low grade PIN by the architectural pattern and cellularity, and importantly, progressive nuclear atypia, including hyperchromasia, chromatin clumping, and prominence of nucleoli (31). PIN lesions were present in the VP of 83 % of mice at 2-3 months of age and 100 % from 4 to 12 months, with progression to lesions regarded as high grade present in 88 % of mice from 5-8 months of age and 100 % of mice older than 8 months (31). Although the current Bar Harbor Classification does not allow for grading of PIN per se, the descriptions of progressive nuclear atypia and architectural changes with PIN progression ultimately leading to invasive carcinoma in some animals in this model are exemplary. Lesions initially reported as invasive adenocarcinomas were detected as early as 7 months of age in the prostate, occurring in the VP and DLP in 19 % and 3 %, respectively. After 8 months, mice with reported carcinomas in the VP and DLP were 40 % and 13 %, respectively. Papillary, tufting, or cribriform patterns were described for adenocarcinoma (31), although it is not clear how or if these were distinguished from precursor lesions (PIN). The former two patterns are quite typical of PIN and rarely observed in frank prostate carcinoma in the human (i.e., except in prostatic ductal carcinoma (7, 9)) and all three patterns are described for PIN in this mouse model. Lesions demonstrating microinvasion were classified as carcinoma, and the illustrated examples and those reviewed by the Prostate Pathology Panel (e.g., Figure 8a) would be considered unequivocal invasion by most pathologists. As expected, these foci of early stromal invasion occurred in spatial relationship to PIN (designated high grade in that study) (31). In this same report of prostate lesions in the C3(1)-SV40 mouse, no metastases were observed (31), whereas subsequent studies demonstrated occasional pulmonary metastases, particularly associated with the even more common invasive morphologically similar carcinomas in the periurethral and bulbourethral glands (40).

Epithelial proliferation and apoptotic rates and possible Ras and p53 mutations were investigated in lesions initially designated as LGPIN, HGPIN, and adenocarcinoma (31). However, it is not clear if the latter group was confined to those lesions exhibiting unequivocal stromal invasion (i.e., vs. glandular patterns seen in PIN). In the C3(1)-SV40 early region mouse, proliferation rates detemined by PCNA immunostaining were low in normal prostate, increased in progressively severe PIN, and highest in lesions designated as adenocarcinoma (31). This increase in cells immunostaining for proliferation markers is similar to that reported for human PIN and adenocarcinoma (102), although the percentages of positive cells are higher in the mouse model (31). Apoptosis levels determined by in situ end labelling of fragmented DNA were low in normal prostate and increased in PIN and lesions designated as adenocarcinoma (31). Again, increase in apoptosis with progressive grades of PIN and in adenocarcinoma is similar to that reported in human Pca, although the levels are apparently higher in the mouse model (31). This correlates with observations in routine histologic examination of C3(1)-SV40 and other Tag-based models where mitotic figures and apoptotic bodies are readily seen and increasingly prominent with greater severity of PIN, whereas these are rarely observed in human HGPIN lesions, an impression supported by rigorous counts of mitoses and apoptotic bodies in human tissue sections ((103). Initial studies also indicate that specific molecular alterations may accompany neoplastic development and progression in the C3(1)-SV40 early region mouse. Two of 11 (18 %) PIN lesions investigated had Ha-ras mutations (at codon 61), whereas four of 12 (33 %) of carcinoma lesions had detected mutations: two Ha-ras mutations at codon 61, one Ha-ras mutation at codon 84, and one Ki-ras mutation (31). One carcinoma lesion had a p53 mutation in exon 7 (31). Although ras mutations are apparently overall uncommon in human Pca, they do occur, including with well documented geographic variation [Anwar, 1992 #823; Konishi, 1997 #824; Watanabe, 1994 #825] and with involvement of the specific codons mutated in the mouse model (104-107). That genetic

changes similar to those described in human Pca occur in GEM bodes well for the successful application of these models to elucidation of alterations potentially relevant to human Pca as well as for the translation of successful interventional trials in mouse models to carefully selected human patient subsets.

sPB (-426 bp)-SV40 Early Region (TRAMP): Greenberg *et al.* initially described neoplastic prostate lesions in 3 lines of founder mice created in both C57BL/6 and FVB mice with the short probasin promoter (sPB) and the SV40 early region with or without use of the chicken lysozyme matrix attachment region (MAR) sequence (85). One line with low levels of transgene expression demonstrated prostate epithelial hyperplasia with questionable mild dysplasia at 33 wks. In contrast, one founder mouse created in C57BL/6 with cointegrated MAR sequences showed high levels of Tag protein expression and developed an extensively invasive, apparently poorly differentiated carcinoma at 10 weeks (85). Focal residual prostate glands reportedly showed features of PIN, suggesting origin from a precursor lesion. This mouse died before a line could be established. Line 8247, designated the TRAMP model for "transgenic adenocarcinoma of mouse prostate", has been more thoroughly characterized and now extensively utilized by multiple investigators. Importantly, the histopathologic phenotype may show some variation depending on genetic background (Norm Greenberg, personal communication and unpublished observations of members of the Pathology Panel Review), so rigid attention should be paid to the genetics of the lines employed in breeding "TRAMP" mice and the background should be specified by investigators. In the Greenberg laboratory as in the original reported series, mice heterozygous for the sPB-SV40 early region are maintained in a pure C57BL/6 background and transgenic males are obtained as [TRAMP x C57BL/6]F1 or [TRAMP x FVB]F1 offspring. A possible relationship of metastatic potential to genetic background was subsequently reported (2).

TRAMP mice develop prostate specific lesions, characterized by precursor PIN lesions and rapid development of metastatic poorly differentiated carcinoma, including to lymph nodes and lung (2). By immunostaining, Tag expression in the TRAMP mouse prostate precedes epithelial hyperplasia. Nine week old transgenic mice show prostate epithelial nuclear Tag immunostaining. Subsequently, ten to twelve wk old mice show changes compatible with progressively more severe PIN, with epithelial stratification, including some cribriform glands, and enlarged, hyperchromatic nuclei. TRAMP mice between 18 and 24 weeks show more severe forms of such prostate epithelial proliferations, with cribriform glands and features of increased cellular turnover, such as abundant mitoses and apoptotic bodies (2). Stromal hypercellularity is also noted and was quite prominent in sections of TRAMP mice provided by NIEHS investigators for the Bar Harbor Pathology Workshop as well as appreciable in material from the originating laboratory (Table 1). During the 18-24 wk time frame in TRAMP mice, poorly differentiated metastases are noted in lymph nodes (31 % of mice 18-24 wks) and lung (36 % of mice at 24 wks) (2). An even higher frequency of lymph node (100 %) and pulmonary (67 %) metastases were present in a smaller number of TRAMP mice examined at 28 wks (2). Interestingly, one mouse developed well characterized osteoblastic bone metastasis in the vertebral column, documented at 22 wks. Hence, the pattern of metastases in the TRAMP mouse, including lymph node, lung, and bone, is similar to that of human Pca. As described further below, the morphologic features of the largest foci of unequivocally invasive tumors and those of the metastases in this model are suggestive of NE differentiation. As already described, visceral (lung, liver) metastases are characteristic of human prostate NE carcinomas. Identifying modifying factors, such as genetic background or particular molecular alterations in individual animals, that contribute to bone metastases may ultimately allow for models with

enhanced proclivity for bony metastases. This is a highly desirable objective in GEM from the perspective of understanding factors responsible for this common end-stage process in human Pca and for testing therapeutic agents to prevent or ameliorate this particularly deleterious outcome in human patients. Some previously illustrated primary tumors in the TRAMP model appear to represent invasive adenocarcinomas, distinct from the background precursor lesions (Figure 8). Prostate tumors described as well differentiated, moderately differentiated, and poorly differentiated carcinoma have been described in the literature, including in subsequent hormone manipulation and other molecular studies (2, 61, 108) as well as incorporated into a six-tiered grading scheme subsequently pubished (109) and used in interventional trials, including by other investigators (110-112). This spectrum of lesions noted in TRAMP mice is classifiable in the proposed Bar Harbor system.

The high grade PIN lesions are appropriately classified as PIN. Descriptors describing progressive involvement, architectural growth patterns, and progressive nuclear atypia can be added as described above. Many prostate sections corresponding to lesions classified as well differentiated adenocarcinoma were felt by most MMHCC panel pathologists to represent primarily in situ lesions, even if characterized by apparently increased gland spaces. Similar to even more exuberant forms of such glandular and stromal proliferations in LPB-Tag mice (see below), these lesions are generally symmetric and fairly uniform and diffuse. Although they may progress from more focal earlier PIN lesions, the extensive and essentially diffuse involement showing lobular expansion by proliferating epithelium and small acini that appear to connect up to larger more central duct profiles and with associated diffuse hypercellular stroma are in contrast to criteria such as focality and clearly invasive architecturally distinct foci recommended for recognition of unequivocal invasive carcinoma (e.g., as illustrated in Figure 8). In such models, these robust atypical epithelial and stromal proliferations likely represent a consequence of essentially uniform expression of the transgene driving cell proliferation or altering apoptosis in a fairly diffuse manner. However, illustrated examples (including in reviewed material) in which small glands extend out from such involved lobules and are clearly distinct from the background of more extensive or uniform involvement (e.g., Figure 8E) were felt by consensus to represent invasive adenocarcinomas. Recognition of such foci may be facilitated by a true desmoplastic response (see above). Although a consensus was not reached regarding whether such desmoplasia was evident in the examples provided, it has been noted by some of the involved pathologists (M.I., unpublished observations). When the entire focus is composed of glands (e.g., Figure 8E), the lesion is appropriately classified as well differentiated based on criteria described above. Again, note this is different than the classification in human Pca, in which invasive gland forming lesions in association with HGPIN are typically classified as moderately differentiated, as composed predomiantly of Gleason pattern 3 Pca (Tables 3 and 4). Metastases composed entirely or even predominantly of malignant glands (as opposed to more solid lesser differentiated foci) have not been reported. Of course, metastasis is NOT a sensitive indicator of invasive carcinoma in the human prostate (see above in section on Invasive Carcinoma in Classification Scheme). However, the metastatic potential of such gland-forming invasive foci remains to be demonstrated in any model.

Other definitions of well differentiated adenocarcinoma in previously published grading schemes, that is "epithelial cells obviously invading through the fibromuscular stroma layer and/or the presence of rounded nuclei with condensed chromatin within the fibromuscular stroma which is increased to more than 3-4 layers" (109) do not necessarily represent well differentiated adenocarcinoma in the Bar Harbor System. Invasion into the stroma will be classified as either microinvasive carcinoma or frank invasive carcinoma, as described above, but should be designated

45

as well differentiated adenocarcinoma only if composed exclusively or predominantly of well formed discernible glands. Further, it was the consensus opinion of the Pathology Committee that positive transgene immunostaining should not be utilized as a sole criterion for designating invasive carcinoma in any model, just as it should not be used as a sole defining criterion for metastases from the prostate when seen in lymph nodes or other distant tissues. For example, Tag positive immunostaining has been variably noted in stromal cells in multiple SV40 or large T-antigen based models (multiple Pathology Panel members, unpublished observations). In this particular situation of trying to discern possible stromal invasion by carcinoma, especially where a stromal response or associated stromal hypercellularity has been described, more conventional markers such as CK immunostaining in possible invasive foci are considered more reliable and definitive. Lesions satisfying currently recommended criteria for a designation of well differentiated adenocarcinoma in this model have not been seen to be spatially associated with foci previously designated as moderately or poorly differentiated carcinoma (R.B., M.I., unpublished observations), such that the relationship between these lesions (e.g., as in progressive dedifferentiation felt to occur with invasive carinoma progression in human Pca) is not clearly established yet. Conceivably, less differentiated or NE tumors could arise more directly in association with PIN in this as in other models (32, 37).

Typical examples of lesions previously described as moderately differentiated carcinoma in the TRAMP model (61, 109) were uniformly thought to have morphologic features of NE carcinoma (Figure 9). These clearly destructive invasive and potentially metastatic lesions showed histologic features, such as rosetting and chromatin characteristics, highly reminiscent of invasive tumors unequivocally shown to have NE differentiation by immunophenotypic and ultrastructural examination in other models (32, 37). However, as outlined above in the approach to tumors with possible NE differentiation (Table 5), it was the opinion of the Pathology Committee that similar confirmation of NE differentiation of these particular invasive lesions should be attempted by interested investigators in the TRAMP model as well. Some other published examples of moderately differentiated adenocarcinoma do appear to show glandular differentiation (e.g., Figure 3c in (109)), and if truly invasive based on properties described herein, these may be classifiable as adenocarcinoma, with differentiation status based on extent of glandular formation as described in the current proposal (Table 3). Further, although nuclear characteristics may be useful in the recognition of carcinoma, neither these nor the presence/frequency of mitoses or apoptosis should be incorporated in assessing the differentiation of invasive gland forming carcinomas as in previously utilized schemes (61, 109). Finally, lesions reported and described as poorly differentiated carcinoma, well represented in supplied material for review, were felt to most likely represent small cell carcinomas (or poorly or less differentiated NE carcinomas). Moderately and poorly differentiated foci, or NE carcinoma and small cell carcinoma (Figure 9) are seen to coexist, with admixed and transitioning foci, supporting a possible relationship between these invasive carcinomas and supporting the recommendation to not separately designate them as distinct entities (Table 2). Instead, typical small cell carcinoma is considered a subtype of NE carcinoma. Again, when such poorly differentiated foci are encountered in GEM models, especially those accompanied by hypercellular and potentially atypical stroma, consideration should also be given to the possibility of a sarcoma. Immunostaining protocols should include a panel to address carcinoma, NE carcinoma, and sarcoma or electron microscopy should be employed. Chromogranin and other NE marker immunostaining can be very focal and weak in such poorly differentiated small cell carcinomas. It was felt by the Pathology Panel that the NE differentiation and hence small cell carcinoma classification of these poorly differentiated carcinomas in the TRAMP model should be

appropriately confirmed by interested investigators. Subsequently, synaptophysin immunostaining has shown positive staining in these poorly differentiated lesions in TRAMP (e.g., Figure 9l), but not those previously designated as moderately differentiated (e.g., Figure 9j,k) (N.M., Greenberg, personal communication). These results support the suspected NE differentiation of the poorly differentiated, small cell carcinoma appearing foci. Possible NE differentiation in the lesions previously designated as moderately differentiated remains to be further addressed.

When TRAMP mice are castrated at 12 wks, the PIN lesions are seen to become atrophic (61), suggesting that the PIN lesion in this model is androgen responsive. The same appears to be true for the PIN lesions in LPB-Tag mice, as they respond similarly to castration (29, 54). In both models, the hypercellular stroma seems to persist, such that atrophic or regressed PIN glands are seen surrounded by a residual hypercellular stroma (29, 54, 61) (Figure 10). In TRAMP mice castrated at 12 wks and sacrificed at 18 or 24 wks, 3 of 7 and 8 of 10 mice, respectively, developed invasive tumors adjacent to such atrophic foci. These androgen independent tumors are reported to be more poorly differentiated with an increased metastatic rate (61). However, when TRAMP mice were castrated at four wks of age (prior to the peak level of androgens and sexual maturation that occurs at 6 wks), 43% of the mice developed tumors that were smaller but looked histologically similar to the tumors seen in intact mice. These data indicated that a significant percentage of neoplasms in TRAMP mice are already androgen-independent by four wks of age (108). In intact TRAMP mice 18-24 wks old, 35 % were classified as having lesions previously designated as well differentiated adenocarcinoma, 38 % "moderately differentiated", and 27 % "poorly differentiated" tumors. In contrast, 100 % of the tumors that developed in the TRAMP mice castrated at 12 wks and sacrificed at 18 and 24 wks were poorly differentiated. Note, this is a different phenomenon than the likely artefactual histologic "upgrading" of human Pca with standard 3-month neoadjuvant combined Lupron/Flutamide androgen-deprivation treatment. In this latter case, androgen sensitive tumor foci in the prostate are seen in the RP specimen to undergo changes such as nuclear pyknosis and cytoplasmic clearing that along with "collapse" of acinar structures can lead to the appearance of a more solid or poorly differentiated growth (9, 65, 66). This potential histologic upgrading is an underlying reason why it is generally recommended to not grade human Pca following standard androgen deprivation therapy. Although in such pretreated RP specimens, tumor foci are commonly seen that do not show these typical cytologic features of pre-treatment, it is unlikely that such brief anti-androgen therapy leads to selection of androgen insensitive tumors. Of course, such selection pressures may occur with long term anti-androgen treatment in patients with recurrent or advanced Pca and whether or not this could occur in some patients in long term anti-androgen chemoprevention trials remains to be seen. Although NE carcinomas with morphology compatible with both the lesions previously designated as moderate and poorly differentiated carcinoma have been observed to be potentially androgen independent in other models, the above results in castrated TRAMP mice are intriguing. These studies suggest that androgen deprivation may accelerate the progression to poorly differentiated and possibly small cell carcinoma. It would be interesting to note if molecular differences relating to possible altered androgen signaling or "upregulation" of signaling mechanisms bypassing androgen dependence could be detected in these different tumor morphologies in the same sections in intact mice.

TRAMP mice have been observed to develop poorly differentiated metastases when only a complex branching or papillary large and small acinar proliferation was present in the prostate, and which is not clearly distinguishable from an in situ proliferation. A morphologically similar invasive tumor is not necessarily identifiable in the prostate at the time of widespread metastases of poorly differentiated carcinoma. This same phenomenon has occurred in other transgenic mouse

models. Histologic progression ("dedifferentiation") of the tumor within the metastasis is a theoretical possibility. There are also sampling issues, wherein a small invasive, yet potentially metastatic tumor could be undetected in the prostate. However, caution must be exerted in GEM models with regard to the primary source of metastatic lesions. Neoplastic proliferations in the TRAMP mouse appear to be limited to the prostate, when considering other sampled organs and tissues (2). However, as described above, when androgen-dependent promoters are employed in creation of GEM models, it is possible that transgene expression and neoplasia development can occur in other androgen regulated male accessory glands, such as the periurethral gland and bulbourethral gland (37, 40). Multiple examples of bulbourethral gland involvement by tumors compatible with NE carcinoma were observed in GEM slides in the Pathology Study Set, including in TRAMP mice sections provided by different institutions (Figure 11). Whether or not involvement of such sites is primary or secondary, such tissues should be examined according to protocols described below. Consensus recognized definitive glandular differentiation is not present in metastatic foci in TRAMP, but these do express Tag oncoprotein, suggesting their origin from Tag positive tissue sites. With models that develop stromal hypercellularity, perhaps even including atypia, consideration must be given to metastatic sarcoma. Sarcomas have not been reported in TRAMP. Metastases to lymph nodes (more typical of carcinoma) and the apparent lack of Tag expression in the prostate stroma also argue against this in the TRAMP model. Normal lymphoid tissue is also Tag negative (2). Cytokeratin and more recently illustrated NE marker immunostaining and ultrastructural analyses may be useful in classifying metastatic tumors.

Multiple translational studies have been performed in TRAMP, examining the possible alteration with tumor progression of several genes or proteins thought to be important in human Pca. The results of such studies have in general shown similar alterations as in human Pca, and represent excellent examples of the possible utility of transgenic mice in Pca research. Multiple interventional trials have also been conducted in TRAMP mice (110-112). Compared to non transgenic mouse prostates, decreased immunostaining of E-cadherin was reported in areas compatible with PIN in an 18-wk old mouse (2). Lymph node metastases also showed decreased E-cadherin immunostaining (2). These results parallel the decreased E-cadherin expression observed in human Pca, which correlates with grade and may have prognostic significance (113-115).

Kaplan et al. (116) characterized alterations in the insulin-like growth factor (IGF) axis in the TRAMP model. IGF-I mRNA was increased in prostates from 30 wk old TRAMP mice and metastatic lesions compared to prostates from 12 wk old TRAMP mice, and increased serum levels of IGF-I were detected in TRAMP mice as early as 12 wks. In contrast, IGF-I mRNA was not increased in prostates (most of which have poorly differentiated tumors) or metastases of TRAMP mice castrated at 12 wks and sacrificed at 24 wks of age. IGF1 receptor (IGF1R) and IGF2R mRNA were decreased in prostates and metastatic lesions of castrated but not intact TRAMP mice (116). These studies suggest that in TRAMP mice the organ-confined lesions could be IGF-I-dependent, whereas metastatic and advanced/poorly differentiated androgen-independent tumors may be IGF1R-independent. These interesting results parallel human epidemiologic studies correlating increased serum levels of (IGF)-I with increased Pca risk (117). In a recent study in the TRAMP model, increased microvessel density with progression from the PIN/well differentiated adenocarcinoma stage to the more poorly differentiated and androgen insensitive advanced tumors was associated with a "switch" from VEGFRI to VEGFRII expression (118). This was paralleled by studies in human prostate tissues, showing increased VEGFRII in cancer vs. benign (118).

LPB-Tag: Eleven LPB-Tag founders were generated, numbered as 12T-n where n = 1 to 11, utilizing the long probasin promoter (LPB) to drive the prostate epithelial expression of a modified SV40 early region (36). These LPB-Tag lines have been collectively referred to as "LADY" by their developers, emphasizing their recognized differences from the TRAMP model described above. The LPB promoter is approximately 11,500 bp, adding upstream enhancers to the sPB –426/+28 promoter, which results in higher transgene expression (36). Although the large T antigen is expressed, the region of the SV40 early region encoding the small t-antigen was modified, such that the small t antigen is not expressed (36). There are some general similarities between this "LADY" model and the TRAMP model, such as the lobular expansion by proliferating atypical epithelium with hypercellular stroma in the anterior and dorsal lobes and the apparent NE differentiation of the advanced and metastatic tumors (previously confirmed in LPB-Tag mice (37). However, there also very appreciable phenotypic dissimilarities. In addition to being on different genetic backgrounds, the differences in the employed promoter and transgene are likely fundamentally responsible for the different phenotypes.

In the LPB-Tag mice, six founders established seven transgenic lines (line 12T-7 diverged into a 12T-7 fast (f) and a 12T-7 slow (s) line), where each received a different transgene copy number from the founder and which demonstrate different rates of neoplastic growth of the prostate (36). In all of the lines, epithelial proliferation with atypical, enlarged, and hyperchromatic nuclei begins focally, and the nuclei of such transformed cells are immunoreactive with an antibody to the SV40 Large T antigen (36). In the fast growing lines, such as 12T7f, 12T7s, and 12T5, the DPs (DLPs) and APs quickly show changes that account for the profound prostate enlargement in these mice. There is a fairly uniform and symmetric lobular expansion with atypical epithelium surrounded by markedly hypercellular stroma (Figure 5a). There is clearly the creation of new glandular spaces compared to the wild type prostate, with small acini surrounding and apparently connecting up to the more central larger duct profiles. The more peripheral small gland profiles show similar marked nuclear atypia as the more central glands/ducts. Although new gland spaces exist, the fairly uniform and symmetric nature of this process has led to its interpretation as a likely in situ process (16, 29, 36), an opinion which was shared by the Bar Harbor Pathology Panel. As it begins focally, is characterized by obvious nuclear atypia, and progresses both in extent and degree, this lesion satisfies recommended Bar Harbor classification criteria for PIN. Further, this lesion appears to have invasive potential, with occasional documented progression to invasive adenocarcinoma and less differentiated carcinomas (16, 29, 36). However, as the morphology of this in situ lesion is different from other described mPIN lesions, including that occurring within the VP of these same mice, descriptive modifiers have been attached, such as "lobular expansion by atypical epithelium with hypercellular stroma or PIN, LEHS" (16, 29).

The epithelial proliferations in the AP and DLP of faster growing LPB-Tag lines are consistently associated with hypercellular stroma. The stromal proliferation appears to be a uniform and diffuse process, likely a consequence of the genetic manipulations involved. Such stromal hypercellularity may result as a paracrine effect from the proliferating epithelial cells. However, as described elsewhere, attention needs to be given in this and other models to the possible direct transgene expression in and consequent proliferation of stromal cells. The hypercellular stroma typically shows phenotypic features compatible with prostate stroma, even at later stages with extreme hypercellularity (Figure 5a). In addition, there is commonly an apparent condensation of stroma immediately underneath neoplastic epithelium, particularly with advanced ages (16, 29, 36). These foci, similar in appearance to those illustrated in Figure 5c, have oval to spindle nuclei, with scant cytoplasm, and increased atypia. In advanced stages the nuclear morphology of these cells is

49

quite similar to the immediately adjacent neoplastic epithelium, such that distinguishing atypical epithelium from these underlying cells is difficult. Similar foci have been noted in combined epithelial and stromal proliferative lesions in the seminal vesicles of this model and were noted in seminal vesicle sections of TRAMP slides (e.g., those provided by NIEHS investigators for the Pathology Panel). Whether these atypical stromal foci in closer proximity to the atypical epithelium are derived from stroma or from epithelial mesenchymal transformation accompanying the neoplastic process remains to be addressed. Interestingly, the marked epithelial and stromal proliferation that occurs in the AP and DP/DLP of the fast growing LPB-Tag lines is not seen in the VP. In the VP, neoplastic epithelial proliferation occurs without hypercellular stroma and without altering the normal gland profiles, such that the PIN lesions are characterized by stratification of enlarged hyperchromatic nuclei within gland profiles similar to wild type. Similar mPIN lesions are seen in all prostate lobes of the slower growing LPB-Tag line 12T-10 (37).

Against the background of marked lobular expansion and hypercellular stroma, discerning possible microinvasion as the extension of tumor cells through glandular basement membranes into surrounding stroma in the AP or DLP of the fast growing LPB-Tag lines can be difficult. Micro-acinar architecture and cells with enlarged clear cytoplasm at the base of PIN containing ducts/glands are suspicious for invasion. For example, such lesions have been observed prior to the time points of more extensive invasion and metastasis in the 12T-10 line (37). In the fast growing lines, foci of unequivocal stromal invasion have been observed (16, 29, 36), further supporting the precursor nature of the PIN lesions described above. In addition, focally architecturally distinct extension of gland forming atypical epithelium into surrounding periprostatic loose connective tissue/adipose tissue is occasionally observed, somewhat analogous to lesions described and illustrated above as well differentiated adenocarcinoma in TRAMP mice (Figure 8e). Efforts should be made to distinguish such foci from a more physical "herniation" of proliferating glandular and stromal tissue into the loose periprostatic connective tissue. A true desmoplastic response or altered nuclear and cytoplasmic features in such foci would support invasion. In addition to these areas of extension into tissue surrounding the hypercellular fibromuscular stroma, foci are occasionally noted within the stroma in which there are more crowded small gland profiles that are architecturally distinct at lower magnifications compared to the more uniform symmetric lobular expansion. Such foci often show altered nuclear and cytoplasmic features (Figure 8d). Such lesions were recognized by consensus of the Bar Harbor Pathology Panel as invasive carcinoma (these foci are typically microinvasive; more frankly invasive depends on extent, such as > 1mm).

The large size of the neoplastic prostate in the fast growing LPB-Tag lines limits maintaining these mice for prolonged periods of time (past 5-6 months). During this time progression to unequivocal invasive carcinoma, including NE carcinoma, occurs uncommonly. In a recent survey, invasive NE carcinoma was observed in the VP of 1 of 10 12T-5 mice 19-25 wks old, invasive adenocarcinoma with extension into fat was seen in the DLP and invasive NE carcinoma in the VP in 4 and 2, respectively, of 18 12T7s mice 21-26 wks old, and invasive adenocarcinoma with extension into fat was noted in the DLP and/or AP of 3 of 20 12T7f mice 15-20 wks old (S.B.S., unpublished observations)[4]. Similar to that reported in 12T-10 mice, occasional mice of faster growing lines show atypical hyperplasias and frankly invasive NE carcinomas in the bulbourethral and periurethral glands (101). Rarely do these faster growing lines develop metastatic carcinoma. However, when mice from these transgenic lines were castrated at late stages of prostatic neoplasia (e.g., 16-24 wks), the primary prostate PIN lesion regressed, with atrophy and residual hypercellular stroma. In many such mice there developed an extensive, frankly invasive, and metastatic poorly differentiated carcinoma with NE differentiation (appropriately classified as NE carcinoma using

50

criteria described herein) (29, 54)[4]. Such tumors are immunoreactive for the Tag antigen, but are only weakly positive or are negative for AR immunostaining (54). Whether such tumors arise spontaneously now that the mouse can be carried out to an older age or whether androgen deprivation exerts selective pressure as speculated above for similar studies in the TRAMP model is not clear. Castration studies provide a possible modification of the model to allow for study of emergence of androgen insensitive tumors, and the more recently characterized 12T-10 line (described below) appears to progress through reproducible stages of PIN, to invasive and metastatic androgen insensitive NE carcinoma spontaneously.

Similar to other LPB-Tag lines, the prostate in the 12T-10 mouse shows progressive epithelial proliferation with marked nuclear atypia diagnostic of mPIN. However, the epithelial proliferation appears to conform much more to normal gland profiles, without prominent lobular expansion and stromal hypercellularity (37). As such, the initial lesions are more morphologically analogous to human PIN (Figure 6). In contrast to some of the other LPB-Tag lines, prostate enlargement in the 12T-10 line is slower (36). However, the PIN lesion predictably progressed to microinvasive carcinoma and more extensive foci of invasive carcinoma, both with and without definitive glandular differentiation (37). By 44 wks of age, most of these 12T-10 mice were reported to develop metastatic poorly differentiated carcinoma in lymph nodes, lung, and liver (Figure 8) (37). The more extensive locally invasive tumors and the metastatic lesions show histologic features of NE differentiation, including scant cytoplasm, granular ("salt and pepper") chromatin, and rosette formation. NE differentiation was confirmed by immunohistochemical studies (e.g., chromogranin) and ultrastructurally, and appears to be present in a progressively greater fraction of cells with progression of PIN (37). Overall, in a characterization of 52 mice aged 2 to 12 months, 100 % of the mice ≥ 2 months had PIN (previously described as high grade based on nuclear features), with foci of microinvasion noted in 20, 40, 80, and 100 % of mice 4, 5, 6, and ≥ 7 months, respectively. Definitive foci of invasion, with glandular or NE differentiation, were present in 40 % of mice 6-7 months of age and in > 80 % of mice ≥ 8 months of age. Metastases in retroperitoneal lymph nodes, liver, or lung were present in 66 % of mice ≥ 6 months and 88 % of mice ≥ 9 months, correlating with the presence of histologically similar invasive tumor in the prostate. The invasive and metastatic NE tumors are Tag immunopositive but are only weakly positive or are negative for AR immunostaining, suggesting possible androgen independence. The latter is supported by the existence of morphologically similar or identical tumors in castrated other LPB-Tag lines. The metastatic capability of the advanced NE tumor was also demonstrated by the development of similar visceral metastases in nude mice with subcutaneous transplants of the 12T-10 tumor. Primary and metastatic tumors showed similar protein profiles, distinct from those of benign prostate, as assessed by matrix assisted laser desorption ionization time-of-flight mass spectrometry (37). The allograft has been sequentially passaged in nude mice more than ten times, with identical NE differentiation, and growth is unaffected by castration, further confirming its androgen independence (119).

Recent studies have begun addressing altered expression of genes with tumor progression or the possible occurrence of similar molecular alterations in LPB-Tag mice as in human Pca. Similar to recent reports showing upregulation of 15-lipoxygenase-1 (15-LOX-1) and cyclooxygenase-2 (COX-2) in high grade (Gleason score 8-10) human Pca (120, 121), studies using enzyme activity assays, mRNA quantitation, and immunostaining show the murine 12/15-LOX homologue of human 15-LOX-1 is increased in PIN and invasive and metastatic carcinoma and COX-2 is increased in PIN in castrated fast growing lines and intact 12T-10 LPB-Tag mice (122). Others have observed increased expression of the murine 12/15-LOX in prostatic neoplasia in TRAMP

51

mice (Uddhav Kelavkar, personal communication). In contrast to human 15-LOX-2, which is essentially uniformly expressed in differentiated secretory cells of benign prostate and reduced or absent in HGPIN and most Pcas (60, 121, 123), the murine homologue 8-LOX (124) is not expressed in wild type or LPB-Tag prostates (122).

Recent studies have shown inhibition of human Pca cell line proliferation by synthetic thiazolidinedione and potentially endogenous ligands for the nuclear receptor peroxisome proliferator activated receptor gamma (PPARγ) (125-128). A small phase II clinical trial showed potential benefit of a PPARγ agonist in patients with advanced Pca, including hormone refractory Pca (127), although the *in vivo* mechanism for the latter effect remains to be defined. The PPARγ agonist rosiglitazone (Avandia™) inhibited angiogenesis and metastases in the allograft model established from the LPB-Tag 12T-10 advanced NE tumor (129) and inhibited metastases in intact LPB-Tag mice from multiple lines (101). Finally, in bigenic mice established from crossing the fast prostate growing LPB-Tag 12T7f line to a line expressing a dominant negative mutant of the TGFβ type II receptor in the prostate under a metallotheionein promoter (MTDNIIR), there was an acceleration of the phenotype, with invasive adenocarcinoma reported at earlier time points compared to PIN-alone lesions in either parental strain and an increased incidence of metastases in bigenic mice (130). These studies support the potentially important role of altered TGFβ signaling in Pca progression.

CR-2-SV40 Early Region Mice: The transgenic mouse CR-2-SV40 employing a cryptidin-2 promoter and the SV-40 early region in FVB/N mice represents a novel model of NE carcinoma of the prostate (32). The transgene construct was originally intended to express the SV40 early region in intestinal paneth cells, but instead resulted in expression in the mouse prostate with 100 % development of prostatic neoplasia. Transgene expression in the prostate is limited to a subset of cells that show NE differentiation (32). The reproducibity of the CR-2 promoter to direct transgenes to prostate NE cells was indicated by its ability to direct the unrelated human growth hormone gene to prostate NE cells (32)

In the initial characterization of the CR-2-SV40 model, 100 % of mice in four lines 5-7 months of age were noted to have prostate tumors. Two subsequently well characterized lines had 100 % penetrance of the prostate lesion. Transgene expression begins around 7 to 8 wks, with focal emergence of lesions compatible with PIN occurring at 8 to 10 wks (32). By 12 wks, all prostates had multifocal PIN and in 70 % there was focal microinvasion into the stroma. The illustrated lesions interpreted as invasion through the basement membrane satisfy the criteria of microinvasive or early invasive carcinoma outlined herein. Recognition of such is facilitated by the general lack of a hypercellular stroma in this model, and confidence in the classification of early lesions as microinvasive is gained by the unequivocal progression to more extensive invasive carcinomas (Figure 8c). By 16 wks, 90 % of prostates had invasion, with 25 % containing more extensive local invasive disease characterized as tumors ≥ 3mm, composed of nodules of poorly differentiated carcinoma. Foci of lymphovascular and perineural invasion were also noted (32). The frequency and extent of local invasion progressed, such that 100 % of prostates at 24 wks contained large tumor nodules composed of sheets of cells without glandular differentiation. These tumors had histologic and cytologic features highly suggestive of NE differentiation, including oval/spindle cells with scant cytoplasm, granular chromatin, and rosette formation. NE differentiation was confirmed by immunostaining for synaptopysin and chromogranin and by electron microscopic examination (32). Furthermore, studies at early time points showed the coexpression of NE markers

52

and the large T-antigen in proliferating cells. During evolution of these PIN lesions, coexpression of large T-antigen and NE markers was maintained (32).

These studies indicate that the CR-2 promoter specifically targets prostate NE cells. The PIN and subsequent invasive carcinoma thus arise from neoplastic transformation of the NE cell population within normal prostate glands, and this evolving tumor has NE differentiation from its inception. This appears to be a distinct mechanism from the above models of confirmed or possible NE carcinoma, in which the SV40 early region or large T antigen transgenes are presumbably targeted to prostate epithelial cells, which can differentiate into secretory cells. It is not possible to exclude expression in androgen responsive epithelial cells (even basal cells) prior to terminal differentiation into luminal secretory cells. Such cells also likely give rise to the NE cells in normal prostate. Transgene expression could also alters normal luminal cell differentiation. As such, the possibility that PIN lesions in these other models show progressive NE differentiation should be considered along with the possibility that later stage invasive tumors show progression to NE differentiation (37). The possible androgen dependence of the NE tumor development in CR-2-SV40 mice was investigated. In 8 wk old prostates of the transgenic mice, cells immunopositive for Tag were negative for androgen receptor (AR). At later time points, invasive Tag-immunopositive tumor cells remained negative for AR. Furthermore, although castration resulted in expected atrophy of benign prostate glands, the nature and extent of the PIN and invasive tumor at 10, 16, and 24 wks was not altered by castration at 4 wks (32).

In addition to invasive NE prostate tumors, CR-2-SV40 mice predictably develop metastatic tumor. Metastases were present in 40 % of mice at 24 wks, involving abdominal lymph nodes, liver, lung, and bone marrow and showing expected cytologic features of NE carcinoma (32). The precise frequency of bone metastases and a possible osteoblastic component have not been described in detail. Invasive tumors were not noted in other organs. Interestingly, though, mild degress of epithelial proliferation with atypia are occasionally noted in periurethral and bulbourethral glands (Figure 11h) (P.A.H., unpublished observations). This may reflect transgene expression in a potentially very minor normal NE cell population in these tissues. In the human, the prostate has the highest percentage of NE cells within the genitourinary tract. In chromogranin immunostained wild type mouse prostates, there is an extremely minor normal population of immunophenotypically NE cells (32, 37). How this compares to the frequency of such cells in other male accessory glands remains to be demonstrated. However, in the CR-2-SV40 mouse, although these other male accessory glands may be secondarily involved by local extension from prostate tumors, they do not appear to give rise to frankly invasive carcinomas (P.A.H., unpublished observations).

Elegant gene expression studies and bigenic mouse models have been utilized to begin characterizing the molecular mechanisms responsible for tumor progression in the CR-2-SV40 mouse. Recent studies in human Pca have shown increased expression of the transcription factor EGR1 (early growth response factor 1) and decreased expression of NAB2, a corepressor which may modulate EGR1 transcriptional activity (131, 132). Compared to CR-2-SV40/$Egr1^{+/+}$ and CR-2-SV40/$Egr1^{+/-}$ mice, CR-2-SV40/$Egr1^{-/-}$ mice on a similar FVB/N x C57Bl/6 background had improved survival and reduced invasive tumors at 35 wks by MRI examination (90). Tag transgene expression was not effected and PIN lesions developed at the same rate in CR-2-SV40/$Egr1^{-/-}$ mice as in controls. Proliferation and apoptotic rates as determined by Ki-67 immunostaining and TUNEL assays were also not different between the two groups. Importantly, blinded histopathologic analysis showed that CR-2-SV40/$Egr1^{-/-}$ mice had a delay or inhibition of the transition from PIN to invasive carcinoma. Five of 6 and 6 of 6 control mice at 25 and 35 wks had

foci of invasive carcinoma, whereas invasion in CR-2-SV40/*Egr1*^{-/-} mice was only present in 1/5 and 2/5 at 25 and 35 wks, respectively. This inhibition of the transition from PIN to invasive carcinoma was paralleled by an inhibition of angiogenesis (at 25 wks) and reduced expression of the potentially EGR1 regulated genes TGFβ1 and PDGF-A in PIN and tumor foci in CR-2-SV40/*Egr1*^{-/-} mice compared to controls (90). Impaired progression to invasive tumor was also demonstrated in the TRAMP/ *Egr1*^{-/-} mice (examined at 20, 25, and 35 wks) by the same investigators (90).

Nkx3.1 knockout mice and Nkx3.1 knockout x PTEN knockout mice: Alterations in genes implicated in normal tissue specific development and maintenance of function may play unique roles in site specific neoplasms. Nkx3.1 is a prostate selective homeobox gene implicated in normal prostate development (47). Interest in this gene in prostate neoplasia is supported by common loss of heterozygosity (LOH) in human Pcas of 8p21, where Nkx3.1 maps to (133). LOH at this region also occurs in the majority of human PIN lesions (134). Interestingly, mutations in the Nkx3.1 gene have not been detected in human Pcas (135), whereas absent or reduced protein expression determined by immunostaining has been observed in both PIN and Pca, with increased frequency in hormone refractory and especially metastatic Pca (136). Such results suggest that if Nkx3.1 is a tumor suppressor gene in human Pca, the second allele may be inactivated by epigenetic mechanisms. Proliferation of human PC3 and rodent AT6 Pca cell lines, which do not express Nkx3.1, was inhibited by transfection of exogenous Nkx3.1 (3). Tumor growth in nude mice was also inhibited by overexpression of exogenous Nkx3.1. In contrast, overexpression of a mutated derivative that codes for a protein that is inactive in DNA binding had no inhibitory effect on cell line proliferation or tumor growth in mice. These studies suggest specific growth suppressing biologic functions for this putative tumor suppressor gene product (3).

In the adult mouse, Nkx3.1 is expressed selectively in the prostate (AP, DLP, VP) and BUGs, without detectable expression in seminal vesicle and other Wolffian duct derivatives (50). In situ hybridization in sections of mouse embryos at 14.5 to 17.5 days (prior to and during prostate formation) showed Nkx3.1 expression in regions where prostatic buds arise as well as in the developing BUG (50). In the neonatal period wherein extensive prostate ductal outgrowth and branching occurs, Nkx3.1 expression persisted in all prostatic lobes, with highest expression noted toward the most active growing regions of the distal ends of the developing ducts (50). Nkx3.1 expression also continued in the developing BUGs. Both abnormal development/differentiation and neoplastic epithelial proliferation have been described in the prostates of Nkx3.1 knockout mice. Mice homozygous for a null mutation of Nkx3.1 (Nkx3.1 -/-) displayed morphologic alterations compatible with prostate ductal hypoplasia in all lobes. Ductal tip number was reduced based on quantitative analysis of Nkx3.1 -/- vs. wild type mouse sections at 12 wks of age (50). Reduced ductal complexity was accompanied by documented abnormalities in secretory differentiation, including the reduced or defective production of specific prostatic secretory proteins (50). Compared to wild type mice, BUGs in Nkx3.1 -/- mice were smaller and showed reduction in differentiated mucin producing cells, an increase in ductal cells, and reduced production of specific secretory proteins (50).

Reduced ductal complexity in Nkx3.1 -/- is accompanied by prostate epithelial cell proliferation. The AP in Nkx3.1 -/- mice showed epithelial hyperplasia as early as 4 wks, with stratification of luminal cells without appreciable nuclear atypia. However, by 12 wks, foci of nuclear atypia and pleomorphism were noted. Such lesions appear to progress, wherein at one year, the AP shows marked epithelial hyperplasia with focal nuclear atypia (50). Similar, but less pronounced lesions are noted in the DLP at 1 year, where milder degrees of epithelial hyperplasia

54

are accompanied by focal nuclear atypia, initially reported as severe dysplasia (50). Progression to frank invasive carcinoma was not noted in any lobe. A similar but less pronounced phenotype of hyperplasia with dysplasia was noted in both the AP and DLP of hetetozygous knockout mice, indicating haploinsufficiency for the reported phenotype (50). The histologic impression of hyperplasia (Figure 4f,g) was supported by documented increases in cellular proliferation, based on quantitation of Ki-67 immunostaining in AP sections of 6 wk old Nkx3.1 -/- and Nkx3.1 +/- compared to wild type mice (50).

A more recent report described the progressive phenotypic alteration in older Nkx3.1 knockout mice, as well as explored the possible impact of genetic background on lesion severity (3). In Nkx3.1 homozygous and heterozygous knockout mice, progressively severe alterations in both epithelial hyperplasia and nuclear atypia were noted in non-blinded histopathologic analysis by one of the members of this MMHCC Prostate Pathology Committee (R.D.C.) and in blinded analysis by the involved investigators. The focal nature of the initial lesions and the progression in epithelial proliferation and nuclear abnormalities satisifies the definitions of mPIN as outlined herein. In a mixed C57Bl/6J/129/SvImJ background, 11 of 16 Nkx3.1 -/- mice aged 12 to 24 months were noted to have PIN. Compatible with previous observations of haploinsufficiency in younger mice, a lower percentage (4 of 11) of heterozygous knockout mice developed histologically similar PIN lesions (3). PIN lesions were described as demonstrating epithelial cell proliferation, with papillary and cribriform architecture, and nuclear atypia manifested as enlarged nuclei with vesicular chromatin and prominent nucleoli with readily identifiable mitotic figures. Similar PIN lesions were noted in 12-15 month old mice in inbred C57Bl/6J, FVB/N, and 129/SvImJ backgrounds, with possible reduced frequency of PIN lesions in the 129/SvImJ background (3). In none of the mice up to 2 years of age were these PIN lesions accompanied by frank invasive carcinoma. This model would thus appropriately be classified according to the current proposed Bar Harbor classification scheme (Table 2) as showing PIN without documented progression to invasive carcinoma. Interestingly, in an effort to begin analyzing possible potential for progression, a novel tissue recombination model was employed. Prostate ducts of 12-15 month old wild type and Nkx3.1 -/- mice were combined with fetal rat or mouse urogenital sinus mesenchyme and implanted under the renal capsule of SCID mice for 1-2 months. Initial and serial passages of wild type mice show usual prostate architecture, with well organized ducts surrounded by fibromuscular stroma and containing a typical single layer of columnar secretory epithelium and associated underlying basal cells. In contrast, serial passages of Nkx3.1 -/- tissue recombinants showed progression to greater histopathologic architectural complexity, with smaller acinar profiles, cribriforming, and solid growths within the ducts and a focally attenuated surrounding stroma, but without progression to frank invasion into surrounding stroma (3). The tissue recombinant studies support potential for lesion progression in this model, although not yet to invasive carcinoma per se. Such studies also raise consideration for similar studies to address potential for progression in other GEM PIN models, as alluded to above for transplantation studies. It would be of interest to see how PIN lesions derived from models with know progression in intact mice would behave in initial recombinants or serial passages in this tissue recombinant model. Such studies may allow for validation of this novel approach to detect PIN lesions with true potential for progression to adenocarcinoma in newly generated models. More experience with the histologic interpretation of such recombinants may also allow incorporation of their results into future classification strategies.

The development of epithelial hyperplasia and dysplasia compatible with mPIN with the loss of expression of Nkx3.1 in the prostate was recently confirmed in a model of prostate selective Nkx3.1 knockout (35). Using loxP-mediated recombination, mice with a conditional Nkx3.1 allele

(*Nkx3.1^{flox}*) were crossed with *Actin-Cre* transgenic mice for Nkx3.1 deletion in the germ line or with *PSA-Cre* transgenic mice made with a 6 kb fragment of the PSA promoter to achieve prostate specific Nkx3.1 deletion in adult mice. *Nkx3.1^{-/-}* (homozygous non-selective knockout), *Nkx3.1^{+/-}* (heterozygous non-selective knockout), *PSA-Cre^+Nkx3.1^{-/flox}*, *PSA-Cre^+ Nkx3.1^{flox/+}*, and *PSA-Cre^+Nkx3.1^{flox/flox}* mice were examined by blinded histologic analysis. Epithelial hyperplasia and dysplasia were noted in both Nkx3.1-/- and Nkx3.1+/- mice (35), as noted in earlier studies with targeted gene disruption by homologuous recombination in ES cells (50). The lesions in the heterozygous mice again indicated haploinsufficiency for the phenotype. Also, as previously noted, no invasive carcinoma was seen in mice aged up to one year (35). In mice made with the PSA-Cre+ transgenic mice, there was no Cre activity detected in the prostates at 3 wks, but it was evident at 10 wks and 30 wks, with recombination particularly apparent in the VPs and DLPs. In mice with the conditional knockout of Nkx3.1 in the prostates, epithelial hyperplasia and focal lesions designated as PIN were noted. PIN lesions showed nuclear enlargement with prominent nucleoli. Although not rigorously demonstrated to temporally progress in extent, the cytologic and other features of this lesion are compatible with mPIN reported previously in non-conditional Nkx3.1 knockout mice. Such PIN lesions were present in 8 of 9 *PSA-Cre^+Nkx3.1^{flox/flox}* mice aged 21-25 wks as well as 4 of 11 *PSA-Cre^+ Nkx3.1^{flox/+}* mice aged 15-35 wks, the latter again supporting that loss of one Nkx3.1 allele is sufficient to initiate PIN development. PIN lesions were further characterized as showing increased proliferation by Ki-67 immunostaining and partial disruption of the basal cell layer using immunostaining with the mouse anti-human HMWCK antibody 34βE12 (35). Interestingly, in PIN lesions developing in *PSA-Cre^+ Nkx3.1^{flox/+}* mice, immunostaining for Nkx3.1 was reduced in many dysplastic cells in PIN foci compared to normal and hyperplastic foci (35).

Cooperativity in the development of prostatic neoplasia was recently described in mice with loss of function in both Nkx3.1 and the putative tumor suppressor PTEN (34). The prostate and other organ pathology in mice with germline knockout of PTEN is described below. In the study by Kim et al., *Nkx3.1^{+/-}* and *Pten^{+/-}* mice were bred in a mixed C57BL/6J-129/SvJ background to produce the following genotypes: *Nkx3.1^{+/+}; Pten^{+/+}*, *Nkx3.1^{+/-}; Pten^{+/+}*, *Nkx3.1^{-/-}; Pten^{+/+}*, *Nkx3.1^{+/+}; Pten^{+/-}*, *Nkx3.1^{+/-}; Pten^{+/-}*, and *Nkx3.1^{-/-}; Pten^{+/-}* (34). Compatible with past results, single mutant mice with heterozygous or homozygous deficiency of Nkx3.1 (and wild type PTEN) and examined at three month intervals up to 15 months developed prostate epithelial hyperplasia with less severe dysplasia than that noted in PTEN +/- mice in this and other studies. In this study, PTEN mutant mice with wild type Nkx3.1 (i.e., Nkx3.1+/+; Pten +/-) developed foci of severely dysplastic epithelium. However, blinded analysis of the prostate pathology showed that the compound mutant mice with loss of function for both Nkx3.1 and PTEN showed cooperativity in the development in the AP and DLP of a lesion designated as "HGPIN/early carcinoma". These lesions were characterized by multifocal epithelial proliferation into the gland/duct lumens accompanied by nuclear enlargement and atypia, with prominent nucleoli and frequent mitotic figures (Figure 7 i,j). The higher proliferative rate in such foci was confirmed by Ki-67 immunostaining (34). The rationale for the inclusion of the term "early carcinoma" in the designation is not clear. The illustrated or described lesions do not satisfy the criteria described above for microinvasive or invasive carcinoma. Immunostaining for endoglin (CD105) demonstrated increased vessels in the apparent cribriform lesions filling some duct lumens. This raises consideration about newly formed associated vessels and stroma and the existence of "back to back glands" within duct lumens, although the overall duct and lobular architecture was not altered. Whether such lesions will eventually be associated with unequivocal destructive invasion into the surrounding fibromuscular stroma in this or other models remains to be seen. The progressive extent

and severity of the in situ lesions in this model served as a basis for a separately reported classification scheme for progressively severe PIN (82). The authors reported that no increase in the occurrence of LGPIN was seen in compound mutants. Again, the MMHCC Consensus Classification does not currently allow for grading of PIN as analogous to such grades in human PIN, and so we do not recommend the specific use of terms LGPIN and HGPIN. However, this study also illustrates that modifiers in PIN-like lesions can allow for the development of scoring schemes that may be applicable within any individual model or that may be useful in studies attempting to discern an altered phenotype with blinded histologic analysis (e.g., to characterize a phenotype in a new model, in bigenic crosses involving existing mice, or in treatment trials in an existing model). In the study by Kim et al., cooperativity was seen between loss of Nkx3.1 and Pten function as manifested by decreased latency for the development of the lesion referred to as HGPIN/early carcinoma in blinded histopathologic analysis (34). At 6 months, such lesions were seen in 60 % of $Nkx3.1^{-/-}$; $Pten^{+/-}$ mice and 36 % of $Nkx3.1^{+/-}$; $Pten^{+/-}$ mice, but only in 10 % of the $Nkx3.1^{+/+}$; $Pten^{+/-}$ mice. At one year of age, such lesions were noted in all of the compound mutant mice ($Nkx3.1^{-/-}$; $Pten^{+/-}$, $Nkx3.1^{+/-}$; $Pten^{+/-}$) in contrast to 34 % of the single mutant heterozygous PTEN knockout mice ($Nkx3.1^{+/+}$; $Pten^{+/-}$) (34).

Compared to strong nuclear immunostaining in histologically normal prostate luminal epithelial cells, Nkx3.1 immunostaining, but not mRNA expression, was reduced in the lesions designated as HGPIN/early carcinoma in the $Nkx3.1^{+/-}$; $Pten^{+/-}$ compound mutants (34). Nkx3.1 immunostaining was also reduced or absent in foci designated as atypical hyperplasia, LGPIN, and HGPIN in Pten +/- single mutants (with wild type Nkx3.1) and in Nkx3.1 heterozygous knockouts with wild type Pten. Similar to recent studies utilizing human tissue microarrays that showed reduced Nkx3.1 protein in PIN and Pca (136), immunostaining of 27 human specimens showed reduced or absent Nkx3.1 in 56 % and 26 % of Pcas, respectively (34). Further, analysis of lesions in $Nkx3.1^{+/-}$; $Pten^{+/-}$ compound mutants did not demonstrate loss of the wild type Nkx3.1 allele, in contrast to the common allelic loss of Pten in such lesions (34). Hence, similar to that postulated in human PIN and Pca, the results in this model and the selective Nkx3.1 knockout mouse described above suggest that silencing of the wild-type Nkx3.1 allele and thus complete loss of Nkx3.1 expression may be important for neoplastic development or progression and that this may occur via epigenetic inactivation.

ARR₂PB-FGF8b transgenic mice: Fibroblast growth factor 8 isoform b (FGF8b) is increased in Pca cell lines and in the malignant epithelial cells of Pca (137, 138). Further, FGF8b and its receptors are increased in human PIN (139). In situ hybridization demonstrated increased expression of FGF8 in the PIN lesions of the fast growing LPB-Tag lines 12T7f and 12T7s (described above) compared to wild type mice, with RT-PCR indicating FGF8b as the major FGF8 species (140). FGF8b was also detected in TRAMP-C cells derived from the TRAMP model (140).

To further characterize a possible role of FGF8b in prostate carcinogenesis, four productive transgenic mouse lines were established using the 468 bp small composite probasin promoter (141) to overexpress FGF8b in the prostate (140). The transgene was expressed in all prostate lobes, as well as in the ductus deferens, seminal vesicles, and epididymis, but not in other examined tissues. Line 3 was most extensively characterized, with histopathologic examination of mice from one to 24 months. Overexpression of FGF8b in the prostate led to multifocal epithelial hyperplasia, evident as early as 2-3 months in the VP and LP, followed by similar lesions in other lobes. Foci with increased nuclear atypia were noted, with temporal progression in extent and in architectural and cytologic abnormalities, indicative of mPIN. Flat, tufting, papillary and cribriform architectures

were noted. Based primarily on the degree of nuclear atypia, such lesions were classified as low grade (LGPIN) and high grade (HGPIN). Mitotic figures were appreciable, with an increase noted in lesions designated as high grade. These foci designated as high grade demonstrated increased nuclear size and hyperchromasia and prominent nucleoli (Figure 7h). Regarding the time course of progression, epithelial hyperplasia was noted in the VP and/or LP of 6 of 7 mice one to six months old, with atypia designated as LGPIN in 2 of 7. Hyperplasia was noted in all mice up to 14 months of age. Lesions referred to as LGPIN were present in 3 of 9 mice seven to twelve months old and 10 of 14 mice thirteen to eighteen months old. In this latter age group, lesions designated as high grade were noted in 4 of 14 mice, whereas these high grade lesions were noted in the prostate of 12 of 16 mice nineteen to twenty-one months and 3 of 11 mice twenty two to twenty four months of age. Such lesions were noted to partially or completely fill gland lumens and occasionally impinge on an attenuated or fragmented fibromuscular stroma, but no foci of unequivocal invasion were noted (140).

Other pathologic alterations noted in the prostate of ARR$_2$PB-FGF8b mice included a lesion designated as papillary hyperplasia, stromal hypercellularity, and stromal lymphocytic infiltrates. Papillary lesions protruding into gland lumens, with fibromuscular stroma containing vessels and variable epithelial nuclear atypia, were designated as papillary hyperplasia. It is not certain whether such lesions constitute hyperplasias or papillomas, as described in the section on the Bar Harbor classification scheme above, although they were noted to be multiple in individual animals. These lesions increased in frequency in ARR$_2$PB-FGF8b mice, and were identified in 6 of 27 mice > 18 months of age (140). Stromal hypercellularity, with a smooth muscle phenotype, also increased with age. It was noted as early as 6 months, was present in 6 of 14 mice thirteen to eighteen months old, and in 16 of 27 mice > 18 months of age (140). Occasionally, stromal proliferation was associated with prominent intraluminal protrusion of lesions regarded as potential papillomas, with "phyllodes-like" growth noted. Stromal inflammation, with an infiltrate of predominantly CD3 positive T-lymphocytes was common, also increasing with age. Intraepithelial inflammation was not a typical feature, and as detailed above, such lesions are not classified as active prostatitis. Admixed acute inflammatory cells with epithelial infiltration and glandular disruption was noted in only 2 of 56 animals (140). Mild chronic inflammation was also noted in the stroma of the ductus deferens, epididymis, and seminal vesicles, the other sites where the transgene is expressed (140). The ARR$_2$PB promoter successfully employed in the creation of this FGF8b GEM model has also been used to establish mice selectively expressing Cre recombinase in the prostate (142). Such mice have recently been employed to begin making selective prostate knockout mice (143).

Models Not Reviewed at the Bar Harbor Pathology Workshop, with Characteristics Inferred from Meeting Presentations and/or Literature Descriptions and Published Photomicrographs:

Fetal globin SV40: During efforts to target the SV40 early region to embryonic erythroid cells utilizing a human fetal Gγ-globin promoter, Perez-Stable et al. observed non-erythroid expression of Tag in embryonic tissues and in tumors in adult mice (86). In one line, referred to as Gγ/T-15, prostate tumors were observed in 50 % of male mice 5-7 months old and adrenocortical tumors were noted in 50 % of similarly aged female mice. In several other lines, hibernoma tumors in brown adipose tissues were noted (86). Tag expression was present in prostate tumors, but was not detectable in the prostate prior to tumor development as determined by Rnase protection assays. The histopathology of the prostate tumors was described as nests of anaplastic carcinoma cells with intervening bands of fibrovascular stroma, compatible with undifferentiated or NE carcinoma (86).

Electron microscopy showed membrane bound vesicles in the apical cytoplasm, consistent with secretory differentiation. Dense core neurosecretory granules were not identified, but chromogranin A RNA was detected. CK8 protein was detected by Western blot. As described above, CK8 expression is not incompatible with an NE tumor, with dot-like perinuclear immunostaining being characteristic. Immunohistochemistry examination was not included. However, the ultrastructural features are indicative of epithelial/secretory differentiation, suggesting mixed NE and secretory epithelial differentiation. The ability of the Gγ-globin promoter to direct gene expression in prostate tissues was supported by experiments with mouse prostate tumor derived cell lines and human Pca cell lines (86). However, the occurrence of tumors in adrenal and adipose tissues indicates the lack of selectivity of the promoter for driving expression of other transgenes as well as the need to carefully exclude other primary sources for any detected metastases.

A subsequent report more fully characterized the time course and frequency of tumor development as well as the natural history of the prostate tumors in the Gγ/T-15 line. Tag was expressed in the adult prostate, including before the presence of grossly discernible tumor. Grossly evident tumors in the urogenital area were noted between 16 and 24 wks. (144). In hemizygous transgenic males, 50 % had tumors at 16-20 wks., and 75 % had tumors at ages > 20 wks. In contrast, 100 % of homozygous transgenic males had tumors at 16-20 wks. Histologic examination of urogenital blocks in mice of this age range showed apparent origin within the prostate, rather than in other male accessory glands. Tumors in both the VP and DP were illustrated. Intraepithelial neoplasia was noted in some acini near to these large discreet tumor masses, but no foci of apparent invasion specifically in association with these PIN glands (i.e., early or microinvasion) were described. The extent and degree of the PIN lesions illustrated appears to be less than that observed in other SV40 based models described above.

The prostate tumor in the Gγ/T-15 GEM appears to be associated with frequent and extensive metastases. Visible tumor was evident in renal lymph nodes, adrenal glands, and kidney in 7/7, 3/7, and 3/7 mice respectively, at necroscopy. However, histologic confirmation and exclusion of possible primary in the adrenal glands (known to occur in other Gγ-SV40 lines and females of this line) was not provided. Further, the possibility of micrometastases in the lung in 4/7 and bone and thymus in 2/7 mice each was indicated by Rnase protection assays for Tag expression. Histologic confirmation was not provided. Although Tag was not expressed in non-prostate sites by similar assays in adult mice prior to prostate tumor formation, as the promoter is not selective, it is not possible to exclude expression in other sites at these later ages when prostate tumors are present. However, the results are certainly suggestive of possible wide spread metastases, including to sites similar to human Pca, such as abdominal or pelvic lymph nodes, bone, and lung. The metastatic capacity of the prostate tumor was further demonstrated by allografting into nude mice, although the number of such studies and the pattern and time course of metastases was not reported. The tumor in this model appears to be androgen independent. In hemizygous males castrated at 4-6 wks. and sacrificied at 20-28 wks., four of an apparently examined six mice developed prostate tumors of similar histology as intact transgenics. This frequency is similar to the 75 % observed in similarly aged intact hemizygous mice (144). The effect of castration on metastases was not reported.

Immunoblots again showed expression of CK8 in the prostate tumors. Without correlation to the tumor histology as in immunohistochemistry, it is not possible to exclude contamination from entrapped normal prostate glands or expression in a pattern more compatible with NE differentiation. The latter was again implied by the presence of chromogranin A RNA. The authors have subsequently noted Tag expression in PIN lesions (Perez-Stable, C., unpublished observations). In additional reported studies, molecular alterations in the prostate tumors in Gγ/T-15

59

included increased p53, Rb, and bcl-2 RNA levels as well as reduced expression of mouse DLP secretory protein and the gap-junction protein connexin 32 (144).

Hence, this mouse represents a potentially useful model for PIN and aggressive and metastatic tumors, with both epithelial and NE differentiation. However, it would be desirable from the pathology perspective to have a more detailed time course of histopathologic alterations in the prostate, including the possible progression of PIN, the relationship of PIN to possible early invasive forms, and glandular vs. NE differentiation in early vs. late and metastatic lesions. In addition, histology of the metastases, including possible bone metastases, and immunohistochemistry for NE markers in primary and possible metastatic tumors would be desirable.

BK5-IGF-1 mouse: DiGiovanni and colleagues reported a transgenic mouse with prostatic neoplasia developing as a consequence of expression of human IGF-1 in the prostate (33) driven by a bovine keratin 5 promoter (BK5) that targets transgene to the basal layer of multiple epithelia (145). BK5-IGF-1 mice showed expression of IGF-1 in the prostate. That this expression results in activation of the IGF receptor (IGF-1R) was supported by the demonstration of receptor phosphorylation. Mice 2-3 months old dmonstrated epithelial hyperplasia in male accessory glands, and the prostates of all mice ≥ 6 months of age showed epithelial hyperplasia in all prostate lobes. Nuclear stratification and atypia compatible with PIN were identified. Importantly, reduced immunostaining of basal cells was noted in such dysplastic glands, suggesting that PIN in this GEM may be accompanied by progressive loss of a basal cell layer as in human PIN.

Invasive carcinoma with glandular differentiation was noted, with extension into periprostatic fat and invasion into seminal vesicles and pelvic muscles observed, including in mice as old as 14 months (33). Overall, 19 of 38 mice (50 %) ≥ 6 months developed invasive carcinomas, including 7 adenocarcinomas in the VP, 11 adenocarcinomas in the DLP, and 2 poorly differentiated carcinomas, with small cell NE differentiation (in older mice). It is not possible to more definitively classify the differentiation of the adenocarcinomas based on the criteria proposed herein on the basis of published photomicrographs alone. However, unequivocal well formed glands were illustrated. No metastases were noted, and absence of metastatic capability was also observed in tumors that were grafted into the renal capsule of male athymic mice, despite the capacity for local growth (33). This mouse model presents a potentially important advance in GEM models of Pca, in addition to results supporting a role for the IGF axis in prostate neoplasia. Although it would be desirable for the MMHCC pathology panel to review actual glass slides, this is perhaps the best reported demonstration thus far of unequivocally locally invasive tumors with definitive glandular differentiation. Although rare NE tumors were noted, the model did not quickly progress to large NE tumors, with the apparent maintenance of an adenocarcinoma phenotype with advancing age. The slow time course may limit the utility of this model. Further, the lack of prostate specific transgene expression may limit the utility of the promoter for establishment of other GEM models and needs to be kept in mind regarding possible primary tumor sites if metastases are noted with an accelerated phenotype in crosses using this mouse. Despite these concerns, it is very promising for the field in general that an apparently invasive adenocarcinoma can develop in a mouse expressing as a transgene a gene that has been implicated as important in human Pca development.

PTEN knockout and PTEN +/- x p27 -/-: PTEN (phosphatase and tensin homologue deleted from chromosome 10) is a dual specificity phosphatase and a putative tumor suppressor gene located on the long arm of chromosome 10 (10q23). LOH involving 10q23 occurs in human Pca,

with biallelic inactivation occurring in some organ confined and particularly in advanced Pcas (146-148). In GEM, homozygous mutational inactivation of PTEN results in embryonic lethality (149). Several published reports and unpublished models included within the MMHCC (Table 1) have now demonstrated prostate lesions classifiable as PIN in heterozygous genomic PTEN "knockout" models (PTEN +/-) (30, 149, 150) (Figure 7). In a mouse model made by targeted disruption of *Pten* exons 4 and 5 (which code for the phosphatase and flanking domains), ten of 10 chimeric mice made from *Pten* +/- ES cells and aged 16 to 30 wks and seven of 7 *Pten* +/- mice 6 to 12 months old showed prostatic lesions described as hyperplastic and dysplastic (149). The focality and progression of these lesions was not specifically addressed., but based on other similar models reviewed within the context of the MMHCC Pathology Panel, the prostatic lesions in PTEN +/- mice appear to represent lesions classifiable as mPIN according to the Bar Harbor Classification.

The perceived epithelial proliferation in the above study was accompanied by increased mitotic figures and was confirmed by quantitation of the proliferative index determined by Ki-67 immunostaining, which showed a marked increase in *Pten* +/- vs. wild-type mice (149). The atypia prompting these lesions to be described as "dysplastic" was not specified, but examples of PTEN +/- mice (aged 6-12 months) from different investigators in the Bar Harbor study set show nuclear enlargement with vesicular nuclei and frequently prominent nucleoli (Figure 7). The nuclear atypia in such mice is thus more reminiscent of that seen in human HGPIN than is the atypia seen in SV40 early region and large T antigen mice. In another *Pten* +/- model with genomic mutational inactivation generated by targeted disruption of the phosphatase encoding exon 5, three of eight male mice aged 6-22 weeks had prostate lesions classified as PIN and three others had focal epithelial hyperplasia, apparently without atypia (150). Again, the nature of the atypia supporting the classification of PIN was not described. The epithelial proliferation was supported by Ki-67 immunostaining. Prostatic lesions in older mice were not described. According to the currently described consensus Bar Harbor classification, the requirements for focality and progression of extent of involvement and/or nuclear atypia would not have been adequately satisfied for a designation of PIN in the prostates of these reported mice (150). However, as alluded to above, the collective experience in PTEN +/- mice from various labs is indicative of PIN as defined herein. Without additional genetic manipulations, PTEN +/- mice have only rarely progressed to invasive carcinoma in the prostate, with one example seen in an aged mouse by one of the panel pathologists (R.D.C., unpublished observation).

Compatible with its possible role in regulating cell proliferation and/or functioning as a tumor suppressor gene in other organs, PTEN +/- mice also develop hyperplastic, dysplastic, and neoplastic proliferations in several other tissue sites. Chimeric mice from PTEN +/- ES cells and PTEN +/- mice develop intestinal (particularly colonic) glandular epithelial proliferative and dysplastic lesions, with occasional progression to lesions showing lamina propria invasion. Less frequently observed were skin epidermal acanthosis and orthokeratosis (149). Chimeric mice also developed abnormal proliferations of testicular stromal cells compatible with gonadostromal tumors and rare thyroid epithelial proliferations (149). In the other described report (150), in PTEN +/- mice 20-56 wks old, 12 % died or were sacrificed because of morbidity, and thymic enlargement, splenomegaly, and lymphomas were described in up to seven of these 30 mice (150). In a thorough systematic analysis of the *Pten* +/- mice, there was a marked predilection to small and large intestinal polyps, documented in all examined mice 7-18 wks old and potentially increasing in extent and size with age. Most were due to lymphoid aggregates, but also described were frequent epithelial hyperplastic lesions, with rare dysplasia (150). Lymph node hyperplasia is a characteristic feature of these mice, as is an endometrial epithelial lesion in female mice described as analogous to

human complex atypical hyperplasia. A less common neoplatic proliferation of thyroid follicular epithelium was also observed (150).

In a more recent report, all PTEN +/- mice aged between 9 and 16 months developed bilateral adrenal medullary tumors (similar to human pheochromocytomas). Approximately two-thirds of all mice developed thyroid neoplasms reported as follicular carcinomas (whether based on capsular penetration or vascular invasion, criteria routinely used in human pathology, and not just on cytologic atypia was not described). Approximately two-thirds of female mice developed endometrial epithelial neoplastic proliferations described as analogous to human complex atypical hyperplasia. Finally, a smaller percentage of all mice developed dysplastic (cytologically atypical) epithelial proliferations of the small intestine, large intestine, and lung (approximately 23 %, 11 %, and 6 %, respectively). Approximately half of male PTEN +/- mice aged 9-16 months developed PIN in the prostate, involving the dorsolateral and anterior prostate (30). Illustrated lesions are similar to those included in this study (Figure 7), with cribriform and tufting epithelial proliferations having nuclear atypia. Invasive carcinoma or metastases were not described in the PTEN +/- mice.

The described phenotype is reportedly accelerated in crosses between PTEN +/- mice and mice with heterozygous and particularly homozygous deletion of CDKN1b, encoding p27^{KIP1} (30). Reduced or absent expression of the cyclin dependent kinase inhibitor p27^{KIP1} has been correlated with an adverse prognosis in human Pca (151). Targeted disruption of CDKN1b alone in mice (p27 -/-) has been reported to result in only mild epithelial hyperplasia (152). Similar observations of absence of phenotypic alteration or only mild epithelial hyperplasia have been made by other investigators in p27 +/- mice (C. Abate-Shen, R.D.C., unpublished observations). However, survival was reduced in PTEN +/- x p27 +/- and particularly PTEN +/- x p27 -/- mice compared to PTEN +/- mice (30). PTEN +/- x p27 -/- had a mean survival of only approximately 15 wks (compared to 51 wks for PTEN +/- mice). The mortality in PTEN +/- x p27 -/- was apparently due primarily due to intestinal obstruction, as these mice had common involvement of the small and large intestines by extensive "polypoid outgrowths". These mice also uniformly had neoplastic proliferations in the adrenal medulla, thyroid, and endometrium (in the female group), with 100 % incidence at 3-5 months and significantly greater involvement of thyroid, endometrium, and small intestine compared to PTEN +/- mice at 9-16 months. 100 % of PTEN +/- x p27 -/- developed prostate neoplasia, with lesions designated as PIN involving the DLP in all mice and the AP in approximately 85 %. Progression to frank invasion, described as rupture of the basement membrane of normal ducts/glands, occurred in 25 %. Unfortunately, as these mice do not survive beyond the approximately 15 wk time point, it is not possible to discern if these foci would progress to more extensive invasive lesions, with or without glandular differentiation, and metastases.

With models involving pathology in multiple organ systems, it is important for pathologists to also bear in mind two potentially complicating issues. Firstly, not only should the relationship of any invasive focus in the prostate to adjacent PIN lesions be noted, but also the pathology in adjacent viscera, such as large intestine, should be noted in order to exclude possible direct extension of carcinoma from other organs. Secondly, if metastases are detected, the possible development of carcinomas in several other sites complicates the issue of determining a prostate vs. other primary site. In addition to careful attention to histologic features, future development and characterization of possible prostate specific markers for the mouse for immunohistochemical staining of metastatic foci may be helpful (i.e., analogous to human PSA). Further validation and application of other techniques, such as tissue proteinomics for detection of tissue and tumor specific protein profiles (37), may also facilitate identification of primary sites.

Future development of tissue selective PTEN and p27 knockouts and crosses of these animals will most likely reduce the development of neoplasms in other sites. This will not only eliminate the complicating factor of other possible primaries when interpreting any metastatic lesions, but should allow for the survival of these animals to longer time points, at which the reported PIN and early invasive carcinoma lesions will have the potential to progress to more advanced lesions.

Protocols in characterization of prostate lesions in GEM:

Necropsy in newly established models and prostate dissection:
   Ages for sampling: In order to fully characterize a GEM model, the suggested timing of sampling should include timepoints that mark the sexual maturity and reproductive milestones of the mouse, in addition to timepoints determined by the investigator based on previous findings, published reports, and expected or determined natural history. Such general time points would include sampling at

1. Day 1: time of birth
2. Week 3: time of weaning
3. Week 6: time of reaching sexual maturity
4. Week 40: time of end of reproductive capability

Prostate dissection and tissue submission: The method of prostate dissection and tissue submission for histology depends in part on the intended use of the tissues, particularly whether ancillary studies such as gene expression analyses are being performed. Histologic examination and tissue based analyses such as immunohistochemistry and in situ hybridization are routinely performed on standard formalin fixed paraffin embedded sections. Caution should be observed regarding the duration of exposure of tissues to 10 % buffered formalin, which is adequate for most if not all analyses. If tissues are not to be processed right away, tissues or cassettes with tissues in them should be switched to 50 or 70 % ethanol after four to six hours. Prolonged exposure to formalin can reduce tissue antigenicity, compromising some subsequent immunohistochemical or in situ hybridization analyses.

   Separate identification of individual prostate lobes (grossly or in microscopic sections) and characterization of pathology in specific lobes is mandatory. For analyses only involving histopathologic assessment and possible subsequent immunohistochemical and/or in situ hybridization analyses on paraffin sections, the prostate and associated organs can be submitted "en bloc" as described below. For protocols involving submission of snap frozen tissues, the individual lobes of the prostate can be dissected with the aid of a dissecting microscope, as illustrated in Figure 2. Lobe dissection is accomplished after removal of the entire genitourinary bloc (prostate lobes, seminal vesicles, ampullary glands, proximal ductus deferens, bladder, proximal urethra) following transection of the urethra. The individual prostate lobes can be weighed and representative portions of each can be snap frozen and the remaining tissue fixed and processed for standard paraffin sections. High quality RNA can be obtained from tissues procured in this manner. Representative portions of both right and left lobes or an entire lobe from one side can be snap frozen and the remaining tissue from specifically designated lobes can then be submitted in its entirety in individual tissue cassettes. If such protocols are employed, sections of seminal vesicles and the remaining genitourinary bloc should be submitted (in a similar fashion as described below and shown in Figure 12), to allow for sampling of the ampullary and periurethral glands. Following a

63

single transverse cut of this portion of tissue through the urethra (with or without prostate lobes attached), both transected surfaces can be embedded down so that initial sections from the block are at the cut surface. Pathologic alteration of the prostate and associated organs can distort the normal anatomy here and can modify the level of this initial cut somewhat. If, for example, the periurethral glands are of interest and are not well represented in the initial histologic section, additional cuts into the block allow for examination of levels thus extending both proximally and distally along the urethra. The anatomy of the mouse prostate and techniques of dissection are illustrated in tutorials at the Web sites indicated in Appendix Six.

The extent to which paraffin blocks are sectioned for H & E stained slides depends upon the nature of the study being conducted and the focality of lesions being detected. For example, in the use of already characterized models that have documented progression to fairly extensive lesions in a reasonably reproducible time course and in which genetic manipulations or pharmacologic interventions are being examined and pathology is an endpoint, one slide per animal may be sufficient if adequate numbers of animals are included. The ability to achieve statistical significance may be impacted by the magnitude of the biologic effect being investigated and the focality of the lesions. Several examples with pathology as the assessed endpoint have been reported, and an idea of the required mouse numbers can be gleaned from past studies cited herein. Even when only one section per prostate lobe is initially stained, several additional sections can be prepared on charged slides, either for possible subsequent staining or ancillary immunohistochemical or other studies.

In sections obtained to characterize a new model, wherein the extent of any phenotypic alterations are uncertain, more extensive sectioning of paraffin blocks would typically be required. However, we do not recommend necessarily H & E staining of all serial sections, at least in initial assessments. Serial sections (e.g., 15-30 sections on 15 slides, with one to two per slide) can be obtained on charged slides. Despite the slightly greater cost compared to un-charged slides, this will better allow for ancillary immunostaining or in situ hybridization. Every third or every fifth slide can be stained initially. If lesions are present, the intervening slides from adjacent sections can be used for ancillary procedures to provide further characterization of focal lesions. If lesions are not identified, additional intervening sections can always be stained with H & E. It is impossible to make rigid recommendations that will apply to all studies, and these are intended as general guidelines.

A method for tissue submission of the male accessory glands en bloc is demonstrated in Figure 12. Procedures have been described previously (1, 153), and a detailed protocol is included in Appendix 2.

Ancillary studies:

Immunohistochemistry: Immunohistochemistry is a vital component in the characterization of GEM models and in the assessment of the effects of treatment interventions or genetic crosses. Many examples have been described in the sections for the individual models reported above. Immunohistochemical assays for antigens of special interest include the determination of expression of the particular transgene employed in a given GEM model (e.g. Tag), alteration of expression of specific proteins accompanying tumor progression (e.g., PTEN, NKX3.1, p53), and modification of proteins reflecting activation of certain signaling pathways during tumor progression (e.g., phosphoAKT). The results of many such assays were described herein, and interested investigators are referred to the specific publications for assay methodology and results. In addition, there is a growing number of commonly employed immunostains that may have particularly broad utilization in model characterization as well as in interventional trials. A list of these antigens and some of the specific antibodies and tissue fixation conditions that have been successfully employed is shown in

64

Table 6. These include markers of epithelial differentiation, including basal and luminal cell subpopulations and NE differentiation. In addition, immunohistochemical staining for proliferation markers, such as PCNA and Ki-67, can be useful for demonstrating increased proliferation with progression as well as determining effects on proliferation of genetic crosses or therapeutic interventions. Similarly, multiple antibodies have been employed to stain endothelial cells in the mouse in order to assess microvessel density and to determine altered patterns of angiogenesis with tumor progression or the effects of genetic crosses or therapeutics on tumor angiogenesis.

In addition to polyclonal antibodies, murine monoclonal antibodies are routinely used to stain mouse sections. The indicated references in Table 6 provide specifics regarding antigen retrieval, secondary antibodies, blocking strategies, and detection techniques. Protocols for polyclonal and monoclonal antibody immunostains are provided in Appendix Three. Additional Immunohistochemistry information can be found at:
http://ccm.ucdavis.edu/tgmouse/protocols/protocol_find_os.cfm

In situ hybridization: In situ hybridization (ISH) is a vital component in the characterization and utilization of GEM models of prostatic neoplasia. Applications include documentation of transgene expression in new transgenic models, as well as lost expression in knockout or selective knockout models. Although not quantitative, ISH is highly specific, and certainly adequate for detecting major alterations in mRNA expression. Despite less precise resolution than immunostaining in tissue sections, it is typically sufficient to demonstrate epithelial vs. stromal localization. ISH may be useful for demonstrating altered expression of specific genes with tumor progression or with therapeutic intervention. It is anticipated that ISH will be useful in confirming results of cDNA microarrays when novel genes are indicated as expressed in a given model, as well as indicating the site of such gene expression. The techniques are established and more widely available than laser capture microdissection coupled to quantitative gene expression analyses. ISH may be a suitable screening option, that can then be supplemented by quantitative techniques if needed. It is recommended that investigators involve collaborators with technical expertise in ISH. Protocols are provided in Appendix Four.

Apoptosis assays: Apoptosis may be useful to assess and even quantitate in the analysis of possible progression in new GEM models. Quantitating apoptosis may be useful in the investigation of possible beneficial effects with certain therapeutic interventions. Increased apoptosis has been noted with tumor progression in some models of mPIN and invasive carcinoma. When possible, and particularly in therapeutic trials, apoptotic cells should be quantitated in a blinded manner, either by cell counting or by computer assisted image analysis. Techniques for assessing apoptosis in tissue sections are described in Appendix Five.

Electron microscopy: Several studies have successfully employed ultrastructural analysis in characterization of tumor cell differentiation or other aspects of GEM model characterization (31, 32, 37, 86). In general, standard techniques are applied. Protocols are available at:
http://www.hms.harvard.edu/core/em.html

Acknowledgements:

References

1. Suwa, T., Nyska, A., Haseman, J. K., Mahler, J. F., and Maronpot, R. R. Spontaneous lesions in control B6C3F1 mice and recommended sectioning of male accessory sex organs, Toxicol Pathol. *30:* 228-234, 2002.

2. Gingrich, J. R., Barrios, R. J., Morton, R. A., Boyce, B. F., DeMayo, F. J., Finegold, M. J., Angelopoulou, R., Rosen, J. M., and Greenberg, N. M. Metastatic Prostate Cancer in a Transgenic Mouse, Cancer Res. *56:* 4096-4102, 1996.

3. Kim, M. J., Bhatia-Gaur, R., Banach-Petrosky, W. A., Desai, N., Wang, Y., Hayward, S. W., Cunha, G. R., Cardiff, R. D., Shen, M. M., and Abate-Shen, C. *Nkx3.1* mutant mice recapitulate early stages of prostate carcinogenesis, Cancer Res. *62:* 2999-3004, 2002.

4. McNeal, J. E. Normal and pathologic anatomy of prostate, Urology. *17 (suppl):* 11-16, 1981.

5. McNeal, J. E. Cancer volume and site of origin of adenocarcinoma in the prostate: relationship to local and distant spread, Hum Pathol. *23:* 258-266, 1992.

6. Epstein, J. I. Non-neoplastic diseases of the prostate. *In:* D. G. Bostwick and J. N. Eble (eds.), Urologic Surgical Pathology, pp. 307-340. St. Louis, MO: Mosby, 1997.

7. Epstein, J. I. and Wojno, K. J. The prostate and seminal vesicles. *In:* S. S. Sternberg (ed.) Diagnostic Surgical Pathology, Vol. 2, pp. 1893-1942. Philadelphia, PA: Lippincott Williams & Wilkins, 1999.

8. Argani, P., Walsh, P. C., and Epstein, J. I. Analysis of the prostatic central zone in patients with unilateral absence of wolffian duct structures: further evidence of the mesodermal origin of the prostatic central zone, J Urol. *160:* 2126-2129, 1998.

9. Bostwick, D. G. Neoplasms of the Prostate. *In:* D. G. Bostwick and J. N. Eble (eds.), Urologic Surgical Pathology, pp. 342-421. St. Louis, MO: Mosby, 1997.

10. McNeal, J. E., Redwine, E. A., Freiha, F. S., and Stamey, T. A. Zonal distribution of prostatic adenocarcinoma. Correlation with histologic pattern and direction of spread, Am J Surg Pathol. *12:* 897-906, 1988.

11. Greene, D. R., Wheeler, T. M., Egawa, S., Dunn, J. K., and Scardino, P. T. A comparison of the morphological features of cancer arising in the transition zone and in the peripheral zone of the prostate, J Urol. *146:* 1069-1076, 1991.

12. Bostwick, D. G. Prospective origins of prostate carcinoma. Prostatic intraepithelial neoplasia and atypical adenomatous hyperplasia, Cancer. *78:* 330-336, 1996.

13. Noguchi, M., Stamey, T. A., McNeal, J. E., and Yemoto, C. E. M. An analysis of 148 consecutive transition zone cancers: Clinical and histological characterisitics, J Urol. *163:* 1751-1755, 2000.

14. Jack, G. S., Cookson, M. S., Coffey, C. S., Vader, V., Roberts, R. L., Chang, S. S., Smith, J. A., Jr., and Shappell, S. B. Pathologic parameters of radical prostatectomy for clinical stages T1c versus T2 prostate adenocarcinoma: Decreased pathological stage and increased detection of transition zone tumors, J Urol. *168:* 519-524, 2002.

15. Stamey, T. A., Donaldson, A. N., Yemoto, C. E., McNeal, J. E., Sozen, S., and Gill, H. Histological and clinical findings in 896 consecutive prostates treated only with radical retropubic prostatectomy: epidemiologic significance of annual changes, J Urol. *160:* 2412-2417, 1998.

16. Shappell, S. B., Masumori, N., Thomas, T., Case, T., Paul, M., Kasper, S., and Matusik, R. J. Transgenic mouse models of prostate carcinoma: Anatomic, histopathologic, and molecular considerations. *In:* E.-N. Lalani and P. D. Abel (eds.), Prostate Cancer: Scientific and Clinical Aspects: Bridging the Gap, pp. (in press). London: Imperial College Press, 2002.

17.   Epstein, J. I., Partin, A. W., Sauvageot, J., and Walsh, P. C. Prediction of progression following radical prostatectomy. A multivariate analysis of 721 men with long-term follow-up, Am J Surg Pathol. *20:* 286-292, 1996.

18.   Wheeler, T. M., Dillioglugil, O., Kattan, M. W., Arakawa, A., Soh, S., Suyama, K., Ohori, M., and Scardino, P. T. Clinical and pathological significance of the level and extent of capsular invasion in clinical stage T1-2 prostate cancer, Hum Pathol. *29:* 856-862, 1998.

19.   Epstein, J. I., Carmichael, M. J., Partin, A. W., and Walsh, P. C. Small high grade adenocarcinoma of the prostate in radical prostatectomy specimens performed for nonpalpable disease: pathogenetic and clinical implications, J Urol. *151:* 1587-1592, 1994.

20.   Xue, Y., Verhofstad, A., Lange, W., Smedts, F., Debruyne, F., de la Rosette, J., and Schalken, J. Prostatic neuroendocrine cells have a unique keratin expression pattern and do not express Bcl-2: cell kinetic features of neuroendocrine cells in the human prostate, Am J Pathol. *151:* 1759-1765, 1997.

21.   Xue, Y., Smedts, F., Verhofstad, A., Debruyne, F., de la Rosette, J., and Schalken, J. Cell kinetics of prostate exocrine and neuroendocrine epithelium and their differential interrelationship: New perspectives, Prostate, suppl. *8:* 62-73, 1998, 1998.

22.   Cohen, R. J., McNeal, J. E., Edgar, S. G., Robertson, T., and Dawkins, H. J. Characterization of cytoplasmic secretory granules (PSG) in prostatic epithelium and their transformation-induced loss in dysplasia and adenocarcinoma, Hum Pathol. *29:* 1488-1494, 1998.

23.   Cohen, R. J., Glezerson, G., Taylor, L. F., Grundle, H. A. J., and Naude, J. H. The neuroendocrine cell population of the human prostate gland, J Urol. *150:* 365-368, 1993.

24.   Brawer, M. K., Peehl, D. M., Stamey, T. A., and Bostwick, D. G. Keratin immunoreactivity in the benign and neoplastic human prostate, Cancer Res. *45:* 3663-3667, 1985.

25.   Hedrick, L. and Epstein, J. I. Use of keratin 903 as an adjunct in the diagnosis of prostate carcinoma, Am J Surg Pathol. *13:* 389-396, 1989.

26.   O'Malley, F. P., Grignon, D. J., and Shum, D. T. Usefulness of immunoperoxidase staining with high-molecular-weight cytokeratin in the differential diagnosis of small-acinar lesions of the prostate gland, Virchows Arch A Pathol Anat Histopathol. *417:* 191-196, 1990.

27.   Cunha, G. R., Donjacour, A. A., Cooke, P. S., Mee, S., Bigsby, R. M., Higgins, S. J., and Sugimura, Y. The endocrinology and developmental biology of the prostate, Endocr Rev. *8:* 338-362, 1987.

28.   Price, D. Comparative aspects of development and structure in the prostate. *In:* E. P. Vollmer and G. Kauffmann (eds.), Biology of the prostate and related tissues, pp. 1-28. Washington, D.C.: US Government Printing Office, 1963.

29.   Matusik, R. J., Masumori, N., Thomas, T., Case, T., Paul, M., Kasper, S., and Shappell, S. B. Transgenic mouse models of prostate cancer. *In:* M. Matzuk, C. W. Brown, and T. R. Kumar (eds.), Contemporary Endocrinology: Transgenics in Endocrinology, pp. 401-425. Totowa, N.J.: Humana Press, Inc., 2001.

30.   Di Cristofano, A., De Acetis, M., Koff, A., Cordon-Cardo, C., and Pandolfi, P. P. Pten and p27KIP1 cooperate in prostate cancer tumor suppression in the mouse, Nature Genet. *27:* 222-224, 2001.

31.   Shibata, M. A., Ward, J. M., Devor, D. E., Liu, M. L., and Green, J. E. Progression of prostatic intraepithelial neoplasia to invasive carcinoma in C3(1)/SV40 large T antigen transgenic mice: histopathological and molecular biological alterations, Cancer Res. *56:* 4894-4903, 1996.

32.   Garabedian, E. M., Humphrey, P. A., and Gordon, J. I. A transgenic mouse model of metastatic prostate cancer originating from neuroendocrine cells, Proc Natl Acad Sci, USA. *95:* 15382-15387, 1998.

33.   DiGiovanni, J., Kiguchi, K., Frijhoff, A., Wilker, E., Bol, D. K., Beltran, L., Moats, S., Ramirez, A., Jorcano, J., and Conti, C. Deregulated expression of insulin-like growth factor 1 in prostate epithelium leads to neoplasia in transgenic mice, Proc Nat Acad Sci, USA. *97:* 3455-3460, 2000.

34.   Kim, M. J., Cardiff, R. D., Desai, N., Banach-Petrosky, W. A., Parsons, R., Shen, M. M., and Abate-Shen, C. Cooperativity of Nkx3.1 and Pten loss of function in a mouse model of prostate carcinogenesis, Proc Natl Acad Sci, USA. *99:* 2884-2889, 2002.

35.   Abdulkadir, S. A., Magee, J. A., Peters, T. J., Kaleem, Z., Naughton, C. K., Humphrey, P. A., and Milbrandt, J. Conditional loss of *Nkx3.1* in adult mice induces prostatic intraepithelial neoplasia, Mol Cell Biol. *22:* 1495-1503, 2002.

36.   Kasper, S., Sheppard, P. C., Yan, Y., Pettigrew, N., Borowsky, A. D., Prins, G. S., Dodd, J. G., Duckworth, M. L., and Matusik, R. J. Development, progression and androgen-dependence of prostate tumors in transgenic mice: A model for prostate cancer, Lab Invest. *78:* 319, 1998.

37.   Masumori, N., Thomas, T. Z., Case, T., Paul, M., Kasper, S., Chaurand, P., Caprioli, R. M., Tsukamoto, T., Shappell, S. B., and Matusik, R. J. A probasin-large T antigen transgenic mouse line develops prostate adeno- and neuroendocrine-carcinoma having metastatic potential, Cancer Res. *61:* 2239-2249, 2001.

38.   Chow, P. H., Yuen, A. C., and Cheng, L. Y. Quantitative electrophoretic study of the modification of sperm plasma membrane by the ampullary gland in the golden hamster, Arch Androl. *34:* 53-61, 1995.

39.   Donjacour, A. A., Thomson, A. A., and Cunha, G. R. Enlargement of the ampullary gland and seminal vesicle, but not the prostate in *int-2/Fgf-3* transgenic mice, Differentiation. *62:* 227-237, 1998.

40.   Shibata, M., Jorcyk, C. L., Devor, D. E., Yoshidome, K., Rulong, S., Resau, J., Roche, N., Roberts, A. B., Ward, J. M., and Green, J. E. Altered expression of transforming growth factors during urethral and bulbourethral gland tumor progression in transgenic mice carrying the androgen-responsive C3 (1)5' flanking region fused to SV40 large T antigen, Carcinogenesis. *19:* 195-205, 1998.

41.   Nistal, M. and Paniagua, R. Non-neoplastic diseases of the testis. *In:* D. G. Bostwick and J. N. Eble (eds.), Urologic Surgical Pathology, pp. 457-565. St. Louis, MO: Mosby, 1997.

42.   Steers, W. D. 5alpha-reductase activity in the prostate, Urology. *58:* 14-24, 2001.

43.   Takahashi, K., Nakayama, K., and Nakayama, K. Mice lacking a CDK inhibitor, p57Kip2, exhibit skeletal abnormalities and growth retardation, J Biochem (Tokyo). *127:* 73-83, 2000.

44.   Yang, A., Kaghad, M., Wang, Y., Gillett, E., Fleming, M. D., Dotsch, V., Andrews, N. C., Caput, D., and McKeon, F. p63, a p53 homolog at 3q27-29, encodes multiple products with transactivating, death-inducing, and dominant-negative activities, Mol Cell. *2:* 305-316, 1998.

45.   Signoretti, S., Waltregny, D., Dilks, J., Isaac, B., Lin, D., Garraway, L., Yang, A., Montironi, R., McKeon, F., and Loda, M. p63 is a prostate basal cell marker and is required for prostate development, Am J Pathol. *157:* 1769-1775, 2000.

46.   Yang, A., Schweitzer, R., Sun, D., Kaghad, M., Walker, N., Bronson, R. T., Tabin, C., Sharpe, A., Caput, D., Crum, C., and McKeon, F. p63 is essential for regenerative proliferation in limb, craniofacial and epithelial development, Nature. *398:* 714-718, 1999.

47.   He, W. W., Sciavolino, P. J., Wing, J., Augustus, M., Hudson, P., Meissner, P. S., Curtis, R. T., Shell, B. K., Bostwick, D. G., Tindall, D. J., Gelmann, E. P., Abate-Shen, C., and Carter, K. C. A novel human prostate-specific, androgen-regulated homeobox gene (NKX3.1) that maps to 8p21, a region frequently deleted in prostate cancer, Genomics. *43:* 69-77, 1997.

48.   Podlasek, C. A., Duboule, D., and Bushman, W. Male accessory sex organ morphogenesis is altered by loss of function of Hoxd-13, Dev Dyn. *208:* 454-465, 1997.

49.   Podlasek, C. A., Clemens, J. Q., and Bushman, W. Hoxa-13 gene mutation results in abnormal seminal vesicle and prostate development, J Urol. *161:* 1655-1661, 1999.

·50.   Bhatia-Gaur, R., Donjacour, A. A., Sciavolino, P. J., Kim, M., Desai, N., Young, P., Norton, C. R., Gridley, T., Cardiff, R. D., Cunha, G. R., Abate-Shen, C., and Shen, M. M. Roles for Nkx3.1 in prostate development and cancer, Genes Dev. *13:* 966-977, 1999.

51.   Reyes, A. O., Swanson, P. E., Carbone, J. M., and Humphrey, P. A. Unusual histologic types of high-grade prostatic intraepithelial neoplasia, Am J Surg Pathol. *21:* 1215-1222, 1997.

52.   Reese, J. H., Freiha, F. S., Gelb, A. B., Lum, B. L., and Torti, F. M. Transitional cell carcinoma of the prostate in patients undergoing radical cystoprostatectomy, J Urol. *147:* 92-95, 1992.

53.   Grignon, D. J. and O'Malley, F. P. Mucinous metaplasia in the prostate gland, Am J Surg Pathol. *17:* 287-290, 1993.

54.   Masumori, N., Vaikunth, S., Thomas, T. Z., Thomas, J., Tsukamoto, T., Case, T., Paul, M., Lee, H., Price, R. R., Caurand, P., Caprioli, R., Kasper, S., Shappell, S., and Matusik, R. J. Regrowth of prostate tumor after castration in probasin-large T antigen transgenic mice - longitudinal study with MRI, J Urol. *(abstract):*, 2000.

55.   Cheville, J. C. and Bostwick, D. G. Postatrophic hyperplasia of the prostate. A histologic mimic of prostatic adenocarcinoma, Am J Surg Pathol. *19:* 1068-1076, 1995.

56.   Amin, M. B., Tamboli, P., Varma, M., and Srigley, J. R. Postatrophic hyperplasia of the prostate gland: a detailed analysis of its morphology in needle biopsy specimens, Am J Surg Pathol. *23:* 925-931, 1999.

57.   De Marzo, A. M., Marchi, V. L., Epstein, J. I., and Nelson, W. G. Proliferative inflammatory atrophy of the prostate: implications for prostatic carcinogenesis, Am J Pathol. *155:* 1985-1992, 1999.

58.   Shah, R., Mucci, N. R., Amin, A., Macoska, J. A., and Rubin, M. A. Postatrophic hyperplasia of the prostate gland: neoplastic precursor or innocent bystander?, Am J Pathol. *158:* 1767-1773, 2001.

59.   Ruska, K. M., Sauvageot, J., and Epstein, J. I. Histology and cellular kinetics of prostatic atrophy, Am J Surg Pathol. *22:* 1073-1077, 1998.

60.   Shappell, S. B., Boeglin, W. E., Olson, S. J., Kasper, S., and Brash, A. R. 15-lipoxygenase-2 (15-LOX-2) is expressed in benign prostatic epithelium and reduced in prostate adenocarcinoma, Am J Pathol. *155:* 235-245, 1999.

61.   Gingrich, J. R., Barrios, R. J., Kattan, M. W., Nahm, H. S., Finegold, M. J., and Greenberg, N. M. Androgen-independent prostate cancer progession in the TRAMP model, Cancer Res. *57:* 4687-4691, 1997.

62.   Bostwick, D. G. and Qian, J. Effect of androgen deprivation therapy on prostatic intraepithelial neoplasia, Urology. *58 (2 Suppl 1):* 91-93, 2001.

63.   Roberts, R. O., Lieber, M. M., Bostwick, D. G., and Jacobsen, S. J. A review of clinical and pathological prostatitis syndromes, Urology. *49:* 809-821, 1997.

64.	Epstein, J. I., Grignon, D. J., Humphrey, P. A., McNeal, J. E., Sesterhenn, I. A., Troncoso, P., and Wheeler, T. M. Interobserver reproducibility in the diagnosis of prostatic intraepithelial neoplasia, Am J Surg Pathol. *19:* 873-886, 1995.

65.	Civantos, F., Marcial, M. A., Banks, E. R., Ho, C. K., Speights, V. O., Drew, P. A., Murphy, W. M., and Soloway, M. S. Pathology of androgen deprivation therapy in prostate carcinoma. A comparative study of 173 patients, Cancer. *75:* 1634-1641, 1995.

66.	Vaillancourt, L., Tetu, B., Fradet, Y., Dupont, A., Gomez, J., Cusan, L., Suburu, E. R., Diamond, P., Candas, B., and Labrie, F. Effect of neoadjuvant endocrine therapy (combined androgen blockade) on normal prostate and prostatic carcinoma. A randomized study, Am J Surg Pathol. *20:* 86-93, 1996.

67.	Brawer, M. K. Prostatic intraepithelial neoplasia: A premalignant lesion, Hum Pathol. *23:* 242-248, 1992.

68.	Bostwick, D. G. High grade prostatic intraepithelial neoplasia, Cancer. *75:* 1823-1836, 1995.

69.	Bostwick, D. G., Pacelli, A., and Lopez-Beltran, A. Molecular biology of prostatic intraepithelial neoplasia, Prostate. *29:* 117-134, 1996.

70.	Weinstein, M. H. and Epstein, J. I. Significance of high grade prostatic intraepithelial neoplasia on needle biopsy, Hum Pathol. *24:* 624-629, 1993.

71.	Brawer, M. K., Bigler, S. A., Sohlberg, O. E., Nagle, R. B., and Laange, P. H. Significance of prostatic intraepithelial neoplasia on prostate needle biopsy, Urology. *38:* 103-107, 1991.

72.	Bostwick, D. G., Amin, M. B., Dundore, P., Marsh, W., and Schultz, D. S. Architectural patterns of high-grade prostatic intraepithelial neoplasia, Hum Pathol. *24:* 298-310, 1993.

73.	Yasunaga, Y., Shin, M., Fujita, M. Q., Nonomura, N., Miki, T., Okuyama, A., and Aozasa, K. Different patterns of p53 mutations in prostatic intraepithelial neoplasia and concurrent carcinoma: Analysis of microdissected specimens, Lab Invest. *78:* 1275-1279, 1998.

74.	Kronz, J. D., Allan, C. H., Shaikh, A. A., and Epstein, J. I. Predicting cancer following a diagnosis of high-grade prostatic intraepithelial neoplasia on needle biopsy: data on men with more than one follow-up biopsy, Am J Surg Pathol. *25:* 1079-1085, 2001.

75.	Rubin, M. A., de La Taille, A., Bagiella, E., Olsson, C. A., and O'Toole, K. M. Cribriform carcinoma of the prostate and cribriform prostatic intraepithelial neoplasia. Incidence and clinical implications, Am J Surg Pathol. *22:* 840-848, 1998.

76.	Wilcox, G., Soh, S., Chakraborty, S., Scardino, P. T., and Wheeler, T. M. Patterns of high-grade prostatic intraepithelial neoplasia associated with clinically aggressive prostate cancer, Hum Pathol. *29:* 1119-1123, 1998.

77.	McNeal, J. E. and Yemoto, C. E. Spread of adenocarcinoma within prostatic ducts and acini: morphologic and clinical considerations, Am J Surg Pathol. *20:* 802-814, 1996.

78.	Gleason, D. Histologic grading and clinical staging of carcinoma of the prostate. *In:* M. Tannenbaum (ed.) Urologic Pathology: The Prostate, pp. 171-198. Philadelphia, PA: Lea & Febiger, 1977.

79.	Dawkins, H. J., Sellner, L. N., Turbett, G. R., Thompson, C. A., Redmond, S. L., McNeal, J. E., and Cohen, R. J. Distinction between intraductal carcinoma of the prostate (IDC-P), high -grade dysplasia (PIN), and invasive prostatic adenocarcinoma, using molecular markeres of cancer progression, Prostate. *44:* 265-270, 2000.

80.	McNeal, J. E. Prostatic microcarcinomas in relation to cancer origin and the evolution to clinical cancer, Cancer. *71 (3 Suppl):* 984-991, 1993.

81.	Kronz, J. D., Shaikh, A. A., and Epstein, J. I. High-grade prostatic intraepithelial neoplasia with adjacent small atypical glands on prostate biopsy, Hum Pathol. *32:* 389-395, 2001.

82. Park, J.-H., Walls, J. E., Galvez, J. J., Kim, M., Abate-Shen, C., Shen, M. M., and Cardiff, R. D. Prostatic intraepithelial neoplasia in genetically engineered mice, Am J Pathol. *161:* 727-735, 2002.

83. Masumori, N., Tsuchiya, K., Tu, W. H., Lee, C., Kasper, S., Tsukamoto, T., Shappell, S. B., and Matusik, R. J. An allograft model of androgen independent prostatic neuroendocrine carcinoma derived from LPB-Tag transgenic mouse line, J Urol. *submitted:*, 2002.

84. Maroulakou, I. G., Anver, M., Garrett, L., and Green, J. E. Prostate and mammary adenocarcinoma in transgenic mice carrying a rat C3(1) simian virus 40 large tumor antigen fusion gene, Proc Natl Acad Sci,USA. *91:* 11236-11240, 1994.

85. Greenberg, N. M., DeMayo, F., Finegold, M. J., Medina, D., Tilley, W. D., Aspinall, J. O., Cunha, G. R., Donjacour, A. A., Matusik, R. J., and Rosen, J. M. Prostate cancer in a transgenic mouse, Proc Natl Acad Sci, USA. *92:* 3439-3443, 1995.

86. Perez-Stable, C., Altman, N. H., Brown, J., Harbison, M., Cray, C., and Roos, B. A. Prostate, adrenocortical, and brown adipose tumors in fetal globin/T antigen transgenic mice, Lab Invest. *74:* 363-373, 1996.

87. Epstein, J. I., Walsh, P. C., Carmichael, M., and Brendler, C. B. Pathologic and clinical findings to predict tumor extent of nonpalpable (stage T1c) prostate cancer, JAMA. *271:* 368-374, 1994.

88. Epstein, J. I., Chan, D. W., Sokoll, L. J., Walsh, P. C., Cox, J. I., Rittenhouse, H., Wolfert, R., and Carter, H. B. Nonpalpable stage T1c prostate cancer: prediction of insignificant disease using free/total prostate specific antigen levels and needle biopsy findings, J Urol. *160:* 2407-2411, 1998.

89. Thorson, P., Vollmer, R. T., Arcangeli, C., Keetch, D. W., and Humphrey, P. A. Minimal carcinoma in prostate needle biopsy specimens: Diagnostic features and radical prostatectomy follow-up, Mod Pathol. *11:* 543-551, 1998.

90. Abdulkadir, S. A., Qu, Z., Garabedian, E., Song, S.-K., Peters, T. J., Svaren, J., Carbone, J. M., Naughton, C. K., Catalona, W. J., Ackerman, J. J. H., Gordon, J. I., Humphrey, P. A., and Milbrandt, J. Imparied prostate tumorigenesis in Egr-1-deficient mice, Nature Med. *7:* 101-106, 2001.

91. Bastacky, S. I., Walsh, P. C., and Epstein, J. I. Relationship between perineural tumor invasion on needle biopsy and radical prostatectomy capsular penetration in clinical stage B adenocarcinoma of the prostate, AmJ Surg Pathol. *17:* 336-341, 1993.

92. Egan, A. J. M. and Bostwick, D. G. Prediction of extraprostatic extension of prostate cancer based on needle biopsy findings: Perineural invasion lacks significance on multivariate analysis, Am J Surg Pathol. *21:* 1496-1500, 1997.

93. Holmes, G. F., Walsh, P. C., Pound, C. R., and Epstein, J. I. Excision of the neurovascular bundle at radical prostatectomy in cases with perineural invasion on needle biopsy, Urology. *53:* 752-756, 1999.

94. Maru, N., Ohori, M., Kattan, M. W., Scardino, P. T., and Wheeler, T. M. Prognostic significance of the diameter of perineural invasion in radical prostatectomy specimens, Hum Pathol. *32:* 828-833, 2001.

95. McNeal, J. E. and Yemoto, C. E. Significance of demonstrable vascular space invasion for the progression of prostatic adenocarcinoma, Am J Surg Pathol. *20:* 1351-1360, 1996.

96. Herman, C. M., Wilcox, G. E., Kattan, M. W., Scardino, P. T., and Wheeler, T. M. Lymphovascular invasion as a predictor of disease progression in prostate cancer, Am J Surg Pathol. *24:* 859-863, 2000.

97. Goldstein, N. S., Begin, L. R., Grody, W. W., Novak, J. M., Qian, J., and Bostwick, D. G. Minimal or no cancer in radical prostatectomy specimens. Report of 13 cases of the "vanishing cancer phenomenon", Am J Surg Pathol. *19:* 1002-1009, 1995.

98. DiGiuseppe, J. A., Sauvageot, J., and Epstein, J. I. Increasing incidence of minimal residual cancer in radical prostatectomy specimens, Am J Surg Pathol. *21:* 174-178, 1997.

99. Ohori, M., Wheeler, T. M., Dunn, J. K., Stamey, T. A., and Scardino, P. T. The pathologic features and prognosis of prostate cancer detectable with current diagnostic tests, The Journal of Urology. *152:* 1714-1720, 1994.

100. Tetu, B., Ro, J. Y., Ayala, A. G., Johnson, D. E., Logothetis, C. J., and Ordonez, N. G. Small cell carcinoma of the prostate part I: A clinicopathologic study of 20 cases, Cancer. *59:* 1803-1809, 1987.

101. Vader, V., Roberts, R. L., Manning, S., Tu, W. H., Case, T., Shook, M. F., Olson, S. J., Matusik, R. J., and Shappell, S. B. A peroxisome proliferator activated receptor gamma (PPARg) agonist inhibits metastases in a transgenic mouse model of prostate carcinoma (Pca), Mod Pathol abstract, 2002.

102. Montironi, R., Galluzzi, C. M., Diamanti, L., Giannulis, I., Pisani, E., and Scarpelli, M. Prostatic intra-epithelial neoplasia: expression and location of proliferating cell nuclear antigen in epithelial, endothelial and stromal nuclei, Virchows Arch A Pathol Anat Histopathol. *422:* 185-192, 1993.

103. Giannulis, I., Montironi, R., Galluzzi, C. M., de Nictolis, M., and Diamanti, L. Frequency and location of mitoses in prostatic intraepithelial neoplasia (PIN), Anticancer Res. *13:* 2447-2451, 1993.

104. Anwar, K., Nakakuki, K., Shiraishi, T., Naiki, H., Yatani, R., and Inuzuka, M. Presence of ras oncogene mutations and human papillomavirus DNA in human prostate carcinomas, Cancer Res. *52:* 5991-5996, 1992.

105. Watanabe, M., Shiraishi, T., Yatani, R., Nomura, A. M., and Stemmermann, G. N. International comparison on ras gene mutations in latent prostate carcinoma, Int J Cancer. *58:* 174-178, 1994.

106. Carter, B. S., Epstein, J. I., and Isaacs, W. B. ras gene mutations in human prostate cancer, Cancer Res. *50:* 6830-6832, 1990.

107. Gumerlock, P. H., Poonamallee, U. R., Meyers, F. J., and deVere White, R. W. Activated ras alleles in human carcinoma of the prostate are rare, Cancer Res. *51:* 1632-1637, 1991.

108. Eng, M. H., Charles, L. G., Ross, B. D., Chrisp, C. E., Pienta, K. J., Greenberg, N. M., Hsu, C. X., and Sanda, M. G. Early castration reduces prostatic carcinogenesis in transgenic mice, Urology. *54:* 1112-1119, 1999.

109. Gingrich, J. R., Barrios, R. J., Foster, B. A., and Greenberg, N. M. Pathologic progression of autochthonous prostate cancer in the TRAMP model, Prostate Cancer and Prostatic Diseases. *2:* 70-75, 1999.

110. Wechter, W. J., Leipold, D. D., Murray, E. D., Jr., Quiggle, D., McCracken, J. D., Barrios, R. S., and Greenberg, N. M. E-7869 (R-Flurbiprofen) inhibits progression of prostate cancer in the TRAMP mouse, Cancer Res. *60:* 2203-2208, 2000.

111. Gupta, S., Ahmad, N., Marengo, S. R., MacLennan, G. T., Greenberg, N. M., and Mukhtar, H. Chemoprevention of prostate carcinogenesis by alpha-difluoromethylornithine in TRAMP mice, Cancer Res. *60:* 5125-5133, 2000.

112.   Mentor-Marcel, R., Lamartiniere, C. A., Eltoum, I. E., Greenberg, N. M., and Elgavish, A. Genistein in the diet reduces the incidence of poorly differentiated prostatic adenocarcinoma in transgenic mice (TRAMP), Cancer Res. *61:* 6777-6782, 2001.

113.   Umbas, R., Isaacs, W. B., Bringuier, P. P., Schaafsma, H. E., Karthaus, H. F., Oosterhof, G. O., Debruyne, F. M., and Schalken, J. A. Decreased E-cadherin expression is associated with poor prognosis in patients with prostate cancer, Cancer Res. *54:* 3929-3933, 1994.

114.   Ross, J. S., Figge, H. L., Bui, H. X., del Rosario, A. D., Fisher, H. A., Nazeer, T., Jennings, T. A., Ingle, R., and Kim, D. N. E-cadherin expression in prostatic carcinoma biopsies: correlation with tumor grade, DNA content, pathologic stage, and clinical outcome, Mod Pathol. *7:* 835-841, 1994.

115.   Cheng, L., Nagabhushan, M., Pretlow, T. P., Amini, S. B., and Pretlow, T. G. Expression of E-cadherin in primary and metastatic prostate cancer, Am J Pathol. *148:* 1375-1380, 1996.

116.   Kaplan, P. J., Mohan, S., Cohen, P., Foster, B. A., and Greenberg, N. M. The insulin-like growth factor axis and prostate cancer: lessons from the transgenic adenocarcinoma of mouse prostate (TRAMP) model, Cancer Res. *59:* 2203-2209, 1999.

117.   Chan, J. M., Stampfer, M. J., Giovannucci, E., Gann, P. H., Ma, J., Wilkinson, P., Hennekens, C. H., and Pollak, M. Plasma insulin-like growth factor-I and prostate cancer risk: a prospective study, Science. *279:* 563-566, 1998.

118.   Huss, W. J., Hanrahan, C. F., Barrios, R. J., Simons, J. W., and Greenberg, N. M. Angiogenesis and prostate cancer: identification of a molecular progression switch, Cancer Res. *61:* 2736-2743, 2001.

119.   Masumori, N., Tu, W. H., Kasper, S., Tsukamoto, T., Shappell, S. B., and Matusik, R. J. Allograft model of androgen independent prostatic neuroendocrine carcinoma derived from LPB-TAG transgenic mouse line, J Urol. *abstract:*, 2001.

120.   Kelavkar, V. P., Cohen, C., Kamitani, H., Eling, T. E., and Badr, K. F. Concordant induction of 15-lipoxygenase-1 and mutant p53 expression in human prostate adenocarcinoma: correlation with Gleason staging, Carcinogenesis. *21:* 1777-1787, 2000.

121.   Shappell, S. B., Manning, S., Boeglin, W. E., Guan, Y., Davis, L., Jack, G. S., Roberts, R. L., Coffey, C. S., Wheeler, T. M., Breyer, M. D., and Brash, A. R. Alterations in lipoxygenase and cyclooxygenase-2 catalytic activity and mRNA expression in prostate carcinoma, Neoplasia. *4:* 287-303, 2001.

122.   Shappell, S. B., Olson, S. J., Manning, S., Roberts, R. L., Masumori, N., Boeglin, W. E., Hannah, S. E., Vader, V., Shook, M. F., Thomas, T. Z., Brash, A. R., and Matusik, R. J. Elevated expression of 12/15-lipoxygenase and COX-2 in a murine model of prostate carcinoma, Proc Am Assoc Cancer Res. *abstract:*, 2002.

123.   Jack, G. S., Brash, A. R., Olson, S. J., Manning, S., Coffey, C. S., Smith, J. A., Jr., and Shappell, S. B. Reduced 15-lipoxygenase-2 immunostaining in prostate adenocarcinoma: Correlation with grade and expression in high grade prostatic intraepithelial neoplasia, Hum Pathol. *31:* 1146-1154, 2000.

124.   Jisaka, M., Kim, R. B., Boeglin, W. E., Nanney, L. B., and Brash, A. R. Molecular cloning and functional expression of a phorbol ester-inducible 8S-lipoxygenase from mouse skin, J Biol Chem. *272:* 24410-24416, 1997.

125.   Kubota, T., Koshizuka, K., Williamson, E. A., Asou, H., Said, J. W., Holden, S., Miyoshi, I., and Koeffler, H. P. Ligand for peroxisome proliferator-activated receptor gamma (Troglitazone) has potent antitumor effect against human prostate cancer both in vitro and in vivo, Cancer Research. *58:* 3344-3352, 1998.

126. Butler, R., Mitchell, S. H., Tindall, D. J., and Young, C. Y. F. Nonapoptotic cell death associated with S-phase arrest of prostate cancer cells via the peroxisome proliferator-activated receptor gamma ligand, 15-deoxy-delta12,14-prostaglandin J2, Cell Growth Diff. *11:* 49-61, 2000.

127. Mueller, E., Smith, M., Sarraf, P., Kroll, T., Aiyer, A., Kaufman, D. S., Oh, W., Demetri, G., Figg, W. D., Zhou, X. P., Eng, C., Spiegelman, B. M., and Kantoff, P. W. Effects of ligand activation of peroxisome proliferator-activated receptor gamma in human prostate cancer, Proc Natl Acad Sci, USA. *97:* 10990-10995, 2000.

128. Shappell, S. B., Gupta, R. A., Manning, S., Whitehead, R., Boeglin, W. E., Schneider, C., Case, T., Price, J., Jack, G. S., Wheeler, T. M., Matusik, R. J., Brash, A. R., and DuBois, R. N. 15-hydroxyeicosatetraenoic acid (15-HETE) activates peroxisome proliferator activated receptor gamma and inhibits proliferation in PC3 prostate carcinoma cells, Cancer Res. *61:* 497-503, 2001.

129. Vader, V., Roberts, R. L., Guan, Y.-F., Manning, S., Masumori, N., Olson, S. J., Shook, M. F., Coffey, C. S., Boeglin, W. E., Brash, A. R., Matusik, R. J., and Shappell, S. B. A synthetic PPARgamma agonist reduces tumor metastases and angiogenesis in a murine model of advanced androgen-insensitive prostate carcinoma. Proc Am Assoc Cancer Res. *43:* 1083a, 2002.

130. Tu, W. H., Thomas, T. Z., Masumori, N., Tsukamoto, T., Kasper, S., Roberts, R. L., Moses, H. L., Shappell, S. B., and Matusik, R. J. Role of TGF- beta pathway in prostate carcinogenesis, J Urol. *abstract:*, 2001.

131. Eid, M. A., Kumar, M. V., Iczkowski, K. A., Bostwick, D. G., and Tindall, D. J. Expression of early growth response genes in human prostate cancer, Cancer Res. *58:* 2461-2468, 1998.

132. Abdulkadir, S. A., Carbone, J. M., Naughton, C. K., Humphrey, P. A., Catalona, W. J., and Milbrandt, J. Frequent and early loss of the EGR1 corepressor NAB2 in human prostate carcinoma, Hum Pathol. *32:* 935-939, 2001.

133. Vocke, C. D., Possatti, R. O., Bostwick, D. G., Florence, C. D., Jennings, S. B., Strup, S. E., Duray, P. H., Liotta, L. A., Emmert-Buck, M. R., and Linehan, W. M. Analysis of 99 microdissected prostate carcinomas reveals a high frequency of allelic loss on chomosome 8p21-22, Cancer Res. *56:* 2411-2416, 1996.

134. Emmert-Buck, M. R., Vocke, C. D., Pozzatti, R. O., Duray, P. H., Jennings, S. B., Florence, C. D., Bostwick, D. G., Liotta, L. A., and Linehan, W. M. Allelic loss on chromosome 8p12-21 in microdissected prostate intraepithelial neoplasia, Cancer Res. *55:* 2959-2962, 1995.

135. Voeller, H. J., Augustus, M., Madlike, V., Bova, G. S., Carter, K. C., and Gelmann, E. P. Coding region of NKX3.1, prostate-specific homeobox gene on 8p21, is not mutated in human prostate cancers, Cancer Res. *57:* 4455-4459, 1997.

136. Bowen, C., Bubendorf, L., Voeller, H. J., Slack, R., Willi, N., Sauter, G., Gasser, T. C., Koivisto, P., Lack, E. E., Kononen, J., Kallioniemi, O. P., and Gelmann, E. P. Loss of NKX3.1 expression in human prostate cancers correlates with tumor progression, Cancer Res. *60:* 6111-6115, 2000.

137. Tanaka, A., Furuya, A., Yamasaki, M., Hanai, N., Kuriki, K., Kamiakito, T., Kobayashi, Y., Yoshida, H., Koike, M., and Fukayama, M. HIgh frequency of fibroblast growth factor (FGF) 8 expression in clinical prostate cancers and breast tissues, immunohistochemically demonstrated by a newly established neutralizing monoclonal antibody against FGF 8, Cancer Res. *58:* 2053-2056, 1998.

138. Dorkin, T. J., Robinson, M. C., Marsh, C., Bjartell, A., Neal, D. E., and Leung, H. Y. FGF8 over-expression in prostate cancer is associated with decreased patient survival and persists in androgen independent disease, Oncogene. *18:* 2755-2761, 1999.

139. Valve, E. M., Nevalainen, M. T., Nurmi, M. J., Laato, M. K., Martikainen, P. M., and Harkonen, P. L. Increased expression of FGF-8 isoforms and FGF receptors in human premalignant prostatic intraepithelial neoplasia lesions and prostate cancer, Lab Invest. *81:* 815-826, 2001.

140. Song, Z., Wu, X., Powell, W. C., Cardiff, R. D., Cohen, M. B., Tin, R. T., Matusik, R. J., Miller, G. J., and Roy-Burman, P. Fibroblast growth factor 8 isoform b overexpression in prostate epithelium: A new mouse model for prostatic intraepithelial neoplasia, Cancer Res. *62:* in press, 2002.

141. Zhang, J., Thomas, T. Z., Kasper, S., and Matusik, R. J. A small composite probasin promoter confers high levels of prostate-specific gene expression through regulation by androgens and glucocorticoids in vitro and in vivo, Endocrinol. *141:* 4698-4710, 2000.

142. Wu, X., Wu, J., Huang, J., Powell, W. C., Zhang, J., Matusik, R. J., Sangiorgi, F. O., Maxson, R. E., Sucov, H. M., and Roy-Burman, P. Generation of a prostate epithelial cell-specific Cre transgenic mouse model for tissue-specific gene ablation, Mech Dev. *101:* 61-69, 2001.

143. Huang, J., Powell, W. C., Khodavirdi, A. C., Wu, J., Makita, T., Cardiff, R. D., Cohen, M. B., Sucov, H. M., and Roy-Burman, P. Prostatic intraepithelial neoplasia in mice with conditional disruption of the retinoid x receptor alpha allele in prostate epithelium, Cancer Res. *62:* in press, 2002.

144. Perez-Stable, C., Altman, N. H., Mehta, P. P., Deftos, L. J., and Roos, B. A. Prostate cancer progression, metastasis, and gene expression in transgenic mice, Cancer Res. *57:* 900-906, 1997.

145. DiGiovanni, J., Bol, D. K., Wilker, E., Beltran, L., Carbajal, S., Moats, S., Ramirez, A., Jorcano, J., and Kiguchi, K. Constituitive expression of insulin-like growth factor-1 in epidermal basal cells of transgenic mice leads to spontaneous tumor promotion, Cancer Res. *60:* 1561-1570, 2000.

146. Steck, P. A., Pershouse, M. A., Jasser, S. A., Yung, W. K., Lin, H., Ligon, A. H., Langford, L. A., Baumgard, M. L., Hattier, T., Davis, T., Frye, C., Hu, R., Swedlund, B., Teng, D. H., and Tavtigian, S. V. Identification of a candidate tumour suppressor gene, MMAC1, at chromosome 10q23.3 that is mutated in multiple advanced cancers, Nat Genet. *15:* 356-362, 1997.

147. Wang, S. I., Parsons, R., and Ittmann, M. Homozygous deletion of the PTEN tumor suppressor gene in a subset of prostate adenocarcinomas, Clin Cancer Res. *4:* 811-815, 1998.

148. Cairns, P., Okami, K., Halachmi, S., Halachmi, N., Esteller, M., Herman, J. G., Jen, J., Isaacs, W. B., Bova, G. S., and Sidransky, D. Frequent inactivation of PTEN/MMAC1 in primary prostate cancer, Cancer Res. *57:* 4997-5000, 1997.

149. Di Cristofano, A., Pesce, B., Cordon-Cardo, C., and Pandolfi, P. P. Pten is essential for embryonic development and tumour suppression, Nature Genet. *19:* 348-355, 1998.

150. Podsypanina, K., Ellenson, L. H., Nemes, A., Gu, J., Tamura, M., Yamada, K. M., Cordon-Cardo, C., Catoretti, G., Fisher, P. E., and Parsons, R. Mutation of *Pten/Mmac1* in mice causes neoplasia in multiple organ systems, Proc Natl Acad Sci, USA. *96:* 1563-1568, 1999.

151. Macri, E. and Loda, M. Role of p27 in prostate carcinogenesis, Cancer Metastasis Rev. *17:* 337-344, 1998.

152. Cordon-Cardo, C., Koff, A., Drobnjak, M., Capodieci, P., Osman, I., Millard, S. S., Gaudin, P. B., Fazzari, M., Zhang, Z. F., Massague, J., and Scher, H. I. Distinct altered patterns of p27KIP1 gene expression in benign prostatic hyperplasia and prostatic carcinoma, J Natl Cancer Inst. *90:* 1284-1291, 1998.

153. Suwa, T., Nyska, A., Peckham, J. C., Hailey, J. R., Mahler, J. F., Haseman, J. K., and Maronpot, R. R. A retrospective analysis of background lesions and tissue accountability for male accessory sex organs in Fischer-344 rats, Toxicol Pathol. *29:* 467-478, 2001.

154.   Serra, R., Johnson, M., Filvaroff, E. H., LaBorde, J., Sheehan, D. M., Derynck, R., and Moses, H. L. Expression of a truncated, kinase-defective TGF-beta type II receptor in mouse skeletal tissue promotes terminal chondrocyte differentiation and osteoarthritis, J Cell Biol. *139:* 541, 1997.

155.   Crabtree, J. S., Scacheri, P. C., Ward, J. M., Garret-Beal, L., Emmert-Buck, M. R., Edgemon, K. A., Lorang, D., Libutti, S. K., Chandrasekharappa, S. C., Marx, S. J., Spiegel, A. M., and Collins, F. S. A mouse model of multiple endocrine neoplasia, type 1, develops multiple endocrine tumors, Proc Natl Acad Sci USA. *98:* 1118-1123, 2001.

156.   Schreiber-Agus, N., Meng, Y., Hoang, T., Hou Jr, H., Chen, K., Greenberg, R., Cordon-Cardo, C., Lee, H.-W., and DePinho, R. A. Role of Mxi1 in ageing organ systems and the regulation of normal and neoplastic growth, Nature. *393:* 483-487, 1998.

Table 1: Genetically Engineered Mouse (GEM) Models of Prostatic Neoplasia Reviewed by the Bar Harbor Pathology Workshop

Category	Model	Transgene or knockout	Background	Promoter or Selectivity of Knockout	Reference
Cell Cycle	C3(1)-SV40	SV40 Early Region		C3(1)	(84)
	TRAMP	SV40 Early Region	C57Bl/6 x FVB	Short PB	(85)
	TRAMP	SV40 Early Region		Short PB	Herbert, R., unpublished
	LPB-Tag 12T10	SV40 Large T antigen	CD1	Long PB	(36, 37)
	LPB-Tag 12T5	SV40 Large T antigen	CD1	Long PB	(36)
	LPB-Tag 12T7s	SV40 Large T antigen	CD1	Long PB	(36)
	LPB-Tag 12T7f	SV40 Large T antigen	CD1	Long PB	(36)
	CR2-SV40	SV40 Early Region	FVB	CR2	(32)
	p27 +/-	p27 knock out	C57	Genomic knockout, heterozygous	Abate-Shen, C., unpublished
Growth factors/Signal pathways	MT-TGFα	Rat TGFα	B6D2F1	MT	Coffey, R.J., unpublished
	PB-ras	H-ras		PB	Schreiber-Agus, N., unpublished
	PB-FGF8b	FGF, isoform b	B6D2F1	ARR$_2$PB	(140)
Receptors	MT-DNIIR	TGFβRII dominant negative	B6D2F1	MT	(154); Moses, H., unpublished
Tumor Suppressors	PTEN +/-	PTEN knock out	Balb/c x 129	Genomic knockout, heterozygous	Wu, H., unpublished
	PTEN +/-	PTEN knock out	SVJ129	Genomic knockout, heterozygous	Abate-Shen, C., unpublished
	Men1$^{TSM/1}$	Men1 knock out	NIH Black Swiss 129/SvEvTacFBR	Genomic knockout, heterozygous	(155)
Homeobox genes	Nkx 3.1 -/-	Nkx 3.1 knockout	129/SvImj x C57Bl/6J	Genomic knockout, homozygous	(50)

Bigenics[4]	LPB-Tag 12T-7f x MT-DNIIR	See Above	(130)
	MT-TGFα x MT-DNIIR	See Above	Cutler, S., Coffey, R.J., unpublished
	Nkx +/- x Pten +/-	See Above	(34)
	Pten +/- x p27 +/-	See Above	Abate-Shen, C., unpublished
	Nkx +/- x Pten +/- x p27 +/-	See Above	Abate-Shen, C., unpublished
	Pb-ras +/+ x mxil -/-	See Above	(156); Schreiber-Agus, N., unpublished

Table 2: Hierarchical Classification of Disorders of the Mouse Prostate and Other Male Accessory Glands: The Bar Harbor Classification

Prostate

Disorders of Development:
    Agenesis/Aplasia
    Hypoplasia

Metaplasia (e.g., transitional, squamous, adenomatous or intestinal)

Atrophy

Inflammatory Disorders
    Prostatitis
        Active/Chronic Active
        Granulomatous

    Abscess
    Coagulative necrosis
    Fibrosis

Non-neoplastic proliferations of the Prostate/Hyperplasia
    Epithelial Hyperplasia
        Focal
            With Atypia
            Without Atypia
        Diffuse
            With Atypia
            Without Atypia
    Stromal Hyperplasia
        Focal
            With Atypia
            Without Aypia
        Diffuse
            With Atypia
            Without Atypia
    Combined Epithelial and Stromal Hyperplasia (extent – focal or diffuse and presence or absence of atypia should be specified)

Neoplastic Proliferations of the Prostate
    Benign
        Adenoma
        Papillary or papilloma

Table 2: Hierarchical Classification of Disorders of the Mouse Prostate and Other Male Accessory Glands: The Bar Harbor Classification – continued

Prostatic Intraepithelial Neoplasia (PIN)/Neoplastic Proliferation of Potential Pre-malignant Potential
      With document progression to invasive carcinoma
      Without documented progression to invasive carcinoma

Carcinoma (invasive)
      Microinvasive Carcinoma
      Invasive Carcinoma
            Adenocarcinoma
                  Well differentiated
                  Moderately differentiated
                  Poorly differentiated
            NE carcinoma
                  Small cell carcinoma
            Undifferentiated carcinoma
            Squamous cell carcinoma
             Spindle cell/Sarcomatoid carcinoma
            Mixed carcinoma (specify components)
                  Adenosquamous carcinoma

Sarcoma
      Leiomyosarcoma
      Rhabdomyosarcoma
      Chondrosarcoma
      Osteosarcoma
      Sarcoma, NOS

Carcinosarcoma

Periurethral and Bulbourethral Glands

Disorders of Development

Atypical hyperplasia

Carcinoma
      Adenocarcinoma
      NE carcinoma
      Poorly differentiated carcinoma

Table 3: Differentiation Classification of Human Prostate Adenocarcinoma

Differentiation	Gleason Score	Common Gleason Pattern	Histologic/Cytologic Description
Well differentiated	2-4	One	Typically TZ tumors; circumscribed proliferation of fairly uniformly sized, closely spaced tumor glands; also BPH-like larger glands with ample clear (?lipid) cytoplasm with well defined cell borders, basally situated relatively bland nuclei
		Two	Typically TZ tumors; partially circumscribed, closely spaced but more variably sized tumor glands with ample generally clear cytoplasm, somewhat similar to benign prostate glands
Moderately differentiated	5-6	Three	Common PZ tumors, although can be seen in TZ; in PZ, commonly associated with HGPIN; small acinar forming, more infiltrative with greater intervening stroma and/or infiltration between benign glands; eosinophilic protein-rich cytoplasm
Moderately Poorly differentiated	7	Four	Common in PZ tumors possibly reflecting "dedifferentiation" with increased tumor growth; also can occur in TZ; characterized especially by gland-fusion and large irregular cribriform proliferations (i.e., no longer discreet gland formation, but still features of adeno differentiation)
Poorly differentiated	8-10	Five	Characterized by infiltrating cords of cells and single cells; large solid growths, including with comedo necrosis

Table 4: Differentiation Classification of Mouse Prostate Adenocarcinoma

Differentiation	Histologic Description
Well differentiated	Composed exclusively or predominantly of discreet, well formed glands
Moderately differentiated	Gland formation clearly evident, but focal to extensive areas are composed of fused glands or more solid areas
Poorly differentiated	Tumor is composed predominantly or exclusively of more solid sheets or nests, with either rare gland formation histologically or cells demonstrated to have secretory differentiation by ancillary techniques

Table 5: NE Carcinoma. Considerations and Classification in GEM Prostate

---

Summary of Neuroendocrine (NE) Differentiation in Human and GEM Prostate Carcinoma

- The relationship between NE differentiation determined immunophenotypically and prognosis in human Pca is not established.
- Glandular differentiation and NE differentiation in human Pca and potentially in GEM tumors are not mutually exclusive. In human Pca:
  - NE differentiation may be demonstrated in usual acinar carcinoma.
  - Small cell carcinomas are commonly seen in association with usual acinar carcinoma or arise in patients with a prior diagnosis of more usual acinar adenocarcinoma.
  - Small cell carcinomas have a variable immunophenotype regarding presence of usual NE markers. Small cell carcinoma in the human is diagnosed on the basis of its cytologic appearance.

Approach to tumors in GEM with histologic features suggestive of NE differentiation.

- Tumors with light microscopic appearance similar or identical to those illustrated as NE carcinoma herein (that have been substantiated by immunohistochemistry and electron microscopy), should be regarded as potentially being NE carcinomas. NE differentiation should be confirmed by ancillary techniques.
  - Immunostaining should employ at least two different markers, e.g., chromogranin and synaptophysin. Positive immunostaining for either is sufficient to designate such tumors as NE carcinoma (when morphology is as shown for NE carcinoma herein). Punctate perinuclear CK8 immunostaining is supportive but less specific.
  - Positive immunostaining for NE markers can be substantitated by ultrastructural examination in order to demonstrate dense core neurosecretory granules.
  - Negative immunostaining should be followed by electron microscopy. As NE type granules can be focal and small in number, examination should be rigorous. Consultation with members of the MMHCC Pathology panel is encouraged. If NE type secretory granules are identified, they are sufficient to designate such tumors as NE carcinoma (when morphology is as shown for NE carcinoma herein).
  - In the absence of immunohistochemical or ultrastructural confirmation of NE differentiation, tumors with suggestive morphology can be designated as carcinoma with NE differentiation or NE features.
- Tumors with glandular differentiation (adenocarcinoma) or without histologic features of either glandular or NE differentiation (poorly differentiated carcinoma) that have NE differentiation demonstrated by immunohistochemistry or electron microscopy can be designated as adenocarcinoma (or carcinoma) with NE differentiation. The specific ancillary techniques employed and their results should be specified.
- Tumors with cytologic features typical of small cell carcinoma in human lung and human prostate should be designated as small cell carcinoma, regardless of the immunophenotype. It is encouraged that immunohistochemistry for NE markers still be performed on these tumors in order to collect potentially useful data for future classification.

Table 6: Immunohistochemical Assays Utilized in Characterization of Prostate Lesions in GEM

Antigen	Target Cells or Structures	Antibody	Company	Dilution	Tissue Fixation [a]	Application	Referen
CK8	Luminal epithelium	PH182 Sheep polyclonal	Binding Site, San Diego, CA	1:200	Form.[b]	Demonstration of luminal cells; e.g., in PIN vs. basal cell hyperplasia	(82)
Pan-Cytokeratin	All epithelial cells	CK-P polyclonal	Dako	N.S.[c]	Para.[d]	Verify epithelial vs. mesenchymal differentiation	(34)
CK5 (HMWCK)	Basal Cells	Anti Mouse CK5 polyclonal	Covance, Berkeley, CA		Form.	Demonstration of basal cells, which are present in benign glands; various alterations have been described in mPIN; fragmentation of basal cell layer is seen in human HGPIN; documentation of basal cell hyperplasia	(33)
CK14 (HMWCK)	Basal Cells	Anti-CK14 monoclonal	BioGenex Laboratories, San Ramon, CA	N.S.	Para.		(34)
		PH503 Sheep polyclonal	Binding Site, San Diego, CA	1:200	Form.		(82)
p63	Basal Cells		Santa Cruz Biotechnology, Inc.	N.S.	Form.		(3)
Chromo-granin	Neuroendocrine Cells	Anti bovine SP-1	Incstar, Stillwater, MN	1:500	Form.	Demonstration NE differentiation; multiple markers should be employed, as staining can be rare/focal and variable for different NE antigens	(32)
			Dia-Sorin, Inc.	1:1000			(37)

Synapto-physin	Neuroendocrine Cells	Anti-human synaptophysin[e]	Dako	1:200[e]	Form.		(32)
E-cadherin	Luminal epithelial cells	C20820	Transduction Laboratories	N.S.	Form.	Documentation of possible altered expression during progression from benign to PIN to Pca, as in human Pca	(2)
				1:800	Form.		(82)
				1:100	Para.		(35)
Smooth muscle actin	Contractile stromal cells	A2537 Mouse Monoclonal	Sigma, St. Louis, MO	1:1000	Form.	Stains fibromuscular stroma, which can be attenuated or fragmented in mPIN; may stain stromal lesions when differential is carcinoma (CK positive) vs. sarcoma	(82)
Laminin	Basement membrane	L9393	Sigma, St. Louis, MO	1:1000	Form.	Stains basement membrane, which is seen around benign glands and mPIN; insufficient data thus far for mouse Pca	(82) (8:

PCNA	Proliferating Cells	PC10	Santa Cruz Biotechnology, Inc.	1:400	Para.	Assessment of proliferation rates, reported as increased in mPIN as in human PIN; useful endpoint for treatments or genetic manipulations that may alter neoplastic cell proliferation, when assessed blindly (counting or image analysis)	(31)
		PC10[f]		1:50[f]	Form.		(37)
Ki67	Proliferating Cells	CLKi67	Novocastro, Newcastle, UK	1:1800	Form.		(82)
		Anti-Ki67 rabbit polyclonal	Vector, Burlingame, CA	1:2000	Para.		(35)
CD31	Endothelial Cells	Anti-C31 rat monoclonal	PharMingen, San Diego, CA	1:50	Form.	Determination of microvessel density: tumor angiogenesis with lesion progression; to discern alterations in angiogenesis with genetic or treatment effects when assessed blindly (counting or image analysis)	(118)
Endoglin (CD105)	Endothelial Cells	Monoclonal	Dako	N.S.	Para.		(34)
von Willebrand factor	Endothelial Cells	Polyclonal	Dako	N.S.	Form.		(90)

Androgen Receptor (AR)	AR postive cells	06-686	Upstate Bio-technologies, Lake Placid, NY	1:1000	Form.	No clear relationship between routine immuno-staining and hormone sensitivity in human Pca; may be altered with progression in some GEM models	(82)
		N-20	Santa Cruz Biotechnology, Inc.	1:100	Form.		(37)

a

b

c NS, not specified

d

e Detected with indocarbocyanine (Cy3)-conjugated donkey anti-rabbit IgG and confocal microscopy

f horseradish peroxidase-conjugated

Figure Legends:

Figure 1: Gross and microscopic anatomy and zone of origin of prostate adenocarcinoma in the human prostate. A) Gross photograph showing a cross section of a prostatectomy specimen in which the transition zone (TZ) is markedly expanded by fleshy nodules of BPH (black arrowheads). The TZ is demarcated from the posteriorly and laterally located peripheral zone (PZ) by fibrous tissue (black arrows) compressed by the expanding TZ. Medially, the urethra (white arrows) is slit-like due to compression by the BPH-expanded TZ. Lateral aspects of the PZ are indicated (white arrowheads). **B)** Gross photograph showing a cross section of a prostatectomy specimen in which the TZ and PZ appear somewhat spongy due, in part, to dilated, atrophic glands. Note the homogenous, tan-gray tumor nodule in right posterolateral PZ (arrowhead). This is a common area of involvement for usual PZ tumors. A tumor in this posterior location would likely be palpable as a discrete, firm nodule on digital rectal examination. Prostate carcinoma is not typically discernible grossly, especially with smaller tumors detected by PSA screening (urethra, arrow). **C, D, E)** Low, intermediate, and high magnification photomicrographs of normal central zone (CZ) glands in a prostatectomy specimen. **C)** The CZ surrounds the ejaculatory ducts (arrowhead), which penetrate the prostate parenchyma and empty into the urethra at the verumontanum, a raised posterior ridge at approximately the junction of the mid and apical third of the prostate. The CZ is located in the posterior medial aspects of the prostate and occupies more tissue towards base. **D,E)** CZ glands are larger in diameter than usual PZ glands and have more irregular luminal contours due to papillary infoldings. Roman arches (arrowheads), imparting a cribriform architecture (arrowheads), are common in CZ glands. However, normal CZ glands lack cytologic atypia, a feature that helps to distinguish them from PIN on transrectal biopsy. **F)** High magnification of normal benign PZ glands in radical prostatectomy specimen. Compared to usual acinar prostate carcinoma, benign glands are larger and have a tufted or undulating luminal border. Benign glands have two distinct cell layers, the basal cells and the differentiated luminal secretory cells. Basal cells are not always discernible or distinguishable from adjacent underlying stromal cells by light microscopy. Secretory cells may be variably stratified or pseudostratified, but lack features of cytologic atypia that are characteristic of PIN. Secretory cells in benign glands typically exhibit a clear to granular, faintly eosinophilic cytoplasm which is variably disrupted at the luminal border due to ongoing apocrine-type secretion. **G)** Intermediate magnification of HMWCK immunostaining (CK 903) of benign prostate glands in radical prostatectomy specimen. The basal cell layer is circumferentially intact in multiple, adjacent gland profiles. Basal cell hyperplasia is evident focally (arrowhead). **H,I)** Typical human TZ tumor. **H)** Whole mount section, in which TZ and PZ are easily identified due to the expansion of the TZ by BPH nodules (arrowheads) composed of hyperplastic glandular and stromal elements. Tumor (asterisk), a Gleason score 2 + 3 = 5 carcinoma, is outlined by ink dots and is clearly located within the TZ, and extending into the anterior aspect of the prostate (black arrow). Urethra and periurethral region where prostatic ducts enter, shown by white arrow at level of verumontanum. **I)** High power photomicrograph, showing a common TZ tumor morphology, corresponding to Gleason pattern 2. Tumor is composed of intermediate to large glands, with ample, fairly clear cytoplasm. Nuclei are basally located and some are pyknotic. Scattered large more vesicular nuclei with prominent nucleoli were also present confirming the carcinoma diagnosis.

89

Occasional inta-luminal dense pink secretions (more typical of carcinoma than benign glands) are noted (arrowheads). **J,K)** Typical human PZ tumor. **J)** Whole mount section showing outlined PZ tumor (asterisk), a Gleason score 3 + 4 = 7 carcinoma, in right posterolateral aspect of the gland. Expansion of the TZ by nodules of glandular and stromal hyperplasia (BPH changes, arrowheads) is evident. Note the extension of the PZ laterally (arrows). **K)** Intermediate power photomicrograph of tumor in J, showing stromal invasion by discrete, well formed glands (arrows) in a Gleason pattern 3 component and the transition to a higher grade Gleason pattern 4 focus (*), where more solid-like growth of fused glands is evident. Note occasional crystalloids and dense pink secretions within lumens of carcinoma glands (arrowheads).

Figure 2: Anatomy and histology of the mouse prostate. A) Gross photograph of wild-type mouse prostate, removed "en-bloc" with the urinary bladder and left and right seminal vesicles, showing the normal anatomic relationships of individual prostate lobes. The anterior/ventral aspect of the block is toward the top of photograph. Note the relationship of the anterior prostate or coagulating gland (AP) to the seminal vesicles (SV). Dorsal prostate (DP); lateral prostate (LP); ventral prostate (VP); urinary bladder (BL); urethra (UR). **B)** Gross photograph of separately dissected wild type mouse prostate lobes positioned to show their normal, relative anatomic relationships. Separating the various lobes with the aid of a dissecting microscope allows for the determination of individual lobe weights and snap freezing individual lobe portions, as well as histologic examination. Procedures for histologic examination of intact DP, LP, VP and adjacent structures are described in the Protocols section and illustrated in Figure 12. **C)** Intermediate power photomicrograph of adult wild type mouse anterior prostate. The anterior prostate shows the most complex luminal architecture compared to the other lobes of the mouse prostate, including frequent mucosal folds protruding into the gland lumens (arrowheads). See text for a more detailed histologic description . **D)** Low power photomicrograph showing adjacent dorsal (D) and lateral (L) prostate lobes of an adult, wild type mouse. A thin rim of fibromuscular stroma and then more peripherally located loose connective tissue surrounds individual glands in both the lateral and dorsal lobes. Note the differences in the epithelial cell thickness and luminal diameters in the lateral and dorsal prostate and the increased amount of eosinophilic secretory product in the glands in the dorsal prostate compared to the lateral prostate (see text for details). **E)** High power photomicrograph of adult, wild type mouse dorsal prostate. Note the thin rim of fibromuscular stroma surrounding individual gland profiles (arrowheads). Low **(F)** and high **(G)** magnification photomicrographs of mouse ventral prostate. Only a thin rim of fibromuscular stroma surrounds individual glands (arrowheads), with loose connective tissue extending between individual gland profiles. This is in contrast to the greater amount of contractile fibromuscular stroma surrounding all the gland lobules in the human prostate. See text for descriptions of nuclei, cytoplasm, and nature of secretions. **H)** A high molecular weight cytokeratin (CK5) immunostained section from adult, wild type mouse prostate shows the well defined basal cell layer that is often circumferential and extends into the normal, short luminal infoldings (arrowheads).

Figure 3: Hypoplasia, metaplasia, atrophy, and inflammation in human and mouse prostate. A) Abnormal or delayed development, consistent with hypoplasia, in section of AP from GEM. The prostate was small and ill defined grossly. Although suboptimal histologic section, reduced gland profiles with associated prominent stroma (arrowheads) can be

90

appreciated, surrounded by conspicuous nerve ganglia (*). (Low power photomicrograph of AP from 19 wk old homozygous SMAD3 knockout mouse, *Smad3 -/-;* W.Tu, R.Coffey, R.J.Matuisk, unpublished observations). **B) Human** prostate from prostatectomy specimen, low power photomicrograph showing normal primary periurethral ducts, which are typically at least partially lined by urothelium, extending out from urethra (with partially denuded lining) in lower left. **C)** High power photomicrograph of transrectal biopsy specimen from **human** prostate showing prominent transitional metaplasia. Patient in blinded chemoprevention trial and may or may not have received long term treatment with 5α-reductase inhibitor. Note, normal urothelium as well as transitional metaplasia will immunostain with antibodies to high molecular weight cytokeratin, similar to basal cells and basal cell hyperplasia. Transitional metaplasia, which can be seen with basal cell hyperplasia, is recognized by histologic resemblance to normal urothelium, including such features as frequent nuclear grooves. **D)** Transitional metaplasia in GEM prostate. High power photomicrograph showing portions of three gland profiles with epithelial stratification, flattening of cells toward the surface, dense eosinophilic cytoplasm, and nuclear features also compatible with transitional metaplasia. Intraepithelial (and stromal) inflammatory cells and some epithelial reactive changes are present as well. Section from DLP of an LPB-Tag 12T7s mouse castrated at 22 wks and sacrificied at 29 wks. **E)** Mucinous metaplasia in prostate epithelium of GEM, characterized by large cytoplasmic vacuoles compressing nuclei to basal aspect in cells highly reminiscent of intestinal goblet cells (e.g., top right). High power photomicrograph of prostate from 24 month old Pb-Ras mouse (N. Schreiber-Agus, R.D.C., unpublished observations). **F)** Atrophy (spontaneous, not treatment related) in peripheral zone of **human** prostatectomy specimen. Low power showing dilated glandular profiles with flat lumens on left and very typical shrunken lobules on right. These appear hyperchromatic on scanning magnification because of the high nuclear to cytoplasmic ratio due to scant cytoplasm. Recognition of lobular architecture is a useful feature. Especially when associated with inflammation, atypia with mildly enlarged nucleoli can be present. An at least partial basal cell layer would be present on HMWCK immunostaining. **G)** Active prostatitis histologically (i.e., not necessarily associated with clinical symptomatology) in section of a **human** prostatectomy specimen. High power shows multiple gland profiles involved, with intraluminal and intraepithelial inflammatory cells, including neutrophils, as well as inflammation in surrounding stroma. Glands are partially atrophic, with dilated, angular profiles, and shrunken eosinophilic cytoplasm. Reactive atypia can be present, and mitotic figures can even occasionally be found. **H)** Nonspecific granulomatous prostatitis in human prostatectomy specimen. High power photomicrograph shows sheet like growth of histiocytes and admixed inflammatory cells, without well formed granulomas or giant cells (see text for details). **I)** Atrophy and inflammation, including "active prostatitis", in section of castrated GEM (LPB-Tag 12T7s castrated at 22 wks, sacrificed at 29 wks). Three dilated gland profiles with somewhat flattened epithelium and inflammatory cells within epithelium, stroma, and periprostatic connective tissue are present. Residual hypercellular stroma, not well demonstrated, is seen focally adjacent to dilated gland in bottom left. The extent of intraepithelial and stromal inflammation in this example is more pronounced than that typically seen in human specimens from patients treated with anti-androgens prior to radical prostatectomy for prostatic carcinoma.

Figure 4: Epithelial Hyperplasia in the Human and Mouse Prostate. A-C) Low, intermediate, and high magnification photomicrographs demonstrating histologic features of benign prostatic hyperplasia (BPH) in a section from a radical prostatectomy specimen. Similar changes can be found in specimens from simple prostatectomy and transurethral resections of the prostate (TURP) performed for symptomatic BPH. BPH consists of nodules of hyperplastic glandular and stromal elements that occur in the transition zone of the **human** prostate, **A)** Low power shows the circumscribed, nodular growth pattern. **B, C)** Glands may be increased in number and may have increased epithelial tufting (arrowheads), but are otherwise fairly normal in appearance. BPH is not associated with cytologic atypia (i.e., nuclear and nucleolar enlargement) that is seen in PIN in the peripheral zone. Stromal hypercellularity without atypia is commonly noted in foci of BPH. **D)** Basal cell hyperplasia at edge of BPH nodule in **human** prostate. High power photomicrograph showing some gland profile with a well defined basal cell layer (arrowheads), other gland profiles with stratified or multiple layers of small basal cells (arrows), and some composed of solid balls or nests of basal cells (asterisk). Typical stromal hypercellularity seen with basal cell hyperplasia in the TZ is appreciated at top and far bottom left. **E)** Clear cell cribriform hyperplasia in TZ of **human** prostatectomy specimen. This entity is occasionally observed as an incidental finding in association with BPH nodules, but can also be seen in the CZ. In contrast to cribriform carcinoma or cribriform HGPIN, there is no significant cytologic atypia in clear cell cribriform hyperplasa. Basal cells are often quite conspicuous in these foci, either as a well defined, circumferential layer(arrowheads) or as small focal tufts of basal cell hyperplasia. Mild stromal hypercellularity can be appreciated focally (asterisk). **E, F)** Epithelial hyperplasia in **mouse** prostate. Low and high power photomicrographs of a cribriform proliferation within a preexisting gland lumen is noted (asterisks), with essentially normal surrounding stroma (arrowhead). AP from 22 month Nkx 3.1 -/- mouse. In the focus shown, there is no appreciable cytologic atypia. Atypia, if present in hyperplasia, should be noted and described. Some of these mice show foci of epithelial atypia that progresses in extent and severity, compatible with mPIN. As epithelial proliferation with nuclear atypia are the morphologic hallmarks of PIN, criteria of focality and progression need to be addressed for the appropriate distinction of hyperplasia with atypia and PIN (see text for details).

Figure 5: Combined epithelial and stromal proliferations in GEM: PIN vs. hyperplasia vs. benign neoplasms. A) Combined epithelial and stromal proliferation in a GEM prostate. Low power photomicrograph of DLP of a LPB-Tag 12T5 mouse at 19 wks, shows marked lobular expansion by a fairly symmetric and uniform proliferation of atypical epithelial cells (arrowheads) with hypercellular stroma (arrows). In stromal hyperplasia, the stromal elements may be fairly normal in appearance but show increased cellularity or they may show cytologic atypia, which should be described. Occasionally, hyperplastic stromal elements are more condensed and consist of crowded spindle cells with scant cytoplasm more immediately adjacent to atypical epithelium. In the LPB-Tag 12T5 mouse and related fast growing LPB-Tag lines this epithelial lesion begins focally and quickly progresses in extent to an essentially diffuse lesion, and occasionally progresses to invasion. Thus it has been regarded as PIN with a morphology distinct from PIN occurring within pre-existing gland spaces (see text). In SV40 or large T antigen GEM models with such exuberant and diffuse atypical glandular and stromal hyperplasia, the distinction between true invasion vs. herniation of glandular and stromal proliferations into

periprostatic loose connective tissue or fat can sometimes be difficult (see text for details). **B)** Photomicrograph showing a somewhat similar symmetric, lobular expansion of glands in a 16 wk old TRAMP mouse prostate by atypical prostatic epithelium and a mildly hypercellular stroma (arrowheads). This is a somewhat uniform and symmetric epithelial lesion in which the small, peripheral acini appear to connect to the larger, more central lumen (asterisk), with similar cytologic atypia. The stromal hyperplasia shown here is not in response to invasion and can be seen diffusely surrounding all three illustrated gland profiles. The distinction between lesions like those shown in Figs. 5A and 5B as PIN vs. adenocarcinoma can be difficult. Histologic features that help to distinguish adenocarcinoma, such as architecturally distinct foci and desmoplasia, are described in the text. The consensus of the Pathology Committee was that lesions like those shown in Figs. 5A and 5B represent in situ lesions. Compare these in situ lesions to the well differentiated adenocarcinoma shown in Fig. 8E. **C)** Hypercellularity of stroma (arrowheads) admixed with proliferating atypical glands (arrows) in 24 wk old TRAMP mouse prostate. These markedly hypercellular stromal elements consist of spindle cells with scant cytoplasm (arrowheads). Foci with these characteristics are also common in AP and DLP of fast growing LPB-Tag lines (see text), and are different in appearance from the more smooth muscle appearing hypercellular stroma also noted. These foci are usually seen in immediate apposition to atypical epithelium. The reactive vs. neoplastic nature of this type of stromal proliferation or possible epithelial-mesenchymal transformation have not been thoroughly addressed. Cytologic atypia and mitotic activity can be noted. Possible prostatic stromal origin for poorly differentiated spindle cell lesions in metastatic foci should be considered in GEM models with such characteristics. Ancillary techniques desribed in the Protocols section can be useful for distinguishing metastatic carcinoma vs. sarcoma. **D)** Markedly atypical epithelial and admixed stromal proliferation in DLP of 25 wk LPB-Tag 12T7s **mouse.** The overall histologic appearance of the lesion shown here is very similar to the background glandular and stromal proliferations seen in these mice, and may constitute a simple physical herniation or protrusion of glands and stroma into duct lumens (asterisks). Whether these lesions thus represent a focal exaggeration of the atypical epithelial hyperplasia or mPIN and stromal hyperplasia vs. distinct neoplasms is not established. These foci are common with increasing age in the fast growing LPB-Tag lines and can show associated stromal edema, with an appearance reminiscent of phyllodes tumors in human breast, as have been described in TRAMP mice. **E)** Low power photomicrograph of multiple gland or duct lumens with intraluminal epithelial and stromal proliferations (asterisks) in prostate of a TRAMP **mouse.** Lesions with these characteristics have had the descriptor "phyllodes-like" added to them, because of their histologic resemblance to this human tumor, most often found in the breast. Lesions with these histologic features are very rarely encountered in the human prostate. In the mouse lesions, the surface of the intraluminal component is typically covered by epithelium, and the polypoid portion contains an admixture of small glands and stroma. The small gland profiles in the polypoid portion often appear to connect to the surface epithelium, and the stroma is variably hypercellular, hyalinized, or edematous. Histologically, such foci have many features compatible with the designation of papilloma. In SV40 or Tag based models, they are always seen in a background of more general atypical epithelial and stromal proliferation. A consensus was not reached on the nature of these lesions based solely on their histologic features. Whether they constitute hyperplasia, as a focal exaggeration of a more general process, or distinct clonal neoplasms arising against a hyperplastic background remains to be established. If encountered, either of these classifications

93

is appropriate, however, their histologic features should be described along with the appearance of the rest of the prostate. The term "phyllodes-like" can be added as a purely histologic descriptive adjective, but this term does not imply any biologic relationship of these lesions to phyllodes tumors found in human tissues. **F-H)** Low, intermediate, and high power photomicrographs of a discrete papillary lesion compatible with papillary hyperplasia or a papillary adenoma (papilloma) in a GEM prostate. This lesion protrudes into and partially fills the lumen (arrowheads) of the lateral prostate from a 73 wk old ARR$_2$Pb-FGF8b mouse. The lesion shows an expansile rather than destructive growth pattern. **(G)** A well vascularized stroma (arrows) is associated with the epithelial proliferation. Papillary structures (arrowheads) are present although the papillae are less evident in foci where the epithelium is more crowded **(H)** Focal cytologic atypia with nuclear enlargement and macronucleoli (arrowheads) are also evident in these regions. In addition to discreet papillary lesions like the one illustrated here, lesions consistent with mPIN are also seen in these mice.

Figure 6: PIN lesions in human prostate and SV-40 and Large T antigen based mouse models. A) Invasive acinar-forming Gleason pattern 3 (Gleason score 3 + 3 = 6) adenocarcinoma (arrowheads) in association with HGPIN (arrows) in **human** radical prostatectomy specimen. Compare the smaller glands of the invasive carcinoma to the larger (normal) sized HGPIN containing gland. The HGPIN gland demonstrates nuclear stratification, enlargement, and atypia, with hyperchromasia apparent at this lower magnification. Note the substantial amount of intervening stroma (asterisk) between the unequivocally invasive glands and the adjacent HGPIN gland. **B) Human** HGPIN, with tufting intraluminal proliferation of markedly atypical epithelial cells (arrowheads), with nuclear enlargement and prominently enlarged nucleoli (arrows). Macronucleoli are characteristic of human HGPIN. The cytologic atypia is similar to that typically appreciable in invasive adenocarcinoma. **C) Mouse** prostatic intraepithelial neoplasia (mPIN) showing focal involvement of multiple gland profiles (arrowheads) by stratified cells with nuclear enlargement and atypia, resulting in a hyperchromatic appearance evident at this intermediate magnification. Section of C3(1)-SV40 mouse prostate at 9 months. Foci of residual more normal appearing epithelium are clearly present (arrows). Progression in extent and the degree of cytologic atypia is compatible with mPIN. In this model, as in other reviewed SV40 and Tag based models, there is documented progression to invasive carcinoma, often in association with such mPIN lesions. mPIN with documented progression to invasive carcinoma is a specific subcategory designated in the Bar Harbor Classification. **D)** PIN in GEM prostate, with extensive involvement of most illustrated gland profiles (arrowheads). Tufting and focally cribriform atypical epithelial proliferations are noted, with general maintenance of normal duct/gland architecture. Nuclear hyperchromasia is appreciable even in this low power photomicrograph. Section of prostate from 8 wk old TRAMP mouse. mPIN in this model has documented progression to association with invasive tumor. **E)** High power photomicrograph demonstrating architectural and cytologic features of mPIN in 3 month old C3(1)-SV40 **mouse**. Nuclear stratification, enlargement/elongation, and hyperchromasia are pronounced (arrowheads). Irregular nuclear membranes, occasional prominent nucleoli, and mitoses are also appreciable in such lesions. **F)** mPIN in TRAMP **mouse** prostate, showing epithelial tufting and marked nuclear hyperchromasia, completely involving three shown gland profiles (asterisks), with a portion of one adjacent gland profile showing somewhat more normal cells (arrowhead). **G)** PIN in VP of 24 wk LPB-Tag 12T-10

mouse showing tufting and micropapillary proliferation of atypical epithelial cells (arrowheads), within an otherwise architecturally normal pre-existing gland, without associated hypercellular stroma. Nuclear enlargement/elongation and particularly hyperchromasia are evident (arrows). Progression to invasive carcinoma is documented in this mouse. **H)** PIN in CR2-SV40 mouse, showing focal stratification of atypical epithelial cells with enlarged, hyperchromatic nuclei (arrowheads). More normal appearing gland profiles are seen at top right and bottom left (asterisk). These lesions progress in extent, compatible with mPIN, and are associated with documented invasive carcinoma. Such early PIN foci show colocalization of Tag antigen and NE markers.

Figure 7: PIN in non-SV40/Tag mouse models. A,B) mPIN in AP of 11 month old PTEN +/- mouse. A) Intermediate magnification showing prominent cribriform epithelial proliferation within preexisting gland profiles (arrowheads), with more normal appearing prostate gland profiles at bottom (arrows) and portion of seminal vesicle at right (asterisk). B) Higher magnification showing 2 adjacent involved gland profiles (arrowheads), with tufting and cribriform growth and possibly mildly reactive surrounding stroma (asterisk). Epithelial nuclear atypia includes enlarged nuclei with vesicular chromatin and prominent nucleoli (arrows), similar to that typical in human HGPIN. The degree of atypia and progression in extent are compatible with mPIN. Spontaneous progression to invasive carcinoma is not a characteristic outcome in this model, with only rare possible invasion noted in older (> 1 yr) mice (R.D.C., unpublished observations). **C,D)** mPIN in DLP sections of PTEN +/- x p27 +/- mice. C) Intermediate magnification showing focal prominent cribriform proliferation (arrowheads) within a gland lumen in an 8 month old mouse. D) Higher magnification showing cytologic atypia in cribriform mPIN in 6 month old PTEN +/- x p27 +/- mouse, with enlarged nuclei and scattered prominent macronucleoli (arrows). Note the essentially normal surrounding thin fibromuscular stroma. Progression to frank invasion has not been observed in these mice (C. Abate-Shen, R.D.C., unpublished observations), although it was reported in up to 25 % of PTEN +/- x p27 -/- mice by other investigators (30). (See text for more details). **E)** Intermediate power photomicrograph of cribriform epithelial proliferation in multiple glands (arrowheads) in AP of 16 wk old MT-TGFα mouse. Atypia and progression in this mouse are compatible with mPIN. (S.Cutler, R.J.Coffey, R.L.R., S.B.S.; unpublished observations). **F)** High power photomicrograph showing mild degrees of focal epithelial stratification (arrowhead) and nuclear atypia, characterized by mild nuclear enlargement and occasional prominent nucleoli (arrows). VP section from 16 wk. old MT-DNIIR mouse. Atypia and progression are compatible with mPIN (Moses, H.A., Jr., Matusik, R.J., R.L.R., S.B.S.; unpublished observations). Characterization of models with potentially subtle phenotypes including relatively mild epithelial proliferation and atypia is supported by the inclusion of adequate age-matched controls and blinded histopathologic analysis. Additional possible supportive objective analyses (e.g., for documenting progression) include quantitative assessment of indices of proliferation and apoptosis. See text for details. **G)** mPIN, showing complex cribriform and microacinar epithelial proliferation, with nuclear atypia, extensively involving a gland lumen (arrowheads). A relatively uninvolved gland profile is shown at bottom right (arrows). High power photomicrograph of LP from 24 month old Pb-ras x mxil +/+ mouse (N. Schreiber-Agus, R.D.C., unpublished observations). **H)** mPIN, showing cribriform epithelial proliferation, with nuclear atypia, including enlarged nuclei and focally prominent nucleoli. Section of LP from 82 wk old ARR₂Pb-FGF8b mouse.

Figure 8: Microinvasive carcinoma and invasive adenocarcinoma in prostates of GEM.
A) Microinvasion occurring in association with PIN lesion in LP of 7 month old C3(1)-SV40 mouse. High power magnification showing extension of single cells and cords and small nests of cells (arrowheads) into thickened stroma underlying cribriform mPIN. **B)** Microinvasive carcinoma in association with PIN in LP of 40 wk old LPB-Tag 12T-10 mouse. Small nests of atypical cells with hyperchromatic nuclei, generally scant cytoplasm, and without evident glandular formation are invading into the stroma (arrowheads) surrounding a PIN containing gland. **C)** Progression to more extensive invasion in mouse Pca model. Section of prostate from CR2-SV40 mouse showing almost circumferential invasion into the thickened stroma (arrowheads) surrounding a residual mPIN-containing gland (between asterices). Invasion is in the form of individual cells and cords and nest of cells, with apparent focal rosetting (arrows). A PIN containing gland is also seeen adjacent to this focus (middle), with more normal appearing gland at bottom right corner. **D)** A microinvasive focus of well differentiated adenocarcinoma (demarcated by arrowheads). Section of prostate from 16 wk LPB-Tag 12T-7f x MT-DNIIR bigenic mouse. Such a lesion can stand out at low magnification as a more crowded small acinar focus compared to the more diffuse and symmetric lobular expansion by atypical epithelial proliferation (arrows) and hypercellular stroma . On higher maginification as shown, definitive alterations in nuclear and cytoplasmic features are evident, with larger more vesicular nuclei and more densely eosinophilic cytoplasm, compared to adjacent PIN. Similar cytologic alterations are well known with early invasive carcinomas (compared to associated in situ lesions) in a variety of carcinomas in the human, such as cervical and urothelial. This is in contrast to the fairly similar nuclear features of HGPIN and associated invasive acinar Gleason pattern 3 carcinoma in human Pca. **E)** Focus of well differentiated adenocarcinoma in mouse prostate. Section of 24 wk old TRAMP mouse. On the left, there is extension of a focally distinct group of smaller and well formed acini into surrounding stroma and connective tissue (arrowheads). Compared to widespread and essentially diffuse background of PIN containing glands or the diffuse symmetric lobular expansion with admixed large and connecting small gland profiles that is seen in some of the SV40 or large T antigen based models with androgen dependent promoters, the low power focality and architecturally distinct nature of the glands in question is a useful feature for distinction from possible complex in situ or atypical hyperplastic lesions. Although not characteristic of invasive adenocarcinoma in the human prostate, in optimal histologic sections, a desmoplastic response in the surrounding fibromuscular stroma or surrounding looser connective tissue can also facilitate recognition of such foci in the mouse prostate. The invasive focus in this example is uniformly and completely composed of discernible gland formations, indicating the designation of well differentiated, as explained in the text. **F)** Invasive adenocarcinoma in association with mPIN in LPB-Tag 12T-10 mouse prostate. Nests of tumor cells extending into the stroma show definitive gland formation (arrowheads), with clear lumens or light eosinophilic secretions, rather than features of NE rosetting. **G,H,I)** Invasive adenocarcinoma. AP from 38 wk old [C57Bl/6TRAMP/+ x FVB]F1 TRAMP mouse, provided by NIEHS investigators (R.H., unpublished observations). **G)** Intermediate power showing unequivocal invasive small acinar adenocarcinoma (arrowheads), extensively extending into stroma and periprosatic loose connective tissue, with two remaining PIN involved glands seen at top and bottom right. **H)** Higher magnification, showing discreet (arrowheads) and occasionally fused small glands, with nuclear enlargement and nucleoli. **I)** Intermediate power showing very pronounced extension of

96

malignant glands into surrounding periprostatic loose connective tissue (asterices), with possible desmoplastic response (arrowheads). Definitive well formed glands are present. Because of occasional admixed more solid nests and fused glands, the lesion could be appropriately classified as a moderately differentiated adenocarcinoma in the Bar Harbor Classification scheme. This was considered by the Pathology Panel to be the best histologic example of unequivocal invasive adenocarcinoma, with a uniform consensus designation as such. Such a focus was seen in only this particular mouse in material supplied for review.

Figure 9: Invasive NE carcinomas and carcinomas with morphologic features suggestive of NE differentiation in prostate and metastases in GEM models. A-C) Invasive NE carcinoma in CR2-SV40 mouse. A) Intermediate power showing invasive carcinoma (asterices) in association with PIN in multiple gland profiles (arrowheads). B-C) Low and high power photomicrographs of extensively invasive carcinoma. The invasive foci show a generally solid or sheet like proliferation, but with evident rosettes throughout (arrowheads in C). On high magnification, cells with typical nuclear features of NE carcinoma focally have a moderate amount of eosinophilic cytoplasm, particularly evident in areas of rosette formation (arrowheads in C). Note that focal glandular differentiation can be seen in human NE carcinomas. The tumors in these mice are mucin-negative. In addition to the morphology illustrated here, foci in which tumor cells have less cytoplasm and more oval or spindle hyperchromatic nuclei can be seen, similar to human small cell carcinoma,. The PIN, invasive, and metastatic lesions in this model show cytologic, immunophenotypic, and ultrastructural features indicative of NE differentiation. **D-I)** Invasive and metastatic NE carcinoma in the LPB-Tag 12T-10 model. D) Intermediate power showing extensive invasion by NE carcinoma, including extensive areas of "less differentiated" small cell carcinoma (asterices), in VP of a 40 wk old mouse. An entrapped PIN gland is seen (white arrowhead), as are two other PIN containing profiles at top and bottom left (black arrowheads). Some foci in the invasive tumor show "punched out" cribriform like areas with eosinophilia due to cell cytoplasm in areas of rosette formation. Areas in this field with more solid growth and extreme cellularity, with closely spaced oval or spindle cells show focal crush "artefact" or Azzopardi effect, which is also characteristic of human small cell carcinoma. E) Intermediate magnification, showing extensive involvement of periprostatic tissue by NE tumor (asterices), encroaching on adjacent PIN-gland and its surrounding stroma (arrowhead). Extensive rosette formation is evident. F) Strong focal chromogranin immunostaining (apical cytoplasmic granular, arrowheads) in the in situ component (PIN) of 12 month old LPB-Tag 12T-10 mouse, which also had extensive invasive NE carcinoma. G) Focal strong cytoplasmic granular chromogranin immunostaining (asterices) in liver metastasis. H) Metastatic NE carcinoma (asterices) in the liver of a 40 wk old 12T-10 mouse. Liver metastases were common with increasing age in this mouse, and often showed prominent rosetting. NE differentiation was demonstrated in such metastases by chromogranin immunostaining, as in G, and by electrom microscopy. I) Two pulmonary micrometastases (asterices) in 44 wk LPB-Tag 12T-10 mouse. Lung metastases are typically smaller than liver lesions, are often in alveolar septa or peribronchial arterial spaces, and are more typically composed of oval or spindle cells with scant cytoplasm and without prominent rosette formation. **J-L)** Invasive carcinoma with morphologic features suggestive of NE differentiation in TRAMP mouse. J,K) Intermediate and high power photomicrographs of prostate from 24 wk old TRAMP mouse showing extensive destructive invasion (asterices in J) between residual PIN glands (arrowheads in J). The tumor shows

relatively solid growth, but with evident cribriform or gland like spaces, recognizable at lower magnifications, and confirmed at high magnification (arrowheads in K). This lesion, previously reported as moderately differentiated adenocarcinoma, shows most nuclei contain granular chromatin. Admixed spindle or oval cells with more hyperchromatic and/or pyrknotic nuclei and abundant rosette or rosette-like spaces are noted. The consensus opinion of the Pathology Panel was that this morphology was highly suggestive of a carcinoma with NE differentiation, based on experience with human tumors as well as the morphologic similarity to well documented NE carcinomas in other GEM (e.g., compare to Figure 9b,c,d,e). Similar morphology has been noted in metastatic foci. L) Less differentiated focus in prostate from another 24 wk old TRAMP mouse. Tumor previously reported as poorly differentiated carcinoma was felt to show morphologic features of NE differentiation, quite similar to human small cell carcinoma. Tumor is composed of closely spaced oval and spindle cells with scant cytoplasm and hyperchromatic nuclei. Metastatic foci, including pulmonary metastases, can show similar morphology. Similar cytologic features have been noted in the invasive and metastatic tumors in other mouse models (i.e., CR2-SV40, LPB-Tag 12T-10) in which the tumor has been confirmed to show immunophenotypic and ultrastructural NE differentiation. The foci in TRAMP as shown in L and regarded as small cell carcinoma by the Pathology Panel have been subsequently shown to be synaptophysin immunopositive, whereas such staining was not noted in foci as shown in J and K (N. Greenberg, personal communication).

Figure 10: Mesenchymal neoplasms in human prostate and GEM: A,B) Benign stromal nodule in human prostate. **A)** Low power showing circumscribed nature of stromal nodule (asterisk), in this case an incidental finding in a radical prostatectomy for Pca. The characteristic suburothelial location is indicated, with the prostatic urethra shown at top left (arrowhead). Stromal nodules are typically located in the periurethral stroma, where there is little or no gland tissue (e.g., penetrated only by periurethral ducts in posterolateral aspect), interior to the more typical areas of BPH glandular and stromal hyperplasia, with which they are often associated. Proximity to the urethral can lead to obstructive symptoms with larger nodules. **B)** High power showing moderately increased cellularity, with oval to spindle cells similar to normal prostate stroma, often in a somewhat myxomatous or edematous stroma (pale blue) in contrast to more dense usual collagenous stroma. Small vessels are a common conspicuous component (asterisk), as are scattered lymphocytes (arrowheads). Cellular atypia, pleomorphism, and mitotic activity are not appreciated. **C,D)** Leiomyoma (benign smooth muscle tumor) in human prostate. The lesion was a circumscribed 1.3 cm mass protruding from the prostate base noted at the time of radical prostatectomy for Pca. Larger tumors can be symptomatic, but these lesions are uncommon in the prostate. The neoplasm has the same histologic features as similar tumors in other sites, such as the uterine myometrium or soft tissues. Compared to the stromal nodule in A and B, note the more defined fasicular growth, with interlacing bundles of cells typically intersecting at right angles, such that some are cut longitudinally and others in cross section (e.g., asterisk in D). This example is moderately cellular, but at high magnification (D), the cells are generally uniform, and show typical oval or "cigar-shaped" round ended nuclei. Such cells are positive on immunostaining for common smooth muscle markers (e.g., smooth muscle actin, desmin). Given the relative rarity of such neoplasms in the prostate, criteria to identify tumors capable of behaving in a malignant fashion are not as defined as in the uterus. However, infiltrative growth and increased cellularity, and especially necrosis, marked nuclear atypia and

pleomorphism, and any appreciable mitotic activity are compatible with leiomyosarcoma. E,F) Sarcoma consistent with leiomyosarcoma in GEM prostate. The tumor is from an LPB-Tag 12T7s mouse that was castrated at 24 wks. and sacrificed 24 wks. later. Atrophic PIN foci, some with intraluminal "phyllodes-like" projections, are noted at right (arrowheads). Even at low magnification (E), the marked hypercellularity of the spindle cell tumor (asteisk) is evident, as is extensive necrosis (**). At high magnification (F), the tumor is composed of interlacing fasicles of markedly atypical spindle cells. There is marked hypercellularity and the tumor cells show prominent nuclear atypia, including hyperchromasia and pleomorphism. Mitotic figures were numerous. The differential diagnosis includes a poorly differentiated spindle cell or sarcomatoid carcinoma (this mouse had a neuroendocrine carcinoma elsewhere in the prostate) or some other sarcoma, such as malignant fibrous histiocytoma. On immunostaining, this sarcoma would be negative for cytokeratin and strongly positive for smooth muscle markers, such as smooth muscle actin.

Figure 11: Neoplastic involvement of periurethral and bulbourethral glands in GEM. A,B) Atypical hyperplasia in periurethral glands in a 22 wk old C(3)1-SV40 mouse. At low power magnification (A), hyperchromasia in multiple foci of periurethral glands is evident (arrowheads), without apparent architectural distortion. Urethral lumen is to the top/top-right. A single prostate gland profile is seen at bottom, below the muscle between it and the periurethral glands. At higher magnification (B), multiple acinar and/or duct profiles show atypical cells (arrowheads), with nuclear enlargement, hyperchromasia, and chromatin clumping. Stromal invasion in not present. **C,D)** Extensive involvement of periurethral region and prostate by a poorly differentiated carcinoma (with possible NE differentiation) in a 38 wk old C(3)1-SV40 mouse. Low power (C) shows a large tumor focus involving periurethral region (urethral lumen, black asterisk, top), as well as extensive destructive involvement of prostate (white asterices, bottom left). Distinguishing the actual site of origin could be difficult. Note more normal appearing prostate gland lumens at right. The single small nodule of tumor in this region (arrow) would be most compatible with secondary involvement at this site (i.e., extension or spread from tumor of periurethral region or from other part of prostate) as no PIN is present in adjacent portions of prostate. PIN is commonly noted with invasive tumor originating in the prostate. D) High power magnification of the tumor in C, showing occasional gland or rosette formation (arrowhead) Most tumor cells show scant cytoplasm, with a high nuclear to cytoplasmic ratio. Many of the nuclei are hyperchromatic, with occasional nuclear molding, features typical of NE differentiation. The differential diagnosis includes poorly differentiated adenocarcinoma vs. NE carcinoma. Tumors with morphology typical of NE carcinomas (as illustrated for the prostate in Figure 9 and for other accessory glands below) should be designated as such. Immunohistochemistry or electron microscopy can be used to confirm the NE nature suggested by the characteristic histologic appearance. Adenocarcinomas in human, and potentially in mice, may show features of NE differentiation upon ultrastructural or immunohistochemical analysis. In lesions with definitve and predominant glandular differentiation, this can be designated as carcinoma, or adenocarcinoma, with NE differentiation, rather than as NE carcinoma. E) Involvement of bulbourethral gland by a NE carcinoma in a 44 wk LPB-Tag 12T-10 mouse. Focal tumor cell apoptosis is present in center (arrowheads). Urethral lumen is to top left (asterisk). F) Involvement of periurethral glands by NE carcinoma in a 17 wk old LPB-Tag 12T-7s mouse. Urethral lumen (asterisk) and urethral mucosa are to top left. Nuclear features and

rosetting (arrowhead) typical of NE differentiation identifiable by light microscopy alone are present. Note similar morphologic appearance of tumors in E and F to NE carcinomas arising in the prostate as shown in Figure 9. **G)** Extensive involvement of periurethral region (center) and proximal portions of prostate (far right and far left) by poorly differentiated neoplasm compatible with NE carcinoma (including poorly differentiated or small cell carcinoma) in 24 wk old TRAMP mouse. Tumor bulges into urethral lumen (asterices). Focal residual normal periurethral glands are noted at left and bottom left relative to urethral lumen (arrowheads). Whether such tumors in this region are ever found without morphologically identical large tumor apparently arising in the prostate has not been described in this model. The androgen regulation of the periurethral and bulbourethral glands mandates careful examination of these tissues in transgenic mouse models made with androgen-regulated promoters. **H)** Focal atypical hyperplasia apparently involving duct of periurethral gland (arrowheads)in a CR2-SV40 mouse. These tall atypical epithelial cells appear to conform to the normal duct lining. There is nuclear enlargement, hyperchromasia and chromating clumping, and ample eosinophilic cytoplasm. Residual periurethral gland acini are seen (arrows). As this promoter targets a neuroendocrine epithelial cell population in the prostate in an apparently androgen-insensitive manner, it is tempting to speculate whether a minor NE cell population in these other accessory glands is the target for this lesion. In contrast to at least the C3(1)-SV40 and occasional LPB-Tag tumors shown herein, however, these lesions have not been noted to progress to frank carcinoma..

Figure 12: Technique for histologic examination of the prostate with en bloc submission. A) Exposed intact prostate, bladder, and seminal vesicles (GU bloc) following linear ventral abdominal incision. The white curvilinear seminal vesicles are readily apparent. **B)** Schematic diagram of removed GU bloc (anterolateral view), following transection of the urethra (UR). VP, ventral prostate; LP, lateral prostate; DP, dorsal prostate; SV, seminal vesicles; CG, coagulating gland or anterior prostate; DD, ductus deferens; UB, urinary bladder. Horizontal black line indicates the level of transverse sectioning through the urethra to include both DLP and VP, at or near level of SV junction. **C)** Removed GU bloc from animal in A, corresponding to that illustrated schematically in B. The amputated segment of distal urethra is longitudinally oriented at bottom. **D)** Same bloc following transverse section through urethra as indicated in B, generating the lower and middle portions of tissue shown. An additional transverse section through seminal vesicles and AP has been made (top). The free portions of the seminal vesicles can be embedded on end for sectioning. The two portions following the transverse cut through the urethra should be embedded with their cut surfaces downward (sectioning into the cut surfaces). **E)** Microscopic section illustrating the resulting tissue section, allowing typically adequate visualization of DP, LP, and VP, as well as other tissues that may have pathology (e.g., ampullary glands, shown, and periurethral glands, not well visualized in section, but typically demonstrable in deeper sections). 1, urethra in cross section; 2, paired ductus deferens in cross section; 3, paired ampullary glands in cross section; 4, ventral prostate; 5, lateral prostate; 6, dorsal prostate.

Appendices:

Appendix One - Glossary, including definitions of modifiers and descriptive terms:

Cribriform: Adjective referring to a growth pattern in which there are sieve-like spaces, which can be created by epithelial formations resembling roman arches or which can appear as punched out spaces in a more solid growth formation. In human prostate, cribriform epithelial proliferations can be seen in benign (e.g., clear cell cribriform hyperplasia), premalignant (cribriform HGPIN), and invasive processes (e.g., invasive cribriform carcinoma or cribriform intraductal carcinoma). Even in human Pca, circumscribed cribriform lesions with atypia (e.g., in isolation on biopsy) cannot always reliably be distinquished as to cribriform invasive carcinoma or cribriform HGPIN. Although the presence of an even fragmented basal cell layer on HMWCK immunostaines would be indicative of cribriform HGPIN (i.e., a precursor lesion) or cribriform intraductal carcinoma (a likely "post-invasive" lesion or spread of invasive tumor within preexisting ducts), the absence of a basal cell layer does not definitively establish invasive cancer in a cribriform lesion, as HGPIN can extensively lose its basal cell layer.

Desmoplasia: The process of forming fibrous tissue, typically in which an abundantly collagenous stroma in formed in response to infiltrative malignant tumor cells. Particularly early on the stroma can have an edematous component, recognized by a light bluish tent on routine sections. The fibroblasts in the responsive tissue can have a very characteristic appearance, with elongated tapering cytoplasm and prominent nucleoli ("tissue culture fibroblasts"). A desmoplastic response can be seen in a variety of human malignancies in association with invasion through the basement membrane of a pre-existing epithelium (e.g., involved by carcinoma in situ) into underlying stroma, and as such can be useful in histologically diagnosing invasion. However, it is not a characteristic response in human Pca (e.g., in association with invasive carcinoma adjacent to HGPIN).

Diffuse: A general descriptive term implying a widespread process, which can be applied to a variety of pathologic process, in which the anatomic compartment being assessed should be specified. For practical purposes, distinguished from focal or multifocal if 50 % of such a compartment is involved. Examples include: diffuse inflammation of the prostate, in which more than 50 % of total area on the slides involved; diffuse epithelial hyperplasia, if more than 50 % of the gland profiles are involved.

Focal: A general descriptive term implying a process confined to a small percentage of whatever anatomic compartment is being assessed. For practical purposes, distinguished from diffuse if < 50 % of such a compartment is involved, such as in focal hyperplasia. One or a few microscopic sites of involvement by a process often described as rare or focal, respectively. More extensive numbers of sites of involvement, but still < 50 % of whatever anatomic compartment is being assessed, often described as multifocal.

Nodular: Adjective referring to a growth pattern in which there is a discrete, typically circumscribed proliferation, which is either palpable or at least conspicuously visible with the unaided eye or at low power microscopically. Size in cm or mm should be given.

Nuclear atypia: Collective term referring to a variety of nuclear cytologic abnormalities recognizable by light microscopy, and imply a pathologic process, either reactive or dysplastic/neoplatic. Abnormalites can be in size, shape, and chromatin content. *Hyperchromasia* refers to increased overall hematoxylin staining of the nucleus. *Chromatin clumping* or discrete *prominent nucleoli* and irregularities of nuclear contour, as opposed to round or oval nuclei with smooth nuclear contours.

Papillary: Adjective referring to a growth pattern in which a polypoid or more slender projection has a vascular stalk covered by epithelium. Stroma underneath the epithelium and surrounding the vascular network is variable. *Micropapillary* is an adjective sometimes applied in describing an architectural pattern of PIN, in which there is intraluminal protrusion of a particularly pronounced fairly narrow tuft of epithelium that may or may not have a discernible vascular stalk.

Phyllodes tumor:

Rosette:

102

Appendix Two – En bloc submission for histologic examination of the prostate and other male accessory glands:

    A.   Tissue Collection Method for en bloc submission (Figure 12)

          1.   Collect and fix the accessory sex glands (DLP, VP, seminal vesicles, AP or coagulating gland) and urinary bladder as a unit (*en bloc)* along with a 4 mm long segment of the urethra attached for orientation purposes. If possible, any adipose tissue surrounding the tissue *bloc* should be removed when collecting. For optimal fixation, the tissues should be arranged flat on a cardboard square (maintaining the normal anatomic relationships) to minimize twisting and curling during fixation in 10% neutral buffered formalin (NBF). For studies in which immunohistochemical staining and/or in situ hybridization are planned, tissues should be fixed in 10% NBF for 24 hours, and then transferred to 70% ethanol and embedded within 5 days.

        Tissue Trimming

          1.   With the ventral surface of the accessory sex gland unit facing up, identify the urinary bladder and remove it by transecting through the neck of the bladder. Trim the urinary bladder longitudinally and place in a cassette to be embedded separately.

          2.   With the dorsal surface of the accessory sex gland unit facing up, anchor the unit using the urethral stump and section transversely through the dorsolateral prostate juxtaposed to the distal ends of the seminal vesicles and place in a cassette.

          3.   Remove normal sized or mildly to moderately enlarged seminal vesicles and associated coagulating glands from the anterior segment of the accessory sex gland unit and place in a cassette to be embedded separately. If seminal vesicles are markedly enlarged and will not fit into a cassette, section them transversely to remove the lateral aspects. Next, section each seminal vesicle through the frontal plane to include the anterior prostate (coagulating glands) in order to fit inside the cassette. Retain the ventral half of the seminal vesicles for embedding.

    B.   Embedding

          1.   Using the urethral stump as an aid for orientation, embed the distal segment of the transected accessory sex gland unit cut surface down, ensuring that all aspects of the cut surface are in the same plane.

2.   If desired, the opposing anterior segment of the accessory sex gland unit may be embedded cut surface down, ensuring that all aspects of the cut surface are in the same plane. This segment may contain the ampullary gland in addition to the dorsolateral and ventral prostate glands.

3.   Embed the seminal vesicles including the retained half of the frontally sectioned seminal vesicles and coagulating glands, ventral surface down, ensuring that all aspects to tissues are in the same plane.

C.   Microtomy

1.   Gradually face the tissue block containing the distal segment of the accessory sex gland unit in order to obtain a 5-6 micron full-faced section of the dorsolateral and ventral prostate glands for H&E staining. After obtaining this section, additional serial sections (5 or more) should be taken at this time and mounted on charged ("Probe On Plus") slides and retained for later use.

2.   Repeat the previous step every 200 microns until prostate tissue is no longer present; staining the first section for H&E staining followed by additional serial sections

3.   Face the tissue block containing the seminal vesicles to obtain a 5-6 micron full-faced section of the entire seminal vesicles and coagulating glands for H&E staining.

Appendix Three - Immunohistochemical Protocols:

Immunostaining using mAB on mouse sections

I) Deparaffinization and hydration
Treat slides sequentially in the following order in 350 ml staining dishes
Xylene 10 minutes
Xylene 10 minutes
100% EtOH 2 minutes
100% EtOH 2 minutes
95% EtOH 2 minutes
70% EtOH 2 minutes
50% EtOH 2 minutes
diH2O 5 minutes
diH2O 5 minutes

II) Antigen retrieval (microwave boiling method)
Place four covered staining dishes in microwave with turntable. Boil citrate buffer to
heat solution before adding slides.
0.01M citrate buffer, pH 6.0 4 minutes at 80% power level X 4 times
Cool down to RT ~ 30 min
Rinse in diH2O 5 minutes
Rinse in diH2O 5 minutes

III) Blocking endogenous peroxidase activity
diH2O + 3% H2O2 5 minutes
diH2O 2 minutes
Rinse in PBS 2 minutes
Rinse in PBS 2 minutes

IV) Blocking
(Add 1 drop of MOM mouse Ig blocking reagent stock solution to 1.25 ml of PBS)
Incubate sections for 1 hr in working solution of MOM Ig blocking reagent in humid
chamber. Cover sections with Parafilm.
Rinse in PBS 2 minutes
Rinse in PBS 2 minutes

V) Primary Ab incubation
(Add 200 ul of protein concentrate stock solution to 2.5 ml of PBS. Primary and
Secondary Ab will be diluted in MOM Diluent to the appropriate concentration.)
MOM Diluent 5 min
Tip excess of diluent off sections
1??Ab (appropriate dilution) 30 min at RT in humid chamber
Rinse in PBS 2 minutes
Rinse in PBS 2 minutes

VI) Secondary Antibody dilution
(Add 1 ul of stock solution MOM biotinylated anti-mouse IgG reagent to 250 ul of diluent)
2??Ab 10 minutes/humid chamber at RT.
Rinse in PBS 2 minutes
Rinse in PBS 2 minutes

VII) Enhancement with Avidin Biotin Complex
(Add 1 drop of reagent A to 1.25 ml of PBS. Mix. Then add 1 drop of reagent B and mix. Prepare the mix 30 min prior to use.)
ABC 5 minutes/humid chamber RT.
Rinse in PBS 5 minutes
Rinse in PBS 5 minutes

VIII) Chromagen Substrate Visualization
NovaRed (2.5 ml of DiH2O+ 38.5ul of Solution1+ 2 drops of Solution2, 3 & H?O2)
Flood slides individually with NovaRed solution and look under the microscope to see changes on the area of target.
DiH2O (stop Rxn.) 5 minutes

IX) Counterstain and Dehydrate
* Hematoxylin time can be adjusted with the thickness of the sections
Hematoxylin (Harris, 1:4 diluted) 4-5 seconds
DiH2O 2 minutes
DiH2O 2 minutes
0.03% Ammonium Hydroxide 2 seconds
DiH2O 5 minutes
50% EtOH 2 minutes
70% EtOH 2 minutes
95% EtOH 2 minutes
100% EtOH 2 minutes
100% EtOH 2 minutes
Xylene 5 minutes
Xylene 5 minutes
Blot off excess xylene
Clean coverslips with compressed air.
Coverslip with Permount (used when working with organic solvents).
Air dry the slides.

Reagents:
Citrate buffer (Poly Scientific s2307)
Hydrogen peroxide (EM Science HX 0635-1)
Vector M.O.M. Immunodetection Kit/Peroxidase (Vector Labs PK-2200)
NovaRed Substrate Kit/Peroxidase (Vector Labs SK-4800)

Harris modified hematoxylin with acetic acid (mercury-free) (Fisher SH26-500D)
Permount (Fisher SP15-100)

Immunohistochemical staining using polyclonal antibodies

I) Preparation of slides
Select appropriate sections for the experiment
Write all the parameters of the experiment in the notebook and give each parameter chronological
numbers.
Label the slides with appropriate numbers.

For frozen sections
Acetone 10 minutes
Dry sections 5 minutes
Methanol + 3% H2O2 20 minutes
diH2O 5 minutes
diH2O 5 minutes

* Go to step Number III (do not perform any antigen retrieval on frozen tissue sections)

For paraffin-embedded sections
To prevent the sections from falling off they have to be on positively-charged or treated slides and
incubated overnight at 37?C with desiccant.
Deparaffinization and hydration
Treat slides sequentially in the following order in 350 ml staining dishes
Xylene 10 minutes
Xylene 10 minutes
100% EtOH 2 minutes
100% EtOH 2 minutes
Methanol + 3% H2O2 20 minutes
100% EtOH 2 minutes
95% EtOH 2 minutes
70% EtOH 2 minutes
50% EtOH 2 minutes
diH2O 5 minutes
diH2O 5 minutes

II) Antigen retrieval (microwave boiling method)
Place four covered staining dishes in microwave with turntable. Boil citrate buffer
to heat solution before adding slides.
Citrate buffer, pH 6.0 at 95?C 4 minutes at 80% power level X 4 times
Cool down ~ 1hr

Rinse in PBST 5 minutes
Rinse in PBST 5 minutes
(PBST = 1X PBS + 0.1% Tween 20)

III) Blocking
* **Do not** use serum in which primary was derived
During this step the slides have to be transferred to a **flat humid chamber.**
Place a piece of blotting paper smaller than the flat humid chamber and wet the paper. Place 2 wooden
sticks spanning the length of the dish to support the slides.
Each dish can hold 2 rows of 7-8 slides.
Wipe the bottom and edges of the slides. Circle the tissues with the PAP pen to prevent the solutions
from falling off.
Avoid touching the sections.
10% goat serum in 1X PBS 1 hr
PBST 5 minutes
PBST 5 minutes

IV) Primary Antibody dilution
* **All primary antibodies has to be diluted in PBS/1% BSA to avoid adsorption to the container in**
which it was diluted
1??Ab Dilution is in PBS 1% /BSA. All new antibody should be titrated and checked
at different concentrations.
1??Ab(appropriate dilution) overnight/humid chamber at 4?C
PBST #1 5 minutes
PBST #2 5 minutes
PBST #3 5 minutes

V) Secondary Antibody dilution
* **All secondary has to be diluted in PBS/1% BSA to avoid adsorption to the container in which it**
was diluted.
* **Make sure the 2?antibody properly targets the 1??Antibody.**
2??Ab: biotinylated anti-Rabbit (from Vectastain Elite kit)
2??Ab 1: 500 in PBS+ 1% BSA 60 minutes/humid chamber at RT
PBST #1 5 minutes
PBST #2 5 minutes
PBST #3 5 minutes

VI) Enhancement with Avidin Biotin Complex
* Only use with Biotin conjugated Secondary
Should be prepared 30 minutes prior to use.

PBS 5 ml 2 drops A, 2 drops B consecutively
ABC 45 minutes/humid chamber at RT
PBST #1 5 minutes
PBST #2 5 minutes
PBST #3 5 minutes

VII) Chromagen Substrate Visualization

NovaRed (2.5 ml of DiH2O+ 38.5 µl of Solution1+ 2 drops of Solution2, 3 & H?O2)
Flood slides individually with NovaRed solution and look under the microscope to
see changes on the area of target. (It usually takes around 2 to 3 min.)
DiH2O (stop Rxn.) 5 minutes

VIII) Counterstain and Dehydrate
* Hematoxylin time can be adjusted with the thickness of the sections

Hematoxylin (Harris, 1:4 diluted) 4-5 seconds
DiH2O 2 minutes
DiH2O 2 minutes
0.03% Ammonium Hydroxide 2 seconds
DiH2O 5 minutes
50% EtOH 2 minutes
70% EtOH 2 minutes
95% EtOH 2 minutes
100% EtOH 2 minutes
100% EtOH 2 minutes
Xylene 5 minutes
Xylene 5 minutes
Blot off excess xylene
Clean coverslips with compressed air.
Coverslip with Permount (used when working with organic solvents).
Air dry the slides.

Reagents:
Citrate buffer (Poly Scientific s2307)
Hydrogen peroxide (EM Science HX 0635-1)
Vectastain Elite ABC Kit (Vector Labs)
NovaRed Substrate Kit/Peroxidase (Vector Labs SK-4800)
Harris modified hematoxylin with acetic acid (mercury-free) (Fisher SH26-500D)
Permount (Fisher SP15-100)

Appendix Four – In situ hybridization:

Whole-mount and section *in situ* hybridization with digoxygenin-labeled riboprobes
Solutions for in situ *hybridization*

Note: Avoid the use of DEPC-treated solutions, since we have observed that trace amounts of DEPC tend to
reduce the yield during probe synthesis.

10x PBS: 1.37 M NaCl, 27 mM KCl, 43 mM Na2HPO4•7H2O, 14 mM KH2PO4, pH 7.4.

4% paraformaldehyde solution/PBS: Dissolve paraformaldehyde powder (Polysciences) in 1x PBS, pH 7.4, and heat
to 60°C with gentle stirring in a fume hood; do not let temperature exceed 70°C. To dissolve the powder quickly,
add a few drops of 10N NaOH, stir until the solution is completely clear, and adjust pH to 7.4. Filter through
Whatman #1 filter paper to remove undissolved particles, and store on ice (remains fresh for one day). For
convenience, make 20% paraformaldehyde/PBS stock solutions that are frozen at –20°C, and dilute with 1x PBS
for use. Note that paraformaldehyde is highly toxic, and caution should be used to avoid vapor inhalation.

1x PBT: 1x PBS, 0.1% Tween-20 (Sigma).

20x SSC, pH 4.5: 3M NaCl, 0.3M Na3citrate•2H2O. Adjust pH using citric acid.

Pre-hybridization solution: 50% formamide (molecular biology grade; Roche Molecular), 5x SSC, pH 4.5, 50 µg/ml
yeast tRNA (Roche Molecular), 1% SDS, 50 µg/ml heparin (Sigma H-3149). Store at –20°C.

Hybridization solution: Pre-hybridization solution containing 1 µg/ml probe. Since probe concentration is difficult
to determine accurately, we generally dilute the riboprobe at a 1:400 ratio in pre-hybridization solution (*i.e.*, 15 µl
riboprobe in 6 ml prehybridization solution for each well of a 6-well Netwell dish).

Solution I: 50% formamide, 4x SSC, pH 4.5, 1% SDS.

Solution III: 50% formamide, 2x SSC, pH 4.5.

Embryo powder blocking reagent: Dissect mouse embryos at 12.5 – 15.5 dpc (two litters are sufficient), and
Polytron homogenize in a minimum volume of ice-cold 1x PBS. Add 4x volume of ice-cold acetone, vortex and
leave on ice for 30 min. Spin at 10,000g for 10 min at 4°C. Discard the floating material, and rinse the pellet with
2
ice-cold acetone. Allow the pellet to air dry completely on filter paper, and then grind to a fine powder using
mortar and pestle. Store at 4°C.

Pre-absorbed anti-digoxigenin antibody: To prepare 2 ml total volume (sufficient for one Netwell insert for wholemount

in situ hybridization, or 5–6 slides for section *in situ*), heat 0.5 ml TBST with 3 mg embryo powder at 70°C

for 30 min. Vortex, cool on ice, and add 5 µl heat-inactivated sheep serum (Life Technologies) and 1 µl alkalinephosphatase-

conjugated anti-digoxigenin antibody, F(ab)2 fragments (Roche Molecular #1093274). Shake for 1.

hr at 4°C, then pellet by a brief spin. Collect the supernatant and dilute with 1.5 ml 1% sheep serum in TBST.

10x TBS: 1.37 M NaCl, 27 mM KCl, 250 mM Tris-HCl, pH 7.5.

1x TBST: 1x TBS, 0.1% Tween-20, 2 mM levimasole (Sigma).

NTMT: 100 mM NaCl, 100 mM Tris-HCl, pH 9.5, 50 mM MgCl2, 0.1% Tween-20, 2 mM levimasole.

NBT (nitro blue tetrazolium): 75 mg/ml stock solution in 70% DMF, store at –20°C.

BCIP (5-bromo-4-chloro-3-indolyl phosphate): 50 mg/ml stock solution in water, store at –20°C.

Detection solution: Heat 20 ml NTMT containing 10% polyvinyl alcohol (MW 31,000-50,000) (Aldrich 36,313-8) to

70°C with stirring until the polyvinyl alcohol is completely dissolved; the polyvinyl alcohol significantly increases

detection sensitivity. Cool to room temperature by immersion in cold tap water (do not use ice), then add 67.5 µl

NBT stock and 52.5 µl BCIP stock.

Preparation of embryos for whole-mount or section in situ *hybridization*

Dissect mouse embryos from 5.5 to 9.5 dpc in 1x PBS, pH 7.4, and transfer embryos into freshly prepared

4% paraformaldehyde/PBS in 6-well or 12-well dishes containing 74 µm mesh Netwell inserts (Costar #3477 or

3479). Small embryos can be transferred using glass microcapillaries by mouth pipetting with an aspirator tube

assembly. After transfer, examine the wells to ensure that the embryos are not floating on the surface of the

fixative, where they will be destroyed by surface tension; if so, quickly pipet additional fixative to cause the

embryos to sink. Fix 3 to 18 h with gentle shaking at 4°C. Embryos are then dehydrated in the Netwell inserts

through a MeOH series: 25% MeOH/75% PBT, 50% MeOH/50% PBT, 75% MeOH/25% PBT, and then twice in

3

100% MeOH, for 5 min each (see notes below on handling embryos in Netwell inserts). The embryos can be

stored at –20°C in Netwell culture dishes sealed with Parafilm for up to six months. As an alternative to

paraformaldehyde fixation, we have also had success with alchohol-based fixatives such as Histochoice

(Amresco, Inc.) or S.T.F. (Streck Laboratories). Similar procedures can be utilized for small dissected tissues from

later-stage embryos or neonatal mice.

For cryoembedding, transfer the fixed embryos into 30% RNase-free sucrose (Roche Molecular) in 1x

PBS, pH 7.4, and incubate with gentle shaking until the embryos sink to the bottom of the tube; this may take up

to two days. Transfer the embryos to a mixture of OCT (Tissue-Tek) and 30% sucrose/PBS in a 1:1 ratio and shake

gently at room temperature for 2 h. Embryos can be stored at 4°C in 30% sucrose or the OCT/30% sucrose

mixture for up to one week. Embed embryos in OCT under a dissecting microscope to ensure the desired

orientation of specimens, and then snap freeze by immersion in a solution of 2-methylbutane cooled on dry ice.

Store blocks wrapped in aluminum foil at –80°C.

Template preparation and riboprobe synthesis

To create a template for riboprobe synthesis, linearize plasmids containing a suitable T3, T7, or SP6

promoter using a restriction enzyme that creates a 5' overhang or blunt end (transcript initiation can occur on

the opposite strand from a 3' overhang, which should therefore be avoided). After enzyme digestion, extract

with phenol/chloroform/isoamyl alcohol (25:24:1), and precipitate with 0.1 volume 3M NaOAc, 2.5 volumes

EtOH. Resuspend template in 20 µl TE (pH 7.5) at a final concentration of 0.5 µg/ul. Set up riboprobe synthesis as

follow: To a final volume of 20 µl, add 2 µl template (0.5 µg/µl), 4 µl 5x transcription buffer (1 M Tris-HCl, pH 7.5, 1

M MgCl2, 100 mM spermidine, 5 M NaCl), 1 µl 0.2 mM DTT, 1 µl 10 mM CTP, 1 µl 10 mM ATP, 1 µl 10 mM GTP, 1.3

µl 10 mM UTP, 0.7 µl 10 mM digoxigenin-11-UTP (Roche Molecular #1209256), 1.5 µl RNase inhibitor (40 U/µl;

Roche Molecular), and 40 units T7, T3, or SP6 RNA polymerase. Incubate at 37°C for 2 h, then check probe

synthesis by running a 2 µl sample on a 1% agarose gel. While the gel is running, DNase treat the samples by

addition of 1 µl RNase inhibitor, 2 µl RNase-free DNase I (10 U/µl; Roche Molecular), vortex and spin briefly, and

incubate at 37°C for 15 min. Precipitate RNA by addition of 2 µl 0.5M EDTA (pH 8.0), 2.5 µl 4M LiCl2, 75 µl 100%

EtOH on dry ice 15 min, or –20°C overnight. Spin at 4°C 5 min, wash pellet twice with 80% EtOH, and air dry

4

briefly. Resuspend RNA in 50 µl H2O, and store at –20°C for up to 6 months. If pellet is difficult to resuspend,

incubate at 37°C for 10 min, then vortex; repeat if necessary.

The yield of synthesized probe can be estimated on ethidium-stained agarose gels by comparison of
the RNA band(s) (sometimes two bands may be visible) with the DNA template band — the RNA band(s) should
greatly exceed the DNA band in intensity (at least ten-fold). Generally, the quality of the probe synthesis is a
crucial determinant of success for an *in situ* hybridization experiment. If the probe concentration is too low, the
signal will be undetectable; however, if the probe concentration is too high, excessive background staining will
result.

Whole mount in situ *hybridization*

Handling of embryos in Netwell inserts. Mouse embryos prior to 9.5 dpc become nearly invisible in the high
concentrations of formamide used during the hybridization and washing steps. Therefore, if early mouse
embryos are used, all steps of this protocol are performed using 6- or 12-well 74 μm mesh Netwell inserts (Costar
#3477 or #3479). The Netwell inserts can be placed in carriers (Costar #3521) immersed in a reagent tray (Costar
#3517) that can contain 100 ml of solution. To transfer Netwell inserts from one solution to another, it is essential
to remove the Netwell slowly from the first solution and then immerse it quickly in the second. A steady motion
is required to prevent mouse embryos from flattening into a "pancake" due to fluid pressure. After transfer,
monitor the Netwells under the dissecting microscope to ensure that embryos have not stuck to the sides of the
well and are not floating on the surface; if so, these embryos can be dislodged by gentle pipetting. During
hybridization and washing steps, incubate Netwell inserts on the surface of a water bath. Use a larger tray to
hold the reagent tray and make a pinhole on its side to prevent inversion inside the water bath.

Day 1: Pre-treatments and hybridization. Rehydrate embryos through 75% MeOH/25% PBT, 50% MeOH/50% PBT,
25% MeOH/75% PBT, PBT twice, 5 min each. Bleach embryos with 6% H_2O_2 (diluted in PBT from fresh 30%
concentrated stock) for 1 h at room temperature with gentle shaking, then wash 3 times with PBT for 5 min each.
Permeabilize embryos with proteinase K (Roche Molecular #1373196) diluted in PBT at room temperature, for
the appropriate length of time depending on their stage (Table 1); note that proteinase K treatments for
dissected tissues can be extrapolated from this table. Stop proteinase K treatment with freshly prepared 2 mg/ml

5

glycine in PBT, 10 min at room temperature, then wash twice with PBT, 5 min each. Postfix embryos with 4%

paraformaldehyde/0.2% glutaraldehyde (Polysciences #00216A)/PBT, 20 min at room temperature, followed by

two PBT washes, 5 min each. Transfer Netwell inserts into prehybridization solution at 70°C for at least 1 h, then

replace with hybridization solution containing 1 μg/ml probe. Seal the dish with Parafilm, and incubate

overnight on the surface of a 70°C water bath.

Day 2: Washing and antibody addition. Wash embryos 3 times with solution I at 70°C for 30 min each. Wash with 3

times solution III at 65°C for 30 min each. Wash 3 times with TBST at room temperature, 5 min each. Block in 10%

sheep serum (heat inactivated at 56°C for 1 h) in TBST for 90 min at room temperature with shaking. Meanwhile,

prepare the pre-absorbed anti-digoxigenin antibody. After blocking, transfer embryos into the antibody mixture,

and gently shake overnight at 4°C.

Day 3: Washing. Wash with TBST at room temperature, 3 times for 5 min each. Wash with TBST at room

temperature, 5 times for 1 hour or more each time. Leave shaking overnight at 4°C.

Day 4: Detection. Wash in NTMT 3 times for 10 min each at room temperature. Add detection solution and keep

in the dark for 1 to 12 h, monitoring the progress of the staining reaction at hourly intervals using a dissecting

microscope. To stop the staining reaction, wash twice with PBT, pH 5.5, then post-fix for 1 h with freshly made

4% paraformaldehyde/0.1% glutaraldehyde in PBS, followed by washing 3 times with PBS. To clear embryos for

visualization of faint signals and for photography, transfer embryos out of the Netwell inserts into 60 mm petri

dishes or glass watch dishes containing 50% glycerol/PBS, 0.1% NaN3 (the sodium azide is added to prevent

bacterial growth) for 30 min, followed by 80% glycerol/PBS, 0.1% NaN3. Examine the dishes to ensure that the

embryos do not remain floating on the surface of the glycerol; store embryos at 4°C. To section embryos after

whole-mount staining, wash embryos through three changes of PBS, then transfer into 30% sucrose for

cryoembedding as described above.

Section **in situ** *hybridization*

Preparation of cryosections: To obtain acceptable signal intensity using non-radioactive probes to moderately abundant

114

transcripts, it is necessary to perform *in situ* hybridization to cryosections; paraffin sections yield poor

6

signals. Collect 12 μm thick cryosections on Superfrost Plus slides (Fisher), which are used instead of gelatinsubbed

slides for convenience. If multiple probes are to be used in the same experiment, place sequential sections in approximately the same position on each slide in a series, so that adjacent sections can be compared.

Place slides in a tightly-sealed slide box with dessicant, then dry the sections at room temperature overnight; the

box can then be stored at −80°C for up to several months. Before opening the slide box to start the *in situ*

protocol, warm the slide box to room temperature to ensure that the sections remain completely dry.

Throughout this protocol, slides are kept in metal holders and washed in histological staining dishes.

Day 1: Pre-treatments and hybridization. Fix cryosections in fresh 4% paraformaldehyde/PBS at room temperature

for 15 min, then wash twice with 1x PBT for 5 min each. Bleach sections in 6% H2O2 (diluted in PBT from 30%

stock) for 5 min, then wash 3 times with PBT, 5 min each. Permeabilize with 1 μg/ml proteinase K in PBT for 15

minutes at room temperature, with gentle shaking. Stop digestion in freshly prepared 2 mg/ml glycine in PBT for

10 min, then wash twice with PBT, 5 min each. Post-fix with 4% paraformaldehyde/0.2% glutaraldehyde/PBT for

15 min at room temperature, then wash 3 times with PBT. Prehybridize at 65°C for at least 1 h. Transfer slides into

plastic slide mailers that hold 5 slides each (Evergreen Scientific 240-5400-X8k), using an individual slide mailer

for each probe; each slide mailer can hold 15–20 ml hybridization solution with 1 μg/ml probe. Seal the slide

mailers with Parafilm, and incubate overnight at 65°C (or 70°C for increased stringency). After hybridization,

probes can be stored in the slide mailers at −20°C and re-used up to six times.

Day 2: Washing and antibody addition. Wash sections 3 times with solution I at 70°C, 15 min each. Wash 3 times

with solution III at 65°C, 15 min each. Wash 3 times with TBST at room temperature, 10 min each. Block in 5%

heat-inactivated sheep serum/TBST for at least 1 h with gentle shaking. In the meantime, prepare the preabsorbed

anti-digoxigenin antibody. For each slide, drain the 5% serum/TBST solution, add 350–400 μl preabsorbed

anti-digoxigenin antibody on each section, and cover the sections with Parafilm. Incubate slides

overnight at 4°C in a flat humidified chamber that is sealed with wet paper towels and Saran wrap to maintain a
humid environment.

Day 3: Washing and detection. Dip slides into TBST to allow Parafilm to float away, then wash 4 times with TBST
for 15 min each, followed by 3 washes in NTMT for 10 min each. Add detection solution, and let stain in the dark
7
for 2 hr up to 3 days, monitoring staining at periodic intervals using a dissecting microscope. If prolonged
staining is necessary, change the detection solution every 24 hours to minimize precipitation. To stop the
staining reaction, wash twice with PBT, pH 5.5, post-fix 15 min with 4% paraformaldehyde/0.1% glutaraldehyde
in PBS, then wash 3 times with PBS. At this point, if the signal is strong, sections can be lightly counterstained
using Nuclear Fast Red (Vector Laboratories). To mount the slides, dehydrate through 50%, 75%, 95%, 100%,
100% EtOH series, 2 min each, followed by 2 washes in Hemo-De (Fisher), 5 min each. Cover slip the slides using
Permount solution (Fisher) and let air-dry. Sections can be visualized and photographed using a histology-grade
microscope equipped with Nomarski optics.
8

Proteinase K digestion conditions for early mouse embryos
Stage Proteinase K concentration Digestion time
early-late streak 1 μg/ml 2 min
neural plate-early head fold 1 μg/ml 3 min
late head fold 1 μg/ml 4 min
0-10 somites 1 μg/ml 6 min
8.5 dpc 1 μg/ml 8 min
9.5 dpc 5 μg/ml 4 min
10.5 dpc 5 μg/ml 10 min
11.5 dpc 10 μg/ml 10 min
12.5 dpc 10 μg/ml 15 min
13.5 dpc 50 μg/ml 10 min

Appendix Five - Apotosis Assays:

TUNEL on fixed, paraffin-embedded mouse sections (not sure if we need this- I have only used Intergen's Apoptag protocol-this protocol appears unwieldy and scary!)

Materials and Reagents
- **Tris** (1M pH7.2)
- **Na Cacodylate** (1.4M)
- **TBS** (0.05M pH 7.5): make 10X stock (180g NaCl + 120g Tris, fill to 2L with DH2O, then add HCl to pH 7.5) then dilute 1:10 in DH2O to make 1X TBS
- **TBS-T** (TBS 0.05M pH7.5, containing 0.01% Tween 20)
- **Tris-HCl** 0.1M pH 9.2 (1:10 from a stock solution 1M)
- **Deoxyribonuclease I** (DNAse type I, Roche #104 159) make 10mg/ml stock in : 20mM Tris HCl
  pH7.5, 1mMMgCl2 ; stock should be 50% glycerol. Store at –20.
- **H_2O_2 (30%)**
- **$CoCl_2$** (100mM)
- **Xylene** (Warning: toxic) or Hemo-De (Fisher)
- **Ethanol**, absolute.
- **Aminoethylcarbazole (AEC)** (20 mg tablets, Sigma A-6926)
- **N,N-dimethyl formamide** (Fisher D119-500)
- **Glycerol-gelatin mounting medium**
- **Adhesive-coated glass slides** (e.g. Fisher Superfrost Plus cat 12-550-15)
- **WVR/Baxter slide staining holder S7636 or radiotransparent slide holder**
- **DTT** 0.1M
- **Proteinase K** (BM/Roche # 161519)
- **TdT/Terminal Transferase** (BM/Roche #220582)
- **Biotin-16-dUTP** (BM/Roche #1093070)
- **NaCl** (5M)
- **Na Citrate** (1M)
- **Avidin/HRP** (DAKO #P0364) dilute 1:300
- **Acetate Buffer** (pH 5.5): 5.25 ml of 1M acetic acid soln, fill to ~ 400ml with DH2O, then add Na acetate as necessary to obtain a pH of 5.5 (approx 40 ml) and bring to 500 ml with DH2O

Protocol

1. **Deparaffinize the 4μm sections**
   5 min - clean xylene
   5 min - clean xylene
   1 min - absolute ethanol
   1 min - absolute ethanol
   2 min – 95% methanol
   1 min - tap water

1 min - distilled water
2. **Make pre-DNase Buffer:**

Distilled Water	33.2 ml	(To make enough for one set of slides:
1M Tris pH 7.2	1,200 ul	199.2 ml dH2O
1.4 M Na Cacodylate	4.0 ml	7.2 ml 1M Tris
	38.4 ml total	24.0 ml 1.4M Na Cacodylate
		230.4 ml total)

Add 38.4 ul (or 230.4ml) of 0.1M DTT to the Buffer (i.e., 1 ul of DTT for each ml of Buffer)

Then set aside 1 ml of this to be used for the control DNAse slide *

For non-DNAse slides: Let all slides except the DNAse slide soak in the Buffer at RT for 20 min.

* For the DNAse slide: Add 1ul of the stock DNAse I (10mg/ml) to the 1ml of buffer that was set aside (final conc is 20U/ml); wipe off the liquid around the section and apply ~ 50 ul of this DNAse Buffer to the slide, then leave in moist chamber at RT for 20 min. **Make sure that DNase treatment is carried out away from the rest of the samples**

After 20 min, wash the slides in (wash DNAse slide separately):
TBS - 1 min
TBS - 1 min
TBS-T - 1 min
TBS-T - 1 min
4. **Proteinase K treatment**
Add 6 ul of Proteinase K stock (10 mg/ml) to 3ml DH2O (final conc. is 20ug/ml)
Wipe off the liquid around the section on each slide and apply 100 ul per slide
Leave in moist chamber for 20 min at RT
Then wash:
TBS - 1min
TBS - 1min
TBS - 1min
TBS - 1min

5. **Block endogenous peroxidase**
Soak slides in :
3% H_2O_2 in methanol (i.e., 180 ml methanol + 20 ml 30% H_2O_2) - 5 min
TBS - 1 min
TBS - 1 min
TBS-T - 1 min
TBS-T - 1 min
6. **Make TdT/dUTP Buffer**

Make more pre-DNAse Buffer (step 2 above; do NOT add the DTT or DNAse) and add to it
384 ul (or 2304 ul) of 100 mM $CoCl_2$ (i.e., 10 ul per 1 ml of buffer)

Next take out 100 ul of the above buffer *per slide*, and add to it
1ul of TdT + 1ul of Bio-16-dUTP *per slide*

Immerse slides in the remaining $CoCl_2$ Buffer for 2 min (to wash off the TBS-T).
Then wipe off the liquid around each section and apply ~100ul of the TdT/dUTP Buffer to each slide (negative control slide gets $CoCl_2$ Buffer instead).
Leave in moist chamber for 60 min at RT.

7. Make TB Buffer

Distilled Water	182 ml
5M NaCl	12 ml
1M Na Citrate	6 ml

Block TdT reaction in TB Buffer for 5 min. Then wash in :
TBS - 1 min
TBS - 1min
TBS-T - 1 min
TBS-T - 1 min

8. Signal amplification
Make Master Mix: allot 100 ul per slide of TBS-T, then add HRP-conjugated Avidin at 1:300 dilution. Wipe off the liquid around each section and apply ~ 100ul of Master Mix per slide. Leave in moist chamber for 20 min at RT.
Then wash:
TBS-T - 5 min
TBS-T - 5 min
TBS-T - 1 min

9. Color development
Resuspend 1 AEC tablet in 2.5 mL of N,N-dimethylformamide
Then add 25ul of 30% H_2O_2 to 50 ml of acetate buffer (keep away from direct sunlight).
Mix the two solutions together and filter with 45micron filter (optional). Be careful to avoid excessive background staining and reach full development if planning to do double staining.
Then wash :
Tap water - 5 min
Tap water - 1 min
Tap water - 1 min
Tap water - 1 min

10. Counterstaining
Hematoxylin - time varies depending on how fresh the hematoxylin is. Fresh takes only ~20 sec.
Then wash:

Tap water - 1 min
Tap water - 1 min
Tap water - 1 min

11.   **Mounting**
Wipe off liquid around section on each slide and apply water soluble mounting medium
(pre-heat in microwave ~ 10 sec) then put coverslip on. Push out any bubbles with
tweezers.

(MAKE SURE ALL CONTAINERS ARE DNASE FREE!!!!)

Appendix Six – Web sites for additional information:

RENI trimming guide for prostate and seminal vesicles:
http://www. ita.fhg.de/reni/trimming/TR_020.HTM

UC Davis resource site:
http://ccm.ucdavis.edu/tvmouse/prostate/PROSTATE1.htm

Prostate Molecular profiling at NCI:
http://cgap-mf.nih.gov/ProstateExample/

(While this site is primarily for human prostate cancer, it has detailed information on tissue preparation, slide preparation, microdissection, processing of tissue for molecular analysis, DNA, RNA and Proteomic analysis as well as protocols in development)
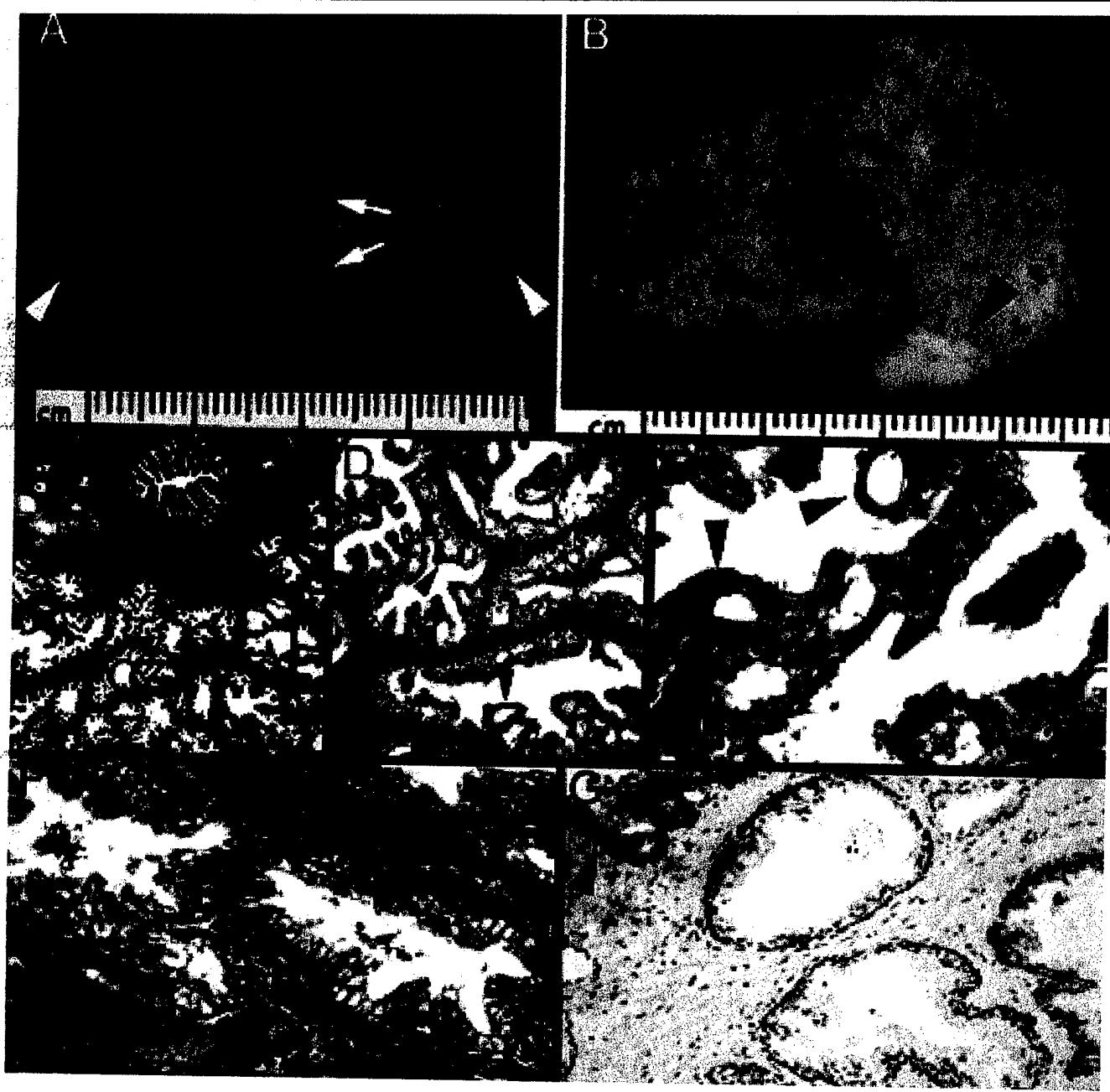
Figure 1A
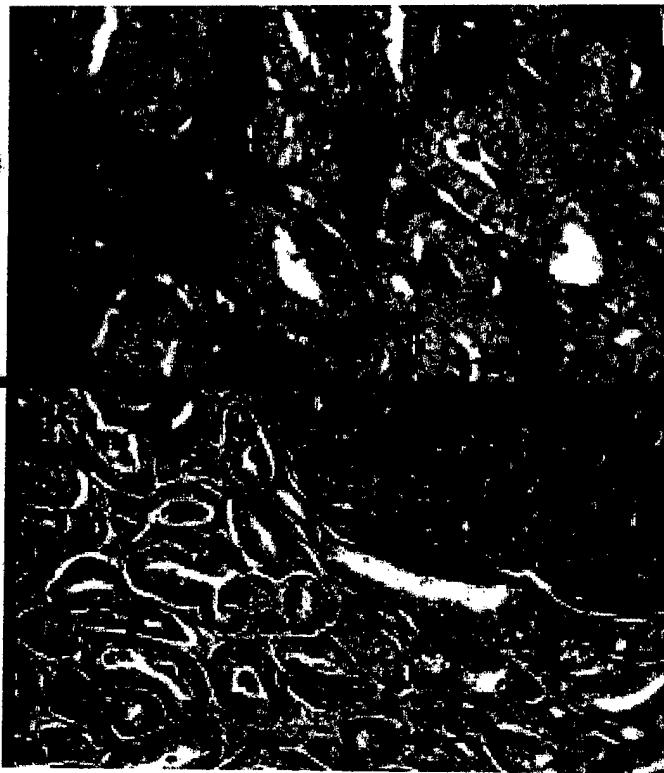
Figure 1B
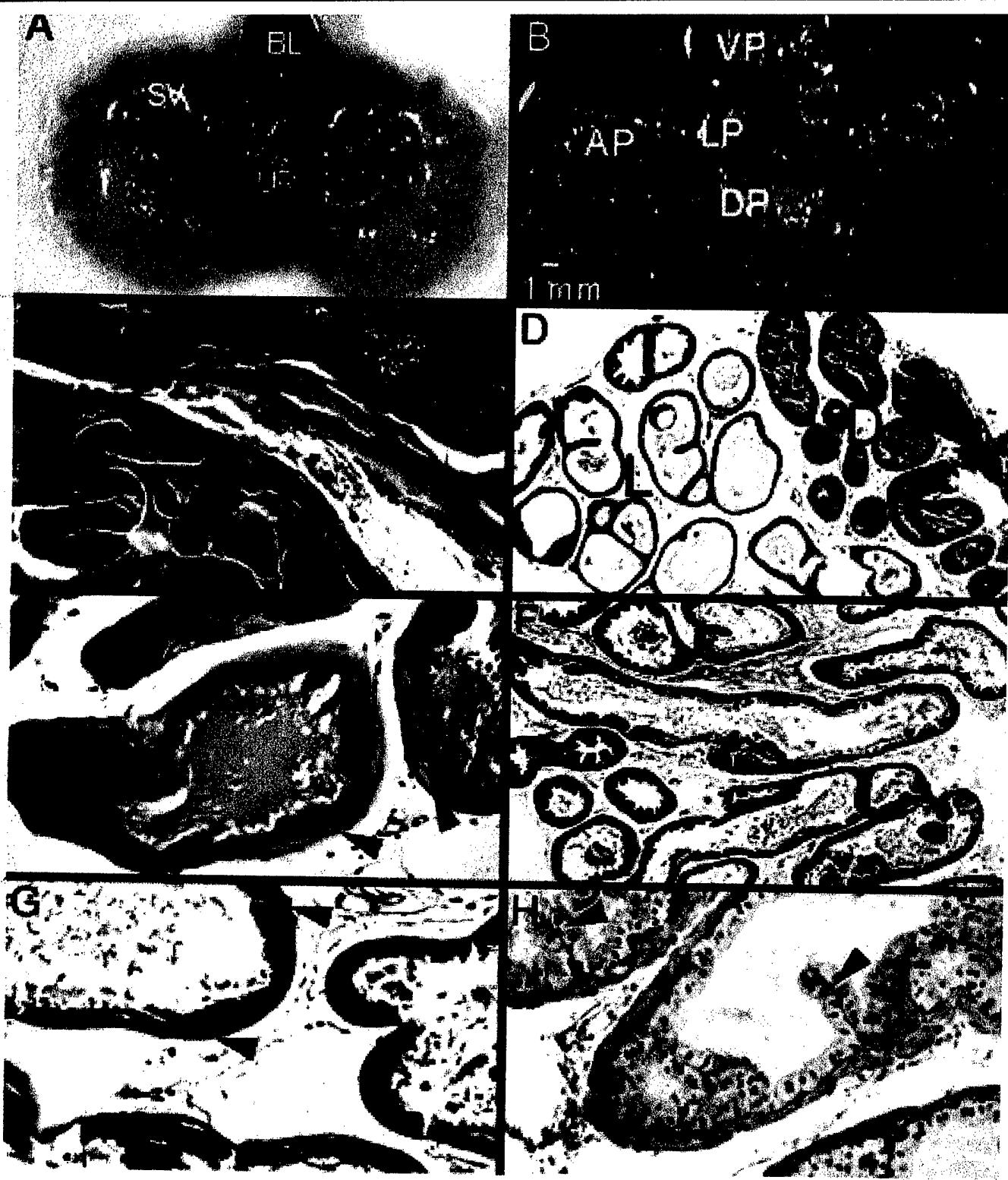
Figure 2
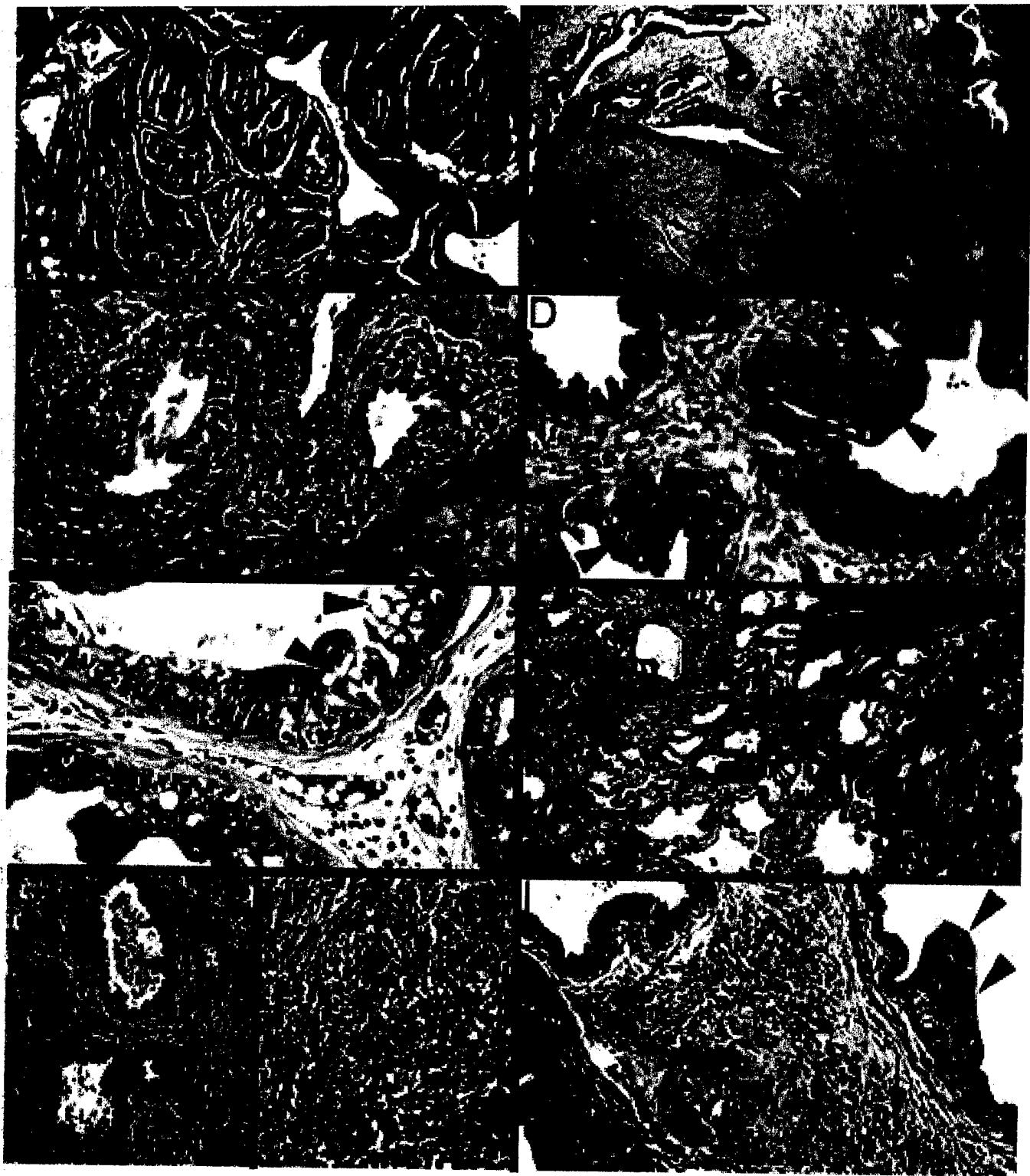
Figure 3
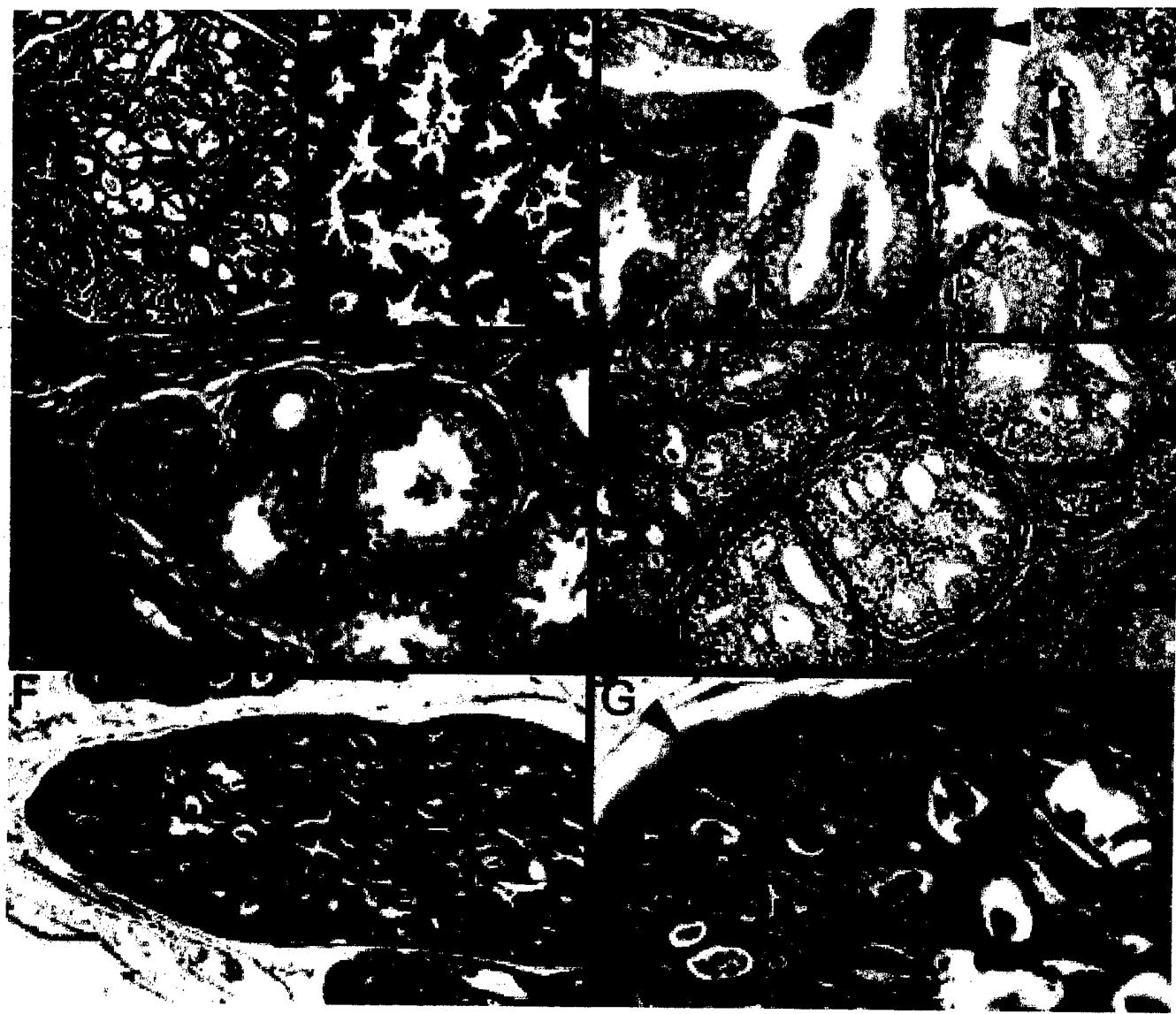
Figure 4
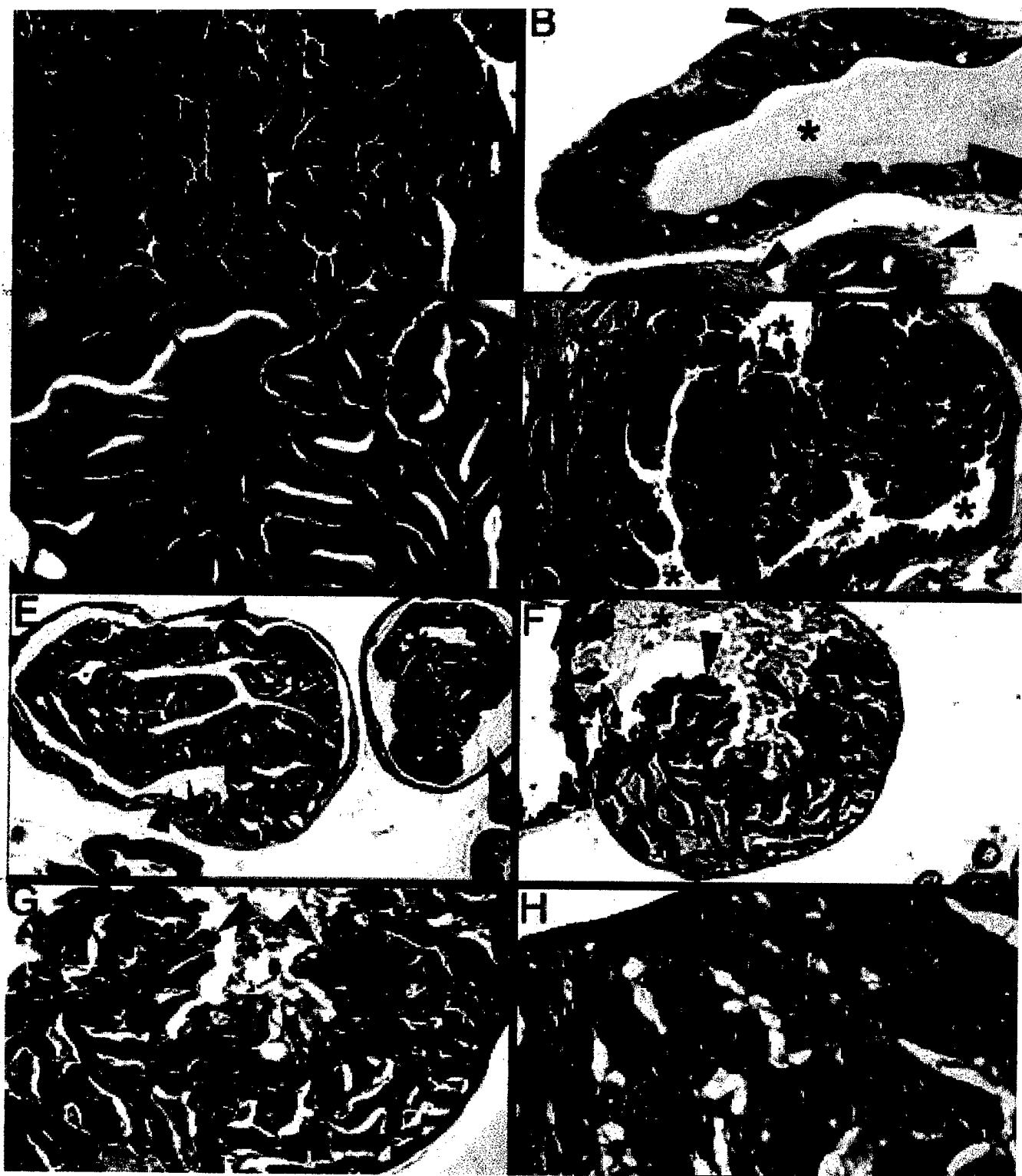
Figure 5
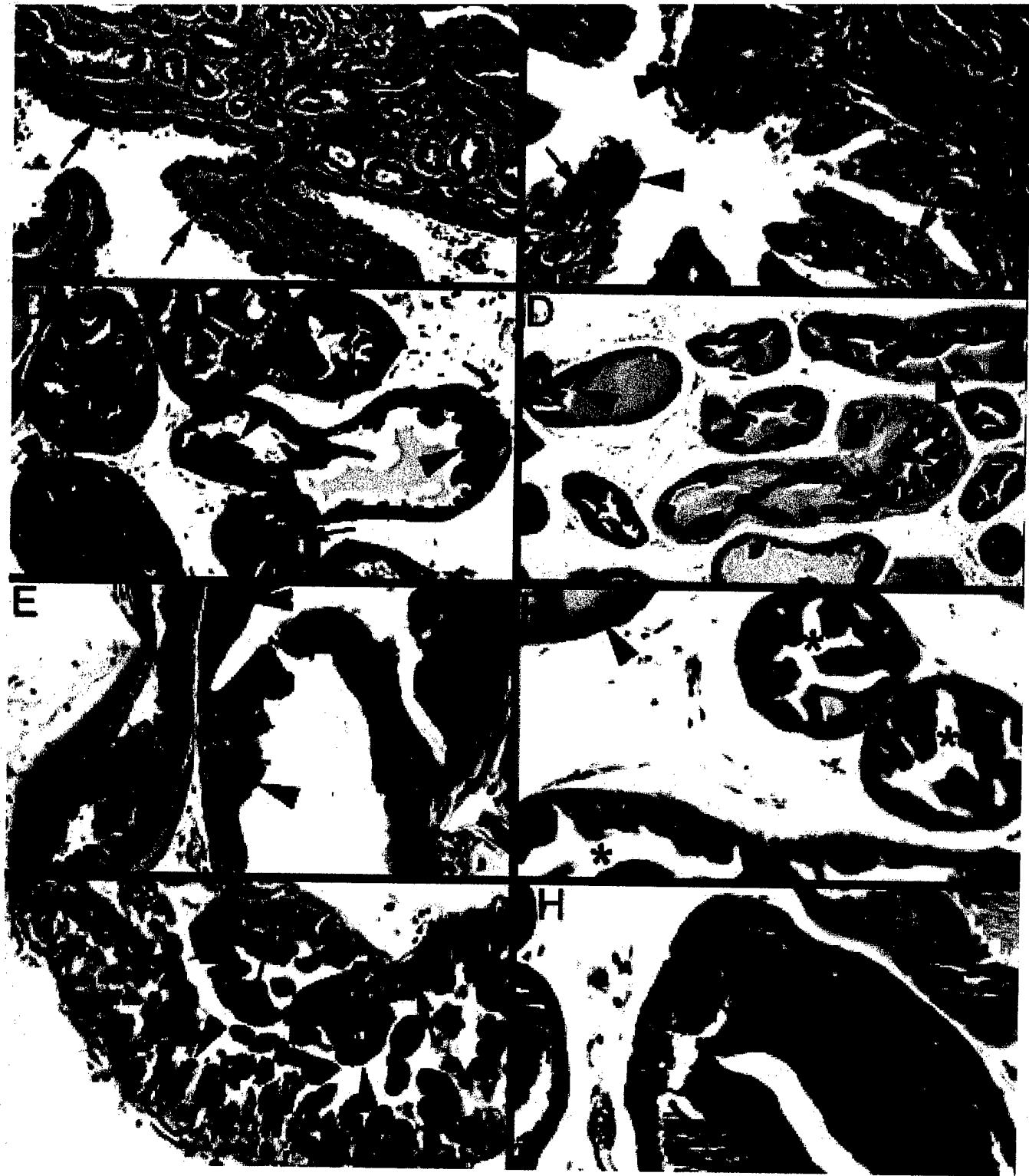
Figure 6
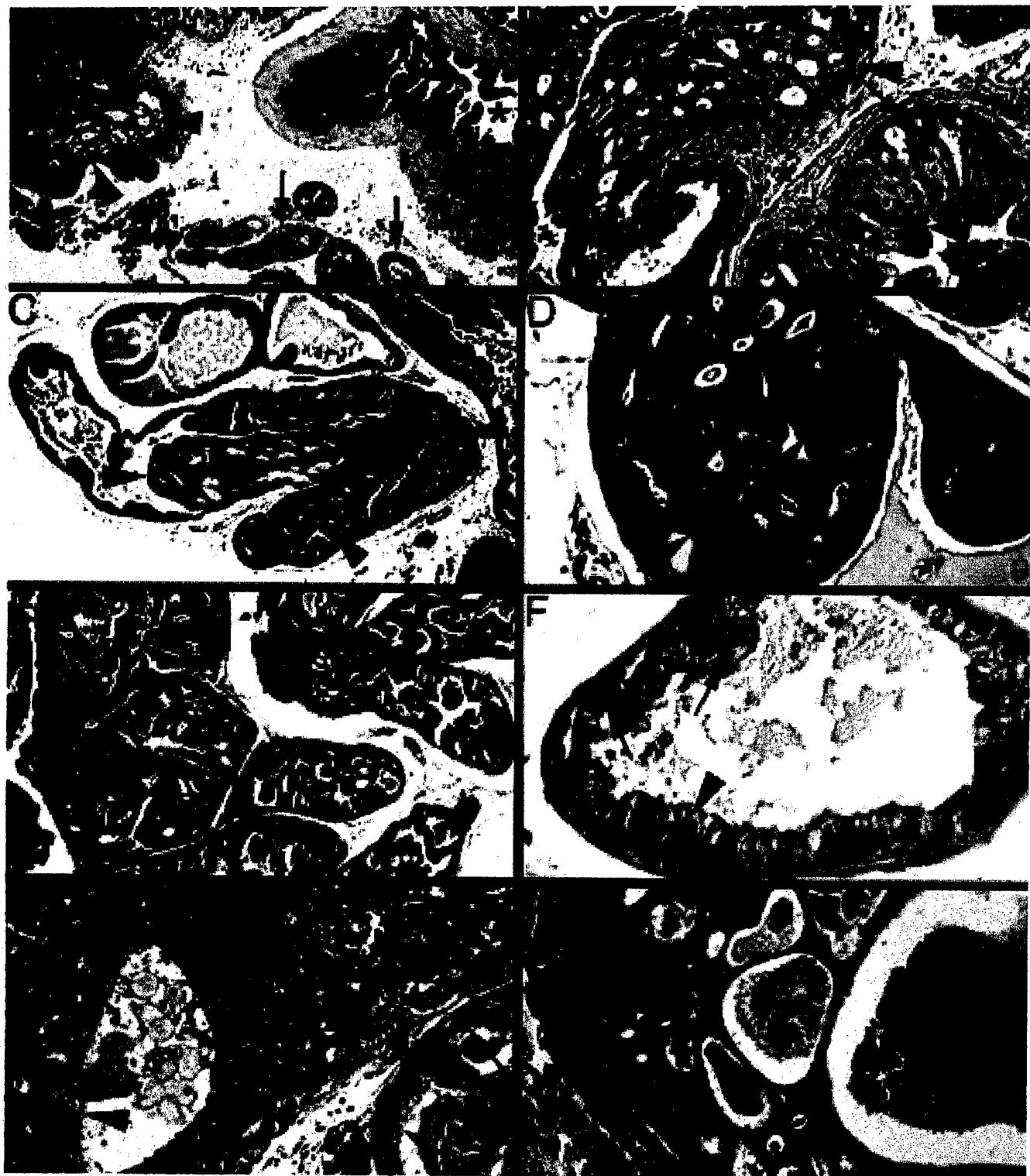
Figure 7
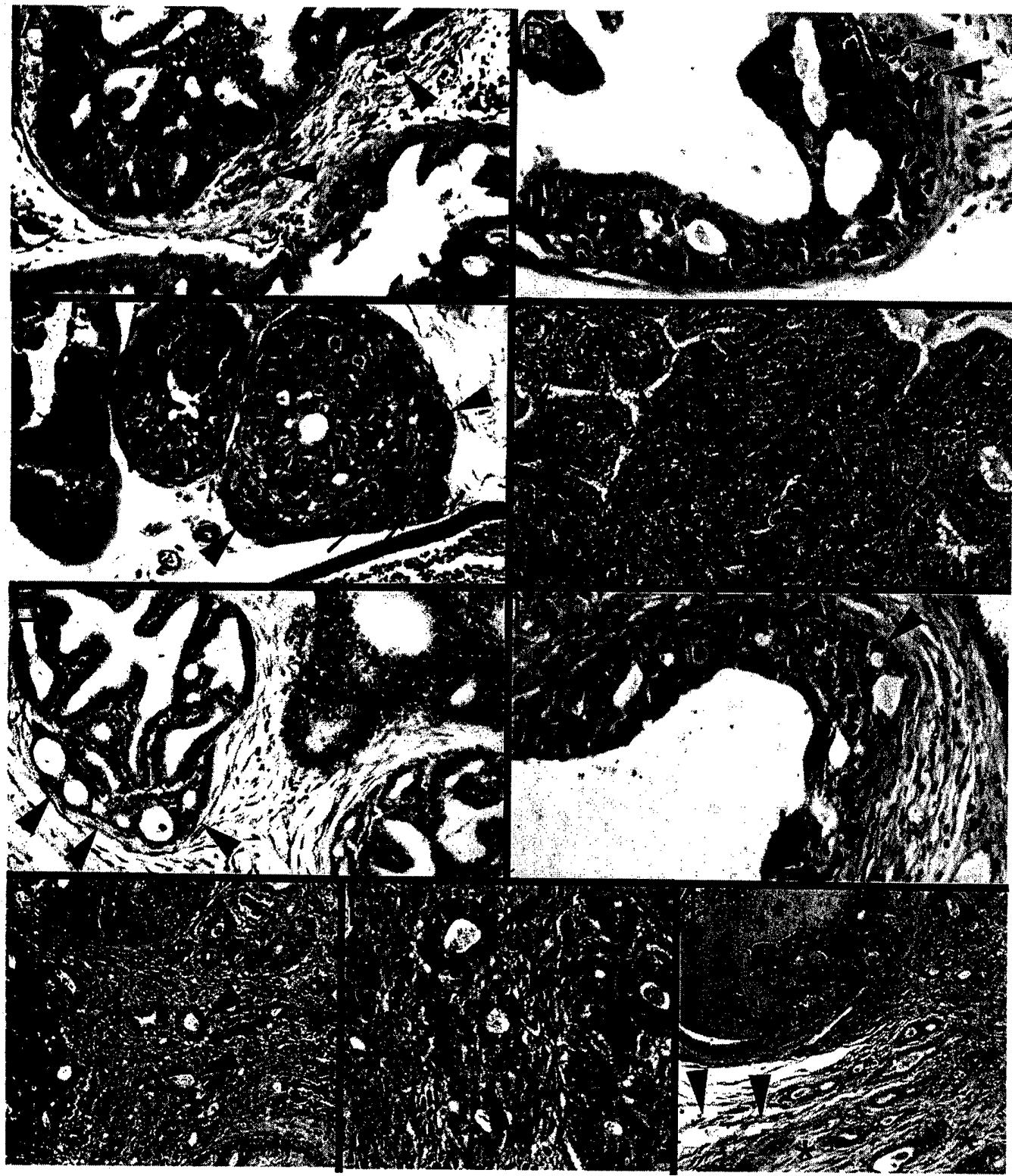
Figure 8
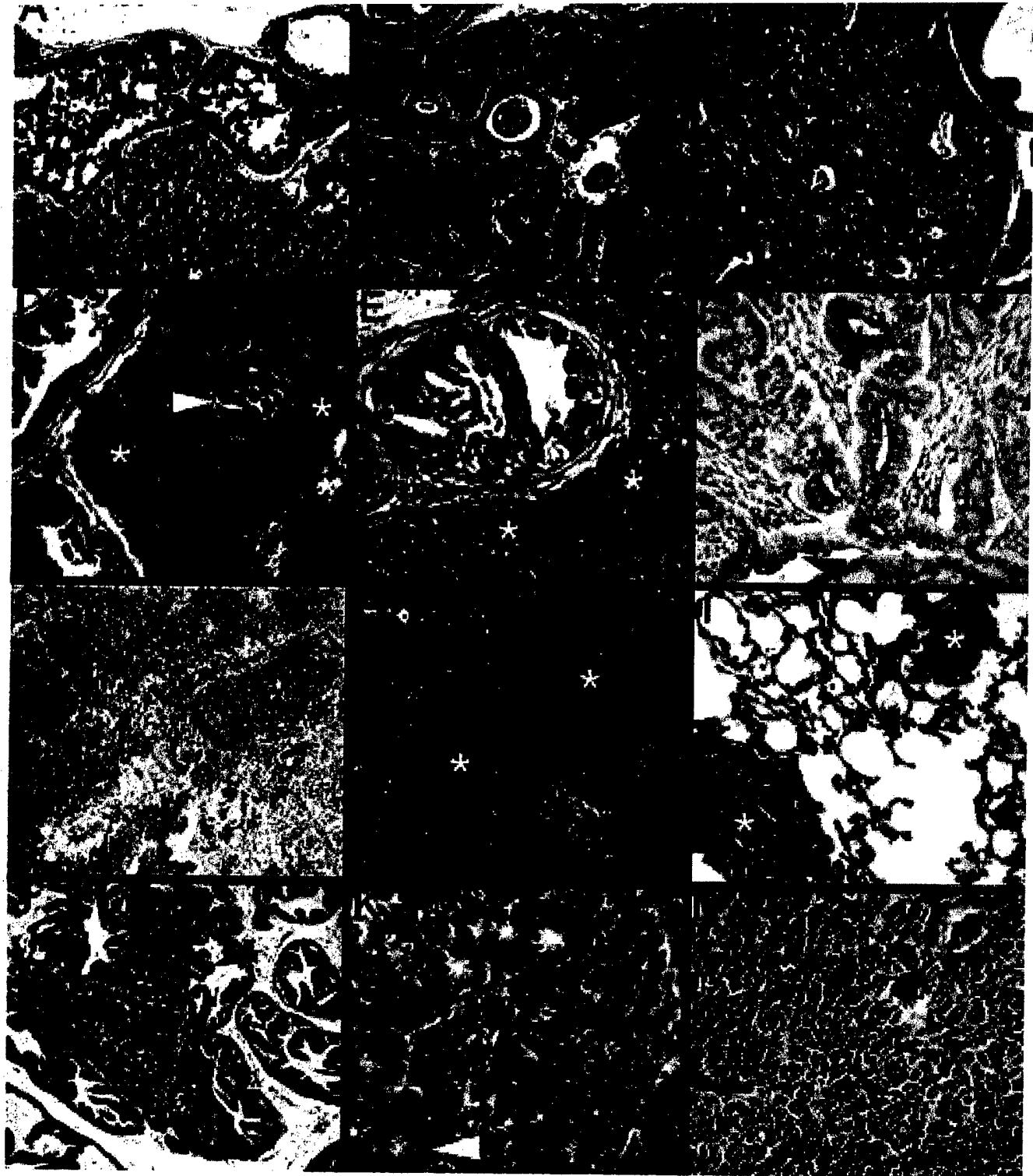
Figure 9

Figure 10

Figure 11